UNIVERSITEIT VAN PRETORIA
UNIVERSITY OF PRETORIA
YUNIBESITHI YA PRETORIA

EXPERIMENTAL INVESTIGATION AND MATHEMATICAL MODELLING OF THERMOPHYSICAL PROPERTIES OF ETHYLENE GLYCOL AND GLYCEROL-BASED NANOFLUIDS

by

SAHEED ADEWALE ADIO

A thesis submitted in partial fulfilment of the requirements for the degree

Philosophiæ Doctor in Mechanical Engineering

in the

Department of Mechanical and Aeronautical Engineering

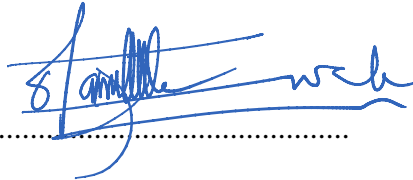Faculty of Engineering, Built Environmental and Information Technology

University of Pretoria

Pretoria

2015

DECLARATION

I, Saheed Adewale Adio, hereby declare that the matter embodied in this thesis, "Experimental investigation and mathematical modelling of thermophysical properties of ethylene glycol and glycerol-based nanofluids" is the result of investigations carried out under the supervision of Dr M Sharifpur and Prof JP Meyer in the Department of Mechanical and Aeronautical Engineering, University of Pretoria, South Africa, towards the awarding of the degree *Philosophiæ Doctor*. I also declare that this thesis has not been submitted elsewhere for any degree or diploma. In keeping with the general practice in reporting scientific observations, due acknowledgement has been made whenever the work described is based on the findings of other researchers.

Signature... Date 31 January, 2016.

DEDICATION

This thesis is dedicated to:

Islaam,

my parents, Mr Tijani Adio Adedeji and Mrs Muibat Omowumi Adio,

my lovely wife, Maimunah, for her unflinching support and sacrifices, and my children,

Al-Haarith, Hibatullaah, Haneefah and Hameemah[‡]

[‡] *Hameemah was born in my absence while I was on the PhD programme*

iii

ACKNOWLEDGEMENTS

I thank almighty Allaah for His infinite mercies, His guidance, the knowledge, good health and the strength he bestowed on me to be able to reach this milestone. He said in the Qur'aan.

"It is Allaah who made for you the night that you may rest therein and the day giving sight. Indeed, Allaah is full of bounty to the people, but most of the people are not grateful" Qur'aan 40 verse 61.

"[He was] grateful for His favours. Allaah chose him and guided him to a straight path" Qur'aan 16 verse 121.

I wish to express my utmost gratitude to my supervisor, Dr Mohsen Sharifpur, for his technical guidance and moral support throughout this study. I thank him for creating a good supervisor-student relationship and for creating time for all my technical challenges.

My deepest thanks go to my co-supervisor and Head of the Department of Mechanical and Aeronautical Engineering at the University of Pretoria, Prof Josua P Meyer, for his technical and financial support, which allowed me to successfully complete this study. He provided the enabling environment and sponsored the needed local and international exposure required for the attainment of this degree.

I would like to acknowledge my siblings, Shadiat, Kafilat and Lateefat, for their prayers, support and love throughout the course of my PhD programme. I thank my in-laws for their assistance to my wife and children back home, for their concerns and prayers. I appreciate you all.

I would also like to thank Ms Tersia Evans (Departmental Postgraduate Administrator), without whom this acknowledgement is incomplete. She makes me feel comfortable (by handling all procurement, space allocation, computer and internet access, etc.) in the Department, which was an important factor in the successful completion of my PhD degree.

I also wish to thank all my postgraduate colleagues and friends, especially Mrs OO Adewumi, Ntumba Tshimanga, Mehdi Mehrabi (PhD), Francis Okafor, Hadi Ghodsinezhad, Adeola Shote, Abiodun Aasa, Daniel Ewim, Garbadeen Ibraheem, Mostafa Mahdavi, Suaib Usman, Mutheba Kadindi, Dickson Ndenguma, Sogo Abolarin and Abubakar Bashir.

Special thanks go to the following staff members of the Department of Mechanical and Aeronautical Engineering at the University of Pretoria: Dr. Lauber Martins, Chris Govender, Donald Keetse, Koos Mthombeni and Danie Gouws.

I sincerely appreciate the concern, love, encouragement, prayers and words of advice that came from my brothers and sister in the deen; Mr Latif, Engr. Olajumoke, Dr Adebesin, Dr Oboirien, Dr Adeleke, Dr Raji, Dr Yusuf, Dr Bello, and Mr and Mrs Akinoso.

Thanks to all the academic and non-academic staff members of the Department of Mechanical Engineering, Obafemi Awolowo University, Ile-Ife, Nigeria, and my employer (the management of Obafemi Awolowo University) for approving my study leave, which afforded me the opportunity to further my studies at the University of Pretoria. In the same vein, I would like to extend special thanks to Dr Obayopo, Dr Muritala, Dr Malomo, Mr Oladosu and Mr Aminu for their unceasing desire to know the progress of my research and their prayers.

I also want to thank my MSc supervisor and mentor, Prof Abraham A Asere for his regular advice.

Finally, I owe a great appreciation to Prof Richard O Fagbenle for his reference during my PhD application process.

ABSTRACT

Title : Experimental investigation and mathematical modelling of thermophysical properties of ethylene glycol and glycerol-based nanofluids

Author : Saheed Adewale Adio

Supervisors : Dr Mohsen Sharifpur and Prof Josua P Meyer

Department : Mechanical and Aeronautical Engineering

University : University of Pretoria

Degree : *Philosophiæ Doctor* (Mechanical Engineering)

Nanofluids are a new class of heat transfer fluids that aim to improve the poor thermal efficiency of conventional heat transfer fluids. The dispersion of nanoparticles into traditional heat transfer fluids, such as water, ethylene glycol, glycerol, engine oil and gear oil, improves the thermal conductivity of base fluids, which has attracted researchers to apply nanofluids in engineering systems. Nanofluids show higher thermal and electrical conductivity. However, in terms of heat transfer performance, viscosity is also important. The viscosity of nanofluids increases due to an increase in the nanoparticle volume fraction, which needs attention and proper experimental investigation to improve the efficiency of nanofluids in heat transfer applications. Consequently, investigation into the effective viscosity of nanofluids is as important as the thermal conductivity.

On the other hand, how nanofluids are prepared can have an effect on the resultant performance. Using an ultrasonication mixer for the dispersion of nanoparticles in the base fluid is one of the most effective and popular methods of preparing nanofluids, especially from the two-step method. Almost all the experimental studies available on nanofluids chose an arbitrary time for the preparation of nanofluids. Choosing an arbitrary time for ultrasonication or any other physical preparation mechanism may be counterproductive. Therefore, in this research, nanofluids are prepared through an optimised two-step method that is assisted with ultrasonic vibration. The resulting homogenised nanofluids are further investigated for the influence of temperature, particle size, volume fraction, base fluid type and particle type on the evolution of the viscosity,

pH and electrical conductivity. The temperature range investigated in this thesis is 20 to 70 ^{o}C; the nanoparticle volume fraction is up to 5%; the base fluids are ethylene glycol (EG) and glycerol, while the nanoparticle types are MgO, Al_2O_3 and SiO_2 in different sizes.

Viscosity is a very important parameter, especially in systems that involve fluid flow (forced or natural convection) and for numerical analysis. However, most generic models in the literature underpredicted the viscosity evolution of nanofluids. Therefore, it is essential that very accurate models need to be developed for the prediction of the viscosity of nanofluids. To this end, this research also models the viscosity of the different nanofluids using dimensional analysis and regression analysis based on the experimental input-output data. Furthermore, artificial intelligence methods, such as the group method of data handling-neural network (GMDH-NN), genetic algorithm-polynomial neural network (GA-PNN) and fuzzy C-mean clustering-based adaptive neuro-fuzzy inference system (FCM-ANFIS) methods, are used to model the relationships between the experimental input parameters and the viscosity of the nanofluids.

Generally, the viscosity of the nanofluids reduced exponentially with temperature increase and the trends are similar to those displayed by the respective base fluids. However, the viscosity of the nanofluids is higher depending on the concentration of the nanoparticles contained in the nanofluids. Suspending nanoparticles in the base fluid increased the viscosity of the resulting nanofluid, and a further increase in the volume fraction of the nanoparticles increased the effective viscosity of the nanofluids. The viscosity trend of the nanofluids of Al_2O_3-glycerol is non-linear to volume fraction increase while MgO-EG nanofluids displayed a linear dependence. Regarding the influence of particle size, smaller particles produced a higher energy dissipation rate due to the higher number density, increased Brownian velocity and particle-particle interactions. Therefore, the viscosity was higher in nanofluid samples prepared from smaller nanoparticles. When the same nanoparticle samples were dispersed in different base fluids, it was found that the relative viscosity is different in the different nanofluids, which suggests that base fluid properties are indispensable when discussing the viscosity of nanofluids.

The pH and electrical conductivity of the base fluids did not change much with an increase in temperature, and their values were smaller than unity. The suspension of nanoparticles saw an increase in the values of both the pH and electrical conductivity. As the volume fraction of suspended particles increased, the value of the electrical conductivity and pH also increased commensurately, until counterion condensation effects set in. Increasing the temperature of the nanofluids led to an increase in the electrical conductivity, while the pH generally reduced with an increase in temperature. Although smaller nanoparticles showed slightly higher electrical conductivity values, pH values were convincingly higher across all the volume fractions. The ionisation process is different for the different base fluids, therefore, the pH and electrical conductivity were different for the same nanoparticles suspended in different base fluids.

The viscosity correlations developed in this thesis through dimensional analysis with regression all gave good agreements with the experimental data. When the correlations were compared with some of the prominent, well-cited models in the open literature, they performed better in producing experimental results. Furthermore, the use of GMDH-NN, GA-PNN and FCM-ANFIS for modelling and predicting the effective viscosity for the nanofluids as a function of particle diameter, temperature and volume fraction are presented. The results of the GMDH-NN, GA-PNN and FCM-ANFIS models all showed very good agreement when compared with the experimental data. Therefore, these models come in handy when using these nanofluids for computational fluid dynamics or any other design analyses.

Keywords: *Nanofluid, effective viscosity, electrical conductivity, pH, MgO, ethylene glycol, Al_2O_3, glycerol, SiO_2, temperature, volume fraction, nanoparticle size, relative viscosity, ultrasonication, energy density, empirical models, dimensional analysis modelling, GMDH-NN, GA-PNN, FCM-ANFIS.*

TABLE OF CONTENTS

LIST OF FIGURES

xiv

xvi

LIST OF TABLES

NOMENCLATURE

a	particle radius (m)
a_a	effective radius of aggregate (m)
a_i	empirical constants
a_{ij}	grand model coefficients
A	empirical parameter
A_b	absorbance
AARD	average absolute relative deviation
AI	artificial intelligence
ANFIS	adaptive neuro-fuzzy inference system
ANN	artificial neural network
APS	average particle size (m)
ATC	automatic temperature compensation
b_I	characteristics of electrolyte
B	empirical parameter
C	correction factor
C_1	empirical constant
CFD	computational fluid dynamics
CL	Cheng and Law
CNT	carbon nanotube
d_p	nanoparticle diameter (m)
d_f	base fluid molecular diameter (m)
d_i	diameter of the ith particle size (m)
D	fractal index
D_a	aggregate diameter (m)
D_{ai}	i^{th} aggregate diameter (m)
D_E	dielectric constant (F/m)
D_x	average particle diameter (m)
DLS	dynamic light scattering
e	Charge (C)

E	empirical constant
E_a	activation energy (J)
EDL	electrical double layer
EDS	energy-dispersive X-ray spectroscopy
EG	ethylene glycol
f_a	agglomeration factor
FCM-ANFIS	fuzzy C-mean clustering-based adaptive neuro-fuzzy inference system
FGM	functionally graded materials
GA	genetic algorithm
GA-NN	genetic algorithm-neural network
GA-PNN	genetic algorithm-polynomial neural network
GMDH	group method of data handling
GMDH-NN	group method of data handling-neural network
GMDH-PNN	group method of data handling-polynomial neural network
HPH	high-pressure homogenisation
JCPDS	Joint Committee on Powder Diffraction Standards
h	thickness of nanolayer (m)
h_s	minimum separation distance between two spheres (m)
I	light intensity of UV-visible ray (Cd)
IEP	isoelectric point
k	specific conductivity
k_b	Boltzmann constant (J/K)
k_H	Huggin's coefficient
K_{bf}	electrical conductivity of base fluid (µS/cm)
K_{nf}	electrical conductivity of nanofluid (µS/cm)
K_p	electrical conductivity of the particle (µS/cm)
l	length of the optical path (m)
L_{ij}	GA-PNN i^{th} output in j^{th} layer
LOC	lab-on-a-chip
m	system property constant
M	number of data points used for the network training

MAE	mean absolute error
MAPLE	matrix-assisted pulsed laser evaporation
MEMS	micro-electro-mechanical systems
MRE	mean relative error
MRF	magnetorheological fluid
MRNF	magnetorheological nanofluid
MSE	means square error
MWCNT	multi-wall carbon nanotube
N_i	number of particles with i^{th} size diameter
n_i	number density of the ions (m^{-3})
NEMS	nano-electro-mechanical systems
Nu	Nusselt number
p	electroviscous coefficient
$\bar{\bar{p}}$	average aspect ratio
PEO	polyethylene oxide
PEMFC	proton exchange membrane fuel cell
PG	propylene glycol
P_i	packing fraction of each class size i
PSD	particle size distribution
Pr	Prandtl number
PVP	polyvinylpyrrolidone
Q	particle surface charge (C)
r	capping layer thickness (nm)
R	adjustable parameter
R_g	universal gas constant (J mol^{-1} K^{-1})
$\Re$	system parameter
Re	Reynolds number
RMSE	root mean square error
SDS	sodium dodecylbenzene sulfonate
SEM	scanning electron microscope
SI	International System of Units

SSE	sum of square errors
SWCNH	single-wall carbon nanohorn
SWCNT	single-wall carbon nanotube
t_o	initial time after preparation (s)
t_3	final time at phase separation (s)
T	suspension temperature (^{o}K)
T_0	reference temperature (^{o}K)
TEM	transmission electron microscope
v_j	binary packing coefficient
V	sedimentation velocity (m/s)
V_B	Brownian velocity (m/s)
VFT	Vogel-Fulcher-Tammann
XRD	X-ray diffraction
z	number of different classes of particle size in suspension

Greek symbols

α	empirical constant
β	diffusion coefficient
γ	empirical constant
$\dot{\gamma}$	shear rate (s^{-1})
γ_{ij}	binary packing fraction
δ	particle centre-centre distance (m)
ε	molar absorptivity (L·mol^{-1}·cm^{-1})
ε_o	permittivity of the vacuum (C² N^{-1} m^{-2})
ε_r	relative permittivity of the medium
$[\eta]$	intrinsic viscosity
ζ	zeta potential (mV)
η_r	relative viscosity
θ	temperature in degree Celsius (^{o}C)
μ_e	electrophoretic mobility (C s kg^{-1})

μ_{eff}	effective viscosity (mPa.s)
μ_i	viscosity corresponding to i^{th} class particle size distribution (mPa.s)
μ_{nf}	nanofluid viscosity (mPa.s)
μ_o	suspending medium viscosity (mPa.s)
μ_s	specific viscosity
μ_∞	intrinsic viscosity at infinite shear rate (mPa.s)
$\mu_{\infty,T}$	viscosity at infinite temperature (mPa.s)
$\pi_1 - \pi_4$	dimensionless parameters
ρ_f	base fluid density (kg/m^3)
ρ_p	nanoparticle density (kg/m^3)
ρ_{nf}	nanofluid density (kg/m^3)
σ	empirical constant
τ	shear stress (N/m^2)
τ_o	yield stress (N/m^2)
υ	crowding factor
Φ	packing geometry of inorganic materials
ϕ	particle volume fraction
ϕ_a	aggregate volume fraction
ϕ_{eff}	effective volume fraction
ϕ_h	hydrodynamic volume fraction
ϕ_i	volume fraction corresponding to i^{th} class particle size distribution
ϕ_j	volume fraction corresponding to j^{th} class particle size distribution
ϕ_m	maximum particle volume fraction
ϕ_{ma}	packing fraction of aggregates
ϕ_z	ultimate packing fraction
φ	nanoparticle mass fraction
φ_i	mass fraction of the aggregate i
ψ	empirical constant

Ψ	molar concentration

Subscripts

0	reference
a	aggregate
b	Boltzmann
B	Brownian
eff	effective
EV	electroviscous
f	fluid
h	hydrodynamic
i	i^{th} class
j	j^{th} class
m	maximum
nf	nanofluid
o	base fluid
p	particle
r	relative
s	separation

Superscripts

mono	monomodal particle distribution
n	empirical constant
x	particle size distribution average

PUBLICATIONS IN JOURNALS AND CONFERENCE PROCEEDINGS

The following list of articles and conference papers were published while this study was in progress. It provided independent peer review and very valuable feedback from reviewers, which were implemented. Therefore, some parts of this thesis have exactly the same content as many of the articles and conference papers that were published. The copyright agreements of the publishers that were signed ensured the necessary permissions.

Published articles in international journals

1. **S.A. Adio**, M. Sharifpur and J.P. Meyer, Investigation into effective viscosity, electrical conductivity and pH of γ-Al_2O_3-glycerol nanofluids in Einstein concentration regime, *Heat Transfer Engineering*, vol. 36, no. 14–15, pp. 1241–1251, 2015.

2. J.P. Meyer, **S.A. Adio,** M. Sharifpur and P.N. Nwosu, The viscosity of nanofluids: a review of the theoretical, empirical and numerical models, *Heat Transfer Engineering*, vol. 37, no. 5, pp. 387–421, 2016.

3. **S.A. Adio**, M. Sharifpur and J.P. Meyer, Factors affecting the pH and electrical conductivity of MgO-ethylene glycol nanofluids, *Bulletin of Materials Science*, vol. 38, no. 5, pp. 1345–1357, 2015.

4. M. Sharifpur, **S.A. Adio**, and J.P. Meyer, Experimental investigation and model development for effective viscosity of Al_2O_3-glycerol nanofluids by using dimensional analysis and GMDH-NN methods, *International Communications in Heat and Mass Transfer*, vol. 68, pp. 208–219, 2015.

5. **S.A. Adio**, M. Sharifpur and J.P. Meyer, Influence of ultrasonication energy on the dispersion consistency of Al_2O_3-glycerol nanofluid based on viscosity data, and model development for the required ultrasonication energy density, *Journal of Experimental Nanoscience*, 2015. **Article in press.**

6. **S.A. Adio**, M. Mehrabi, M. Sharifpur and J.P. Meyer, Experimental investigation and modelling of the effective viscosity of MgO-ethylene glycol nanofluids using dimensional analysis, FCM-ANFIS and GA-PNN modelling techniques, *International Communications in Heat and Mass Transfer*, 2016. **Article in press.**

Manuscripts under review in international journals

7. **S.A. Adio**, M. Sharifpur and J.P. Meyer, Experimental investigation on characterization and the influence of ultrasonic energy density on the dispersion consistency of MgO-EG nanofluids using viscometry approach, *Heat Transfer Engineering*, Submitted in September 2015.

Published refereed conference papers

8. **S.A. Adio**, M. Sharifpur and J.P. Meyer, Investigation into effective viscosity and electrical conductivity of γ-Al_2O_3-glycerol nanofluids in Einstein concentration regime, *Proceedings of the 13th UK Heat Transfer Conference (UKHTC2013),* Imperial College, London, UKHTC2013/92, pp. 1–13, 2–3 September 2013.

9. **S.A. Adio**, M. Sharifpur and J.P. Meyer, Combined influenced of size and sonication on constant shear viscosity of MgO-ethylene glycol nanofluids, *Proceedings of the 15th International Heat Transfer Conference,* Kyoto, Japan, paper IHTC15-8606, 10–15 August 2014. DOI: 10.1615/IHTC15.tpp.008606

10. **S.A. Adio**, M. Sharifpur and J.P. Meyer, Investigation into the pH and electrical conductivity of MgO-ethylene glycol nanofluids, *Proceedings of the 15th International Heat Transfer Conference,* Kyoto, Japan, paper IHTC15-8604, 10–15 August 2014. DOI: 10.1615/IHTC15.tpp.008604

11. M. Sharifpur, **S.A. Adio** and J.P. Meyer, Nanofluid composites: preparation and rheology behaviour for vacuum infusion process, *Proceedings of the 4th International Conference on Composites: Characterization, Fabrication and Application (CCFA-4)*, Tehran, Iran, paper A-10-1350-1, 16–17 December 2014.

12. M. Sharifpur, **S.A. Adio** and J.P. Meyer, Experimental investigation on the viscosity, electrical conductivity and pH of SiO2-Ethylene Glycol Nanofluids, *Proceedings of the 11th International Conference on Heat Transfer, Fluid Mechanics and Thermodynamics (HEFAT2015)*, Kruger National Park, South Africa, pp. 199–204, 20–23 July 2015.

CHAPTER 1:   INTRODUCTION

1.1   BACKGROUND

Energy sustainability demands the efficient management of resources, which includes energy and thermal processes. The global objective is to achieve sustainable and efficient energy development in line with sustainable development goals. Therefore, technological advancement is growing at a geometric rate and, among other things, it is tailored towards the achievement of sustainable energy and energy management processes. Recently, devices such as lab-on-a-chip (LOC), micro-electro-mechanical systems (MEMS), nano-electro-mechanical systems (NEMS), and micro- and nano-processors are required to accomplish high-end precision tasks. For instance, MEMS are currently used for surgical procedures that require high-level precision, especially in human surgery. These devices, from microelectronics to industrial machines, are being made smaller and lighter, but more sophisticated in their intended functions. Consequently, they generate more heat per unit area (high heat flux), which needs to be removed properly through a heat exchange medium, and if not, they will lead to overheating, hot spot, performance reduction and equipment damage.

There are several ways of resolving the thermal management challenges posed by the new and technologically advanced devices. Some of these methods are the use of functionally graded materials (FGM), the geometric modification of heat exchanger microchannels to find optimum configurations, increasing the effective heat transfer surface area, and increasing the convective heat transfer coefficient. The use of FGM raise production costs, which makes affordability a serious concern. On the other hand, microchannel size constraint requires little working fluid. Therefore, heat removal is not efficient. Especially with the conventional heat transfer fluid, increasing the effective heat transfer surface area results in increased weight and size, and increasing the convective heat transfer coefficient incurs greater running cost in terms of the pumping power requirement.

Functionally modified heat transfer fluid is a new class of heat transfer fluid called nanofluid. This new class of fluid is produced from the dispersion of ultrafine particles

(nanoparticles) of metal, metal oxide, non-metals and non-metal oxides in the conventional heat transfer fluid (base fluid), such as water, ethylene glycol (EG), glycerol, propylene glycol (PG) and engine oil. The dispersion was thought desirable in order to modify the transport properties of the conventional heat transfer fluids, since they are characteristically poor in thermal transport properties such as thermal conductivity, heat transfer coefficient and electrical conductivity. The idea of particle dispersion in base fluid can be traced to Maxwell in 1873 [1], when the conductivity of heat transfer fluid was first modified with micrometric particles. The challenges with Maxwell's types of fluid were numerous, ranging from the rapid settling of particles (poor stability), abrasion of flow equipment and significant pressure drops. Recently, researchers have shown that different nanofluids show excellent thermal transport properties, better than conventional heat transfer fluids, good stability and reduced pressure drop in heat exchangers compared to the Maxwell's fluid types. Therefore, nanofluids will provide valuable benefits in industrial processes and systems that require liquid as a working fluid, especially as heat transfer and lubricating fluids.

Numerous applications of nanoparticles and nanofluids cut across the sciences, biomedical sciences, pharmaceuticals and engineering fields. Specifically, in the context of sustainable energy development and thermal management, nanofluids are becoming more essential as the need for efficient thermal management is becoming more important. Nanofluids have capabilities that make them the right candidates for the proper and efficient cooling of MEMS, NEMS, LOCs, fuel cells or larger devices that are found in industrial processes, such as nuclear power plant processes, chemical processes, automobile cooling and large-scale microelectronic cooling systems. These capabilities are centred on their improved thermophysical properties, such as thermal conductivity, electrical conductivity, pH, density, Nusselt number (Nu) and heat capacity. Much research has been carried out to investigate the effects of different parametric inputs, mainly on the thermal conductivity of nanofluids and Nu in different flow configurations.

The viscosity of nanofluids is as important as its thermal conductivity because both the Reynolds (Re) and Prandtl (Pr) numbers are highly influenced by viscosity. It can also be argued that the Nu depends on viscosity, but this thermophysical property is sparingly investigated, especially considering different parameters such as particle size,

2

temperature, volume fraction, different base fluids, different particle types and energy of ultrasonication used during nanofluid preparation. Other poorly investigated properties of nanofluids that are critical to the attainment of their full potential are pH and electrical conductivity, which are important because they are related to the nanofluids' stability. Moreover, the study of electrical conductivity is important for LOCs, fuel cells, electrically conducting adhesives and electrospray technology. Understanding the behaviour of the pH of nanofluids is essential for material selection and corrosion monitoring.

1.2 AIM OF THIS RESEARCH

The aim of this research is to prepare uniformly homogenised and stable Al_2O_3-glycerol, MgO-EG, SiO_2-glycerol and SiO_2-EG nanofluids using an ultrasonication assist mechanism, performing experimental investigations to measure the viscosity, electrical conductivity and pH of the stably prepared nanofluids, as well as proposing accurate models through non-dimensional analysis and artificial intelligence (AI) methods for the prediction of nanofluids' viscosity.

1.3 RESEARCH OBJECTIVES

The specific objectives of this research are as follows:

1. To optimise the ultrasonication process of preparing nanofluid samples by changing the energy input into the preparation in order to determine the best ultrasonication energy required for Al_2O_3-glycerol, MgO-EG, SiO_2-glycerol and SiO_2-EG nanofluids

2. To characterise the nanoparticles and nanofluids using techniques such as transmission electron microscopy (TEM), X-ray diffraction (XRD), energy-dispersive X-ray spectroscopy (EDS), zeta potential (ζ) measurement and UV-visible spectrophotometry

3. To investigate the viscosity, pH and electrical conductivity of the samples prepared in (1) while considering different particle sizes, volume fractions, particle types, temperatures and base fluids

4. To develop viscosity correlations using non-dimensional analysis technique and AI methods on experimental data

3

1.4 SCOPE OF THE STUDY

In this research, the influence of nanoparticle size, volume fraction, nanoparticle type, base fluid type and temperature will only be considered on the effective viscosity, pH and electrical conductivity of nanofluids containing Al_2O_3, MgO and SiO_2 nanoparticles in either glycerol and/or EG base fluids.

Dispersion consistency will be monitored using the viscosity value at room temperature, and the sample with the lowest viscosity value will be taken as the homogenised sample that will be used for further experimental investigations.

The mathematical model for viscosity prediction will be provided for an individual nanofluid type based on the results of the experimental investigations using non-dimensional analysis. Furthermore, the group method of data handling-neural network (GMDH-NN), genetic algorithm-polynomial neural network (GA-PNN) and fuzzy C-mean clustering-based adaptive neuro-fuzzy inference system (FCM-ANFIS) will be employed as AI methods for the modelling of the nanofluid viscosity.

1.5 ORGANISATION OF THE THESIS

This thesis consists of seven chapters. To ensure brevity and clarity, the chapters are divided into sections and subsections. The organisation of the chapters in this thesis is discussed in this section.

Chapter 1 introduces nanofluids as a heat transfer fluid. It also presents the background information on the research study, the aims and objectives of the study and the scope of the work.

Chapter 2 provides literature reviews on the subject of the viscosity, pH and electrical conductivity of nanofluids. The theoretical background gives a detailed account on suspension viscosity models (classical, new theoretical and empirical models). The review of the experimental studies identified key factors that affect nanofluid viscosity. Review of the literature on the use of AI for modelling different thermophysical properties of nanofluids and studies on the pH and electrical conductivity of nanofluids are duly presented.

4

In Chapter 3, the experimental and modelling methodology that is employed in obtaining the experimental data and the mathematical models are presented. It focuses on the materials, equipment used, sample preparation and characterisation procedures. It also gives statistics on the estimation of the total uncertainty in each of the measurements (i.e. viscosity, pH and electrical conductivity data) and details on the modelling approaches used in the thesis.

Chapter 4 presents the experimental results and discussions on the viscosity of nanofluids. The discussion is based on the results of nanoparticles and nanofluid characterisations, the influence of ultrasonication, temperature, volume fraction and nanoparticle size on the viscosity of nanofluids. The influence of different base fluids when the same nanoparticles (type and size) are dispersed and different nanoparticles of similar size in the same base fluid type are also presented.

In Chapter 5, the experimental results of pH and electrical conductivity measurement are presented in light of the different factors: nanoparticle size, temperature, volume fractions and base fluid types.

Chapter 6 develops correlations using non-dimensional analysis and regression on the viscosity data. In the development of the correlations, essential factors, such as nanoparticle size, volume fraction temperature, capping layer thickness, viscosity of the base fluid, the density of the base fluid and the density of the nanofluid, are considered as input parameters. The developed non-dimensional correlations, which are functions of non-dimensional particle size, non-dimensional temperature and volume fraction, are used to predict the viscosity data in this work and are also compared with various well-established viscosity models in the literature. AI methods, such as GMDH-NN, GA-PNN and FCM-ANFIS, are also employed to model the experimental viscosity data.

Chapter 7 provides a general summary of the study's findings. It also presents the conclusions and recommendations for future work.

CHAPTER 2: LITERATURE REVIEW[1, 2]

2.1 INTRODUCTION

Colloidal suspension dates back to Maxwell's study in 1873 [1]. Although the idea behind his study was to create a new class of fluid with improved properties, the imposed problems were numerous for any profitable engineering solutions to be achieved [2].

Two decades ago, Choi [3] came up with a pioneering idea based on Maxwell's study and suspended different nanoparticles in a number of base fluids to produce different nanofluids. His invention opened up a myriad of opportunities in research and development. Nanofluids are colloidal suspensions that contain the following nanoparticles:

- Metallic (Ag, Au, Al, Cu and Ni)
- Non-metallic (graphene, graphite, single-wall carbon nanotube (SWCNT) and multi-wall carbon nanotube (MWCNT))
- Single-metal oxide (CuO, SnO_2, MgO, Fe_2O_3, Fe_3O_4, Al_2O_3, ZnO, TiO_2 and NiO_2)
- Multi-element oxides (indium-tin oxide, $CaCO_3$, $CoFe_2O_4$ and $NiFe_2O_4$)
- Oxides of non-metals and carbides (SiC and SiO_2)

These nanoparticles are suspended in conventional heat transfer fluids, such as water, engine oil, EG, transformer oil, gear oil or a mixture of two or more heat transfer fluids [2, 3].

When compared with the previous colloidal suspensions containing microparticles, it is a special type of fluid with numerous application potentials because of its enhanced thermal conductivity, stability and homogeneity [3, 4]. Micrometric particles in suspensions lead to the abrasion of equipment linings, the clogging of flow paths, significant pressure drops and high pumping power cost requirements. Therefore, its sustainability for heat transfer purposes was impossible. Moreover, nanofluids can reduce the pumping power in engineering equipment significantly and do not pose the problem of clogging and the abrasion of equipment linings and flow paths [5–8]. Therefore, the design and engineering of physical systems are now being tailored towards using nanofluid as a working fluid.

The two most important parameters with the use of nanofluids as heat transfer fluids are their thermal conductivity and viscosity [9–12]. The thermal conductivity and heat capacity of the fluid largely determine the heat removal capacity of the fluid. The higher the thermal conductivity, the more heat the fluid can remove from thermal systems.

High thermal conductivity fluid can also minimise the size of heat exchangers that in turn reduce the overall weight of the equipment. On the other hand, viscosity is important in systems that require flow because flow properties, such as the Re, Pr, Nu, and pressure drop depend very much on viscosity [13]. Therefore, if the viscosity is very high, there will be a penalty on the pumping power required to achieve the system's target.

In the recent past, much research progress has been made with the thermal conductivity of nanofluids [14–24], which are a few of the copious studies that have been carried out on the theoretical and experimental study of the thermal conductivity of nanofluids. However, with regard to the viscosity of nanofluids, very few theoretical models have been developed based on the unique properties of nanoparticles [2, 25]. Most available theoretical models were developed for micrometric suspensions. Notably, there are many different types of empirical models of nanofluids, but their use is often limited to specific types of nanofluids, nanoparticle size and a range of volume fraction [26, 27].

The mismatch between models and experimental results obtained from studies [28–30] on the rheological behaviour of nanofluids is of great concern. In addition, Masoumi et al. [2] and Avsec and Oblak [31] have shown that, despite good agreement between

7

experimental and theoretical results in certain cases, a wide range of constitutive factors need to be incorporated into the models in order to account for the rheological behaviour of nanofluids in widely varying conditions [32].

Other important areas of nanofluids that require proper review and experimental investigations border on the factors that affect the pH and electrical conductivity of nanofluids. Some research has been carried out on the influence of pH on the stability of nanofluids that largely affects both viscosity and thermal conductivity.

However, most of these studies have only focused on pH at room temperature. Since nanofluids are being proposed for high-temperature processes, it is advantageous to also study the influence of temperature on pH, among other factors. The study of the electrical conductivity of nanofluids at this stage in nanofluid research is also necessary because electrically conductive fluids are useful in the manufacture of electrically conductive paint, electrically conductive adhesives [33] and electric field-induced pattern formation in colloids, such as in magnetorheological fluid [34] for lubrication, efficient heat transfer and the semi-active control of vehicle suspensions [35].

Research, development and the implementation of electrospray technology is also an area that mainly depends on knowledge of the electrical conductivity of colloids [36]. Equally, understanding the electrical conductivity evolutions is particularly vital for LOCs and electrophoretic applications, especially for suspensions with a thick electrical double layer (EDL), which is typical of salt-free mediums such as EG, glycerol and PG [37].

2.2 THEORETICAL BACKGROUND OF SUSPENSION RHEOLOGY

The rheology of colloidal suspensions encompasses the study of the behaviour of a suspension in relation to its Newtonian or non-Newtonian properties, and is thus a measure of its viscosity with respect to shear stress and shear rate. A number of factors affect colloidal suspensions (micro/nanoparticles in suspensions). These factors include temperature, particle volume concentration, particle size, particle size distribution (PSD), packing fraction, EDL, the aspect ratio of particles, particle interaction, particle agglomeration, pH, nanolayer and the magnetic properties of some particles [38].

8

2.2.1   Classical theoretical viscosity models

Hypothetical analyses of the possible phenomena affecting the viscosity of nanofluids can be found in the literature, although these analyses are very limited when compared with the depth of the theoretical models that are available on the thermal conductivity of nanofluids. However, several theoretical studies have been conducted on the rheology of general suspensions. The fundamental work of Einstein [39] on the dilute suspensions of uncharged hard spheres based on the vorticity of the particle shear field was the first available theoretical study on the viscosity of suspensions that gave the model in Equation 2.1:

$$\mu_{eff} = \mu_o \left(1 + [\eta] \phi \right),$$ (2.1)

where μ_{eff} is the effective viscosity of the suspension, μ_o is the dynamic viscosity of the base fluid and $[\eta]$ is the intrinsic viscosity of the suspension. This linear equation is based on the assumed absence of interaction between the particles, and the coefficient $[\eta]$ is a function of the shape of the particle, which was derived as 2.5 for hard spheres. This model is valid for particle volume concentration, $\phi \leq 2\%$. Numerous models were developed in efforts to extend Einstein's model to concentrate suspensions [40–43] a few years after Einstein's work. Contrary to the uncharged particle in Einstein's analysis [39], Smoluchowski [40] presented an effective viscosity model for charged particles in electrolyte suspension, given in Equation 2.2:

$$\mu_{eff} = \mu_o \left[1 + 2.5\phi \left\{ 1 + \frac{1}{k\mu_o a^2} \left(\frac{\zeta D_E}{2\pi} \right)^2 \right\} \right],$$ (2.2)

where k is the specific conductivity of the electrolyte, a is the radius of the solid particles, D_E is the dielectric constants of the suspending medium and ζ is the zeta potential of the particle with respect to the electrolytic medium. Based on experimental data, Bull [44] suggested in 1940 that the effective viscosity of a suspension of egg albumen varies with the square of the electrophoretic mobility (a measure of zeta potential). Although, Smoluchowski [40] proposed that the effective viscosity of suspensions varies with the square of zeta potential as well, when this equation was applied to Bull's experimental data,

9

it predicted higher viscosity values. Therefore, Bull [44] proposed a simple model for the effective viscosity at isoelectric point (IEP), the point of zero charge on the particle, to be:

$$\frac{\mu_s}{\phi} = 0.0112 \frac{\mu_e}{\sqrt{k}},$$

(2.3)

where μ_s is the specific viscosity, μ_e the electrophoretic mobility and k the specific conductivity. In 1950, Booth [45] studied the overprediction (of the viscosity of suspension with respect to the effect of electroviscous force between particles and the suspending medium) made by Smoluchowski's model [40]. Therefore, Booth made a quantitative recalculation of the electroviscous force effect on the effective viscosity, which predicted the data of Bull [44] with a good degree of accuracy. The model is given as:

$$\mu_{eff} = \mu_o \left[1 + 2.5\phi \left\{ 1 + \sum_1^\infty b_I \left(\frac{e\zeta}{k_b T} \right)^I \right\} \right],$$

(2.4)

where b_I is the characteristics of the electrolyte, e is the electronic charge on the particles, k_b is the Boltzmann constant and T is the absolute temperature.

In 1922, Jeffery [41] extended the work of Einstein for suspensions that contain ellipsoidal particles. Based on the principle of the dissipation of energy, the model presented was not different from Einstein's Equation 2.1. However, the intrinsic viscosity was provided with two limits (minimum and maximum) for both prolate and oblate spheroids of different ellipticity of the meridian section.

Therefore, as the particles approach spherical in shape, the difference in the limits of the intrinsic viscosity diminishes and hence reduces to Einstein's model. Ward and Whitmore [46] experimented on microsphere-aqueous suspensions in a bid to verify Einstein's equation. They concluded that the intrinsic viscosity given by Einstein is a function of the PSD ratio, which is approximately 4.0 for an infinitely diluted suspension with a PSD ratio of 1:1 and approximately 1.9 for a PSD ratio exceeding 3:1. At a ratio of 1.5:1, Einstein's intrinsic viscosity value of 2.5 was obtained. This was corroborated by the work of Vand [47]. Williams [48] also concluded that PSD is a key parameter affecting the viscosity of colloidal suspension after experimenting with different sizes (4, 8 and

12 µm) of glass spheres in a binary mixture of EG-water base fluid. He fitted the data obtained into the equations of Mooney [49] and Roscoe [50] with relatively good success. Maron and Fok [51] held that the duo of Mooney and Roscoe's models did not satisfactorily predict the experimental data of Williams [48]. Hence, they tried to fit the data with the models of Maron and Fok [51] that had been successfully tested with lattices and latex mixtures. They treated the experimental data with the least-squares method to obtain model constants, and clearly showed that if the intrinsic viscosity of Einstein's model were to be between 3.15 and 3.35, the equations of Mooney [49] and Roscoe [50] would have been a perfect fit to Williams's data.

Applying a different viewpoint, Batchelor [52] considered the influence of interparticle interactions to obtain the model in Equation 2.5 for the relative viscosity of colloidal suspension having volume fraction, $\phi \leq 4\%$. Within the limits of a very low particle concentration, this model approaches Equation 2.1, which means Batchelor's model does not differ from Einstein's model, i.e. at low-volume concentration, the assumption of the non-interaction of particles, as assumed by Einstein [39], is also inherently considered. This is an ideal situation:

$$\mu_{eff} = \mu_o \left(1 + [\eta]\phi + k_H \left([\eta]\phi\right)^2\right), \tag{2.5}$$

where k_H is the Huggin's coefficient, known also as the interaction parameter. This coefficient accounts for interparticle interaction as opposed to hydrodynamic effects [53]. The semi-empirical relationship proposed by Krieger and Dougherty [54] for shear viscosity covering the full spectrum of particle volume concentrations is expressed as:

$$\mu_{eff} = \mu_o \left(1 - \frac{\phi}{\phi_m}\right)^{-[\eta]\phi_m}, \tag{2.6}$$

where ϕ_m is the maximum particle volume fraction at which flow can still occur (i.e. the concentration at which the relative viscosity approaches infinity asymptotically), the intrinsic viscosity $[\eta]$ was given as 2.5 for monodispersed suspensions of hard spheres. However, in practical situations, particles are polydisperse in nature. Hence, the assumption made by Krieger and Dougherty [54] is not valid for all particulate suspensions. This has been accentuated with underpredictions made by this model when

11

applied to viscosity data, for example, when it was applied to Al_2O_3-water nanofluid data [55].

Currently, there are not many unified models that can be used to predict the viscosity of colloids. Most of the available classical models are built around particle volume concentration and, when tested, they all give different predictions as depicted in Figure 2.1. The insets of Figure 2.1 show the degree of variation among these classical models. There is no clear-cut phenomenon to explain the erratic nature of the nanofluid viscosity data presented by different investigators. However, using these models to predict the recent experimental data, as depicted in Figure 2.2 and Figure 2.3 (for Al_2O_3-water and TiO_2-water, respectively), shows their inability to accurately predict the suspension's viscosity.

Generally, the discrepancies in reported viscosity data have mostly been ascribed to agglomeration formation. Chen et al. [53], based on this widespread assertion, extended the theoretical work of Krieger and Dougherty [54], which was based on the packing fraction of monodispersed particles without agglomeration. Chen et al. [53] assumed that if particle agglomerates were spherical, the sphere would be of different sizes. Thus, they derived a modification of Krieger and Dougherty's equation, as presented in Equation 2.7, based on the maximum packing fraction of agglomerates and the fractal index of the agglomerates, which is an indication of the degree of variation in the packing fraction from the centre of the agglomerates to the outer edge.

$$\mu_{eff} = \mu_o \left(1 - \frac{\phi_a}{\phi_m} \right)^{-[\eta]\phi_m}, \tag{2.7}$$

ϕ_a is given by $\phi_a = \phi/\phi_{ma}$, where ϕ_{ma} is the packing fraction of the aggregates. The viscosity was assumed to follow a power law with a fractal index, *D*. Consequently, ϕ_a becomes $\phi_a = \phi(a_a/a)^{3-D}$, where a_a/a is the ratio of the effective radii of aggregates and the primary nanoparticles.

12
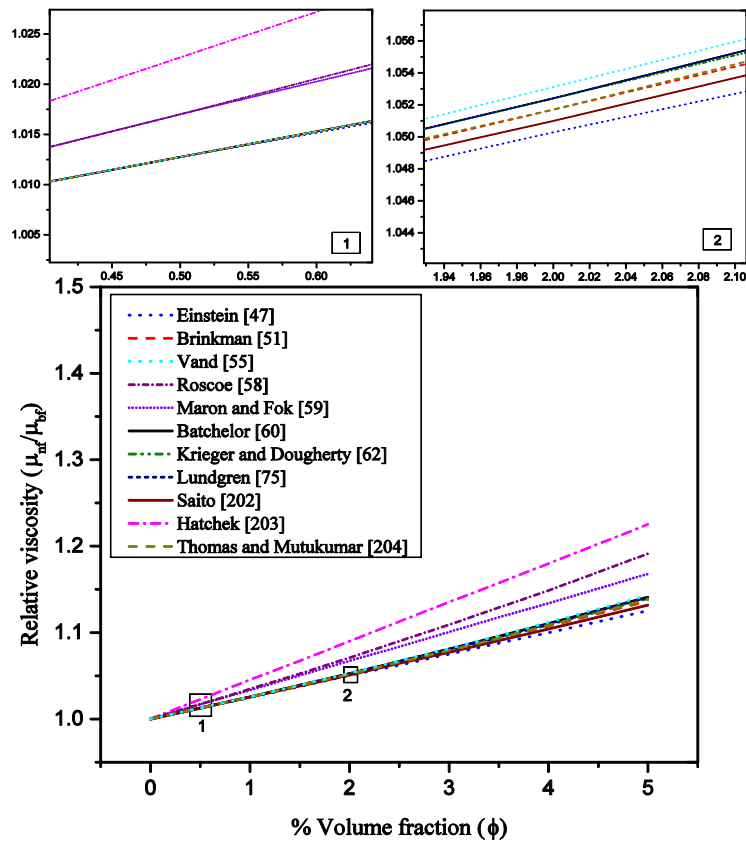
Figure 2.1: Inconsistency in suspension viscosity predictions by different available models. Al$_2$O$_3$-deionised water nanofluids' prediction at 20 ^{o}C. Insets at points 1 and 2 depict the level of discordance in the predicted relative viscosity values, even for models built around particle volume concentration.
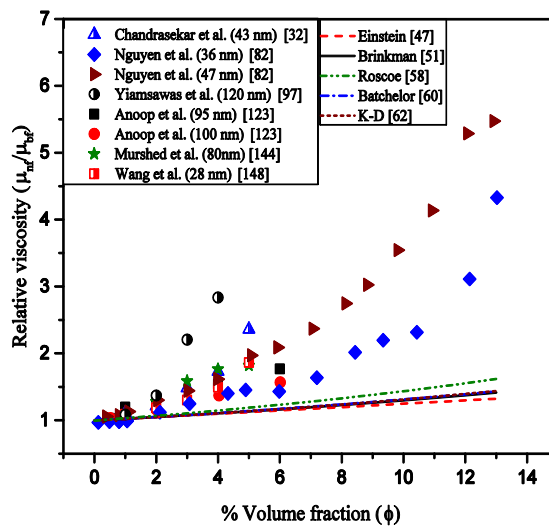
Figure 2.2: Underprediction of Al$_2$O$_3$-deionised water nanofluids by classical models

13
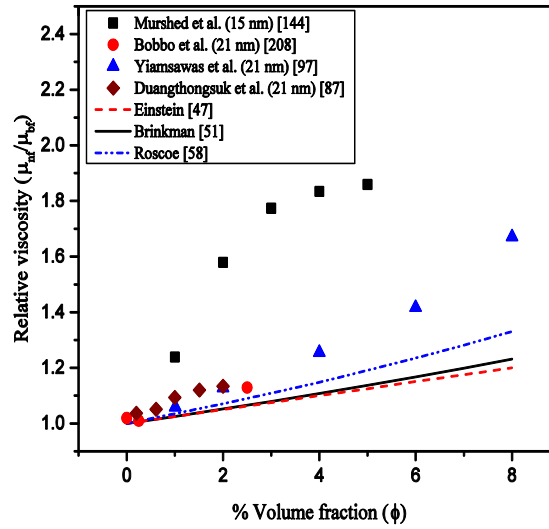
Figure 2.3: Underprediction of TiO$_2$-deionised water nanofluids by classical models

In an attempt to bring together the two separate views: that PSD affects the viscosity of suspension and that agglomeration, which is a function of the interaction between particles, affects the viscosity of suspension, Farris [56] suggested that agglomeration alone could not describe the evolution of nanofluid viscosity and that PSD was seen to play a role in the viscosity trend. Therefore, if the PSD is discrete, the global relative viscosity of the non-interacting monodispersed system of particles in suspensions may be calculated as the product of each independent viscosity as shown in Equation 2.8 [56]:

$$\eta_r = \left(\frac{\mu_1 \phi_1}{\mu_o}\right) \times \left(\frac{\mu_2 \phi_2}{\mu_o}\right) \times \cdots \cdots \times \left(\frac{\mu_z \phi_z}{\mu_o}\right), \tag{2.8a}$$

In general form:
$$\eta_r = \prod_{i=1}^{z} \eta_r\left(\phi_i\right), \tag{2.8b}$$

where ϕ_i is the zth class corresponding particle fraction and z stands for the different average particle sizes contained in the distributions. The viscosity of each monodispersed suspension can also be related to the maximum particle volume fraction, ϕ_m in the model proposed by Chong et al. [57] and given as:

$$\eta_r\left(\phi_i\right) = \left[1 + 0.75\left(\frac{\phi_i / \phi_m}{1 - \phi_i / \phi_m}\right)\right]^2. \tag{2.9}$$

Chong et al. [57] experimentally determined the maximum particle volume fraction of a monodispersed system of glass beads sized in microns using a specially developed orifice viscometer. They reported ϕ_m for their experiment as 0.605 and further proved that plotting

14

the $\phi \cdot \eta_r / (\eta_r - 1)$ vs ϕ and extrapolating up to the point where the two axes' variables meet will give the ϕ_m for any suspension. Storms et al. [58] expanded the work of Chong et al. [57] to understand the effect of polydisperity (the size ratio and percentage volume fraction of smaller particles) on the viscosity of the suspension. It was found that the viscosity depends on the size ratio and percentage volume fraction of the smaller particles present. The model in Equation 2.10 accurately predicted the experimental data of Chong et al. [57]:

$$\eta_r\left(\phi_i\right) = \left[1 + \frac{R\phi_i}{1 - \phi_i / \phi_m}\right]^{3.3\phi_m}, \tag{2.10}$$

where R is an adjustable parameter and varies from 0.7 to 1.25 depending on the size distribution. If ϕ_m is taken as 0.605, as Chong et al. [57] proposed, the exponent in Equation 2.10 becomes 2. It should be noted that equations 2.9 and 2.10 are modified versions of Eilers's equation (see [57]) given below:

$$\eta_r = \left[1 + \frac{2.5\phi}{2\left(1 - \phi / \phi_m\right)}\right]^2. \tag{2.11}$$

While determining ϕ_m for monodispersed and bidispersed suspensions, Dames et al. [59] applied an empirical model in Equation 2.12 to determine the maximum packing fraction for particle sizes; $R_{large} = 270$ nm and $R_{small} = 80$ nm:

$$\phi_m = \phi_z - \left(\phi_z - \phi_m^{mono}\right)^{\left(0.27\left(1 - \frac{D_5}{D_1}\right)\right)}, \tag{2.12}$$

where $\qquad \phi_z = 1 - \left(1 - \phi_m^{mono}\right)^z$ and $D_x = \dfrac{\sum\limits_{i=1}^{z} N_i d_i^x}{\sum\limits_{i=1}^{z} N_i d_i^{x-1}}$,

where ϕ_m^{mono} is the maximum packing fraction of a monodispersed system and it is taken as 0.63, z is the number of modal suspensions (mono, bi or multi), D_x is the x-*th* moment of PSD, i.e. D_1 is the number average of the particle diameter. For a multidispersed mixture of spherical particles, the technique given in Muralidharan and Runkana [60] and Servais et al. [61] can be used to determine ϕ_m from the minimum value of the packing fraction (P) given as:

15

$$\phi_{\mathrm{m}} = \min(P_i), \tag{2.13}$$

where P_i is the packing fraction of each class size i, calculated based on the following:

$$P_i = \sum_{j=1}^{n} \gamma_{ij}\phi_j, \tag{2.14}$$

γ_{ij} is the binary packing coefficient of classes i and j, and ϕ_j is the volume fraction of the class j. The procedures for calculating these two quantities are detailed in Muralidharan and Runkana [60] and Servais et al. [61].

All these earlier studies were done before the invention of nanofluids and, as such, mainly focused on the suspension of micrometric particles in fluid mediums. However, knowledge and ideas have been borrowed from them for recent analyses of the thermophysical properties of nanofluids. Again, some of these models were first published more than 80 years ago. Therefore, the usability of these classical models on nanofluids is a subject that should be critically analysed [62] because many factors that affect colloids in suspensions have been oversimplified in order to achieve a presentable solution. Table 2.1 includes a comprehensive list of other available classical models that were developed by various investigators [47, 49, 50, 52, 54, 63–68] and are applicable to the determination of the viscosity of solid-liquid suspensions. These models differ from one another and no single model can predict data in the entire concentration range up to the maximum concentration possible.

2.2.2   New theoretical models

Researchers have unsuccessfully tried to predict the viscosity of nanofluids using the classical models on the viscosity of suspensions. These models all predate the invention of nanofluids. Therefore, some very salient characteristics, such as nanolayer, pH, EDL, zeta potentials, temperature, capping/nanolayer, interparticle spacing and particle magnetic properties, that influence the thermal properties of suspensions were not considered. Hosseini, Moghadassi and Henneke [25] applied the principle of dimensional analysis on some of the constitutive

16

Table 2.1: Summarised list of the available classical models

Investigators	Classical models	Remarks
Einstein [39]	$\mu_{eff} = \mu_o\left(1 + 2.5\phi\right)$	This model was established on an extremely diluted suspension of rigid solid spheres and a non-interacting medium, and is for a volume fraction of $\phi \leq 0.02$. From the model, it is clear that viscosity is a linear function of volume fraction.
Taylor [42]	$\mu_{eff} = \mu_o\left\{1 + 2.5\phi\left(\dfrac{\mu' + \dfrac{2}{3}\mu}{\mu' + \mu}\right)\right\}$	This is an extension of Einstein's model [39], for liquid-containing drops of another liquid in suspension. The liquid drops have been assumed to be spherical and, for sphericity to be maintained, there must be high surface tension. Therefore, this model is only valid when the condition above is met.
Brinkman [43]	$\mu_{eff} = \mu_o\left(1 - \phi\right)^{-2.5}$	This is an extension of Einstein's model [39] and is for a volume fraction of $\phi \leq 0.04$.
Vand [47]	$\mu_{eff} = \mu_o\left(1 + 2.5\phi + 7.348\phi^2 + ...\right)$	–
Mooney [49]	$\mu_{eff} = \mu_o\exp\left(\dfrac{2.5\phi}{1 - \upsilon\phi}\right)$	This model was formulated on the premise of Einstein's model [39]. It is limited to rigid spherical particles. This is a semi-empirical model as the interaction data, υ (crowding factor), was obtained empirically. The model accounts for suspensions that contain a wide spectrum of continuous size distribution, i.e. for a monodispersed suspension of finite concentration. The crowding factor υ will be different for the particulate suspension of two different diameters, see Mooney [49].
Roscoe [50]	$\mu_{eff} = \mu_o\left(1 - 1.35\phi\right)^{-2.5}$	This model equation was developed for spheres of equal size and high concentrations. For spheres of very diverse sizes, the viscosity is to be predicted with $\mu_{eff} = \mu_o\left(1 - \phi\right)^{-2.5}$. This equation is valid for all concentrations and, as the volume concentration tends towards zero, it reduces to Einstein model [39].
Batchelor [52]	$\mu_{eff} = \mu_o\left(1 + 2.5\phi + 6.5\phi^2\right)$	The effect of interactions between particles was considered in the development of this model. Within the limits of a very low particle volume concentration, this model approaches Einstein's model [39].

Investigators	Classical models	Remarks
Krieger and Dougherty [54]	$\mu_{eff} = \mu_o \left(1 - \dfrac{\phi}{\phi_m}\right)^{-[\eta]\phi_m}$	This model covers virtually the whole spectrum of nanoparticles. The maximum concentration at which flow can occur is ϕ_m and its high shear rate value is 0.605. The intrinsic viscosity is η, with a typical value of 2.5.
Lundgren [63]	$\mu_{eff} = \mu_o \left(1 + 2.5\phi + \dfrac{25}{4}\phi^2 + f(\phi^3)\right)$	This model was proposed considering the Brownian motion of the isotropic suspension of rigid spherical particles. The resulting bulk stress on the particles was taken into account. Within the limits of a very low particle volume concentration, this model approaches Einstein's model [39].
Graham [64]	$\mu_{eff} = \mu_o \left\{1 + 2.5\phi + 4.5 \times \left[\dfrac{1}{(h_s/d_p)(2 + (h_s/d_p))(1 + (h_s/d_p)^2)}\right]\right\}$	This model approaches the model of Einstein [39] and Frankel and Acrivos [68] as the lower and upper limits of the volume fraction tends to zero and infinity, respectively. Cell-based theory was used. The diameters of the spheres were assumed to be uniform and zero inertial, Brownian motion, van der Waals force and electroviscous force were considered.
Saitô [65]	$\mu_{eff} = \mu_o \left(2.5\phi + 14.1\phi^2\right)$	–
Hatschek [66]	$\mu_{eff} = \mu_o \left(1 + 4.5\phi\right)$	This model is applicable for up to 40% solid concentration.
Thomas and Muthukumar [67]	$\mu_{eff} = \mu_o \left(1 + 2.5\phi + 4.83\phi^2 + 6.4\phi^3\right)$	–
Frankel and Acrivos [68]	$\mu_{eff} = \mu_o \dfrac{9}{8}\left[\dfrac{(\phi/\phi_m)^{\frac{1}{3}}}{1 - (\phi/\phi_m)^{\frac{1}{3}}}\right]$	This model was developed using an asymptotic technique to describe the viscosity of suspension within the concentrated limit where maximum volume fraction is obtainable. Uniform solid sphere is assumed to complement Einstein's work from the dilute to the concentrate regime.

Table 2.2: New theoretical models in summary

Investigators	New models	Remarks
Masoumi et al. [2]	$\mu_{nf} = \mu_o + \dfrac{\rho_p V_B d_p^2}{72 C \delta}$ $$\delta = \sqrt[3]{\dfrac{\pi}{6\phi}} d_p$$	This model was developed based on Brownian motion, and considers five parameters (volumetric fraction, temperature, size, particle density and base fluid properties). The models were tested with nanofluids with single- and two-base fluids.
Hosseini et al. [25]	$\mu_{nf} = \mu_o . \exp\left[m + \alpha\left(\dfrac{T}{T_0}\right) + \omega(\phi_h) + \gamma\left(\dfrac{d_p}{1+r}\right) \right]$	This model was formulated using dimensionless groups considering the viscosity of the base fluid, the hydrodynamic volume fraction of nanoparticles, the diameter of the nanoparticles, the thickness of the capping layer of the nanoparticles and temperature as π_1, π_2, π_3 and π_4, respectively. The dimensionless group is defined as: $\pi_1 = \dfrac{\mu_{nf}}{\mu_o}$, $\pi_2 = \phi_h$, $\pi_3 = \dfrac{d}{1+r}$ and $\pi_4 = \dfrac{d}{1+r}.m$ is a system property constant, while α, ω and γ are empirical constants obtainable from the experimental data.
Chen et al. [53]	$\mu_{nf} = \mu_o \left(1 - \dfrac{\phi_a}{\phi_m} \right)^{-[\eta]\phi_m}$	This model is a modification of the model of Krieger and Dougherty [54], and considers the effect of agglomeration. It therefore proposes ϕ_a as the effective volume fraction of agglomerates. The power in the model $\left(-[\eta]\phi_m \right)$ was evaluated to be -1.5125, $\phi_a = \phi(a_a / a)^{3-D}$, where D is the fractal index, and the duo of a_a and a are the radii of the agglomerates and primary particles.

factors affecting the viscosity of nanofluids to obtain a new dimensionless viscosity model. In their analysis, the relative viscosity was defined as a function of dimensionless groups, which contains the following parameters: the viscosity of the base fluid, the hydrodynamic volume fraction of nanoparticles, the nanoparticle's diameter, the thickness of the capping layer and temperature as dimensionless groups π_1, π_2, π_3 and π_4, respectively, as presented

19

in Table 2.2. The model (Equation 2.15) is the result of the combination of the dimensionless parameters:

$$\mu_{nf} = \mu_o \cdot exp\left[m + \alpha\left(\frac{T}{T_0}\right) + \omega\left(\phi_h\right) + \gamma\left(\frac{d_p}{1+r}\right)\right],$$ (2.15)

where μ_{nf} is the viscosity of the nanofluids, μ_o is the viscosity of the base fluid, ϕ_h is the hydrodynamic volume fraction of the nanoparticles, d_p is the diameter of the nanoparticles, r is the thickness of the capping layer, T_0 is a reference temperature, which is taken to be 20 ^{o}C, and T is the working temperature of the nanofluid. In this model, m is referred to as a system property constant, which is a function of the types of nanoparticles, types of base fluids and the interactions between them. Although there was no indication of how the constants α, ω and γ were derived, it is believed that they have been obtained through non-linear regression analysis. The model was tested with limited samples of Al_2O_3-water-based nanofluids, although it claimed good agreement with the experimental data tested. Further analysis of the model revealed that when the volume fraction is zero (i.e. no nanoparticle is suspended), the model does not predict the base fluid's viscosity.

Recent literature revealed that the theoretical analysis of the effective viscosity of nanofluids can be approached as either a single-phase problem or a two-phase problem. Masoumi et al. [2] analysed the dispersion of nanoparticles in a fluid medium as a two-phase problem and considered that five parameters affect the effective viscosity of nanofluids. Parameters such as nanoparticle size, temperature, nanoparticle density, nanoparticle volume fraction and base fluid physical properties were considered. Using the Brownian velocity relation presented by Prasher et al. [69] in Equation 2.16, the effective viscosity was derived as presented in Equation 2.17. A creeping flow assumption around the spherical nanoparticle was used in their derivation. A correction factor was introduced to take care of the simplification of their assumptions. The model was tested in predicting the effective viscosity of CuO-H_2O, CuO-EG, TiO_2-EG, CuO-EG/H_2O and Al_2O_3-H_2O nanofluids. According to the results presented, there was an acceptable level of agreement between the model and the experimental data used.

$$V_B = \frac{1}{d_p}\sqrt{\frac{18k_bT}{\pi\rho_p d_p}}$$ (2.16)

$$\mu_{nf} = \mu_o + \frac{\rho_p V_B d_p^2}{72 C \delta}, \tag{2.17}$$

where k_b is the Boltzmann constant, T is the temperature, ρ_p is the particle density, δ is the distance between the centres of particles, V_B is the Brownian velocity, C is the correction factor and d_p is the particle diameter. δ and the constant C were defined as:

$$\delta = \sqrt[3]{\frac{\pi}{6\phi}} d_p \tag{2.18}$$

$$C = \mu_o^{-1} \left[\left(c_1 d_p + c_2 \right) \phi + \left(c_3 d_p + c_4 \right) \right]. \tag{2.19}$$

Constants $c_1 - c_4$ are obtainable from the experimental data. It should be stated here that this is one of the very few theoretical analyses of nanofluid viscosity in the literature. However, the required procedures, as described by the authors to obtain this set of constants, will not allow for the reproducibility of these constants. Hence, C may be difficult to calculate for nanofluids that differ from those in their work. It is believed that a better presentation of these constants can be made. There is not much evidence that this model has been cited often in comparison with experimental data by other investigators since its publication.

2.2.3 Empirical models

Ward (in Graf [70]) recommended that experimental results should be expressed in the form of Equation 2.20 to allow easy comparison with theoretical models. He further noted that the intrinsic viscosity should be determined experimentally, because it is difficult to evaluate the intrinsic viscosity from the power of three and above theoretically [71]:

$$\mu_{eff} = \mu_o \left(1 + [\eta]\phi + [\eta]^2 \phi^2 + [\eta]^3 \phi^3 + [\eta]^4 \phi^4 + ... \right). \tag{2.20}$$

Cheng and Law (CL) [72] reanalysed the effective viscosity of suspensions based on Einstein's model to provide an exponential formula for the effective viscosity of nanofluids for volume fractions higher than Einstein's concentration regime. The CL model (Equation 2.21), although similar to the general model expression given by Batchelor [52] and Lundgren [63], provided the coefficient of volume fraction up to the

21

power of five. When compared with the experimental data reported by Ward (in Graf [70]), they are in close agreement.

$$\mu_{eff} = \mu_o \left(\begin{array}{l} 1 + 2.5\phi + \left(\dfrac{35}{8} + \dfrac{5}{4}\beta \right)^2 \phi^2 + \left(\dfrac{105}{16} + \dfrac{35}{8}\beta + \dfrac{5}{12}\beta^2 \right)^3 \phi^3 \\[2mm] + \left(\dfrac{1155}{128} + \dfrac{935}{96}\beta + \dfrac{235}{96}\beta^2 + \dfrac{5}{48}\beta^3 \right)^4 \phi^4 + \\[2mm] \left(\dfrac{3003}{256} + \dfrac{1125}{64}\beta + \dfrac{1465}{192}\beta^2 + \dfrac{95}{96}\beta^3 + \dfrac{1}{48}\beta^4 \right)\phi^5 + ... \end{array} \right), \tag{2.21}$$

where β is the diffusion exponent. Avsec and Oblak [31] emphasise that Ward's model, as presented in Equation 2.22, is of little importance to nanoscale viscosity (nanoviscosity) and presented a new model (Equation 2.23) with a simple twist to Ward's expression. This was derived using statistical mechanics owing to the possibility of modelling particulate interaction (nanolayer interaction effect) with statistical mechanics.

$$\mu_{eff} = \mu_o \left(1 + 2.5\phi + (2.5)^2 \phi^2 + (2.5)^3 \phi^3 + (2.5)^4 \phi^4 + ... \right) \tag{2.22}$$

$$\mu_{eff} = \mu_o \left(1 + 2.5\phi_{eff} + (2.5)^2 \phi_{eff}^2 + (2.5)^3 \phi_{eff}^3 + (2.5)^4 \phi_{eff}^4 + ... \right), \tag{2.23}$$

where $$\phi_{eff} = \phi \left(1 + \dfrac{h}{a} \right)^3, \tag{2.24}$$

where ϕ_{eff} is the effective volume fraction, h is the thickness of the nanolayer and a is the particle radius. Apart from the theoretical models presented above, most of the available models for the determination of nanofluid viscosity are correlations from very limited experimental data. These models are not hybrid because they are, in most cases, developed from experimental data with a confined volume fraction of nanoparticles, a few nanoparticle types (mostly one per model), a small spectrum of the nanoparticle size, and mostly spherical or assumed to be spherical in shape [73–78]. Through experimental studies, researchers have observed that the temperature of the studied medium, volume fraction, shear rate and size of nanoparticles affect the effective viscosity of nanofluids [79–81]. However, an exhaustive examination of the existing empirical models shows that, researchers refrained from providing the effect of temperature, shear rate and size of nanoparticles in the majority of the correlations, as they affect nanofluid viscosity in their correlations.

22

Nguyen et al. [79], after a comprehensive investigation of the dynamic viscosity of alumina-water nanofluids considering different nanoparticle volume fractions, sizes and temperatures, only provide individual correlation equations for nanofluid viscosity based on the volume fraction and temperature respectively. In fact, the models with temperature can only predict for 1 to 4% volume fraction, which was inadequate for even their experimental data. Similarly, Vakili-Nezhaad and Dorany [82] provided two empirical models for the same nanofluids (SWCNTs/lube oil) based on volume fraction and temperature. The correlations are polynomial functions of volume fraction and temperature, as given below

$$\mu_{nf} = \mu_o \left(1 + 1.59\phi - 16.36\phi^2 + 50.4\phi^3 \right), \tag{2.25}$$

$$\mu_{nf} = \mu_o \left(1048 - 30.3T + 0.2T^2 \right). \tag{2.26}$$

Equations 2.25 and 2.26 are valid for 0.01 to 0.2% volume fraction and temperatures of 25 to 100 $^\circ$C respectively. In terms of the viscosity of CuO-coconut oil, Rashin and Hemalatha [27] also proposed two separate models to predict the mass fraction and temperature dependence of their experimental data. The mass fraction model, similar to Batchelor's Equation [52], is presented alongside the temperature model in equations 2.27 and 2.28:

$$\mu_{nf} = \mu_o \left(1 + a\varphi - b\varphi^2 \right), \tag{2.27}$$

$$\mu_{nf} = ce^{-0.03T}, \tag{2.28}$$

where φ is the mass fraction of nanoparticle to base fluid, T is the temperature in Kelvin, *a, b* and *c* are parameters from regression analysis and unique to 20 nm CuO-coconut oil nanofluids at a temperature range of 35 to 55 $^\circ$C. Many other researchers present their model as a linear or polynomial function of the volume fraction without considering the effect of either temperature or particle size [83–87]. Furthermore, most researchers who considered more than one constitutive factor presented equations with unbalanced units (see equations 2.26 and 2.28).

Heyhat et al. [13] presented a volume fraction exponential correlation relating the viscosity of alumina-water nanofluid for volume fractions between 0.1 and 2%. Their correlation, presented in Equation 2.29, averaged the effect of volume fraction over the temperature range experimented (20 to 60 $^\circ$C):

23

$$\frac{\mu_{nf}}{\mu_o} = Exp\left(\frac{5.989\phi}{0.278-\phi}\right). \tag{2.29}$$

In 2012, Suganthi and Rajan [88] proposed a modified form of Einstein's equation (Equation 2.30a) by replacing the volume fraction with an agglomerate volume fraction similar to Chen et al. [53]. This was done to account for the effect of agglomeration on the viscosity of nanofluid in the volume fraction range of 0 to 1.5% and temperatures between 10 and 35 ^{o}C.

$$\mu_{nf} = \mu_o\left(1+2.5\phi_a\right), \tag{2.30a}$$

where ϕ_a is related to ϕ using Equation 2.30b:

$$\frac{\phi_a}{\phi} = \left(\frac{D_a}{d_p}\right)^{3-D}. \tag{2.30b}$$

Generally, agglomerates are of different sizes in nanofluids. Therefore, Equation 2.30b can be rewritten in a broader form:

$$\left(\frac{D_a}{d_p}\right)^{3-D} = \sum_{i}^{N}\left(\varphi_i\left(\frac{D_{ai}}{d_p}\right)^{3-D}\right), \tag{2.30c}$$

where φ_i is the mass fraction of the aggregate i, D_{ai} is the diameter of the aggregate i, N is the number of aggregates present and D is the fractal dimension. The diameter of the nanoparticle (ZnO) used by Suganthi and Rajan [88] was 35 to 40 nm. For a volume fraction higher than 1.5% (i.e. 2%), the authors proposed another model: a modified Batchelor's Equation [52], as presented in Equation 2.31, to take care of the effect of particle-particle interactions:

$$\mu_{nf} = \mu_o\left(1+2.5\phi_a+6.1\phi_a^2\right). \tag{2.31}$$

Recently, Suganthi et al. [89] proposed a temperature-based power law correlation (Equation 2.32) to relate the effect of temperature on the viscosity of ZnO-PG nanofluids. Their previous models (equations. 2.30 and 2.31) could not be applied here, probably because the trend of ZnO-PG with increasing volume fraction is directly opposite to the trend in their previous experiment on ZnO-water nanofluids [88]:

$$\mu_{nf} = A\theta^{-B}, \tag{2.32}$$

24

where θ is in ^{o}C, and *A* and *B* are empirical constants, and are different for different volume fractions. Singh et al. [90] offered a correction based on the Arrhenius functional form (Equation 2.33) to predict the temperature dependence of 170 nm SiC-water-based nanofluids at volume fractions of 1.8%, 3.7% and 7.4%:

$$\mu_{nf} = \mu_{\infty,T} \exp\left(\frac{E_a}{R_g T}\right), \tag{2.33}$$

where $\mu_{\infty,T}$ is the viscosity at "infinite temperature", E_a is the activation energy to viscous flow, R_g is the universal gas constant and *T* is the temperature in Kelvin. The viscosity at infinite temperature and the activation energy can be obtained from experimental data using the logarithmic form of the Arrhenius Equation [91]. Abareshi et al. [29] were also able to fit their experimental data at different volume fractions into the Vogel-Fulcher-Tammann (VFT) Equation [92], which took care of the temperature effect alone on nanofluid viscosity as shown below:

$$\frac{\mu_{nf}}{\mu_o}(T) = Ae^{\left(\frac{B}{T+T_0}\right)}. \tag{2.34}$$

Equation 2.34 was fitted for the two limiting volume fractions to produce two sets of the empirical constants *A, B* and T_0. The problem with generating correlation through the regression analysis of a single parameter, such as temperature, is that when large numbers of volume fractions are involved, the empirical constants become huge and untidy. This also depends on the number of constants in the proposed model. For instance, Zyla et al. [93] proposed a nine-order polynomial correlation to fit the viscosity of Y_2O_3-diethylene glycol. The variable in their correlation is the temperature of the nanofluid. The concentration studied was in five levels (5:5:25%). Therefore, according to their model in Equation 2.35, the empirical constants totalled 50.

$$\eta_r = a_0 + a_1 T + a_2 T^2 + a_3 T^3 + a_4 T^4 + a_5 T^5 + a_6 T^6 + a_7 T^7 + a_8 T^8 + a_9 T^9. \tag{2.35a}$$

In a more general form:

$$\eta_r = \sum_{i=0}^{9} a_i T^i, \tag{2.35b}$$

25

where $a_i's$ are the empirical constants and T is the temperature in ^{o}C. Kulkarni et al. [94] gave a correlation, which is one of the few empirical studies that takes care of both the temperature and volume fraction effect on the nanofluid viscosity. Another such work is that of Namburu et al. [26], in which they tried to fit their experimental data to existing equations in the literature. However, the failure of the exercise spurred a new correlation given in Equation 2.36, which considered the effects of both temperature and volume fraction.

$$Log\left(\mu_{nf}\right) = Ae^{-BT}. \tag{2.36a}$$

Equation 2.36a is an empirical model with a correlation coefficient $R^2 = 0.99$, developed for CuO-EG nanofluids with a volume concentration of CuO $\leq 6.12\%$. Constants A and B were calculated as a function of the volume fraction with the correlations below:

$$\left.\begin{array}{l} A = 1.8375\phi^2 - 29.643\phi + 165.56 \\ B = 4\times10^{-6}\phi^2 - 1\times10^{-3}\phi + 1.86\times10^{-2} \end{array}\right\}, \tag{2.36b}$$

where $R_A^2 = 0.987$ and $R_B^2 = 0.988$. The correlation of Nguyen et al. [79] performed better than most of the classical models. However, Yiamsawas et al. [95] showed that the correlations of Nguyen et al. underpredicted their alumina-EG/water experimental data, because the correlations of Nguyen et al. separately considers the volume fraction and temperature effects on the viscosity of nanofluid. Consequently, the correlation below was developed to predict the viscosity of titania-EG/water (20:80) and alumina-EG/water (20:80) with a volume fraction range of 1 to 4%. The experiments were conducted between 15 and 60 ^{o}C, and the diameters of the titanium oxide and aluminium oxide used were 21 and 120 nm, respectively.

$$\mu_{nf} = A\phi^B T^C \mu_o^E, \tag{2.37}$$

where μ_o is calculated based on this expression; $\mu_o = 2.3775 - 0.0461T + 0.0003T^2$, A, B, C and E are empirical constants obtained from regression analysis. Lately, Hemmat Esfe and Saedodin [96] offered a two-variable correlation (temperature and volume fraction) for ZnO-EG nanofluids. Their correlation in Equation 2.38 has an average deviation of 2% from the experimental data, and the stability region over which it was tested is $25 \leq T \leq 50$ ^{o}C and $0.25 \leq \phi \leq 5\%$:

$$\frac{\mu_{nf}}{\mu_o} = 0.9118e^{\left(5.49\phi - 0.00001359T^2\right)} + 0.0303ln(T). \tag{2.38}$$

26

Azmi et al. [97] offered a water-based correlation based on the combined effects of volume fraction, temperature and nanoparticle size on the effective viscosity of nanofluids. Using the data available in the literature on Al_2O_3, CuO and SiC with a particle size ranging from 20 to 170 nm and a volume fraction ≤ 4%, they proposed the following correlation:

$$\frac{\mu_{nf}}{\mu_o} = C_1 \left(1 + \frac{\phi}{100}\right)^{\alpha} \left(1 + \frac{T_{nf}}{70}\right)^{-\gamma} \left(1 + \frac{d_p}{170}\right)^{-\sigma}, \qquad (2.39)$$

where C_1 is an empirical constant dependent on the types of nanofluid, and the exponents α, γ and σ are empirical constants given as 11.3, 0.038 and 0.061 respectively. To test the performance of this model, they carried out new experiments on water-based nanofluids of Al_2O_3, ZnO and TiO_2. Generally, the model is valid for water-based nanofluids of Al_2O_3, CuO, SiC, ZnO and TiO_2 with a particle diameter between 20 and 170 nm, and a volume fraction of $\phi \leq 4\%$. Khanafer and Vafai [98] also developed a three-parameter correlation to predict the viscosity of a Al_2O_3-water nanofluid. Their correlation, shown below, is valid for a volume fraction between 1 and 9%, a temperature between 20 and 70 $^{\circ}$C, and a nanoparticle diameter between 13 and 131 nm. However, the units on both sides of the equation are very different.

$$\begin{aligned}
\mu_{nf} = -0.4491 &+ \frac{28.837}{T} + 0.574\phi - 0.1634\phi^2 + 23.053\frac{\phi^2}{T^2} + 0.0132\phi^3 \\
&- 2354.735\frac{\phi}{T^3} + 23.498\frac{\phi^2}{d_p^2} - 3.0185\frac{\phi^3}{d_p^2}
\end{aligned} \qquad (2.40)$$

The model above accurately predicted the viscosity changes with temperature of some data in the literature. Numerous studies have shown that the addition of nanoparticles to a Newtonian base fluid sometimes turns the fluid to non-Newtonian. An example of this is the recent studies of Yu et al. [99] on aluminium nitride nanofluid, Halelfadl et al. [100], and Aladag et al. [101] on alumina-water and carbon nanotube-water nanofluids. In most situations, despite the non-Newtonian nature of nanofluids, reported correlations only considered temperature and volume fraction, or considered both as input parameters.

According to Syam Sundar et al. [102], it is important to study the behaviour of nanofluids with respect to change in shear rate, therefore empirical correlations should be designed taking cognisance of this parameter. Hernández Battez et al. [81] investigated the rheology

27

of ZnO and ZrO$_2$ suspended in Newtonian polyalphaolefin (PAO 6) base fluid. At low shear rates (0-700 s^{-1}), all nanofluid samples behaved as Newtonian fluid; however, at higher shear rates (10^6 -10^7 s^{-1}), non-Newtonian shear-thinning characteristics with varying trends were observed. This suggests that the effect of shear rate is significant in the characterisation of nanofluid viscosity. Therefore, the following correlations were proposed for the two types of nanofluids (ZnO and ZrO$_2$) respectively:

$$\eta_r(cp) = 52.80 - 9.76 \times 10^{-7} \dot{\gamma} + 0.172\varphi - 0.912T + 1.02 \times 10^{-8} \dot{\gamma}T + 4.24 \times 10^{-3}T^2, \quad (2.41)$$

$$\eta_r(cp) = 53.78 - 9.25 \times 10^{-7} \dot{\gamma} + 0.202\varphi - 0.937T + 9.65 \times 10^{-9} \dot{\gamma}T + 4.39 \times 10^{-3}T^2. \quad (2.42)$$

In the equations above, $\dot{\gamma}$ is the shear rate, φ is the mass fraction and T is the temperature. The correlations were derived using the least-squares approach with $R^2 > 0.995$ in both cases. Earlier, Phuoc and Massoudi [103] noted that the addition of nanoparticles created yield stress within the Fe$_2$O$_3$-water/dispersants (polyvinylpyrrolidone, PVP and polyethylene oxide, PEO) nanofluids. They described the dependence of the yield stress on volume concentrations as $\tau_o = \psi e^{n\phi}$. Using Casson's Equation (see [103]) for flocculated suspended particles described by $\tau^{1/2} = \tau_o^{1/2} + \mu_\infty^{1/2} \dot{\gamma}^{1/2}$ to determine the suspension viscosity at an infinite shear rate for their base fluid plus dispersants, they found that the viscosity values predicted by Casson's Equation were two orders of magnitude lower than the viscosity of the base fluid. Moreover, the model does not consider the effect of particle concentration. Therefore, the following correlation was proposed to characterise the combined effects of shear rate and volume fraction on the viscosity of Fe$_2$O$_3$-water-dispersants (PVP and PEO nanofluids) nanofluid:

$$\mu_{nf} = \mu_\infty + \left(\frac{\psi e^{n\phi}}{\dot{\gamma}} \right)^{1/2} \left[\left(\frac{\psi e^{n\phi}}{\dot{\gamma}} \right)^{1/2} + 2\mu_\infty^{1/2} \right]. \quad (2.43)$$

The data used for the correlation in Equation 2.43 was taken at 25 ^{o}C, where μ_∞ is the intrinsic viscosity at an infinite shear rate, and ψ and n are empirical constants that are dependent on the intercept of the plot of $\left(\mu_{nf} \dot{\gamma} \right)^{1/2}$ against $\left(\dot{\gamma} \right)^{1/2}$ for all the volume fractions considered. A summarised description of other empirical models is given in Table 2.3.

Table 2.3: Summary of available empirical models

Empirical models	Concentration (%)	Size (nm)	Temperature (°C)	Remarks
$\mu_{nf} = \mu_o \left(1 + A \left(\dfrac{\phi}{1-\phi} \right)^n \right)$ [24]	0.33–5	43	25	Al$_2$O$_3$-water nanofluid. Based on mean free path between nanoparticles. *A* and *n* were taken as 5 200 and 2.8, respectively.
$Log\left(\mu_{nf} \right) = A e^{-BT}$ $A = 1.8375\phi^2 - 29.643\phi$ $\quad +165.56$ $R^2 = 0.9873$ $B = 4 \times 10^{-6}\phi^2 - 1 \times 10^{-3}\phi$ $\quad +1.86 \times 10^{-2}$ $R^2 = 0.988$ [26]	1–6.12	29	-35–50	CuO-EG/water (60:40) nanofluid. Newtonian nanofluid. *T* is the absolute temperature in Kelvin. *A* and *B* are empirical curve fit parameters and in this case are functions of ϕ, with $R^2 = 0.99$.
$\mu_{nf}\left(T\right) = \mu_o\left(T\right) A e^{\left(\frac{B}{T+T_0}\right)}$ [29]	0.125–0.75	25–50	30–70	α–Fe$_2$O$_3$-glycerol nanofluid. Non-Newtonian shear-thinning. Based on VFT equation. Obtained μ_{nf} at shear rate of 40 s^{-1} *A* and T_0 are fitting parameters of the shear viscosity. *B* is related to the free activation energy of the fluid (empirically obtainable).
$\mu_{nf} = \mu_o \left(1 - \dfrac{\phi}{0.5}\left(\dfrac{a_a}{a}\right)^{1.3} \right)^{-1.25}$ $In\left(\mu_{nf}\right) = A + \dfrac{1000B}{(T+C)}$ [30]	0.5–2.5	40	5–80	CuO-gear oil nanofluid. Newtonian nanofluid ($\phi = 0.5\%$). Non-Newtonian shear-thinning ($0.5 \leq \phi \leq 2.5\%$). *T* is the absolute temperature in Kelvin. Aggregate size is 200 to 360 nm. *A, B* and *C* are empirical curve fit parameters with deviation ~ 1.4%. μ_{nf} was obtained at 30 °C.
$\mu_{nf} = \mu_o \times 0.4513 e^{0.6965\phi}$ [74]	3–10	300	25	Ni-terpineol nanofluid. Dispersant concentration is 0.5 to 10% of Ni weight. R^2 = 0.9952.

Empirical models	Concentration (%)	Size (nm)	Temperature (^{o}C)	Remarks
$\mu_{nf} = \mu_o\left(1 + 10.6\phi + (10.6\phi)^2\right)$ $In(\mu_{nf}) = A + \dfrac{1000B}{(T+C)}$ [73]	0–8[a]	25	20–60	TiO$_2$-EG nanofluid. Newtonian nanofluid. Agglomerated size is 70 to 100 nm. μ_{nf} predicted the experimental data with R^2 = 0.9989. *A, B* and *C* are empirical curve fit parameters with deviation ~ 1.7%.
$\mu_{nf} = \mu_o \times 13.47 e^{35.98\phi}$ [75]	5–12	7–20	25	TiO$_2$-deionised water nanofluid. μ_{nf} predicted the experimental data with R^2 = 0.98. μ_{nf} was obtained at shear rate of 100 s^{-1}.
$\mu_{nf} = \mu_o\left(\begin{array}{c} 1 + 2.5\phi \\ + A\phi\left(\dfrac{\phi}{\phi_m - \phi}\right)^2 \end{array}\right)$ [77]	0–40			NiO/YSZ-furfuryl alcohol suspension. Empirical viscosity model for ceramic suspensions. Shear rate range is 10 to 1000 s^{-1}. *A* and ϕ_m are obtainable from experimental data.
$\mu_{nf} = A e^{(B/T + C\phi)}$ [78]	1–10	53	-35–90	Al$_2$O$_3$-EG/water (60:40) nanofluid. Non-Newtonian nanofluid shear-thinning (-35 to 0°C). Newtonian nanofluid (0 to 90 ^{o}C). *T* is the absolute temperature in Kelvin. *A*, *B* and *C* are empirical curve fit parameters with R^2 = 0.99.
$\mu_{nf} = \mu_o \times 0.904 e^{0.1483\phi}$ [79]	0.15–13	47	22–25	Al$_2$O$_3$-water nanofluid. No information on the dispersant used.

30

Empirical models	Concentration (%)	Size (nm)	Temperature (°C)	Remarks
$\mu_{nf} = \mu_o\left(1 - 0.025\phi + 0.015\phi^2\right)$ [79]	0.15–12	36	22–25	Al$_2$O$_3$-water nanofluid. No information on the dispersant used.
$\mu_{nf} = \mu_o\left(\begin{array}{c}1.475 - 0.319\phi \\ + 0.051\phi^2 + 0.009\phi^3\end{array}\right)$ [79]	0.15–12	29	22–25	CuO-water nanofluid. No information on the dispersant used.
$\mu_{nf} = \mu_o(1.125 - 0.0007T)$ $\mu_{nf} = \mu_o(2.1275 - 0.0215T + 0.0002T^2)$ [79]	1 and 4	29, 36 and 47	20–70	Al$_2$O$_3$-water and CuO-water nanofluid.
$\mu_{nf} = \mu_o\left(1 + 11\phi\right)$ [83]	0.5–2	200	–	Cu-EG nanofluid. Newtonian nanofluid.
$\mu_{nf} = \mu_o\left(\begin{array}{c}1.005 + 0.497\phi \\ -0.1149\phi^2\end{array}\right)$ [84]	0.3–0.9	60	50–90	Ag-deionised water nanofluid.
$\mu_{nf} = \mu_o\left(A + B\phi + C\phi^2\right)$ [85]	0.2–2	21	15, 25 and 35	TiO$_2$-water nanofluid. *A, B* and *C* are empirical constants for the three different temperatures.
$\mu_{nf} = \mu_o\left(1 + 8.3\phi\right)$ [87]	0–6	190	25	SiO2-ethanol nanofluid. Clearly a linear fit of the type of classical work of Einstein [39].
$\mu_{nf} = \mu_o\left(1 - \dfrac{\phi_a(d_p)}{\phi_m}\right)^{-2}$ $\phi_a(d_p) = \left(\dfrac{D_a}{d_p}\right)^{1.2}\phi$ [87]	0–7	35 and 94	25	SiO$_2$-ethanol nanofluid. Based on Krieger and Dougherty's model [54] and fitted for the particle sizes, with D_a as the aggregated diameter (195 and 352 nm) corresponding to the nanoparticle diameters. ϕ_m is the crowding factor [104].
$In\left(\mu_{nf}\right) = A\left(\dfrac{1}{T}\right) - B$ [94]	5–15	29	5–50	CuO-water nanofluid. Non-Newtonian pseudoplastic and shear-thinning behaviour. T is the absolute temperature in Kelvin. *A* and *B* are empirical constants and depend on the particle volume fraction.

Empirical models	Concentration (%)	Size (nm)	Temperature (^{o}C)	Remarks
$\mu_{nf} = \mu_o \left(1 + \dfrac{\phi}{12.5}\right)^{6.356}$ [102]	0–2	13	20– 60	Fe_3O_4-water nanofluid. Newtonian nanofluids.
$\mu_{nf} = \mu_\infty + \left(\dfrac{\psi e^{n\phi}}{\dot\gamma}\right)^{\frac{1}{2}} \times$ $\left[\left(\dfrac{\psi e^{n\phi}}{\dot\gamma}\right)^{\frac{1}{2}} + 2\mu_\infty^{\frac{1}{2}}\right]$ [103]	0–4	20–40	25	Fe_2O_3-deionised water nanofluid. Considered both shear rate and volume fraction. Shear rates are 26.4, 79.2, 132 and 211 s^{-1}. Non-Newtonian shear-thinning at $\phi \geq 2$ %. Dispersant.
$\mu_{nf} = \mu_o \left(\dfrac{1}{1 - 34.87(d_p/d_f)^{-0.3}\phi^{1.03}}\right)$ $d_f = 0.1\left(\dfrac{6M}{N\pi\rho_f}\right)^{1/3}$ [105]	0.01–7.1	25–200	20–50	Sourced data from the literature. Nanofluids consisting of Al_2O_3, TiO_2, SiO_2 and Cu nanoparticles. d is the diameter. M is the molar mass of the base fluid. N is Avogadro's number.
$\mu_{nf} = 0.935\mu_0 \left(1 + \dfrac{T_{nf}}{70}\right)^{0.5602} \times \left(1 + \dfrac{d_p}{80}\right)^{-0.05915}$ $\times\left(1 + \dfrac{\phi}{100}\right)^{10.51}$ [106]	0.01–5	13–100	20–70	Al_2O_3-water nanofluid. Regression model based on experimental data from the literature. Deviations of -10% to +18%.
$\mu_{nf} = \mu_o \left(1 - \dfrac{\phi}{\Phi}\right)^{-2}$ [107]	0–6.2	–	–	Modelled for polymer melts for different inorganic fillers. Based on Maron-Pierce's Equation $\eta_r = \left(1 - \phi/\Phi\right)^{-2}$; Φ is a constant for packing geometry. Φ is related to the packing geometry of various inorganic materials that fill the polymer melts; $\Phi = 0.54 - 0.0125\bar{\bar{p}}$, where $\bar{\bar{p}}$ is the average aspect ratio. The equation is only applicable above the shear stress of 10^4 dyne/cm^2.

2.3   EXPERIMENTAL STUDIES

There are numerous experimental studies on the thermal properties and behaviour of nanofluids. These studies mainly cut across the determination of nanofluid thermal conductivity [108–110], convective heat transfer [111, 112], performance in heat pipes and microchannels [113–115], the effectiveness of nanofluids in solar heaters and other solar devices [116–119] and the behaviour of nanofluids in car engine radiators [62, 120]. A few of these studies focused on the viscosity of nanofluids and, recently, there has been some new development in the experimental field, as researchers are now investigating the thermal diffusivity and electrical conductivity of nanofluids and how these properties affect thermal properties [37, 121].

2.3.1   Methods of preparation of nanoparticles and nanofluids

The methods of preparation of nanofluids can be divided into two categories: the preparation of dry nanostructures and the subsequent dispersion of the nanostructures in the base fluids, and an infused method of preparing nanostructures in their intended base fluid medium. The first approach is called the two-step method, in which case, nanostructure preparation is the first step in the development of nanofluids. Nanostructures of sizes ranging from 1 to 100 nm are desired for nanofluids [9, 122] and a wide range of nanostructures exist today, ranging from nanowires to nanorods, nanofibres, nanocylinders, nanograins and nanoparticles [91, 123, 124]. These nanomaterials can either be produced from the smallest unit of matter (known as the bottom-up approach) or fractured down from bigger lumps to nanosized materials (known as the top-down approach) [125–127].

The most common methods for the synthesis of nanostructures are broadly classified into physical and chemical methods. Some of the physical methods are pulsed laser ablation [128–130], laser deposition and matrix-assisted pulsed laser evaporation (MAPLE) [122, 131], and ball milling [125–127], while the chemical methods are chemical precipitation [132–134], sonoelectrochemical synthesis [135–140], spray pyrolysis [141, 142], chemical vapour deposition [143–145] and thermal decomposition [146]. Details on other methods in these categories can be found in past publications [147–149]. After the synthesis of the desired nanostructures, the nanostructures are dispersed in any

33

intended base-fluid medium using assisted dispersion with a magnetic stirrer, high shear homogeniser, high-pressure homogeniser and/or ultrasonication (probes and baths) [150, 151]. The production of nanofluids by this first method is very popular and by far the most economical method. It is being produced on an industrial scale. However, there is a problem with the stability of nanofluids prepared using this method. The second method is called the single-step method because the process of making the nanostructures is infused into the method of preparing the nanofluid without any intermediate product, i.e. no dry nanomaterials are produced; rather, the nanofluid is produced in the form of a continuous process [152, 153]. Nanofluids produced with this method are more stable, but this process is very costly, which is one of the reasons why it is yet to reach commercialisation.

Worthy of mention is the biological method of synthesising nanoparticles. Using different biological substances, such as algae [154], fungi [155, 156], plant extracts [157–161], bacteria [162–164], yeast [165–168] and marine sponge [169], two nanoparticles, silver (Ag) and gold (Au), have been successfully synthesised. Thakkar et al. [170] established the need for eco-friendly nanoparticle synthesis vis-à-vis energy saving, poisonous gas reduction and the declining usage of toxic compounds. Therefore, different microorganisms for the production of non-toxic nanoparticles were highlighted. Similarly, Elumalai et al. [157] and Krishnaraj et al. [158] synthesised Ag nanoparticles from different leaf extracts to study their antibacterial activities. Table 2.4 gives an overview of the classifications and different methods that have been used in the synthesis of nanostructures.

2.3.2 Nanofluid stability

The relevance of nanofluids cuts across all phases of science and technology in human development, and this is what makes it one of the fastest-growing research topics in the world today. To unlock the full potential of the novel fluid, many challenges have been faced, most of which have been met to a reasonable degree. However, the problem of the stability of nanofluids persists. A stable nanofluid is when nanoparticles are continually in their Brownian motions without cohesion and are devoid of flocculation, agglomeration and ultimately sedimentation. It may be said that, at a very low nanoparticle volume concentration, stability does not pose a big threat in the face of the present preparation

34

methods of nanofluids. However, in the case of increasing volume concentration as desired by many applications, instability becomes very pronounced vis-à-vis flocculation, agglomeration, settling down and ultimately phase separation. When first prepared with any combination of the different dispersion methods available [150] (especially the two-step method), it displays good dispersion, mostly because of the high shear, pressure or energy impacted into the homogenisation process. However, with time, agglomeration formation occurs [171], as shown in Figure 2.4.

Table 2.4: Overview of classification of preparation methods of nanoparticles

Classification	Methods	Nanostructures	Reference
Physical	Ball milling	γ-Fe_2O_3	[125]
		Fe_2S_4, Fe_2S	[126]
		Si	[127]
	Pulsed laser ablation	Fe_2O_4 and Fe_3C	[128]
		Pd	[129]
		Au	[130]
	Laser deposition and MAPLE	TiO	[122, 131]
Chemical	Chemical precipitation	CdS	[132]
		$CaCo_3$, $Al(OH)_3$,	[133]
		$SrCO_{3,}$ NiCuZn	[134]
	Sonoelectrochemical synthesis	Ag	[135]
		CdSe	[136]
		PbSe	[137]
		Pt	[138]
		Tungsten	[139]
	Spray pyrolysis	SiO_2	[141]
		TiO	[142]
	Chemical vapour deposition	SWCNT	[143, 144]
		SiO_2	[145]
	Thermal decomposition	Tungsten	[146]
Biological	Algae	Au	[154]
	Fungi	Ag	[155, 156]
	Plant and plant extracts	Ag	[157–159]
		Au	[159–161]
	Bacteria	Ag	[162]
		Au	[163, 164]
	Yeast	Au	[165–168]
	Marine sponge	Ag	[169]
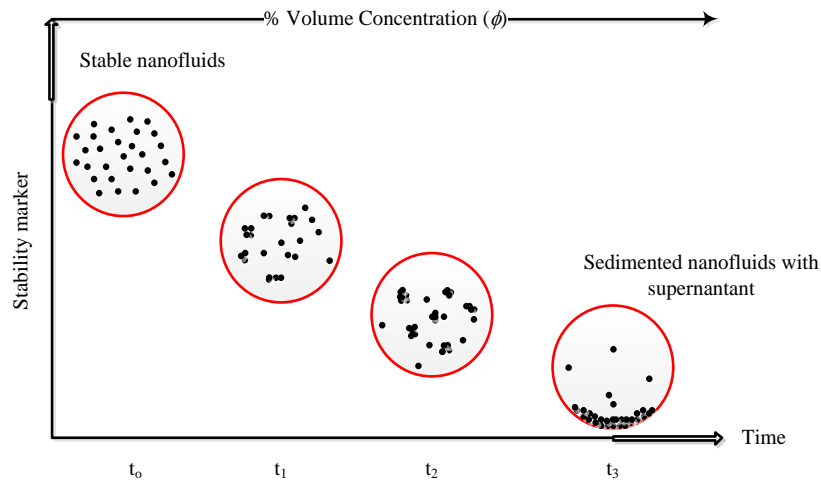
Figure 2.4: Instability sequence in nanofluids. At time t_o, the nanofluid is stable just after preparation by ultrasonication or high-pressure homogenisation (HPH), at t_1, flocculation sets in and degenerates to agglomeration at t_2, which finally sediments at time t_3. As ϕ also increases, the tendency of the instability sequence is high.

The time difference between t_o when a homogeneous suspension is formed and t_3 when full-phase separation occurs is a function of compositions, i.e. particle volume concentration, nanoparticle type, type and concentration of surfactant, shape of particle, type of system (stationary or dynamic), method of preparation, temperature of the suspension and density difference between the nanoparticles and base fluid. For example, exploring three different dispersion methods, namely ultrasonication, ball milling and HPH, Fedele et al. [150] prepared deionised water-based nanofluids of CuO, TiO_2 and single-wall carbon nanohorns (SWCNHs) to study their stability.

With sedimentation rate as a stability marker, and applying static and shake dynamics (i.e. samples were prepared and divided into two, first sets were kept stationary, while the second sets were shaken before measurement), they used dynamic light scattering to monitor the variation in size of dispersed nanoparticles and SWCNHs over a period of 30 days. From their findings, CuO and TiO_2 dispersed using ball milling sedimented four days after preparation, whereas the same nanoparticles dispersed through ultrasonication lasted more than 15 days in suspension. The addition of surfactant to the unstable TiO_2-water nanofluids at varying weight percentages made the nanofluid stable for more than 30 days without any sign of agglomeration or sedimentation.

36

Zamzamia et al. [151] formulated nanofluids of Al_2O_3 and CuO in EG that were stable for 90 days and tested both in double-pipe and plate heat exchangers. Employing wet ball milling, Samal et al. [172] also produced and dispersed nanoparticles of an Al-Cu alloy in deionised water to study its stability at different pH levels. By measuring the zeta potential of the nanofluid as the pH is varied, their results showed that pH is a major driver of the nanofluid's stability, with or without the addition of surface-active agents (surfactant). This is because pH modification has a direct link with the electrostatic condition of the interface between the suspended particles and the fluid medium.

In another investigation, Wang et al. [173] systematically prepared optimised Al_2O_3-water and Cu-water nanofluids using the zeta potential, nanoparticle size and absorbency of the nanofluids as stability indicators. They varied the pH level and surfactant concentration (in this case, sodium dodecylbenzene sulfonate (SDS)) to synthesise a stable nanofluid, indicated by zeta potential and absorbance values. However, at the optimised pH level and surfactant concentration that depicted stable nanofluid, the measured size of nanoparticles in suspension was more than the starting materials by a factor of 7.4 for Al_2O_3 and 7.5 for Cu. It should be noted that the sizes were the minimum obtained when compared to sizes reported at other pH levels and surfactant concentrations. Because the measured size was bigger than the size of the starting materials, one of two things could be inferred here: that the reported starting materials were not actually the size reported, or that there were agglomerations within the nanofluids prepared as the time given for sonication might not have been enough (in this case one hour).

In stability characterisation, the key marker of stability from the available systematic experimental investigations [150–152, 172, 173] can be narrowed down to the following: visual inspection for sedimentation, sedimentation rate measurement, turbidity, zeta potential, UV-visible light absorbance of nanofluids, transmittance and size measurement against time after preparation (for detecting agglomeration and/or a reduction in nanoparticle population). Some researchers have also deduced that rheological characteristics, i.e. Newtonian, signify stable nanofluids, and non-Newtonian characteristics signify otherwise [174]. All these characterisation procedures have their deficiencies, which still prevent the reporting of either qualitative results or a report that represents the actual situation that is encountered in real-life applications. For instance,

37

visual observation of sedimentation is relative to the eyes and, as such, lacks substance in reporting the stability of nanofluids. However, it can be used as a secondary means of characterisation (i.e. to back up a quantitative report on stability). The available quantitative approaches, such as turbidity measurement, zeta potential, UV-visible analysis and nanoparticle size measurement, all have their limitations. Either the volume concentration must be in the dilute regime (usually ≤ 1%), which is not always the case in real-life applications, or the opacity of the nanofluids is disrupting the proper measurement, in which case it must be diluted as well. The idea of a diluted concentration of samples in order to measure any of these stability markers may not represent what is obtainable in the industry where volume concentration of up to 10% might be required for application in heat exchangers and other engineering systems. Moreover, some nanoparticles, such as Fe_2O_3, Fe_3O_4 Cu and CuO, are opaque and a great deal of dilution is required before the abovementioned techniques can be applied to them.

2.3.3 Experimental set-ups

Measuring the viscosity of nanofluids seemingly looks very simple when the scale and sensitivity of equipment requirement are compared with other aspects of the thermal properties of nanofluids. Nevertheless, it is important to state that a good knowledge of the design of the experiment and the control of the variables to stability is required to be able to measure and report accurate data. At least five types of viscometers with different principles of operation have been used in viscosity measurements. These are the capillary tube viscometer [28, 87], vibro-viscometer [9, 175], rotating viscometer (which includes cone-plate, flat plate and concentric geometries) [24, 29, 30, 53, 176], falling ball/falling piston viscometer [79] and cup-type viscometer.

Chen et al. [53] formulated an EG-based TiO_2 nanofluid from dry nanoparticles using the two-step method and in the absence of dispersant. After sonication of the nanofluid samples for 20 hours each, samples were subjected to rheological tests using a Bohlin CVO rheometer that works on the principle of controlled shear stress. Al_2O_3-EG/water nanofluids were prepared and sonicated in the presence of oleic acid as the surfactant for three hours. The suspension was further agitated magnetically for one hour to obtain a uniform homogenisation, after which rheological tests were performed between the temperatures of 20 and 100 $^{\circ}$C using the Brookfield programmable viscometer (model:

38

LVDV-II-Pro), which works by controlling the spindle shearing rate [62]. Chandrasekar et al. [24] used a similar set-up to measure the viscosity of Al_2O_3-water without a dispersant and sonicated for a period of six hours. In a different set-up, Lee et al. [175] used a sine-wave vibro-viscometer operating on a constant resonance frequency to determine the viscosity of aqueous SiC nanofluids.

2.3.4 Parameters involved in the effective viscosity of nanofluids

2.3.4.1 *Temperature*

The reduction in the viscosity of conventional heat transfer fluids, such as water, EG, PG, PAO, engine oil and grease, is an established phenomenon. The rate at which this occurs is commensurate with the intrinsic properties of the fluid (mainly the intermolecular bond strength) [175]. Nanofluids, which are thought of as a better replacement for these conventional fluids, have hardly been in use for two decades and have drawn the attention of many in the industry, research centres and academia. In order to understand and maximise the potential of these new-generation heat transfer fluids, a number of investigations into their behaviours at different elevated temperatures have been carried out. The heating of fluids generally supplies the molecules of the fluid with higher energy. This increase in energy contributes to increased random motion and a weakening of the intermolecular forces holding the fluid molecules. This phenomena results in a reduced resistance of the fluid to shearing force, and by implication, a reduction in viscosity is experienced.

It is important to note that the behaviour of the viscosity of nanofluids to change in temperature does not differ in any way from the behaviour of the conventional fluid, as stated above. Kumaresan and Velraj [177] presented the relationship between temperature and the viscosity of MWCNT-water/EG-based nanofluid at 0.15, 0.30 and 0.45% MWCNT volume fractions. An increase in the viscosity of the nanofluid at temperatures below 25 ^{o}C was initially observed. However, a further increase in temperature showed a corresponding reduction in the viscosity of their nanofluid samples.

It may be concluded that the addition of surfactants in the experiment carried out by Kumaresan and Velraj [177] is probably responsible for the initial behaviour of the nanofluid. In another recent report by Aladag et al. [101], a carbon nanotube (CNT)-

water-based nanofluid was investigated for its rheological properties at low temperatures (2 to 10 ^{o}C). The characteristic of the measured viscosity with respect to the temperature increase was not different from the behaviour of conventional heat transfer fluid as widely reported in literature. Sahoo et al. [78] also considered Al_2O_3-EG/water nanofluid for its rheological characteristics. They found that it exhibited non-Newtonian behaviour at a very low temperature. This behaviour specifically matched the characteristics of a Bingham plastic and it was more pronounced as the concentration of the nanoparticles increased.

Nevertheless, as temperature increased across the volume fractions investigated, the viscosity of the nanofluid decreased exponentially. Similar exponential dependence of viscosity to temperature was observed by Syam Sundar et al. [178] when they investigated the viscosity of nanofluids synthesised from magnetic Fe_3O_2 and EG-water binary mixtures. The temperature of their investigation started from 0 to 50 ^{o}C, with a maximum volume fraction of 1%. Varying the percentage weight composition of the EG-water mixture (60:40, 40:60 and 20:80) did not have any impact on the viscosity-temperature trends of the nanofluids. In fact, if the base fluid involved is the highly viscous type, such as glycerol, the addition of nanoparticles will not impair the established relationship between the viscosities of the nanofluids and temperature, as reported by Abareshi et al. [29].

2.3.4.2 *Volume fraction*

Volumetric concentration is the amount of nanoparticles dispersed in the base fluid, usually less than 10% of the base fluid's volume. Adequate research efforts have gone into discovering the effects of the volume fraction of nanoparticles on the thermophysical behaviour of nanofluids.

Most investigations reported so far show that an increase in the volume fraction of nanoparticles increases the viscosity of nanofluids. For example, Chevalier et al. [87] studied the rheological behaviours of SiO_2-ethanol nanofluids in microchannels and observed a constant Newtonian behaviour of the nanofluid over the range of volume fractions studied (1.1 to 7%) and shear rate values of 5×10^3-5×10^4 s^{-1}. They also found the effective viscosity relative to volume fraction increase, i.e. the viscosity increased as the volume fraction was increased. Corcione [105] analysed different experimental data from

40

the diverse literature for possible parameters that affect the viscosity of nanofluids. His observation centred on the significant increase in the viscosity as the volume fraction increases. Phuoc and Massoudi [103] experimentally observed that for Fe_2O_3-deionised water, the Fe_2O_3 nanoparticle volume concentration is a critical parameter that influences the viscosity of the nanofluid. Across the shear rate range (13.2 to 264 s^{-1}) tested at room temperature, there was a significant viscosity increase for 1 to 4% volume fraction investigated.

Likewise, the viscosity of Al_2O_3-PG at different volume fractions was experimentally investigated by Prasher et al. [104]. Their experimental data was comparable with data from Das et al. [179] and Wang et al. [180], showing the strong dependence of viscosity enhancement on volume concentration. It was further reported that, at a volume fraction of less than 4% investigated, the Al_2O_3-PG nanofluid behaviour was Newtonian and viscosity increased with an increase in volume fraction. Some of the most recent studies also corroborate this finding [13, 181, 182], except for a more recent experimental work by Suganthi et al. [89] on the viscosity of ZnO-PG nanofluid.

Contrary to most publications, the authors discovered that the addition of ZnO nanoparticles to PG up to 2% of volume fraction reduced the viscosity below the viscosity of the base fluid (PG). They offered an explanation in line with the bonding characteristics created between the ZnO nanoparticles and the PG molecules. The hydrogen-bonding network that existed between the PG molecules was weakened by the introduction of ZnO nanoparticles, which translates to viscosity reduction. The effect is similar to the influence of increased temperature on the intermolecular bonding of nanofluids.

Generally, the observed increase in viscosity with the volume fraction of nanoparticles could be explained in view of the fact that an increase in the volume of particles dispersed in the base fluid will result in a pronounced drag effect on individual particles due to Brownian motion. Therefore, the overall drag effect present in the medium will be increased, which, in turn, will lead to increased dissipation of energy. The consequence of this is the observed rise in the nanofluid viscosity.

Furthermore, it can be explained by exploring the particle surface charge mechanism in relation to the suspending medium. When charged nanoparticles are dispersed into a polar base fluid for instance, the attraction of counterion onto the nanoparticle surface occurs and this process creates the formation of EDL. An increase in nanoparticle concentration will reduce the interparticle distance and, by extension, the distance between the EDLs. Therefore, the force of interaction between the EDLs, known as electroviscous force, introduces an additional increase in viscosity [124]. Other forces, such as solvation, hydration, hydrophilic and hydrophobic forces, become very important, because they influence the rheology of nanofluids when the interparticle distance is reduced due to an increase in volume fraction [183].

Particle agglomeration has also been argued to be one of the causes of increased nanofluid viscosity. According to Chen et al. [184], a well-dispersed nanofluid suspension shows lower viscosity compared with the corresponding agglomerated suspension. Increased volume concentration beyond the dilute regime heightens the tendency of agglomeration in nanofluid systems, especially when the van der Waals force of attraction is significant. When agglomeration occurs, it forms a porous particle with the liquid of the suspending medium filling the interstices. This immobile additional liquid in the interstices causes an increase in the effective volume fraction, which leads to a viscosity increase [124].

2.3.4.3 *Shear rate*

The control of the flow property of suspensions is very important in many industrial applications, such as in the manufacture of paint, crude oil drilling, crude oil and petroleum product transportation, as well as in food and consumer products. Rheological studies of these products give insights into the type of control that needs to be applied for efficient product transportation and delivery. For instance, in the petroleum industry where hydrate formation in crude oil transportation creates a flow problem or sometimes a total blockage of the flow path [185], knowledge of the behaviour of hydrate slurry to different shear stress/shear rates among other influencing parameters will make the delivery more efficient and less expensive [186].

The rheology of numerous nanofluids containing different nanoparticles, including carbon nanotubes, has been studied over the past years [73, 76, 187]. Different rheological

42

characteristics, ranging from Newtonian to non-Newtonian shear-thinning, shear thickening, and thixotropic [73, 188], have been reported. In 2003, Tseng and Lin [75] investigated the rheology and structure of TiO_2-water nanofluid and found that at the investigated volume fraction (5 to 12%), the nanofluid exhibited non-Newtonian viscoplastic fluid behaviour as presented in Figure 2.5 (a). As nanoparticles are added to the Newtonian base fluid up to 5%, an initial yield stress was needed to be exceeded before flow could be achieved. This feature puts the nanofluids in the viscoplastic non-Newtonian regime. When flow occurs, an increase in the shearing rate from 0 to 1000 s^{-1} clearly shows shear-thinning structures, except at 5% and a shear rate ≥ 700 s^{-1} (Figure 2.5 (b)).

During this shearing process, agglomerate structures formed in the nanofluid are broken down until they form an ordered arrangement without agglomeration within the limits of high shear rates [75]. To support this point, similar trends and explanations have been offered in a more recent investigation by Yang et al. [189], who investigated the rheology of diamond and Al_2O_3 nanofluids. Two Newtonian base fluids were employed: silicone oil (Syltherm 800) and deionised water. From their findings, the addition of as low as 0.35 and 0.24% of diamond and Al_2O_3 nanoparticles respectively and the omission of stabiliser turns the fluid to non-Newtonian with shear-thinning characteristics. Interestingly, in the stabilised Al_2O_3-deionised water nanofluids sample at 1.28% volume fraction, the nanofluid behaved as a Newtonian fluid, while the non-stabilised counterpart clearly showed a shear-thinning phenomenon without thixotropy.

As stated earlier, the Newtonian characteristic of the stabilised sample was due to the ordered structure of the nanoparticles in suspension (i.e. devoid of agglomeration), while in the non-stabilised sample, there was agglomeration due to dominance of the van der Waals force of attraction, and at low shear rate, it showed high resistance to flow. As the shear rate increased, the agglomerates were broken down and the immobile liquids within the interstices of the porous agglomerates were released, which further reduced the viscosity alongside the ordered structure that was created at a high shearing rate.
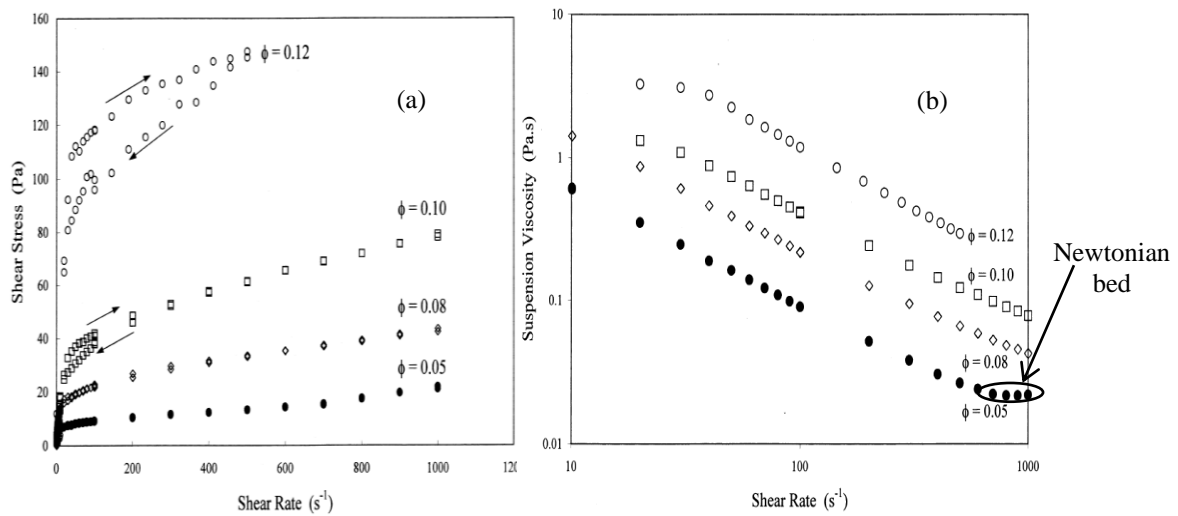
Figure 2.5: Viscosity of TiO$_2$-water nanofluid at different particle volume fractions: (a) the shear stress (τ)-shear rate ($\dot{\gamma}$) curve; and (b) the effective viscosity (μ_{nf})-shear rate ($\dot{\gamma}$) curve [75].

Aladag et al. [101] recently showed that shearing time also influenced the internal microstructure of nanofluids. Investigation on CNT- and Al$_2$O$_3$-water-based nanofluids at three different shearing times and shear rates up to ~ 4000 s^{-1} showed that stabilised CNT and Al$_2$O$_3$ in water responded with shear-thinning thixotropic and shear-thickening thixotropic phenomena respectively. During the ramp-up shear rate (low-high), deagglomeration and/or realignment of agglomerated nanoparticles occurred, which leads to the shear-thinning behaviour. The corresponding shear stress to the ramp-down shear rate (high-low) was lower, which signifies the thixotropic characteristics of the nanofluids, as depicted in Figure 2.6 (a). But in the Al$_2$O$_3$ samples, the characteristic was shear thickening with thixotropic phenomena, as shown in Figure 2.6 (b).

Based on the shearing time experiments, it was clear from Figure 2.6 (b) that when the shearing time was relaxed, sufficient time was provided to rebuild the particle structure, which gave rise to the increased ramp-down shear stress shown for samples sheared for 180 and 240 seconds respectively. Another nanofluid that showed shear thickening behaviour is the dispersion of an Al$_2$O$_3$ in R141b refrigerant up to 0.15% volume fraction [188].

2.3.4.4 *Size of nanoparticles*

A size of 1 to 100 nm particles is desired for nanofluid suspensions [190]. However, particles larger than 100 nm have also been used for the nanofluid production [74, 191].

44

Nguyen et al. [192] investigated the effect of particle size (36 and 47 nm) on the viscosity of Al_2O_3-water nanofluids, and reported that the viscosity of both particles were similar at a volume fraction below 4%. However, at a higher volume fraction, the viscosity was clearly higher in 47 nm. He et al. [193] also observed that a bigger agglomerated size of TiO_2 had higher viscosity compared with a smaller agglomerated size. Contrary reports have shown that smaller particle size led to an increase in viscosity [87, 194–196]. The results from these reports appear to be reasonable given the following explanation.
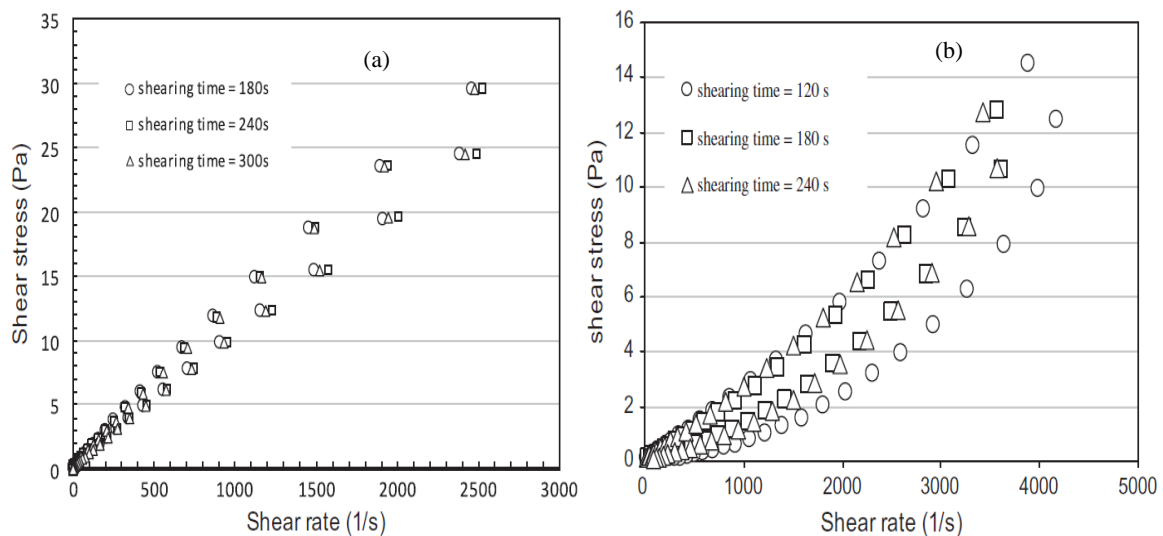
Figure 2.6: Plots of shear stress versus shear rates: (a) the effect of shearing time on the water-based nanofluid of CNTs at 5 ^{o}C, showing shear-thinning thixotropic phenomena; (b) the effect of shearing time on the water-based nanofluid of Al_2O_3 at 5 ^{o}C, showing shear-thickening thixotropic phenomena [101].

When nanoparticles are dispersed in a fluid medium, two major interactions are possible: particle-fluid interaction and particle-particle interaction. These interactions have been termed first and second electroviscous effects respectively [128]. Another prevalent interaction is the van der Waals force of attraction between particles. The electroviscous effect that is present in the nanofluid medium determines the agglomeration and hence the degree of Brownian motion of the particles. For example, if the particle concentration is fixed, a reduced nanoparticle size translates into an increased overall surface area of solid-liquid interaction and solid-solid interaction, i.e. there will be an increase in the electroviscous effect present in the nanofluid, which gives rise to an increase in viscosity. Similarly, if the overall surface area of solid-liquid interface is reduced, the electroviscous

45

effect will be reduced. Thus, a reduction in viscosity had been experimentally observed (Figure 2.7) due to the increased size of nanoparticles [87, 124, 194–198]. A bigger particle size that gives a higher viscosity could be the result of particle agglomeration, as one of the reports clearly stated [193]. Besides, agglomerates trap an immobile fluid in the interstices of the loosely bonded particles, which leads to increased viscosity.
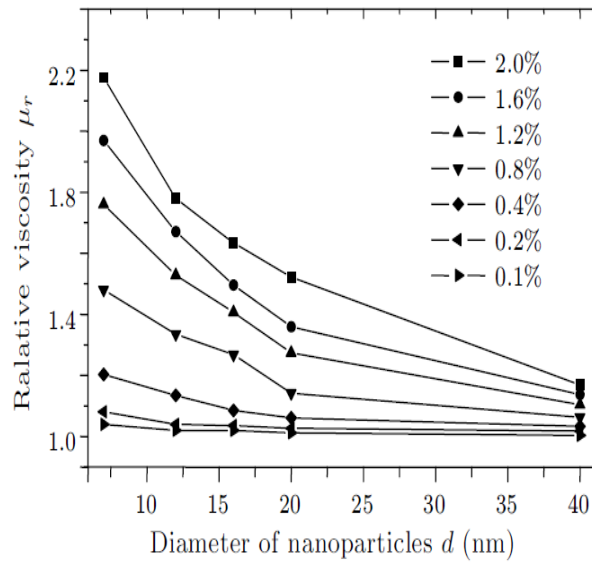
Figure 2.7: The effect of nanoparticle size on the relative viscosity of SiO$_2$-deionised water nanofluid [198].

In Equation 2.1, the intrinsic viscosity [η] was provided as 2.5 for uncharged hard spherical particles. However, due to the different processes of nanoparticle preparation [128, 148], the most correct opinion is that nanoparticles always carry charges. In the absence or reduced strength of electroviscous effect, there will be pH domination of the viscosity evolution in the nanofluid, which may further the enhancement of cluster formation, especially when the pH level of the nanofluid is close to IEP.

The shape of agglomerates determines the intrinsic viscosity and it has been shown to be more than 2.5 when the agglomerate is not spherical [199]. Anoop et al. [124] proposed that the intrinsic viscosity is not a shape function, but rather an electroviscous effect and agglomeration function. Equation 2.44 was derived for the electroviscous intrinsic viscosity, and Equation 2.45 for the agglomeration intrinsic viscosity:

$$[\eta]_{EV} = [\eta](1 + p), \tag{2.44}$$

$$[\eta]_a = [\eta] \times f_a, \tag{2.45}$$

where p is the electroviscous coefficient and f_a is the agglomeration factor, which is taken to be 2, because the agglomerated nanoparticles doubled the starting size of the nanoparticles.

2.3.4.5 *Shape of nanoparticles*

Virtually all reported studies on the thermophysical properties of nanofluids either assumed or worked on spherical nanoparticles, except for those that worked with CNTs and a few other studies on different nanoparticles [91, 200]. Shape factor, which is a measure of the total surface area of particles, is related to the degree of solid-liquid interactions at the interface. Timofeeva et al. [91] note that, as the sphericity of particles reduces, a corresponding increase in shape factor occurs. Consequently, a larger surface area is presented for active solid-liquid interactions. The same authors presented a correlation to describe the viscosity of alumina-EG/water nanofluid with varying shapes.

Although the proposed equation (Equation 2.46) is more of a replica of Batchelor's Equation (Equation 2.5) [52], the authors clarified that the coefficients A_1 and A_2 were higher than that presented in Batchelor's model, even for spherical and non-reacting particles. These coefficients also varied with particle shape.

$$\mu_{nf} = \mu_o \left(1 + A_1 + A_2^2\right). \tag{2.46}$$

The variation in viscosity with respect to the shape of the nanoparticles, as presented in Timofeeva et al. [91], is the only data available with regard to the different shapes of nanoparticles in the same experimental set-up and conditions. Although, some investigations on suspensions of shapes other than spheres had been carried out [200–202], they only considered rod-like shapes. The increase in the shape factor of particles has been thought to be one of the causes of an increase in nanofluid viscosity. However, the viscosity evolution, as presented by Timofeeva et al. [91], was anomalous and lacked a distinctive relationship with the shape or shape factor of the nanoparticles.

Another factor that could cause a difference in the viscosity data of different nanoparticle shapes could lie in the aerodynamics of these shapes in the suspended medium. A

47

streamlined shape poses less resistance to flow compared with an irregular shape or sharp-edged shapes that resist flow because it is difficult for such shapes to fall in ordered streamlines and, as such, they dissipate more energy, which results in the increased viscosity of the suspension. In view of the above, it is imperative that more research is conducted on this topic.

2.3.4.6   *Base fluid properties*

The nanofluid viscosity increase is a multifactorial issue. Base fluid properties, such as density, thermal conductivity, viscosity and pH level, are definitely part of the factors that affect the overall properties of nanofluids, such as stability, thermal conductivity and viscosity. As the name "base fluid" implies, it is the basis on which all enhancements are built. Many conventional heat transfer fluids and different nanoparticles have been experimented with in different mixing ratios. However, research claiming that base fluid properties influence viscosity enhancement has not presented any exhaustive experimental data probing the extent to which the intrinsic properties of base fluids influence the viscosity enhancement of nanofluids.

Nonetheless, Syam Sundar et al. [178] investigated the viscosity of nanofluids that were synthesised from magnetic Fe_3O_2 and three different EG-water mixtures as the base fluids, namely EG:water – 60:40, 40:60 and 20:80. An enhancement of approximately 300% was recorded for the sample prepared from the 60:40 ratio, which was higher than that of other nanofluids. Wang et al. [180] measured the viscosity of Al_2O_3 dispersed in water and EG. In their experiment, the viscosity of Al_2O_3-water increased by 20 to 30% at 3% volume fraction, and it depended on the dispersion method, while for the Al_2O_3-EG sample at 3.5%, the viscosity increase was approximately 40%. Recently, Yu et al. [99] dispersed aluminium nitride into EG and PG as base fluids and studied their thermal conductivity and rheology. The viscosity study shows that the enhancement in EG is approximately 15% higher than the enhancement in PG.This research supports the implication of the base fluid in nanofluid viscosity. However, as conventional heat transfer fluids are the bases for nanofluid synthesis, the same nanoparticles (i.e. particles from the same metal or oxide of metal, equal volume fraction and equal average size) have exhibited different behaviours in the same base fluid medium. Therefore, it is

48

expedient to investigate this topic more deeply to clarify the influence of base fluid on the enhancement of nanofluid viscosity.

2.4 MODELLING NANOFLUID PROPERTIES WITH ARTIFICIAL INTELLIGENCE

Employing the recent high computational power and a knowledge of algorithms, a new window of opportunity has been opened to the nanofluid research community on the prediction models for thermal properties of nanofluids. Rudyak and Krasnolutskii [203] recently performed a computer simulation that employs a standard molecular dynamics method to model the interaction between nanoparticles and the carrier fluid molecules. Based on the interaction potential (basically a geometric function) between the particle and fluid molecule, they simulated the viscosity of lithium-argon and aluminium-argon nanofluids.

In early studies by Huseyin and Muhammet [204], Hojjat et al. [205] and Papari et al. [206], an artificial neural network (ANN) was applied to predict the thermal conductivity of different nanofluids. They showed that ANN predicted the experimental data with a good degree of accuracy. Mehrabi et al. [207] developed two new models for the prediction of thermal conductivity of Al_2O_3-water nanofluids using FCM-ANFIS and GA-PNN alongside experimental data. Recently, Esfe et al. [208, 209] predicted the thermal conductivity of MgO-EG and ZnO-EG nanofluids using ANN.

The use of ANN is now gaining momentum in the prediction of the thermal properties of nanofluids, including the viscosity of different nanofluids. Yousefi et al. [210], Bahiraei et al. [211] and, Karimi and Yousefi [212] successfully applied the ANN and genetic algorithm (GA) to effective viscosity modelling for different nanofluids. Mehrabi et al. [213] developed four different models for the prediction of nanofluid viscosities for four different water-based nanofluids (Al_2O_3, CuO, TiO_2 and SiO_2) based on the FCM-ANFIS modelling technique. The results of the respective models were compared with the experimental data and some prominent correlations from the literature. The degree of prediction of the FCM-ANFIS models was more accurate than the previous theoretical and empirical models. Atashrouz et al. [214], using data from the open literature, recently modelled the viscosity of nine nanofluids based on the hybrid group method of data handling-polynomial neural network (GMDH-PNN) system. The experimental data on

49

Al_2O_3-water, Al_2O_3-EG, Al_2O_3-PG, CuO-water, CuO-EG/water, SiO_2-water, TiO_2-EG and TiO_2-water was used. Nine models were presented for individual nanofluids with an average absolute relative deviation of 2.14%. Employing the GMDH-PNN algorithm, a model can be regarded as a set of neurons in which different pairs of neurons in each layer are connected through a polynomial of the second order, which then produces new neurons in the following layer. This representation can be employed in modelling and predicting highly non-linear experimental data as an inputs-outputs system.

It should be mentioned that these are the few algorithm-based studies on the prediction of the thermal conductivity and viscosity of nanofluids thus far, therefore, researchers need to do more work in this regard to further enrich nanofluid research.

2.5   THE pH OF NANOFLUIDS

The pH becomes important in the engineering of nanofluids given the prospect of available data, emphasising the effect of zeta potential on the thermophysical properties of nanofluids. The electro-kinetic potential of the EDL and zeta potential are two related quantities that influence the electrical-viscosity behaviour of nanofluids. According to Wamkam et al. [215], understanding the influence of pH on nanofluids may facilitate investigations into the fundamental nature of the heat transfer fluids.

Numerous efforts have been focused to study the effect of the pH of nanofluids on their heat transfer characteristics. Rubio-Hernández et al. [199] studied the effect of pH on nanofluids' zeta potential and thickness of the EDL. Timofeeva et al. [197] showed that by adjusting the pH values of nanofluids, one can achieve meaningful reduction in the viscosity value. They reported 34% viscosity reduction by changing the pH of SiC–water nanofluids from 5.5 to 10.3. Conversely, Zhao et al. [216] showed that viscosity increases with pH manipulation. This is probably due to the fact that the effect of pH manipulations on zeta potential values was not monitored and must have affected the stability of the suspension. Therefore, careful manipulation of the zeta potential of the nanofluids needs to be carried out so that stability is not compromised. It has been shown that the van der Waals force of attraction dominates the interaction between nanoparticles when the pH of the nanofluid is at the IEP, because the zeta potential is equal to zero at the IEP, and this hastens the agglomeration rate [171]. The pH and zeta potential of nanofluids have been

50

investigated to determine the IEP, as well as their effects on the agglomeration kinetics (stability) for different nanofluids [217].

Wamkam et al. [215] reported aggregation, precipitation and enhancement in the thermophysical properties (viscosity and thermal conductivity) of water-based nanofluids of ZrO_2 and TiO_2 at IEP pH. When the pH value of ZrO_2-water nanofluid was modified from the IEP, the nanofluid viscosity enhancement was reduced by ~46% because the aggregate size reduced significantly and the nanofluid samples became stable. This is similar to the work of Timofeeva et al. [197] mentioned above.

Xian-Ju and Xin-Fang [218] showed that an optimal pH value at which the nanofluid viscosity is minimum is achievable when they investigated the effect of pH on the viscosity and thermal conductivity of Cu-H_2O and Al_2O_3-H_2O nanofluids. At the optimal pH levels of 9.5 and 8.0 for Cu-H_2O and Al_2O_3-H_2O nanofluids respectively, their results indicated that the nanofluids were stable and had minimum viscosity enhancements for a volume concentration between 0.1 and 0.4%. Li et al. [219] reported that, as the pH of Cu-H_2O nanofluid is moved away from the IEP, the nanoparticles' surface charge increases due to more frequent attacks to the surface hydroxyl groups and phenyl sulfonic group by potential determining ions (H^+, OH^- and phenyl sulfonic group). This leads to increased zeta potential up to the potential at which the dispersion behaviour becomes stabilised. Other similar studies have shown that modifying the pH of a nanofluid suspension beyond the IEP has led to the formulation of stable nanofluids [173, 220–222].

All the literature cited above agree that at IEP, the nanoparticles will aggregate due to insufficient electrostatic force to overcome the effectiveness of the van der Waals forces of attraction. If the pH changes further away from the IEP, the ionic charge state of the particle surface increases, which produces a sufficient electrostatic repulsive force that overcomes the van der Waals forces of attraction. According to the Derjaguin and Landau, Verwey and Overbeek theory, at IEP, the total interaction energy barrier that must be overcome is at its minimum, which allows the formation of agglomerates (resulting from the Brownian motion of the nanoparticles). However, when the pH is adjusted to a value much higher than the IEP's pH, the ionic strength increases. This results in a much higher interaction energy barrier that hinders particle agglomeration. In

51

this state, the aggregates present in the suspension are at the minimum size and the suspension becomes stable [222].

All research conducted on the influence of pH on the zeta potential of nanofluids was carried out at 25 ^{o}C. However, nanofluids are aimed at higher-temperature applications and an important aspect of the pH of nanofluids that has not been explored is the influence of higher temperature, nanoparticle size and volume fraction variation. The pH affects the stability of nanofluids, as it dictates the zeta potential value. Therefore, the effect of temperature, nanoparticle size and volume fraction on the pH of nanofluids needs to be studied. Moreover, nanofluids are meant for high-temperature applications, therefore, it is expedient to study the pH characteristics at elevated temperature. This will further bolster the study of nanofluid stability. Recently, Konakanchi et al. [223] showed that temperature has a significant influence on the pH of different types of water-based nanofluids. At the time this research was conducted, the work of Konakanchi et al. [223] was the only work that studied the influence of the temperature on the pH of nanofluids.

2.6   ELECTRICAL CONDUCTIVITY

The pH and electrical conductivity are two interrelated phenomena that are linked to the ionic configuration and surface charge of the nanoparticles in suspension [224, 225]. Assuming electroneutrality (a situation where the positive ions are balanced with the negative ions) in stable base fluids is acceptable. The introduction of nanoparticles at different volumetric fractions leads to a change in the ionic configuration of the initial system due to the dissociation of the ionic group at the particle surface, adsorption of the ionic group to the particle surface, and the isomorphous substitution of ions, etc.

Nanoparticles have residual charges due to the methods of synthesis. When introduced into a presumably electroneutral base fluid, modification of the ionic strength of the suspending medium far away from the particle surface occurs because the charged particle attracts counterions firmly to its surface. Therefore, there is a deficiency in the counterions and a surplus of particle coions [226] in the base fluid. As a result, the electrical conductivity of the system will be altered. Essentially, the electrical conductivity of nanofluids relates to the surface electrokinetics interplay with the ionic situations in the bulk fluid. The charge characteristic is also interrelated with the EDL,

52

electrophoretic mobility and the electrical conductivity of the nanofluids. The interplay between the electrical conductivity, EDL and the electrophoretic mobility of the nanoparticles in the nanofluids have been shown to influence the stability and effective viscosity of colloidal suspensions [199, 227]. Therefore, the study of the electrical conductivity of nanofluids becomes even more crucial at this stage in nanofluids research.

Presently, little research has been directed towards understanding the enhancement evolution of electrical conductivity in nanofluids. Sarojini et al [33] reported a linear rise in water-based ceramic nanofluids (Al_2O_3, CuO) with an increase in volume fraction and a non-linear behaviour in water-based Cu nanofluid. Ganguly et al. [228] reported a linear increment in the electrical conductivity of Al_2O_3–water nanofluid with an increase in volume fraction. Modesto-Lopez and Biswas [36] reported similar results on TiO_2 ceramic. The thermal and electrical conductivity of CNT and graphene have also been studied [229, 230].

Teng et al. [231] synthesised carbon-water nanofluid using a single-step plasma arc system. The electrical conductivity characterisation of the carbon-water nanofluid showed that the electrical conductivity is higher than the base fluid. Maddah et al. [232] synthesised Ag and Al_2O_3 nanoparticles using the microwave-assisted chemical precipitation method. The nanoparticles were dispersed in water to produce both Ag-water and Al_2O_3-water nanofluids, which showed higher electrical conductivity compared to the base fluid, and the value increased with volume fraction increase.

Wong and Kurma [233] investigated the electrical conductivity of Al_2O_3-water nanofluid among other thermophysical properties. Their results indicated a linear increase in electrical conductivity with an increase in the volume fraction. Similarly, Minea and Luciu [234] experimentally investigated the influence of temperature and volume fraction on the electrical conductivity of stabilised Al_2O_3-water nanofluids. They also showed that the electrical conductivity of the nanofluid increased as both temperature and volume fraction also increased. However, at higher volume fractions, the rate of the electrical conductivity increment started reducing, which was ascribed to the counterion condensation effect in the high surface charge regime. White et al. [37] also experimentally showed that counterion condensation occurs when they investigated the

influence of increasing the volume fraction of ZnO on the electrical conductivity of ZnO/PG nanofluids.

Based on the equivalent cell model as depicted in Figure 2.8, Ohshima [235–238] extensively theorised and modelled the electrokinetics and electrical conductivity of colloids in suspensions to obtain the following equation:

$$K_{nf} = K_{bf}\left\{\frac{1-\phi}{1+2\phi}\left(1-3\phi\left(\frac{e\zeta}{k_bT}\right)f\left(\kappa a,\phi\right)\frac{\sum_{i=1}^{N}z_i^3 n_i^\infty/\lambda_i}{\sum_{i=1}^{N}z_i^2 n_i^\infty/\lambda_i}\right)\right\},\qquad (2.47)$$

where K_{nf} is the electrical conductivity of the nanofluids, K_{bf} is the electrical conductivity of the base fluid, ζ is the zeta potential, n_i is the number density of the ions, k_b is the Boltzmann constant, *T* is the absolute temperature, *e* is the electron charge, z_i is the particle valence, λ_i is the ionic drag coefficient, and κ is the inverse of Debye length. The function $f\left(\kappa a,\phi\right)$ in Equation 2.47 is calculated using:

$$f\left(\kappa a,\phi\right) = \frac{1}{3a^3\zeta(1+\phi)(1+2/\phi)}\times\int_a^b\left(\frac{a^3}{2}+r^3\right)\left(1-\frac{a^3}{r^3}\right)\frac{d\psi^{(0)}}{dr}\,dr. \quad (2.48)$$

In the case of uncharged particles and suspensions with a very large EDL formation around the particles, Equation 2.48 reduces to the form of Maxwell's conductivity model.
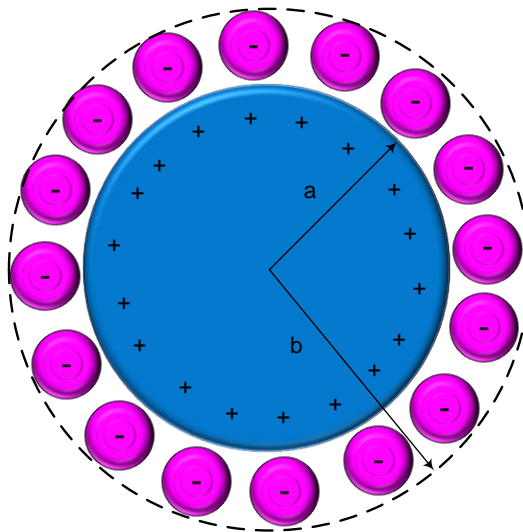
Figure 2.8: Equivalent cell model showing counterions around a positively charged particle.

54

Cruz et al. [239] applied Maxwell's model on conductivity to predict the electrical conductivity of aluminium oxide ceramic suspensions. They prepared their suspension using a 520 nm alumina in distilled water up to a 35% volume fraction. They applied NH_4Cl and HCl to modify the ionic strength and pH of the suspension respectively. Maxwell's equation was also successfully applied to experimental data by Turner [240] to predict and explain the behaviour of the electrical conductivity of suspensions of particles fluidised by an $NaCl_{aq}$ solution. The model predicts the conductivity of liquid-particle systems, such as nanofluids as a function of the individual conductivities of the suspension components (particle and base fluid) and the volume fraction of the dispersed phase (particle) such that:

$$\frac{K_{nf}}{K_{bf}} = 1 + \frac{3(\alpha - 1)\phi}{(\alpha + 2) - (\alpha - 1)\phi}, \tag{2.49}$$

where α is K_{nf}/K_p, and K_p is the electrical conductivity of the nanoparticles. Maxwell's model is valid for low-volume fractions with the assumption that particles are randomly distributed and at distances significantly larger than their sizes. Generally, Maxwell's theory on conductivity evolves, depending on the conducting nature of the dispersed phase [239] according to the following approximations:

i.   If the dispersed phase is an insulating type (i.e. $K_p << K_{bf}$), Equation 2.49 is approximated as $\frac{K_{nf}}{K_{bf}} = 1 - \frac{3}{2}\phi$.

ii.   If the dispersed phase has equal conductivity with the base fluid, then Equation 2.49 is $\frac{K_{nf}}{K_{bf}} = 1$.

iii. If the dispersed phase is conducting particles (i.e. $K_p >> K_{bf}$), Equation 2.49 is approximated as $\frac{K_{nf}}{K_{bf}} = 1 - 3\phi$.

When Ganguly et al. [228] applied the Maxwell model to predict their electrical conductivity data obtained from aqueous alumina nanofluids, the model underpredicted the experimental data. Therefore, they proposed an empirical model based on their experimental data, given as:

$$\left(K_{nf} - K_{bf}\right)/K_{bf} = 3679.049\phi + 1.085799T - 43.6384. \tag{2.50}$$

Note the dependence of the relative electrical conductivity on volume fraction in Equation 2.50 above. Other researchers have shown that their experimental data was underpredicted using Maxwell's model [234, 241]. Therefore, they proposed empirical models consisting of volume fraction, temperature and particle size:

$$K_{nf} = 176.69 + 5.88.41\phi + 13.64T - 86.31\phi^2 + 0.36T^2$$
$$+ 1.07T\phi + 11.06\phi^3 + 0.18T^2\phi + 1.01T\phi^2 \tag{2.51}$$

Unlike the models presented in equations 2.50 and 2.51, in which the two sides of the equations possess different units (unbalanced equations), Konakanchi et al. [241] presented a non-dimensional model with consideration given to temperature, particle size and volume fraction, as presented in Equation 2.52:

$$\frac{K_{nf}}{K_{bf}} = \left[a_1 \left(\frac{T}{T_0} \right)^2 + a_2 \left(\frac{T}{T_0} \right) + a_3 \right] \left[b_1 \phi^2 + b_2 \phi + b_3 \right] \left[c_1 \left(\frac{d_0}{d} \right)^2 + c_2 \right], \tag{2.52}$$

where T_0 and d_0 are reference temperature and particle size (273 $^{\circ}$K and 100 nm respectively); $a_1 - a_3$, $b_1 - b_3$ and c_1 and c_2 are all empirical constants that are obtainable from regression analysis. The range of validity of the model in Equation 2.52 is 273 K $\leq$ $T \leq$ 363 K, 1% $\leq \phi \leq$ 6% and 10 nm $\leq d \leq$ 70 nm.

2.7   CONCLUSION

In this literature review, an attempt was made to cast more light on the understanding of nanofluid viscosity models and their evolution from the classical to numerical models using the findings available in the literature. The pioneering work of Einstein was developed to predict the viscosity of non-interacting and hard microsphere suspension in the dilute regime.

The majority of the subsequent classical research on the viscosity of suspension was carried out to further extend Einstein's work to a concentrated regime. These efforts show the importance of the influence of increase in volume fraction on the viscosity of suspension. However, none of the classical models was developed for the estimation of nanofluid viscosity.

56

Recently, a few new theoretical models were developed, taking into consideration some of the characteristics of nanofluids, such as nanoparticle size, hydrodynamic volume fraction, particle density, agglomerate diameter and capping layer thickness. The empirical models were applied to characterise the behaviour of nanofluids at different nanoparticle volume fractions, sizes, temperatures and shear rates. It was noted that most empirical models were developed considering a single parameter, mostly volume fraction or temperature, and many of them have unbalanced units. However, nanofluid viscosity is affected by multiple factors, such as volume fraction, particle size, particle shape, shearing rate, shearing time, particle agglomeration and base fluid properties. Therefore, the literature review further looked into the factors that affect nanofluid viscosity.

The use of AI methods of ANN, GMDH-PNN, GA and GA-PNN are gaining ground at a rapid rate due to their ability to model highly non-linear systems, such as the thermophysical properties of nanofluids. The ANN-based models have shown good predictions with a reduced average absolute relative devation (AARD), and can take a wide range of influencing factors into consideration compared with most empirical models that are built around a single parameter, such as temperature or volume fraction.

The pH and electrical conductivity of nanofluids are related to their stability. Invariably, these properties are very important because understanding their behaviour with different input variables (such as nanoparticle size, volume fraction, temperature and energy input into the preparation procedure) will guide the understanding of other thermophysical properties of nanofluids. However, comprehensive knowledge of these two parameters with regard to the factors that affect them is lacking in the literature. Consequently, this chapter examined the few existing studies on the pH and electrical conductivity of nanofluids.

CHAPTER 3:   METHODOLOGY[1, 2, 3, 4, 5]

3.1   INTRODUCTION

This chapter deals with the methods that are involved in the experimental investigations and the modelling techniques applied to the properties of the nanofluids used in this thesis. The focus is mainly on the materials and equipment, material characterisation, nanofluid preparation, measurement procedures of thermophysical properties, conditions of measurements and modelling techniques. These will be discussed in detail in the subsequent sections.

3.2   MATERIALS AND EQUIPMENT

3.2.1   Materials

The nanopariticles used in this research are Al_2O_3, MgO and SiO_2. The Al_2O_3 particles are of three different sizes and were procured from Nano Amorphous Inc. (20-30 nm γ-Al_2O_3), MK Nano (80 nm α-Al_2O_3) and US Nanomaterials Inc. (100 nm α-Al_2O_3). According to the manufacturers, the MgO nanoparticles have average particle sizes

---

This chapter has been published in part as:

[1] S.A. Adio, M. Sharifpur and J.P. Meyer, Investigation into effective viscosity, electrical conductivity and pH of γ-Al_2O_3-glycerol nanofluids in Einstein concentration regime, *Heat Transfer Engineering*, vol. 36, no. 14–15, pp. 1241–1251, 2015.

[2] M. Sharifpur, S.A. Adio and J.P. Meyer, Modelling effective viscosity of Al_2O_3-glycerol nanofluid for heat transfer applications using dimensional analysis and GMDH-NN methods on experimental data, *International Communications in Heat and Mass Transfer*, vol. 68, pp. 208–219, 2015.

[3] S.A. Adio, M. Sharifpur and J.P. Meyer, Factors affecting the pH and electrical conductivity of MgO-ethylene glycol nanofluids, *Bulletin of Materials Science*, vol. 38, no. 5, pp.1–13, 2015.

[4] S.A. Adio, M. Sharifpur and J.P. Meyer, Influence of ultrasonication energy on the dispersion consistency of Al_2O_3-glycerol nanofluid based on viscosity data, and model development for the required ultrasonication energy density, *Journal of Experimental Nanoscience*, 2015. Article in press.

[5] S.A. Adio, M. Mehrabi, M. Sharifpur and J.P. Meyer, Experimental investigation and modelling of the effective viscosity of MgO-ethylene glycol nanofluids using dimensional analysis, FCM-ANFIS and GA-PNN modelling techniques, *International Communications in Heat and Mass Transfer*, 2016. Article in press.

58

(APSs) of 20, 40 and 100 nm. On the other hand, the SiO_2 nanoparticle has an APS of 20 nm. Table 3.1 gives some of the physical properties of the nanoparticles. The base fluids, which are EG and glycerol, were procured from Merck Millipore (Germany), both with 99.5% purity. Other materials used during the course of the research are deionised water, KOH and HCl. All the nanopowders were supplied as white powder with a purity of more than 99%. The nanopowders and other materials in this study are of analytical grade and were used as received without further purification. As stated by Gustafsson et al. [242], attempts at the further purification of nanopowders may lead to contamination.

Table 3.1: Physical properties of alumina nanoparticles

Name	Crystallographic stucture	Size[a] (nm)	Shape[a]	Density[a] (g/cm^3) at 20 ^{o}C	Manufacturer
γ- Al_2O_3	Rhombohedral[b]	20–30	Nearly spherical	3.7	Nano Amorphous Inc.
α- Al_2O_3	Hexagonal	80	Nearly spherical	3.5–3.9	Us Nanomaterials Inc.
α- Al_2O_3	Rhombohedral	100	Nearly spherical	3.7	MK Nano
MgO	Cubic/hexagonal	20	Polyhedral	3.58	Nano Amorphous Inc.
MgO	Cubic/hexagonal	40	Polyhedral	3.58	Nano Amorphous Inc.
MgO	Cubic	100	Polyhedral	3.58	Us Nanomaterials Inc.
SiO_2	Amorphous	20	Nearly spherical	2.17–2.66	Nano Amorphous Inc.

[a] As stated by the manufacturer. [b] Cubic by manufacturer's estimation.

3.2.2 Equipment

The weight of the nanoparticles and base fluids were measured using a RADWAG precision balance (AS 220.R2) and a Highland HCB1002 precision balance to prepare predetermined volume fractions. The prepared samples were sonicated using a Q700 ultrasonicator (Qsonica, USA) equipped to measure the total energy impacted in the dispersion process, or Hielscher ultrasonic processor (UP200S) set at 75% amplitude and 80% pulse-pulse. The temperature of the nanofluid samples was controlled using a programmable constant temperature bath (LAUDA ECO RE1225 Silver). The bath was

programmed with a ramp function to achieve a relatively uniform and steady control of the temperature of samples throughout the experiments.

The dispersion process and the stability of the nanofluid were characterised by UV-visible (UV-vis) spectrophotometer (Model 7315 from Jenway, UK) and zeta potential measurement using Zetasizer Nano ZS (Malvern Instrument Inc., UK). The shear viscosity of the nanofluid samples was measured using SV-10 sine wave vibro-viscometer (A&D, Japan). The pH and electrical conductivity were measured using a Jenway 3510 pH meter and EUTECH CON700 electrical conductivity meter, respectively.

3.3 NANOPARTICLES' CHARACTERISATION AND NANOFLUIDS' PREPARATION

The size and morphology of the nanoparticles were verified using a transmission electron microscope (TEM). Samples for the TEM characterisation were prepared by dispersing 0.1% volume fraction of each nanoparticle type in acetone so that a rapid-drying method could be employed for the captures [215]. Heavier base fluids, such as glycerol, EG, PG and engine oil, cannot be used for this purpose as they will cause irreparable damage to the TEM vacuum column. Therefore, the nanoparticles were sonicated for five minutes in the acetone and were characterised using the JEOL JEM-2100F microscope operated at 20 kV.

An XPERT-PRO diffractometer (PANalytical BV, Netherlands) with theta/theta geometry, operating a cobalt tube ($\lambda = 0.1789$ nm) at 35 kV and 50 mA, was used to obtain the X-ray diffraction (XRD) pattern. The XRD patterns of all the nanoparticle samples were recorded in a range of 10 to 90° (2 theta position) with a scanning step size of 0.001° and a counting time of 12.705 seconds per step.

The energy-dispersive X-ray spectroscopy (EDS) was also carried out using a scanning electron microscope (SEM) (JEOL 5800LV) equipped with an energy-dispersive system operated at 20 kV. The EDS system was integrated into the SEM instrument and comprises a sensitive detector for detecting X-ray spectrum, a liquid nitrogen coolant Dewar, and a software for the collection and analysis of energy spectra. During the

60

analysis, the X-ray beams of different elements are characterised into an energy spectrum by the sensitive X-ray detector, after which the software analyses the energy spectrum to determine the specific elements corresponding to the spectrum.

The two-step technique [243] was used for the preparation of the nanofluid samples. The volume fractions of the nanoparticles were determined by calculating the equivalent mass of nanoparticles, using the mass of the base fluid and the densities of both the nanoparticles and base fluid as in Equation 3.1:

$$\phi = \frac{m_p / \rho_p}{m_p / \rho_p + m_{bf} / \rho_{bf}}, \tag{3.1}$$

where ϕ is the volume fraction, m and ρ are the mass and density respectively, for both nanoparticle and base fluid. A precalculated mass of nanoparticles corresponding to a known volume fraction of the desired nanofluid sample was measured using the precision balance and was added to the corresponding base fluid mass. To obtain a homogenised dispersion of nanoparticles in the base fluid, the mixture was sonicated continuously with the ultrasonicator in a 100 ml beaker using a 12 mm stainless steel sonotrode. During this process of homogenisation, the samples were kept in the programmable constant temperature bath and kept at the prevailing room temperature.

The UV-visible spectrophotometry analysis is one of the convenient ways to characterise the dispersion of nanofluid. Using the Beer Lambert Law (Equation 3.2), the light absorbency ratio index of the nanofluid can be calculated.

$$A_b = -\log \frac{I_0}{I} = \varepsilon l \Psi. \tag{3.2}$$

In Equation 3.2, A_b is the absorbance, I_0 is the intensity of the UV-visible light through the blank, I is the intensity of the UV-visible light through the samples, ε is the molar absorptivity, l is the length of the optical path, which is the length of the test section through which light passes, and Ψ is the molar concentration of the particles in suspension.

Concerning Equation 3.2, it can be mentioned that, for a fixed optical path length and molar absorptivity, the absorbency of a suspension is proportional to the concentration of

61

the particles in the suspension. Therefore, a well-dispersed suspension shows a proportional relationship between the absorbance and the concentration [244].

Regarding the zeta potential, the equipment (Zetasizer Nano ZS) measures the electrophoretic mobility of the particles using capillary cells with electrodes at either end to which electric potential is applied. The measured electrophoretic mobility of the particle is then used to calculate the zeta potential using Henry's function. The zeta potential was measured at room temperature (25 ^{o}C) with an applied potential of 10 V. Due to equipment limitations, a dilute concentration of 0.05% was used for the zeta potential measurements, as higher concentrations were beyond the equipment's range.

3.4 VISCOSITY MEASUREMENT

The viscometer used is a sine wave vibro-viscometer with viscosity measurement limits of 0.3 to 10 000 mPa.s. The measuring cup of the apparatus is equipped with a water jacket connected to a programmable thermal bath for efficient temperature control of the sample. The viscometer uses the turning-fork vibration method at a constant resonating frequency of 30 Hz to determine the vicidity of the fluid sample based on power differentials that maintain the resonating frequency. The fluid sample temperature is monitored with a temperature sensor that is affixed equal distances from the vibrating forks. This ensures uniform temperature at the sampling site.

Using an online Windows communication tool, both the viscosity and temperature of the sample can be accurately logged in real time at every second. The viscometer was calibrated using a fluid with known viscosity. In this case, the base fluids were used depending on the type of nanofluid being investigated. For glycerol as a base fluid, the manufacturer-stated viscosity is 1 412 mPa.s at 20 ^{o}C, while for EG it is 16.9 mPa.s at 25 ^{o}C.

After calibration, benchmark tests were carried out between 20 and 70 ^{o}C to confirm the accuracy and repeatability of experimental results using the device. The experimental set-up is shown in Figure 3.1. The benchmark test results show good agreement with the values reported in the literature by Miner and Dalton [245] for glycerol base fluid, and Xie et al. [246] and Pastoriza-Gallego et al. [247] for EG as a base fluid, as shown in

Figure 3.2. The deviation from the literature values was found to be minimal and within the uncertainty of the equipment. Figure 3.3 further stresses the fact that the vibro-viscometer is repeatable in its measurement after running the device to measure from 20 to 70 ^{o}C and 70 to 20 ^{o}C respectively. When traced from the temperature axis to the viscosity axis, the dash double dot line in Figure 3.3 highlights this fact.

3.5 THE pH AND ELECTRICAL CONDUCTIVITY MEASUREMENT

3.5.1 The pH measurement

The pH measurements were carried out using the bench top pH/mV meter (Model 3510, Jenway UK). The device is equipped with an automatic temperature compensation (ATC) thermocouple that can measure temperature in the range of 0 to 100 ^{o}C, and supplied with a combination electrode for the pH measurement. The high impedance meter measures the quantity of the hydrogen ion activity between the range of -2 and 19.999 pH and was calibrated using three-point calibration with the buffers 4, 7 and 10. The pH measurement of the nanofluid samples were all made between 20 and 70 ^{o}C, employing an in-house water jacket connected to the thermal bath in order to produce constant temperature. During the measurement, the samples were continually stirred until the desired temperature was reached, and the slope monitor from the device showed a ready sign before measurements were taken.
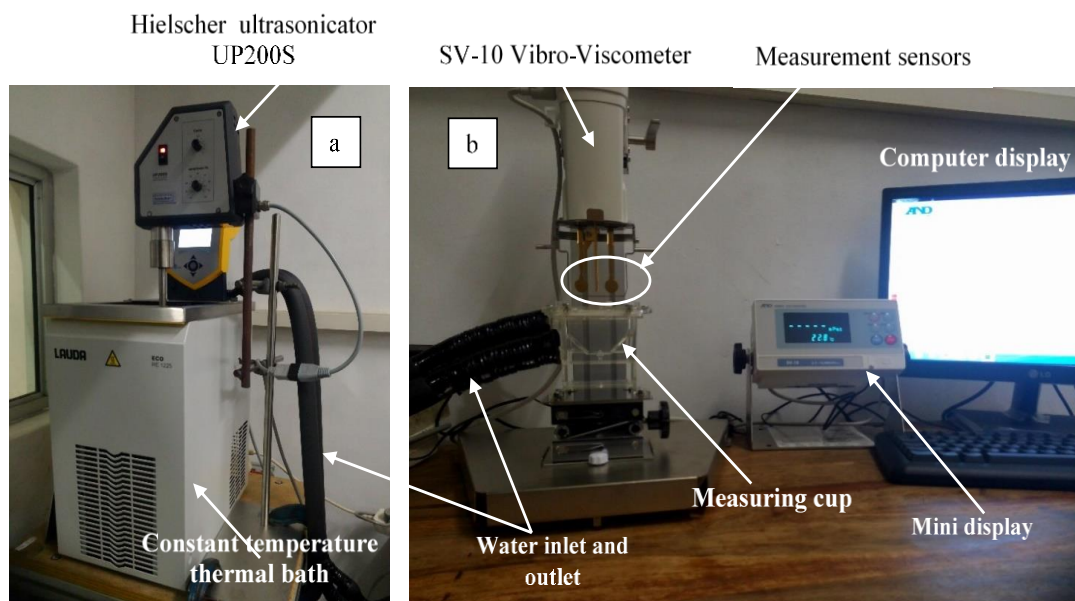
Figure 3.1: Experimental set-up: (a) nanofluid preparation; (b) viscosity measurement.

63
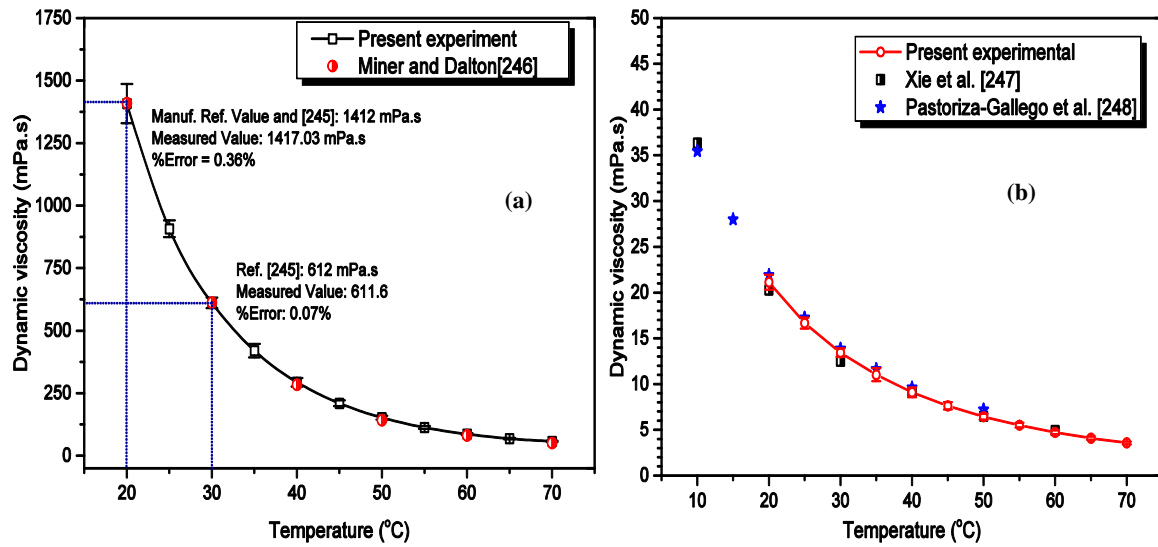
Figure 3.2: Benchmark test with the base fluids and comparison with other experimental data: (a) glycerol; (b) EG.
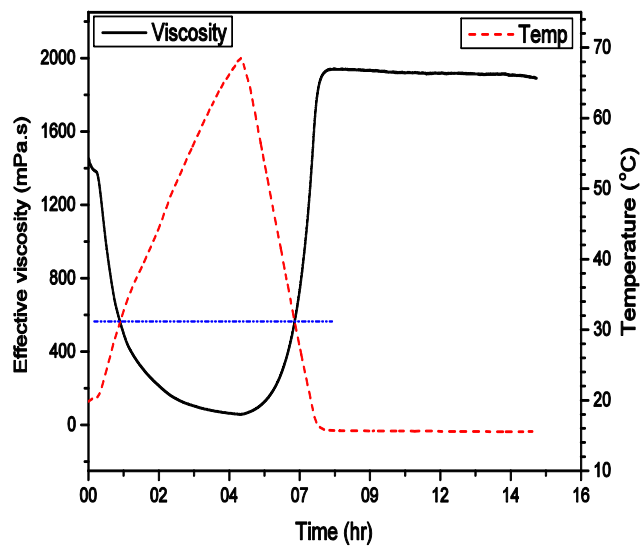
Figure 3.3: Viscosity-temperature-time monitor of the viscometer.

3.5.2   Electrical conductivity measurement

The electrical conductivity of the nanofluid samples was carried out using the EUTECH CON700 conductivity meter. The device is equipped with a two-cell electrical conductivity electrode meter with a nominal cell constant k = 1.0. The apparatus came with a built-in thermistor temperature sensor with ATC. It was calibrated with

64

1 413 μS/cm standard calibration fluid repeatedly at 25 ^{o}C and the measured value does not only agree with the standard value, but was also repeatable, as shown in Table 3.2. The electrical conductivity experiments were also conducted between the temperature of 20 and 70 ^{o}C. Samples were continually stirred and, when the desired temperature was achieved and the slope monitor showed a ready sign, the measurements were recorded. Figure 3.4 shows the schematic diagram of the experimental set-up for the pH and electrical conductivity measurements with the inset showing a pictograph of the measurement site.

3.6   UNCERTAINTY ANALYSIS

Part of the study's objective is to experimentally study the viscosity, pH and electrical conductivity of nanofluids regarding the factors that affect them. Therefore, uncertainty analysis becomes very important in order to illustrate the quality of the experimental results that are presented in this thesis. The uncertainty of any experimental data defines an interval about the data of which the true value is suspected to fall with a specified probability.

Table 3.2: Calibration data of the electrical conductivity meter

Measurement	Temperature (^{o}C)	Electrical conductivity (μS/cm)
First measurements	25.0	1 412
	24.9	1 415
	24.8	1 414
Second measurements	25.0	1 413
	24.9	1 412
	24.8	1 415
Third measurements	25.0	1 412
	24.9	1 415
	24.8	1 415
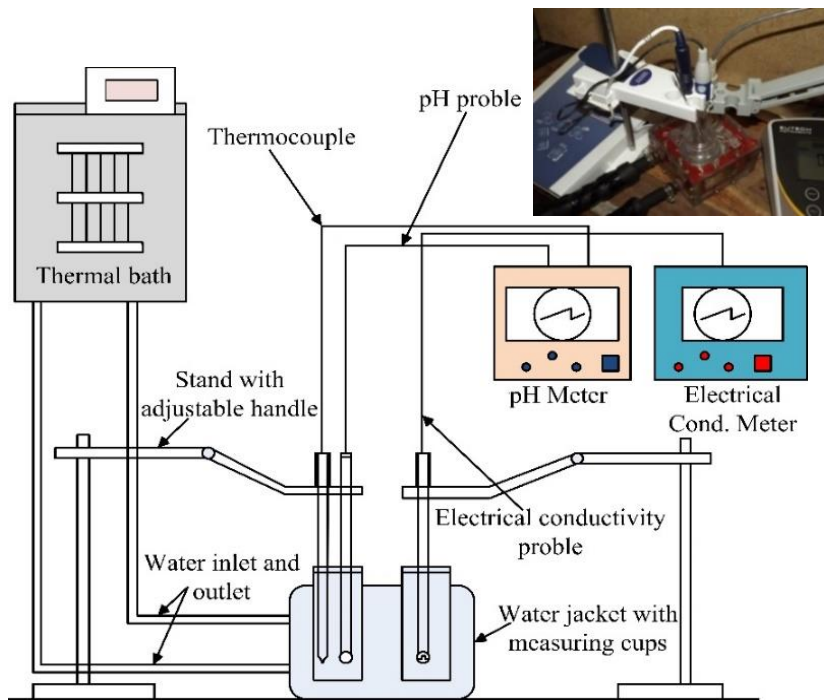
Figure 3.4: Schematic of the experimental set-up with the inset showing a pictograph of the measurement site.

The uncertainty analysis is the process of finding, measuring and combining the errors. In measurement, two error components are generally considered during uncertainty analysis. These components are systematic (bias) and random error (precision). Systematic errors are fixed errors that are repeatable around the measured data under fixed experimental condition. They shift the sample mean away from the true mean by a fixed quantity. This type of error arises from imperfections in the equipment, poor calibration, incorrect assumptions or methods, etc. Random errors, on the other hand, are precision errors that are based on the data set's finite statistics. They bring about a distribution of the measured values about the true mean of the experimental data. Random errors are always present in experimental data due to variation in experimental conditions, electrical noise, vibration, a change in measurement equipment, etc. [248].

The uncertainty (U_M) in a single measurement (X_i) is given in Equation 3.3, where B_i is the systematic error and P_i is the random error. The uncertainty is evaluated at 95% confidence level:

66

$$U_M = \delta X_i = \pm\sqrt{\left(B_i\right)^2 + \left(P_i\right)^2}. \tag{3.3}$$

Estimate of systematic error (B) and random error (P) is given as:

$$\pm U_B = \pm\left(t_{v,p} \times B^*\right), \tag{3.4a}$$

$$\pm U_P = \pm\left(t_{v,p} \times SD_{\bar{X}}\right), \tag{3.4b}$$

where $t_{v,p}$ is the student's t distribution at v degrees of freedom and probability, p (usually 95%), B^* is the estimate of systematic errors and $SD_{\bar{X}}$ is the random standard error of mean uncertainty. Details on the calculation of uncertainty can be found in Figliola and Beasley [248].

3.6.1   Uncertainty in viscosity measurement

The measurement errors relating to the variables in the preparation, temperature and viscosity measurements constitute the uncertainty in viscosity measurements. The weighing balance was used to measure the mass of the samples during the preparation of the nanofluids. The balance measured in the range of 90.291 to 105.277 g with $\pm$ 0.01 g accuracy; therefore, the systematic error of the balance will be propagated into the volume fraction. The accuracy of the viscometer depends on the viscosity value being measured. It is between ±3 and $\pm5\%$. Likewise, the built-in thermocouple has its accuracy as a function of the temperature and is between 0.5 and 2 ^{o}C within the present temperature range. The systematic uncertainty of the viscosity data, which is due to the error introduced by the respective equipment, could be calculated using Equation 3.5 based on the procedure adopted by Kulkarni et al. [249]:

$$U_B = \pm\sqrt{\left(\frac{\Delta\mu}{\mu}\right)^2 + \left(\frac{\Delta T}{T}\right)^2 + \left(\frac{\Delta m}{m}\right)^2}, \tag{3.5}$$

where U_B is the total systematic uncertainty in the viscosity data, μ is the viscosity, T the temperature, m the mass and Δ stands for the accuracy of the device within the measurement range. The random uncertainty in the viscosity data was estimated using Equation 3.4b. Therefore, the total uncertainty in the viscosity data was estimated using Equation 3.6:

$$U_M = \pm\sqrt{\left(U_B\right)^2 + \left(U_P\right)^2}. \qquad\qquad (3.6)$$

Substituting the relevant values and depending on the nanofluid type, volume fraction and temperature, the overall uncertainty in the viscosity data is between 3.43 and 7.06%.

3.6.2 Uncertainty in pH and electrical conductivity measurement

The uncertainty in the pH and the electrical conductivity data were estimated using the principle applied above. The overall uncertainty in the pH data is between 0.71 and 2.5%, while the overall uncertainty in the electrical conductivity data is between 0.71 and 4.96%.

3.7 MODELLING

3.7.1 Dimensional analysis

Most parameters (either variables or constants) possess a unit that is used to describe them analytically. The unit is mainly used to assign numerical values to dimensions, and it is very important in the scientific analysis of different phenomena. Seven fundamental dimensions are shown in Table 3.3. The use of inspectional analysis to non-dimensionalise an equation is often only useful in a situation where the relationship between the parameters is known. However, in emerging areas and in real-life scenarios, relationships between parameters are unknown and the existing theories are not able to explain the phenomenon. In situations like this, the results of experimental observation are often relied on to obtain reliable information.

Dimensional analysis is an important tool for modelling the relationship between physical parameters. It generates non-dimensional parameters that allow the design of experiments and serve as the basis for the comparison of results. It is very useful for the prediction of trends in the relationship between parameters.

In this thesis, dimensional analysis is employed alongside regression analysis based on the experimental data to find the best relationship between the input parameters and the experimental output. The method of repeating variables is used for the non-dimensionalisation of the essential parameters that are considered (nanoparticle size,

68

volume fraction, temperature, capping layer thickness, viscosity of the base fluid, the density of the base fluid and the density of the nanofluid) as input parameters. Details on the step-by-step procedure of repeating the variable used for the dimensional analysis can be found in Cengel and Cimbala [250].

Table 3.3: The fundamental dimensions and their International System of Units (SI) units [250]

Dimensions	Symbol	SI unit
Mass	m	Kilogram (kg)
Length	L	Metre (m)
Time	t	Time (s)
Temperature	T	Kelvin (K)
Electric current	I	Ampere (A)
Amount of light	C	Candela (cd)
Amount of matter	N	Mole (mol)

3.7.2   Artificial intelligence

In recent years, the idea of applying AI techniques to model complex real-life engineering problems has been strengthened due to technological advancements in computational hardware. Presently, many researchers are using knowledge of ANN, group method of data handling (GMDH), GA and fuzzy logic to investigate different complex systems that are essential in the fields of economics, science and engineering. Numerous AI techniques are currently available for use in solving different problems. However, most of these methods are deficient when used individually to model highly non-linear complex systems. Consequently, these techniques are hybridised with other optimisation techniques to create a more robust and flexible hybrid system.

In this thesis, GMDH-NN, GA-PNN and FCM-ANFIS hybrid systems are applied for the AI modelling of the experimental data.

3.7.2.1   *GMDH-NN modelling technique*

The standard multilayer GMDH generally has two major problems. It underperforms when applied for non-parametric modelling, and overfits when applied to time series data,

69

as it tends to produce complex polynomials that cannot model future data suitably [251]. Several other authors have reported high errors generated using this traditional GMDH technique [222, 234, 235]. The standard multilayer GMDH algorithm was first introduced by Ivankhnenko [252] as a learning algorithm to accomplish the generation and selection of model structures based on the neurons that give optimised outputs. This modelling technique is self-organising because it automatically determines the number of layers, and the structure of the inputs of each layer that minimises the objective functions. Thus, it organises an optimal network architecture that best estimates the system being modelled.

Due to the deficiencies of the traditional GMDH modelling technique, numerous researchers have applied different hybrid network systems based on the GMDH algorithms, such as GA-PNN by Mehrabi et al. [207], GMDH-PNN by Atashrouz et al. [214] and GMDH-NN by Abdolrahimi et al. [253]. The traditional GMDH algorithm by Ivankhnenko [252] was limited in terms of the number of independent input variables that could be combined at a time during the iterative procedure. It combines pair input at a time, which leads to the exclusion of the effects of other variables. Therefore, for a highly non-linear system, the algorithm generates less precise models to represent the system. Figure 3.5 represents the traditional GMDH network, with the starred nodes being the optimised ones.

A nanofluids system is one the most complex systems to be encountered in the fields of science and engineering. Therefore, a hybrid GMDH-NN system that is achieved by combining a GMDH and a neural network is chosen in this thesis to model the experimental data. This type of network is based on the formation of several layers from the combination of two or more input variables, and has several neurons in each layer. This hybrid GMDH-NN uses the combinatorial algorithm to optimise the connections between the neurons in each layer. The established relationship between every input and output into the neurons at every stage of the iteration is a multinomial expression in the form of Equation 3.7, known as the Volterra-Kolmogorov-Gabor function.

$$y_i = a + \sum_{i=1}^{N} a_i x_i + \sum_{i=1}^{N}\sum_{j=1}^{N} a_{ij} x_i x_j + \sum_{i=1}^{N}\sum_{j=1}^{N}\sum_{k=1}^{N} a_{ijk} x_i x_j x_k + ..., \qquad (3.7)$$

70

where N is the number of independent variables, $a_{i,j,..}$ is the unknown coefficients or weights, and x_i, x_j, x_k are the independent variables. In a GMDH-NN, the Volterra-Kolmogorov-Gabor neuron function is disintegrated into the quadratic polynomial of the form in Equation 3.8 and the coefficients are determined using the method of the least squares approximation.

$$Y_i = f_i\left(x_i, x_j\right) = a_0 + a_1 x_i + a_2 x_j + a_3 x_i x_j + a_4 x_i^2 + a_5 x_j^2, \qquad (3.8)$$
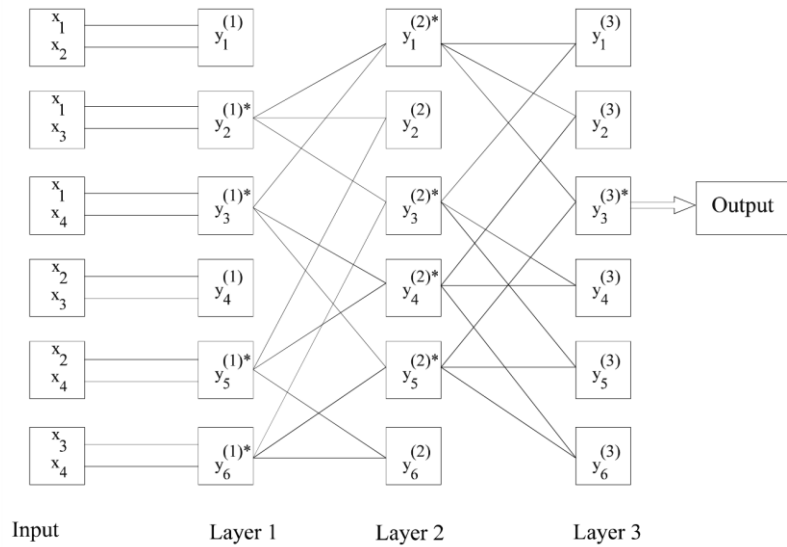
Figure 3.5: Traditional GMDH functional network with pair inputs into each node [251].

When training the GMDH-NN, the experimental data is randomised and divided into two parts. The first part of the data is used for the training and construction of the GMDH-NN structure. During the construction of this network structure, all combinations of input variables are generated and sent to the first layer of the network, and the optimised output from all the functional nodes of this layer will serve as input into the subsequent layer. This procedure is continued as long as the node or the combination of nodes in the new layer produces much better result than the previous layer. However, the construction of new layers can also be stopped if the testing error was reduced by less than 1% or if the number of layers has reached a certain limit that must have been defined.

Another method of constructing the GMDH-NN during training is by dividing the dataset into k portions. Training of the model network is done k times using k-1 parts, each time

71

measuring model performance using a new remaining part. Finally, residuals obtained from all testing parts of the training dataset are added and used for model comparison. The deviation/error between the training data and the GMDH-NN's predicted values is monitored using both the mean absolute error (MAE) and root mean square error (RMSE) as in Equation 3.9 and Equation 3.10 as statistical tools. The coefficients in Equation 3.8 are fitted using the training data set, while the testing data is used to select the most accurate model combination that satisfies the eternal or statistical criterion.

$$MAE = \frac{1}{M} \sum_{i=1}^{M} \left(\left| Y \right|_{train} - Y \right|_{pred} \right) \tag{3.9}$$

$$RMSE = \sqrt{\frac{1}{M} \sum_{i=1}^{M} \left(Y \right|_{train} - Y \right|_{pred})^2} \tag{3.10}$$

3.7.2.2   *GA-PNN modelling technique*

In this thesis, the GA was used to control the GMDH-PNN coefficients, bias coefficients and hidden layers, in order to minimise the training error and thus find the optimal network architecture. The GA is used mainly to find the chromosomes of the network, which are the hidden layers and bias coefficients. A typical flow chart of the hybridisation between GA and GMDH-PNN is given in Figure 3.6.

In the GA-PNN hybrid system, the GMDH learning algorithm applied to the PNN network introduced the GMDH-PNN for the eventual formation of the GA-PNN hybrid system. On the other hand, the hidden layers and the appropriate bias coefficients of the GMDH-PNN (which are necessary for achieving optimal structure and minimising training error) are generated by the GA technique. The GA works by mimicking the evolution process, in which mutated chromosomes combine to produce a new population of chromosomes. The chromosomes from the new population are ranked using their fitness, which can be estimated using the probability of survival, the fitness rank space method and the highest diversity from the best ranking chromosomes. Further information regarding GMDH-PNN architecture and the GA-PNN hybrid system is given in Pesteei and Mehrabi [254], and Mehrabi et al. [207, 255], respectively. This hybrid GA-PNN system approach is similar to the genetic algorithm-neural network (GA-NN) hybrid system used by Karimi and Yousefi [212]and Karimi et al. [256] with the following steps as described below:

72
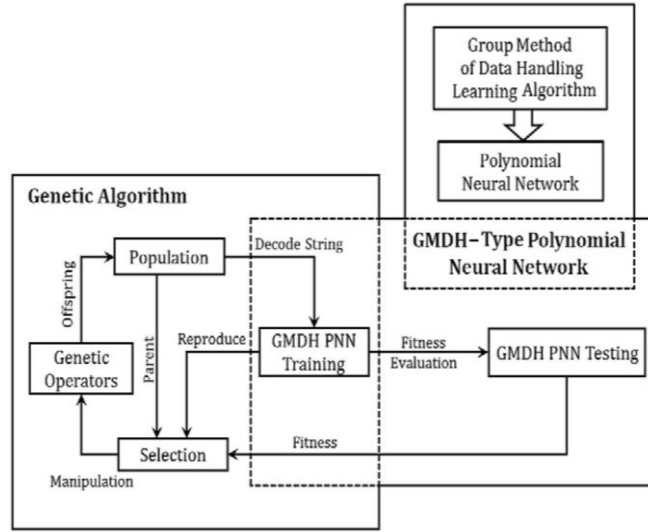
Figure 3.6: The hybridisation between the genetic algorithm and GMDH-PNN techniques [207].

1. Chromosome population initialisation: The weights and bias coefficients of the system are randomly selected to constitute the initial population.

2. Estimation of fitness function: Individual chromosomes are evaluated based on the level of their fitness value. This is calculated by measuring the average deviation of the predicted value from the actual training data value. The fitness function is calculated using the formula below:

$$f_f = \frac{1}{1 + \delta_{MSE}},$$ (3.7)

$$\delta_{MSE} = \frac{1}{M} \sum_{i=1}^{M} \left(Y\big|_{train} - Y\big|_{pred} \right)^2,$$ (3.8)

where f_f is the fitness function, and δ_{MSE} is the mean square error. The chromosome strings are selected based on their fitness value, i.e. the higher the fitness value, the better the chance of producing offspring with a good fitness value and higher diversification index.

3. Population variation through crossover operation: The selected chromosomes are set for crossover, mutation and mating in order to produce new offspring. The new offspring takes its genetic factor from that of the parents, and parents are selected randomly. During the mutation operations, random changes are introduced into the population to

73

change the weight and bias of the chromosome in order to ensure the correctness of the genetic factors. The new weights are passed to the network for training until the objective function is met (i.e. minimising the error margin).

4. The final network architecture is selected based on the chromosome that gives the minimal error. The network is run a number of times to obtain the best set of weights, which are the model coefficients (layer coefficients) that define a well-trained GMDH-PNN. Each time the network is run, a new set of weights was obtained and replaced the old ones [207].

3.7.2.3   *FCM-ANFIS modelling technique*

Numerous arrangements have been proposed for the establishment of an efficient neuro-fuzzy system, however, the adaptive neuro-fuzzy inference system (ANFIS) technique [257] is one of the best techniques. Modelling with ANFIS uses the combination of both fuzzy logic and a neural network to achieve accurate results. The fuzzy logic algorithm computes the best membership functions that allow the inference system to model the input-output relationship of the data correctly. The membership functions are adjusted (adaptive), based on the structure of the data, using the simulation capability of the neural network. The adaptive nature allows the neuro-fuzzy system to learn from the data that is being modelled.

The ANFIS architecture is divided into the introductory part (which consists of the input, input characteristics and input membership functions) and the concluding part (which consists of the output characteristics, output membership functions and output). The introductory and concluding parts are connected by rules. Notably, ANFIS consists of five major layers, with each layer comprising nodes/neurons that are of the same functional family. The first layer is an adaptive layer in which the fuzzy formation takes place. The second layer consists of fixed nodes, and this is where fuzzy rules are performed. In the third layer, the nodes are fixed and the output of this layer is the normalised membership functions. The fourth layer is made up of adaptive nodes, which perform the concluding part of the fuzzy rules. In the fifth layer, a fixed single node computes the overall network output. More detailed information on ANFIS network architecture can be found in Mehrabi et al. [258, 259].

ANFIS can be generated using either of the following structure identification techniques: fuzzy C-mean clustering, subtractive clustering and grid partitioning. Each of these identification techniques follows the steps of mapping the input variables to the input space partitioning, choosing the appropriate input membership functions, followed by the creation of the fuzzy rules, selecting premises and creating the concluding part of the fuzzy rules, as well as selecting the initial parameters for the membership functions. Figure 3.7 shows a typical structure of the ANFIS modelling technique.
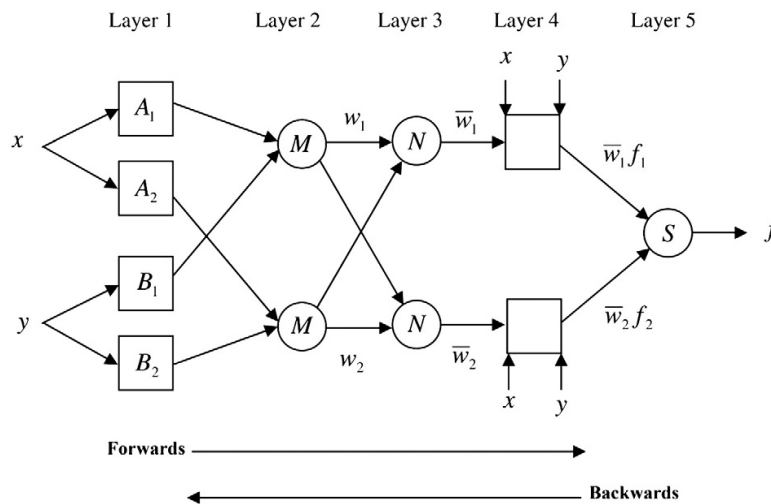
Figure 3.7: ANFIS architecture for a two-input first-order Sugeno fuzzy model with two rules [257].

3.8   CONCLUSION

In this chapter, the materials, equipment, nanofluid preparation and characterisation methodology that are employed in this research have been duly addressed. The experimental procedures for the calibration of the equipment used to measure the thermophysical properties were also discussed. The modelling technique employed in this study are dimensional analysis with regression and computation intelligence, which is implemented using GMDH-NN, GA-PNN and FCM-ANFIS modelling techniques.

CHAPTER 4:   VISCOSITY OF NANOFLUIDS[1, 2, 3, 4]

4.1 INTRODUCTION

Waste heat recovery and cooling are processes that have been integrated into many industrial systems, such as those in the oil and gas, pulp and paper, food, power generation and textile industries. These processes require heat recovery and/or cooling to be mostly performed by means of a flowing fluid. During the past decades, EG, glycerol, water and oil were some of the conventional heat transfer fluids used for this purpose.

Recently, Choi and Eastman [260] used the available modern techniques to produce nanosized materials, which were dispersed in conventional heat transfer fluids, to ultimately produce a nanofluid of Cu in water. This nanofluid has the potential to enhance the heat transfer rate in industrial equipment, thus making industrial heat exchangers more compact.

This will reduce the energy consumption and emission levels (reduced greenhouse gases and global warming potential). However, the addition of nanoparticles to heat transfer fluids increases the viscosity of the fluids, which is why the penalty of pressure drop and increased pump power is still of major concern. Peng et al. [261] established that the

---

This chapter has been published in part as:

[1] S.A. Adio, M. Sharifpur and J.P. Meyer, Investigation into effective viscosity, electrical conductivity and pH of γ-Al$_2$O$_3$-glycerol nanofluids in Einstein concentration regime, *Heat Transfer Engineering*, vol. 36, no. 14–15, pp. 1241–1251, 2015.

[2] S.A. Adio, M. Sharifpur and J.P. Meyer, Influence of ultrasonication energy on the dispersion consistency of Al$_2$O$_3$-glycerol nanofluid based on viscosity data, and model development for the required ultrasonication energy density, *Journal of Experimental Nanoscience*, 2015. Article in press.

[3] S.A. Adio, M. Sharifpur and J.P. Meyer, Combined influenced of size and sonication on constant shear viscosity of MgO-ethylene glycol nanofluids, *Proceedings of the 15th International Heat Transfer Conference,* Kyoto, Japan, paper IHTC15-8606, 10–15 August 2014. DOI: 10.1615/IHTC15.tpp.008606

[4] M. Sharifpur, S.A. Adio and J.P. Meyer, Experimental investigation on the viscosity, electrical conductivity and pH of SiO$_2$-ethylene glycol nanofluids, *Proceeding of the 11th international conference on heat transfer, fluid mechanics and thermodynamics conference (HEFAT2015)*, Kruger National Park, South Africa, pp. 199–204, 20–23 July 2015.

frictional pressure drop of nanorefrigerant (refrigerant-based nanofluid) flowing in a horizontal smooth tube is higher than the base fluid refrigerant, and increases as the volume fraction of the dispersed nanoparticles increases.

In a more recent work by Alawi et al. [262], it was shown that the viscosity and pressure drop of a nanorefrigerant in pipe flow increase with an increase in nanoparticle volume fractions. They also predicted the viscosity of the nanorefrigerant using Brinkman model [43]. However, researchers like Mahbubul et al. [188, 263] and Murshed et al. [5] maintained that the classical models based on Einstein's equation of suspension viscosity, such as the Mooney [49] and Brinkman [43] models that are used in predicting the viscosity of nanofluids, are inapt. Therefore, the rheological behaviour of nanofluids, including viscosity, needs to be evaluated experimentally before implementing them in industrial heat recovery, cooling systems or any other equipment that requires heat transfer fluids for efficient performance.

4.2 CHARACTERISATION AND VISCOSITY OF Al_2O_3-GLYCEROL NANOFLUIDS

Al_2O_3-glycerol nanofluid samples were prepared from the dispersion of three differently sized Al_2O_3 particles in glycerol, and the characterisation of nanoparticles and nanofluids was carried out. The influence of ultrasonication energy density was monitored with viscosity values of the nanofluids, and the optimum value of ultrasonication energy required for proper dispersion (at which point the viscosity is minimised or did not change with dispersion energy) was obtained for every investigated nanofluid type. Therefore, the results presented below are based on uniformly dispersed nanofluid samples.

4.2.1 The characterisation of Al_2O_3 nanoparticles and nanofluids

The results of the characterisation of the Al_2O_3 nanoparticles used in the present work based on TEM imaging are shown in Figure 4.1 (a, b and c). The corresponding size analysis is also as presented in Figure 4.1 (d, e and f). When compared to the physical characteristics of the nanoparticles presented in Table 3.1, the 20-30 nm has an APS of 19 nm; the 80 nm gave an APS of 160 nm (in contrast to the manufacturer's claim) and

77

the 100 nm gave an APS of 139 nm. Hence, the Al_2O_3 size throughout the rest of this thesis will be taken as 19, 139 and 160 nm.
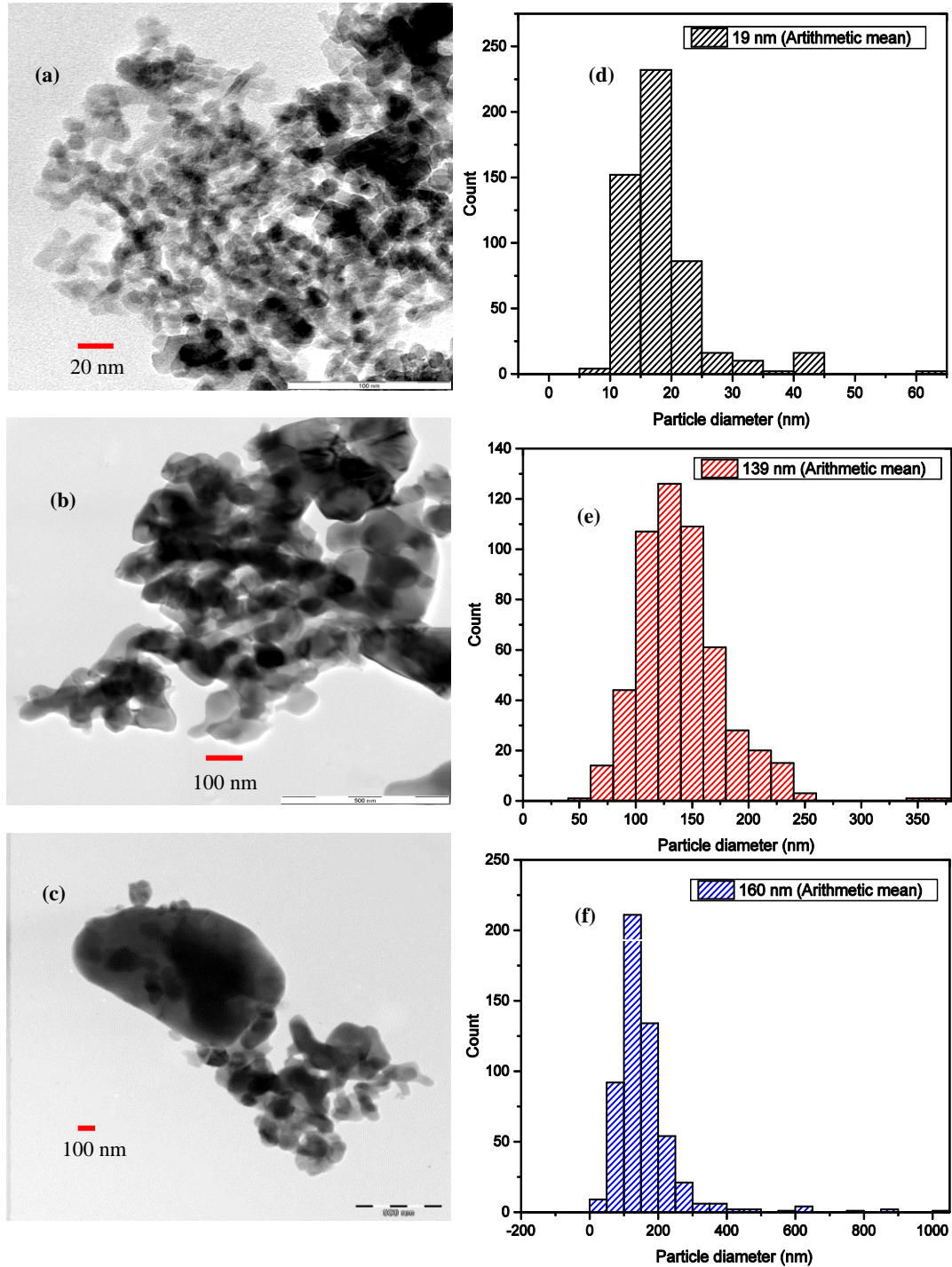
Figure 4.1 TEM image and particle size distribution of Al₂O₃ nanoparticles (a) and (d) 19 nm (b) and (e) 139 nm (c) and (f) 160 nm.

78

In Figure 4.2 (a), the pattern of the XRD peaks was identified as Al_2O_3 with traces of $Al_2(SO_4)_3$, both corresponding to 01-083-2080 and 01-077-0385 file numbers from the Joint Committee on Powder Diffraction Standards (JCPDS). The spectra pattern in Figure 4.2 (a) indicates that the 19 nm sample is in the amorphous phase, while the patterns in Figure 4.2 (b, c) show that the 139 and 160 nm samples are in crystalline form. The peaks also matched Al_2O_3 with traces of $Al_2(SO_4)_3$ (JCPDS file numbers 01-081-2267 and 01-077-0066) for 139 nm and Al_2O_3 (JCPDS file number 90-008-8029) for 160 nm. The black font in the XRD indexing represents Al_2O_3 and the blue font represents $Al_2(SO_4)_3$. The EDS results, which also showed that major components of the nanoparticle samples are aluminium and oxygen, can be found in Appendix A1.

Figure 4.2: XRD pattern for Al_2O_3 nanoparticles: (a) 19 nm; (b) 139 nm; (c) 160 nm. The black font represents corundum and the blue font represents millosevichite.

The UV-visible spectra pattern for all the nanofluids at different volume fractions from 0.01 to 0.035% are presented in Figure 4.3. Very low-volume fractions were chosen for the UV-visible experiment because the absorbance was out of the range for the spectrophotometer at a higher volume fraction. In Figure 4.3 (a, b and c), the Al_2O_3-glycerol 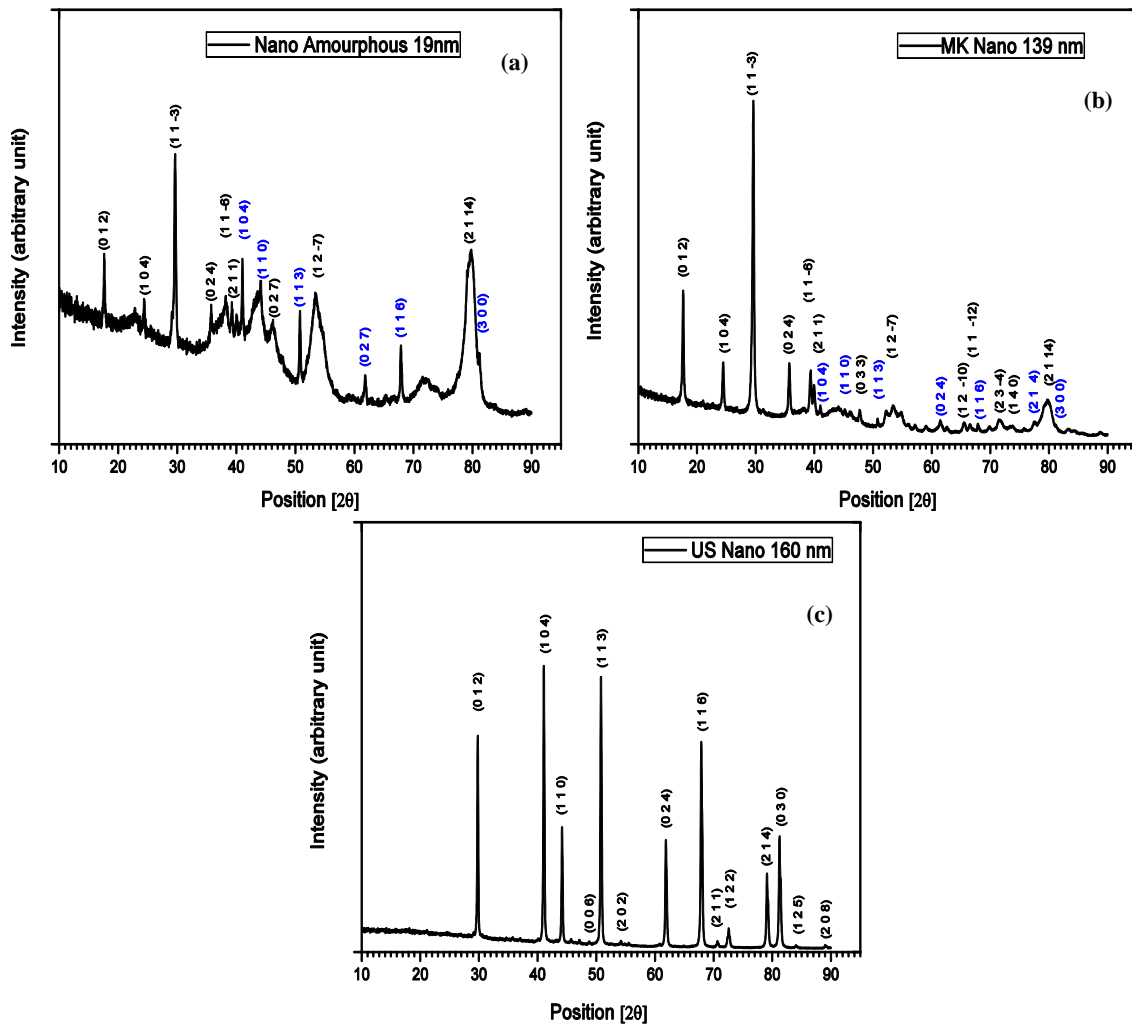nanofluids featured a strong absorption band at around a wavelength of 230 nm, followed by a monotonic decrease in absorbance when increasing the wavelength. The spectra pattern and the strongest peak wavelength corresponds to previous analysis carried out by Piriyawong et al. [264] on Al_2O_3 dispersed in deionised water. In Figure 4.3 (d, e and f), it is clear that the absorbance increases as the nanoparticle concentration increases. It should also be noted that as the absorbance increases by increasing the amount of dispersed Al_2O_3, it shows good dispersion of the nanoparticle in the base fluid as the relationship is linear following Beer's law [244].

The zeta potential characterisation of the Al_2O_3-glycerol nanofluid samples, which shows the level of nanofluid stability, is presented in Table 4.1. The zeta potential values indicate that the Al_2O_3-glycerol nanofluid samples are stable, since the magnitude is greater than 30 mV, which is the threshold of stability of nanofluids [265].

4.2.2 Influence of ultrasonication energy density

The tendency to agglomerate is high when nanofluids are prepared using the two-step method due to the large surface area of nanoparticles. At the beginning of the preparation, this tendency becomes even higher when the base fluid is highly dense and the presence of agglomerates could be seen with the bare eye. The use of an ultrasonication probe has been proven to be effective in deagglomeration, seeing that a strong bonding interaction does not exist between agglomerate particles [266].

As stated in Section 2.3.2, most methods used in studying both nanofluid dispersion and stability are deficient because these methods only take very dilute volume fraction and also dependent on the opacity of the nanoparticle dispersed. The volume fraction studied in this thesis is up to 5% of Al_2O_3 nanoparticles and the available dynamic light scattering (DLS) device takes a maximum volume fraction of 0.05%. As a result, it is difficult to use

the quantitative method of analysis, which is to measure the nanoparticle size (in-situ) as ultrasonication energy is changed.
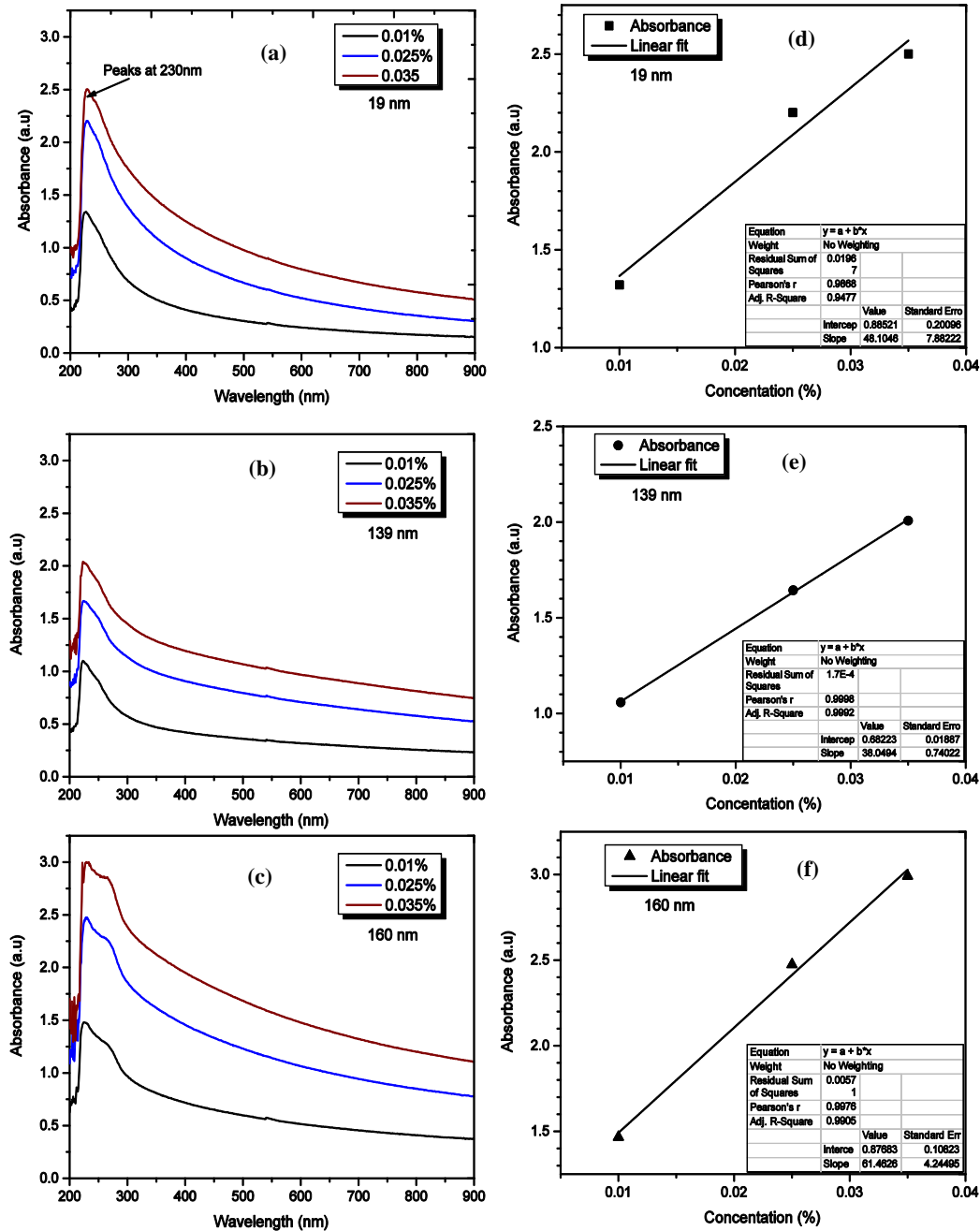

Figure 4.3: UV-visible spectra analysis of Al$_2$O$_3$-glycerol nanofluids: (a, b and c) spectra pattern at different volume fraction and wavelength for 19, 139 and 160 nm respectively; (d, e and f) absorbance of Al$_2$O$_3$ in glycerol at different concentration and 230 nm wavelength for 19, 139 and 160 nm, respectively.

Table 4.1: Zeta potential values for the Al$_2$O$_3$-glycerol nanofluids at 20 $^{\circ}$C

Nanofluid	pH	Zeta potential (mV)
19 nm Al$_2$O$_3$-glycerol	6.44	-504.33
139 nm Al$_2$O$_3$-glycerol	4.09	-79.43
160 nm Al$_2$O$_3$-glycerol	6.26	-243.67

Good dispersion is vital for the achievement of satisfactory nanofluid stability and reduced viscosity. An increase in ultrasonication time/energy has been shown to reduce the size of agglomerates, increase the thermal conductivity and reduce the viscosity as a result of uniform dispersion [89]. Since this experiment is performed on different particle sizes and all the volume fractions investigated are much higher than the DLS device can handle, viscosity values were used to estimate the minimum ultrasonication energy density required for obtaining consistency in the dispersion of nanofluids. This will allow for the determination of minimum ultrasonication energy required for the proper dispersion of the nanoparticles in the base fluid [83].

In Figure 4.4, 19 nm particles became well dispersed in glycerol during a six-hour sonication period (corresponding to 3.0×10^7 kJ/m^3). The trend was repeated for the entire volume fraction investigated on this nanoparticle. However, for the 139 and 160 nm particles, the optimised time for ultrasonication is generally around three hours (corresponding to 1.5×10^7 kJ/m^3) because prolonged ultrasonication beyond this time caused a noticeable increase in the viscosity of the nanofluid samples. The prolonged ultrasonication period led to the coalescence of the particles to reform loose aggregates that allow the entrapment of fluid and cause viscosity increment. This fact has been reported previously [55, 88, 267].

4.2.3 Influence of temperature

In order to highlight the effect of temperature on the effective viscosity of the nanofluid samples, the measured effective viscosities at various volume fractions have been plotted against temperature in Figure 4.5. The effective viscosity of the nanofluids decreases as the temperature increases, with a decreasing slope and displayed asymptotic feature. The

82

trend of the curves is similar in all cases across all particle sizes and volume fractions. In Figure 4.5, the curve of the viscosity of pure glycerol is provided for comparison and it is noticed that the difference between the effective viscosity of the nanofluid and that of pure glycerol reduces as the temperature increases. This is primarily due to the influence of temperature in the weakening of the intermolecular bonding, which drastically reduced the shear resistance of the nanofluid samples.
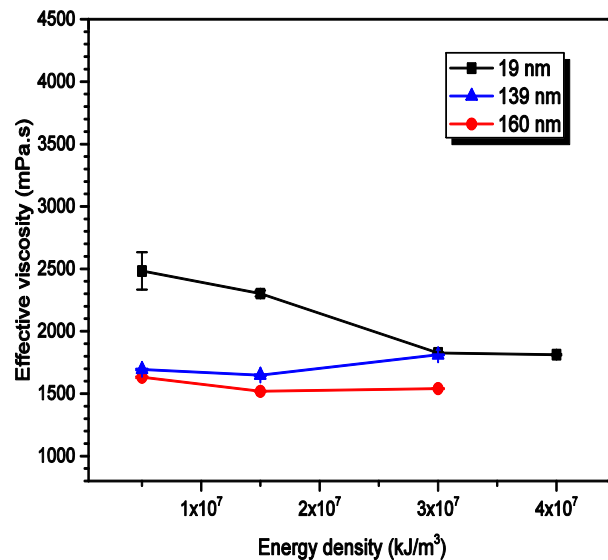
Figure 4.4: The effect of ultrasonication time on effective viscosity at 3% volume fraction.

The relative viscosity of Al_2O_3-glycerol nanofluids at different volume fractions as a function of the working temperature is presented in Figure 4.6. It can be noted that, irrespective of the nanoparticle volume fraction, the relative viscosity was almost constant across the temperature regime. This has an exception for the case of the 5% volume fraction of a 19 nm sample, which can be attributed to the increase in particle-particle interactions at a higher volume fraction. It is noteworthy that the number density of particles present at 5% of 19 nm is much more than 5% of 139 nm, as well as 5% of 160 nm. Therefore, the observed deviation is the cumulative effect of small particle size, effective volume fraction and increased Brownian motion at higher working temperatures. Similar results regarding the behaviour of the relative viscosity of other nanofluids with respect to temperature increase have previously been reported [90, 95, 268].
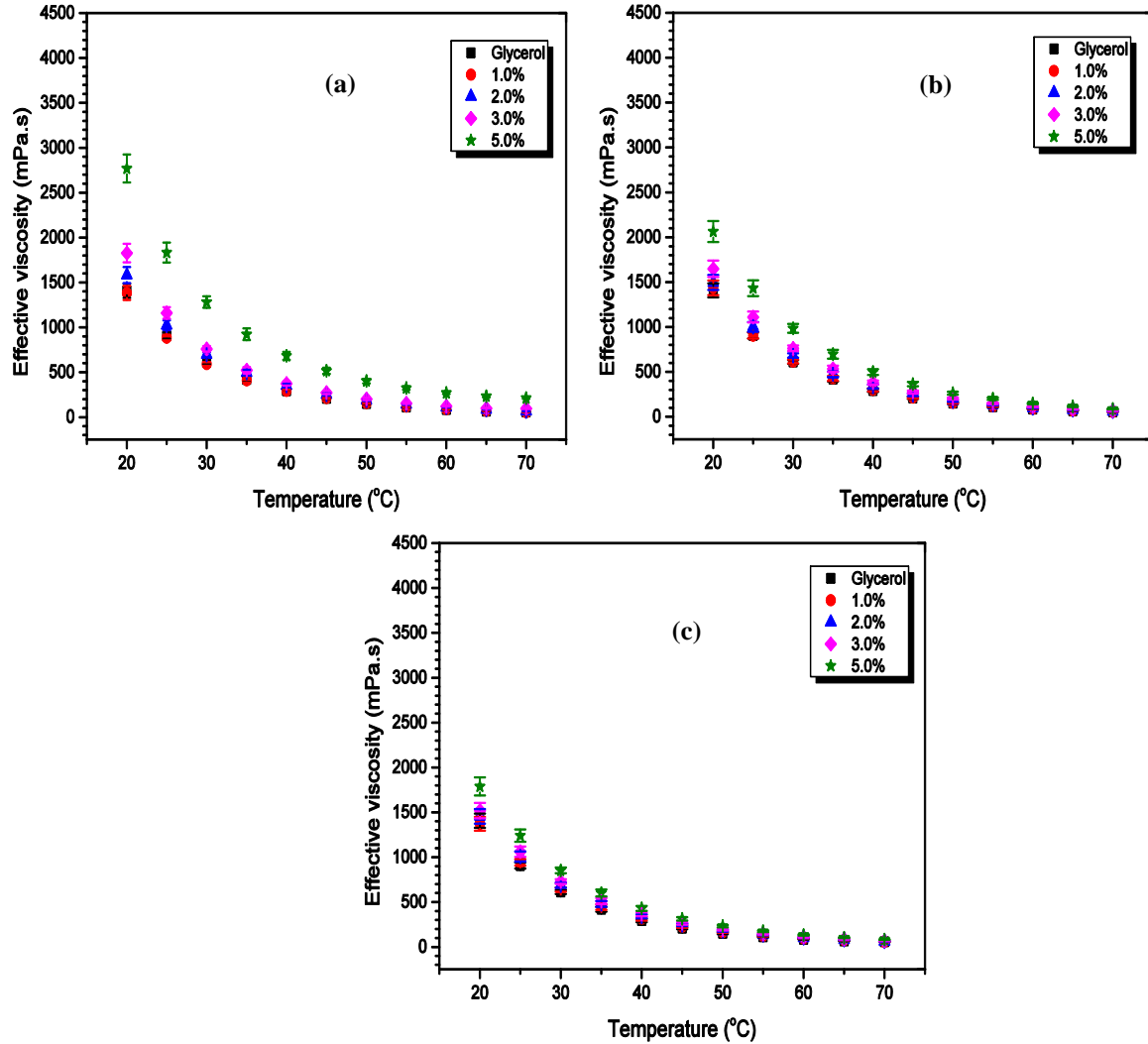
Figure 4.5: The dependence of the effective viscosity of Al₂O₃-glycerol nanofluids on temperature: (a) 19 nm; (b) 139 nm; (c) 160 nm.

84
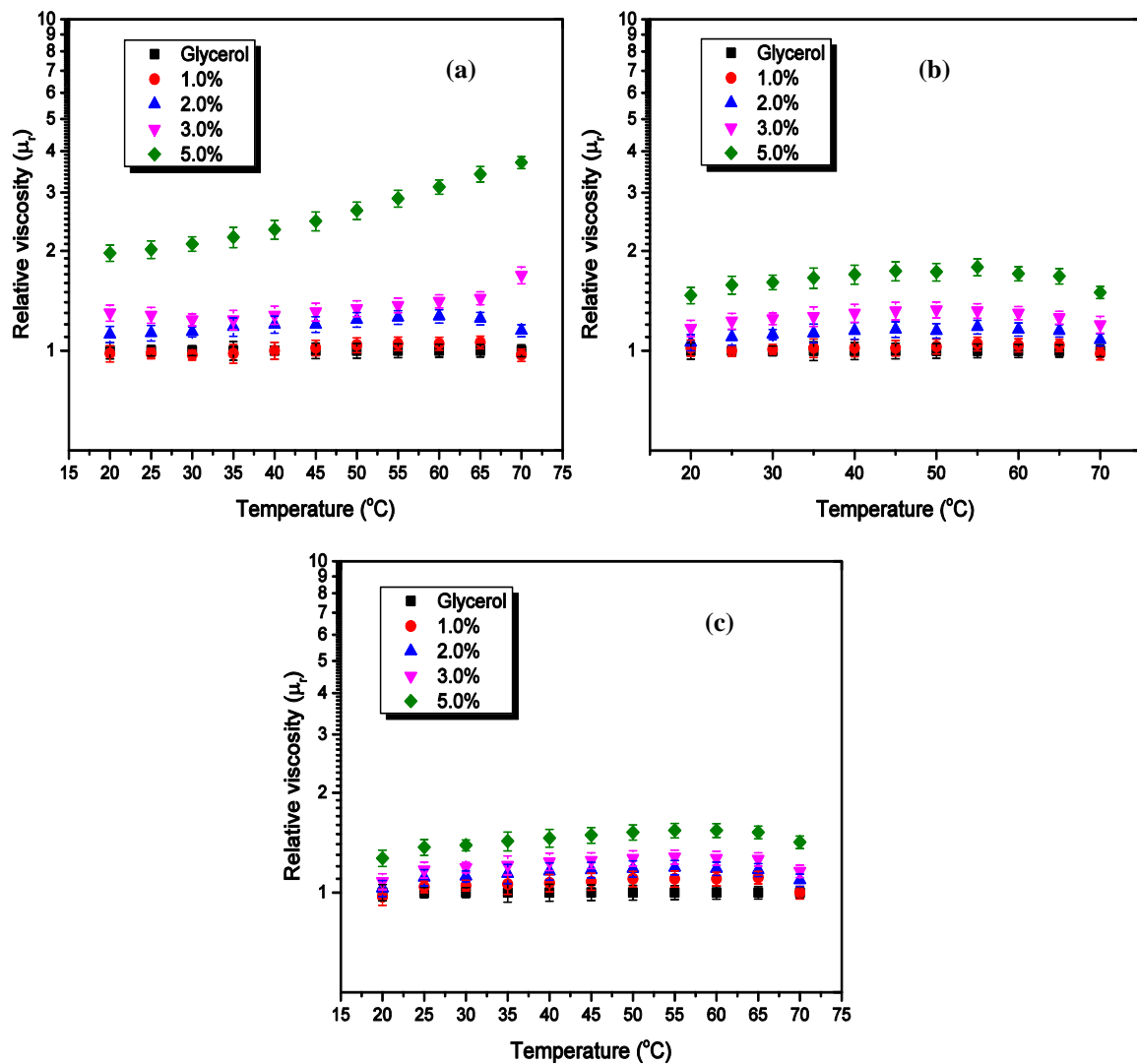
Figure 4.6: Normalised viscosity of Al$_2$O$_3$-glycerol nanofluids with varying volume fraction at different temperatures: (a) 19 nm; (b) 139 nm; (c) 160 nm.

4.2.4 Influence of Al$_2$O$_3$ concentration and size on the dispersion viscosity

The addition of nanoparticles into the base fluid and its influence on the viscosity has been previously studied [96, 246, 269]. These studies have shown that, among other influencing parameters, the addition of particles to base fluid considerably affects the suspension viscosity. An increase in particle concentration brings about an increase in suspension viscosity and the percentage increase depends on factors such as type of particle, base fluids and the size of particles, to mention a few. At a given volume concentration, the Brownian

85

theory confirms that the smaller size particles may translate to an increase in Brownian velocity and particle-particle interactions. This will step up the energy dissipation during the process due to first and second electroviscous effects, which cause the increase in viscosity [124, 197]. Therefore, in suspensions prepared with small particles, the viscosity is higher than suspensions with bigger particles because the particle number density is higher in suspension with smaller nanoparticles [198]. Figure 4.7 displays a steady increase in the relative viscosity as the volume fraction is increased in all the samples of the nanofluids. The highest value was observed in the smallest particle size and vice versa.
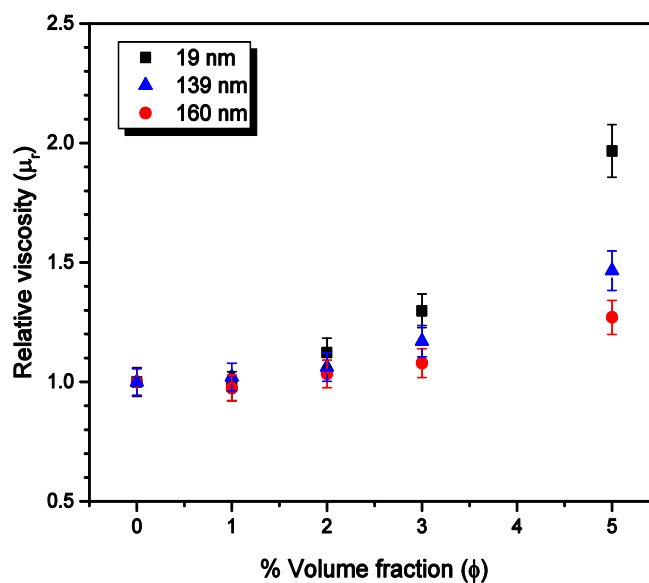
Figure 4.7: The influence of nanoparticle volume fraction on the relative viscosity of Al$_2$O$_3$-glycerol nanofluids.

4.3 CHARACTERISATION AND VISCOSITY OF MgO-EG NANOFLUIDS

The MgO-EG nanofluids were prepared from the three different sizes of MgO nanoparticles as presented in Table 3.1. The nanoparticles and nanofluids were characterised to confirm the particle size, morphology and dispersion state. The influence of ultrasonication energy density was monitored with viscosity values of the nanofluids and the optimum value of ultrasonication energy required for proper dispersion was obtained just as was described in Section 4.2. Therefore, the results presented below are based on uniformly dispersed nanofluid samples.

86

4.3.1   MgO nanoparticles and nanofluids characterisation

The results of the TEM capture of MgO nanoparticles and the corresponding size analysis based on the TEM are presented in Figure 4.8. The measured APS is ~20, ~125 and ~100 nm as against the manufacturer values of 20, 40 and 100 nm respectively. The nanoparticles' morphology is polyhedral, which corresponds with the manufacturer's estimation and is presented in Figure 4.8 (a to c). In Figure 4.8 (d and e), the size distribution of the nanoparticle is representative of the manufacturer's quoted size. On the contrary, Figure 4.8 (f) represents MgO nanoparticles with an APS of approximately 125 nm as against the 40 nm estimated by the manufacturer. The scale bar in Figure 4.8 (c) further supports this observation. Therefore, the estimated TEM size will be taken as the size of the nanoparticles.

Figure 4.9 (a) represents the XRD patterns of all the MgO nanoparticles presented in 3D. The prominent peaks of the patterns are identified with Periclase structure (MgO) from the JCPDS record, having database pdf numbers of 01-087-0651 for 20 and 125 nm MgO, and 01-078-0430 for 100 nm MgO. The peaks' hkl lattice parameters show that the MgO has a cubic crystal lattice system with an Fm3-fm spacing group that corresponds with previously published results [270]. Other peaks identified with the shaded circles in Figure 4.9 (a) correspond to Brucite $(Mg[OH]_2)$ (pdf number 01-083-0114) and were found in the diffraction patterns of 20 and 125 nm with hexagonal structure. The EDS graphs of all the nanoparticle samples also affirm that major components of the samples are magnesium and oxygen, as shown in Figure 4.9 (b to d). When the XRD patterns were compared with those provided by the manufacturers (not shown here), they gave good agreement with a 5 to 10° shift in 2-theta position in the present experiment due to the different X-ray sources used (present experiment: cobalt with $\lambda = 0.1789$ nm; manufacturer: copper with $\lambda = 0.159$ nm were used).

Figure 4.10 shows the UV-visible spectra for the MgO-EG nanofluids at different particle concentrations. The spectra patterns show maximum absorption at about 260 nm. As seen in Figure 4.10 (a, b and c), the spectra patterns are similar, but the absorbance value at a given wavelength increases as the MgO nanoparticle concentration increases. The plots between absorbance and MgO concentration at 260 nm, as presented in Figure 4.10 (d, e

and f), show that the absorbance depends linearly on the MgO nanoparticle concentration, and the data obeyed Beer's Law, as described for Al_2O_3-glycerol in section 4.2.1.
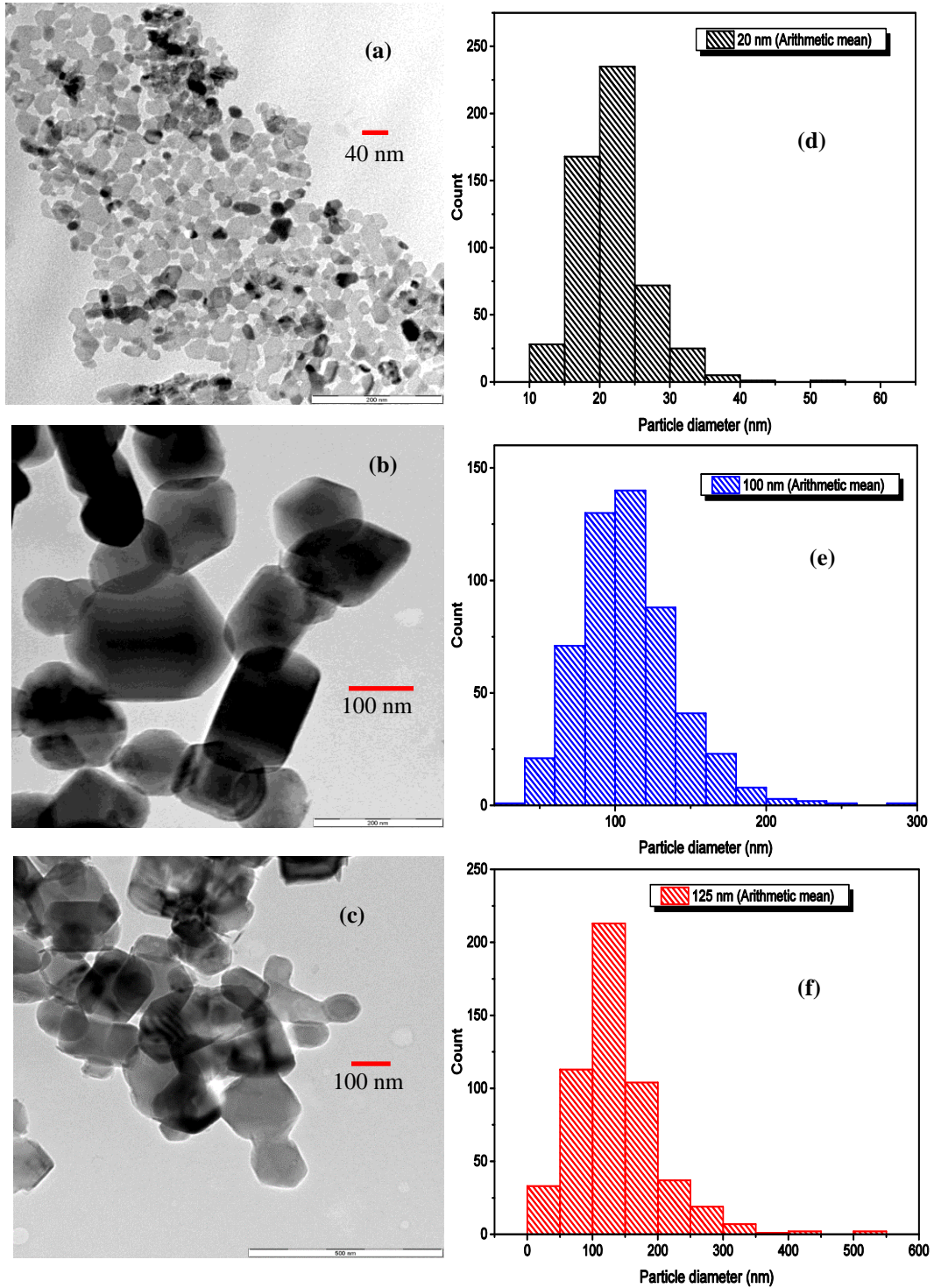
Figure 4.8: TEM image of MgO and PSD: (a and d) 20 nm; (b and e) 100 nm; (c and f) 125 nm.

88
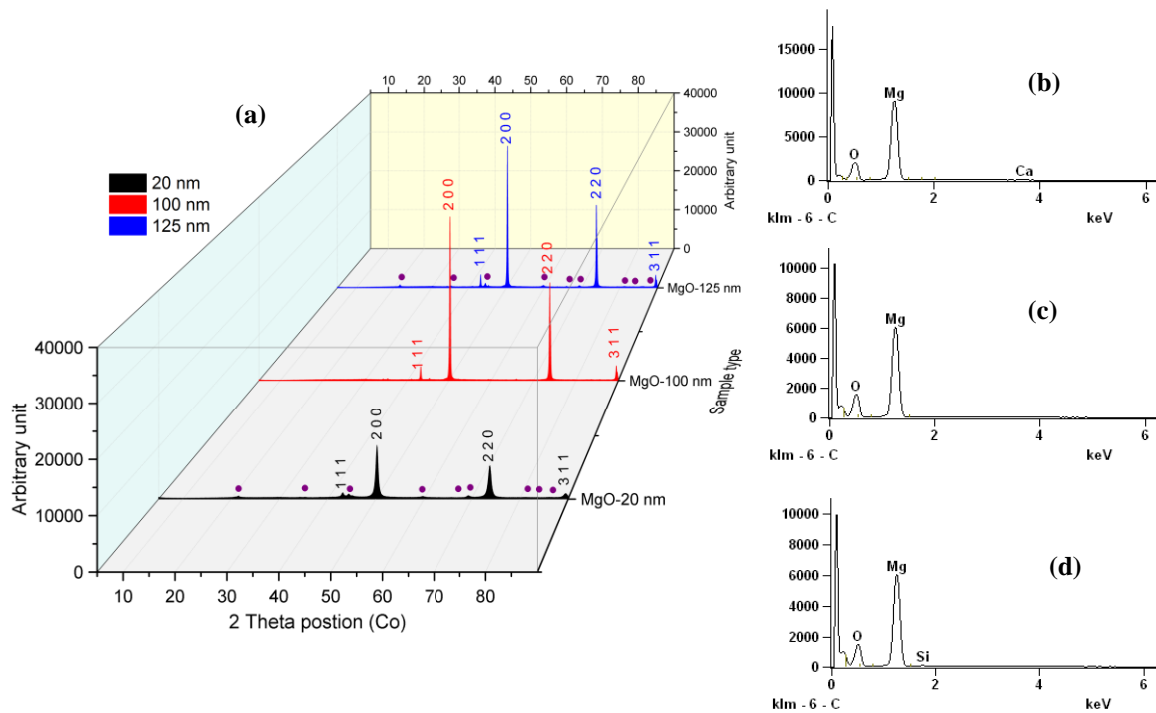
Figure 4.9: XRD and EDS spectra patterns of MgO nanoparticles: (a) XRD spectra of MgO-EG nanofluids; (b, c and d) EDS spectra of 125, 100 and 20 nm MgO respectively.

A nanofluid sample with zeta potential value (absolute value) greater than or equal to the threshold ($\pm$30 mV) is considered stable [265]. The zeta potential of all MgO-EG nanofluid samples in the present experiment is above the threshold without modifying their pH values. Here, zeta potential values of 38.5, 46.5 and 30.3 mV were recorded for 20, 100 and 125 nm, respectively. For the sake of studying the influence of change in pH on zeta potential, the pH of the samples was adjusted using 0.5 M KOH and/or HCl before the measurement was made with at least four repeated measurements. The average of the repeated measurement was taken as the measured value. Figure 4.11 shows the zeta potential behaviour of the nanofluids at different pH values. The inset was taken five days after preparation and it can be seen that the samples used in this experiment are stable as there was little or no sedimentation, even without pH modification or surfactant addition.
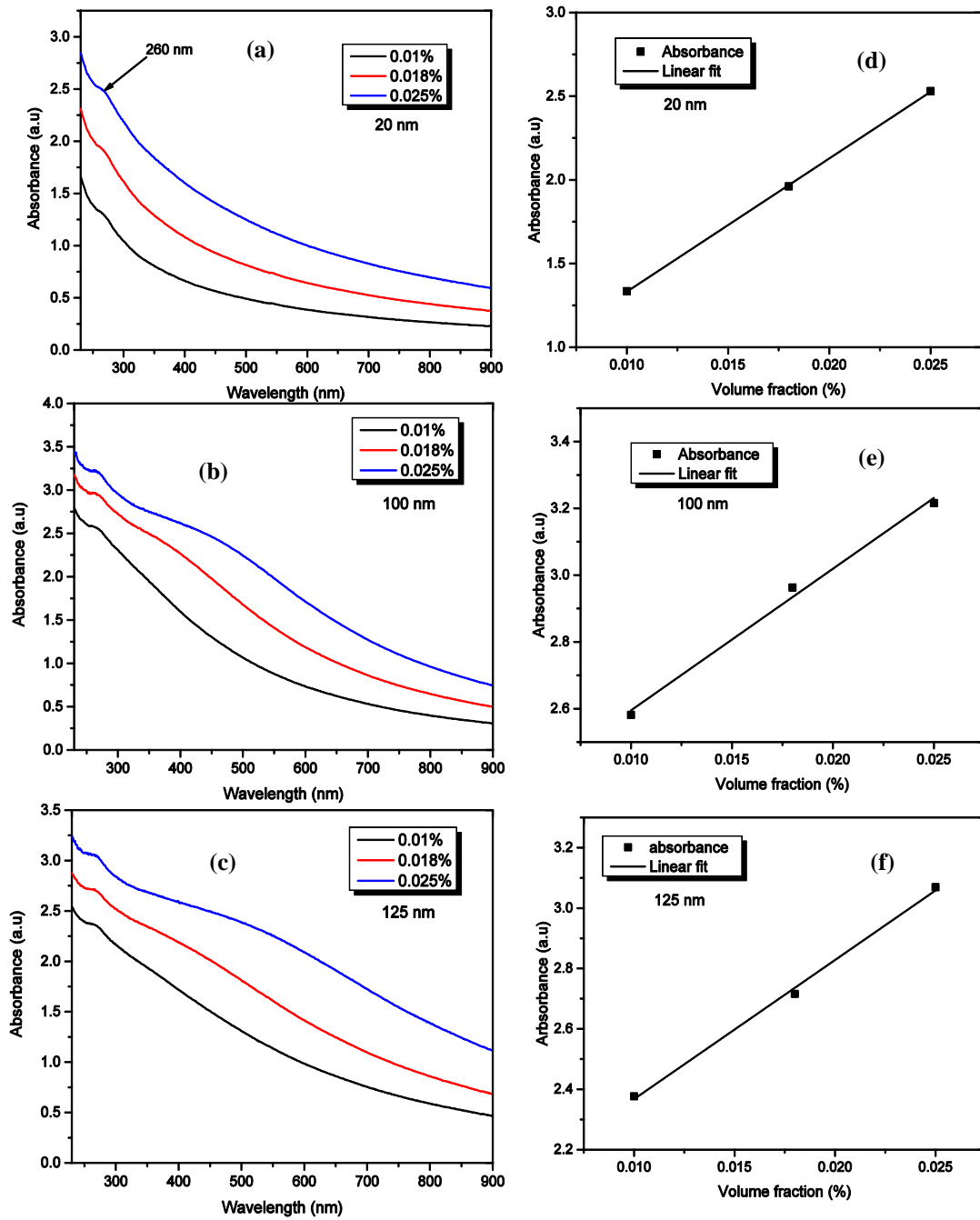
Figure 4.10: UV-visible of MgO-EG nanofluid at different concentration: (a to c) UV-visible spectra between 230 and 900 nm; (d to f) relationships between the absorbance and concentration of the nanofluid at 260 nm.
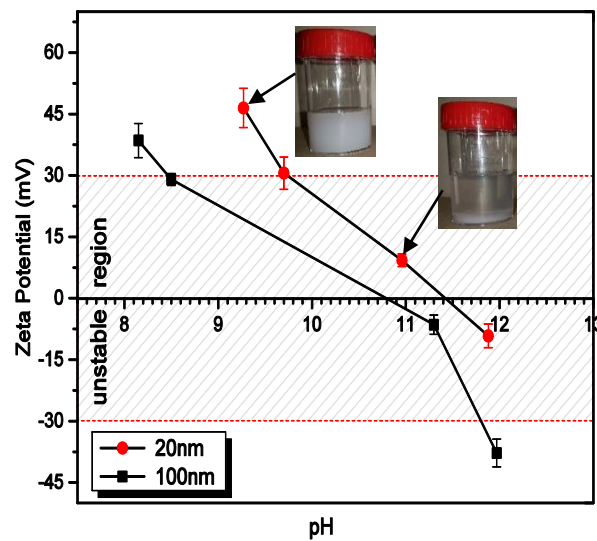
Figure 4.11: The influence of change in pH on the zeta potential of MgO-EG nanofluid.

4.3.2   The influence of ultrasonication energy density

Presented in Figure 4.12 is the plots of the effective viscosity against the energy density applied for the preparation of the MgO-EG nanofluids at 3% MgO volume fraction. The result shows that at 4.364×10^6 kJ/m^3 energy density, the nanofluid samples are all uniformly dispersed (corresponding to 60 minutes of ultrasonication time). Similar trends were obtained for other volume fractions, except the volume fractions 0.1% and 0.5% that were uniformly homogenised at an energy density of 2.183×10^6 kJ/m^3, which is due to the very small fraction of the nanoparticles present. Therefore, other results presented on these nanofluids will be based on the uniformly homogenised nanofluids prepared using the optimum energy density of 4.364×10^6 kJ/m^3. Xie et al. [246] applied ultrasonication for three hours to disperse 20 nm of MgO in EG for a volume fraction up to 5%. Comparing their results with the results obtained for 20 nm of MgO in the present investigation gave good agreement as shown in Figure 4.13. While the energy density applied in their experiment was not mentioned and no data was provided for possible recalculation of their energy input, they applied ultrasonication using three times the period of ultrasonication of the homogenised samples in the present work. Therefore, selecting a predefined value of time for nanofluid preparation, especially in the two-step

method, is counterproductive regarding the energy and time input into the preparation process.
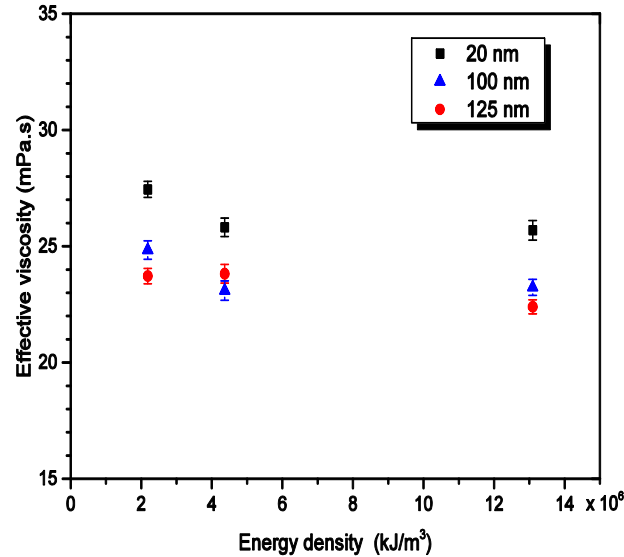
Figure 4.12: The effect of energy density on the viscosity of MgO-EG nanofluids.
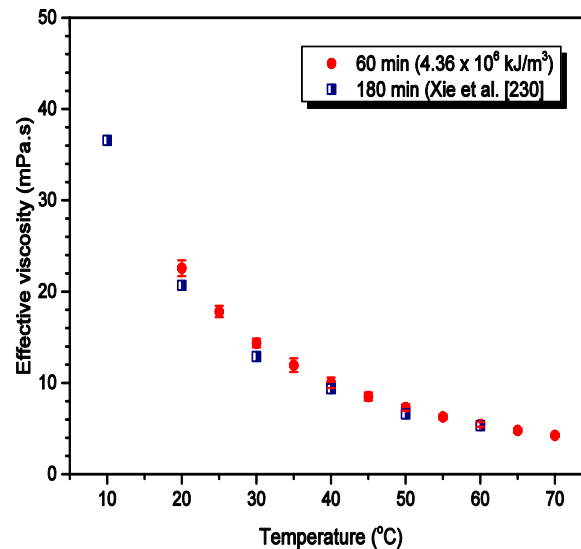
Figure 4.13: Comparison between the present experimental data with Xie et al. [246] at 1% volume fraction.

4.3.3 The influence of temperature

The effective viscosity of the MgO-EG samples decreases exponentially with increasing temperature as presented in Figure 4.14. At all the volume fractions, and irrespective of the particle size, the temperature dependence of the effective viscosity of the MgO-EG

nanofluids is similar to the dependence exhibited by the base fluid. However, the viscosity of the nanofluid is higher depending on the concentration of MgO contained in the nanofluid. At high temperatures (50 to 70°C), the change in effective viscosity from one volume fraction to the other reduces as overlaps of data points were obvious. This is primarily due to the increase in the influence of temperature in the weakening of the intermolecular bonding, which drastically reduced the shear resistance of the nanofluids. Interestingly, the relative viscosity, when plotted against the working temperature for all volume fractions and nanoparticle sizes, presented nearly a flat line, indicating not much change in relative viscosity with temperature (Figure 4.15).
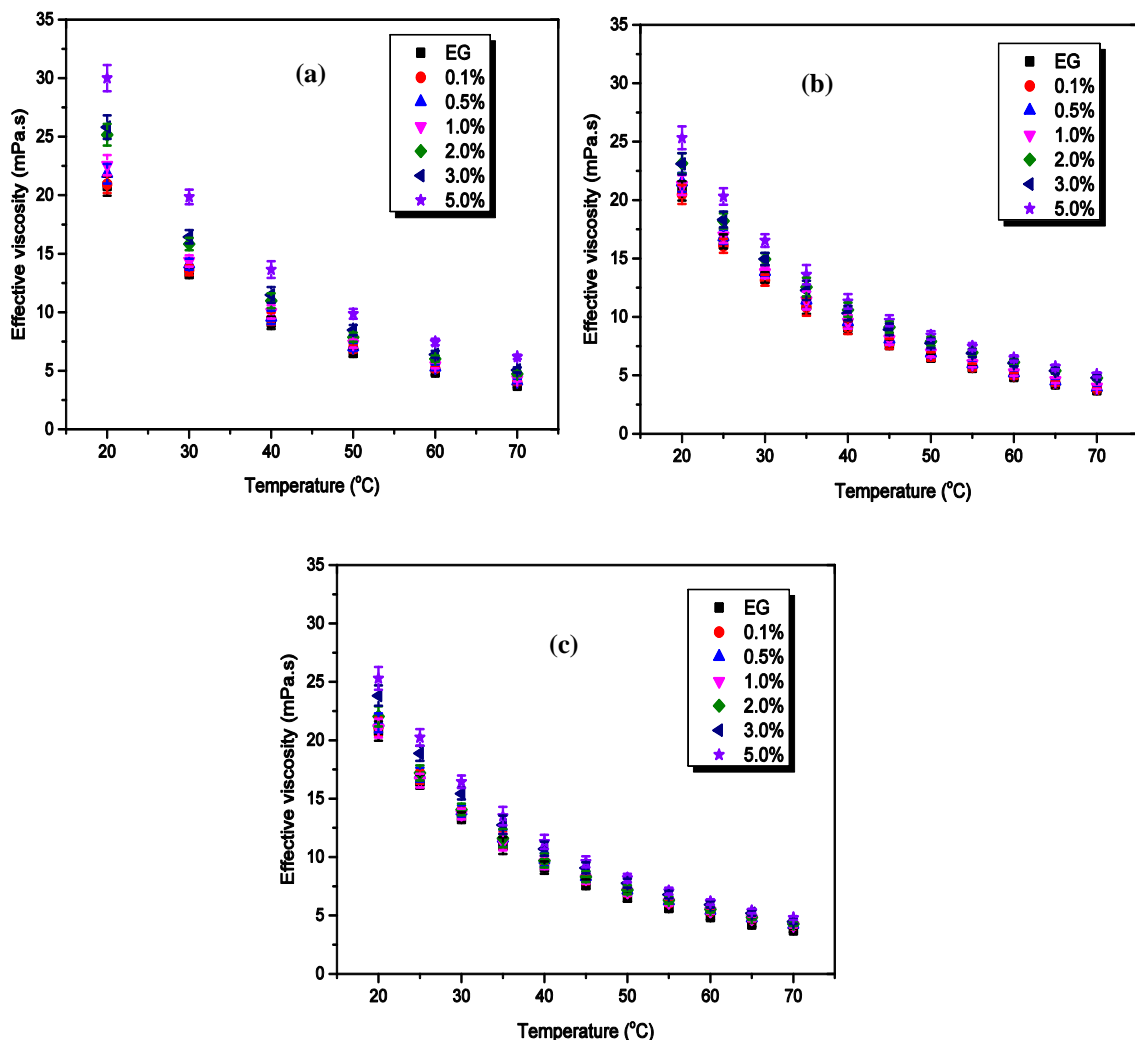
Figure 4.14: The effect of temperature on the effective viscosity at various volume fractions: (a) 20 nm; (b) 100 nm; (c) 125 nm.

93
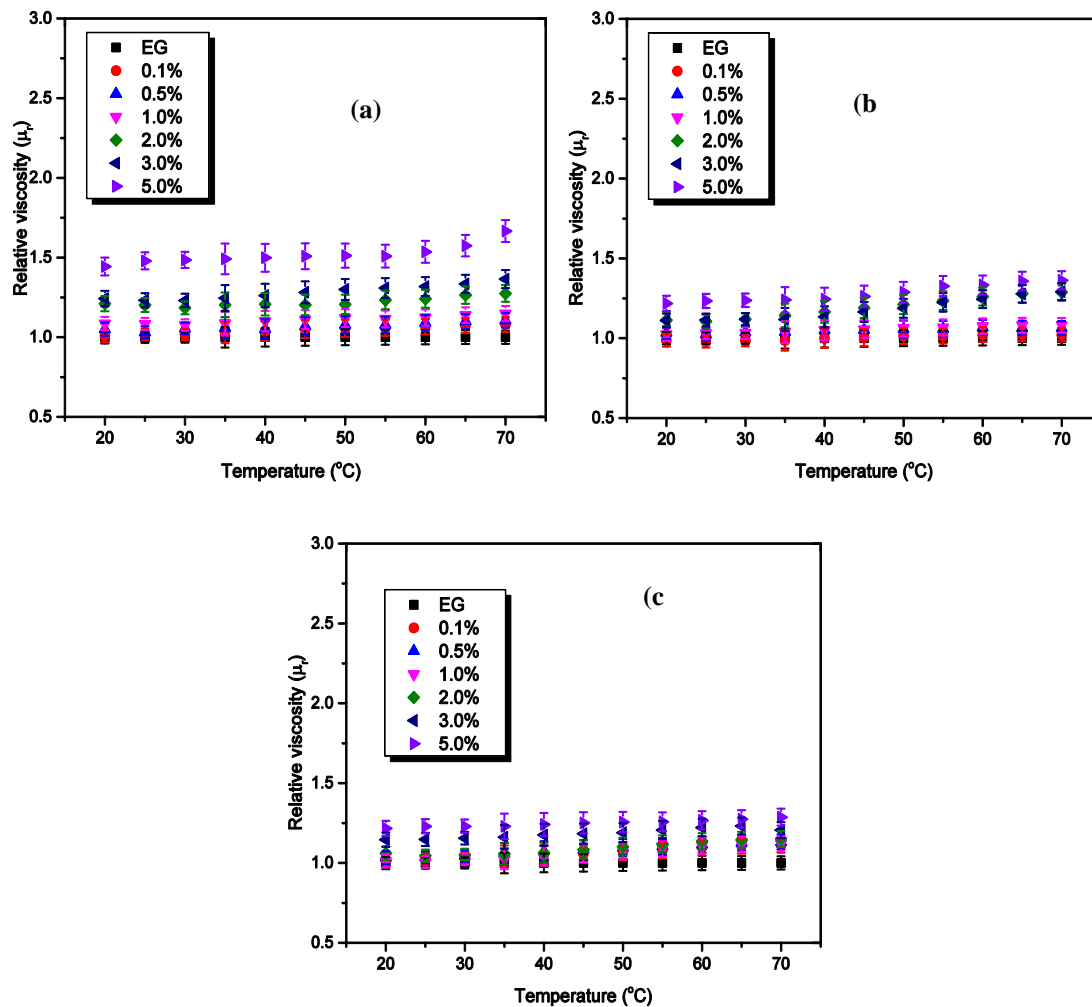
Figure 4.15: Nanofluid relative viscosity at various temperatures: (a) 20 nm; (b) 100 nm; (c) 125 nm.

4.3.4   Influence of volume fraction and particle size of MgO

The dispersion of MgO nanoparticles into the base fluid shows that the viscosity of the resulting fluid is higher than that of the ordinary base fluid as presented in Figure 4.16. Having nanoparticles suspended in the base fluid leads to shear resistance of the nanoparticles on the base fluid layers, and increasing the volume concentration gives a corresponding increase in the shear resistance, which is relative to the viscosity of the nanofluid. Therefore, the higher the volume fraction, the greater the viscosity enhancement of the nanofluid. The 20 nm samples displayed the highest effective viscosity when compared to the 100 and 125 nm samples, because of their smaller size. At the same volume fraction, a smaller particle

94

size translates into a higher number density of particles present in the suspension, thereby increasing the effective volume fraction [77]. This trend is similar to the results of Al_2O_3-glycerol nanofluids discussed in Section 4.2.4. Also obvious in Figure 4.16 is the level of harmony in the relative viscosity of 100 and 125 nm samples for all volume fractions. This is basically a function of their nanoparticle sizes. From the size analysis presented in Figure 4.8, the sizes of 100 and 125 nm MgO are of the same order of magnitude. Unlike the results on Al_2O_3-glycerol nanofluid (Figure 4.7), the relative viscosity of the MgO-EG nanofluid appears to increase linearly with volume fraction increase.
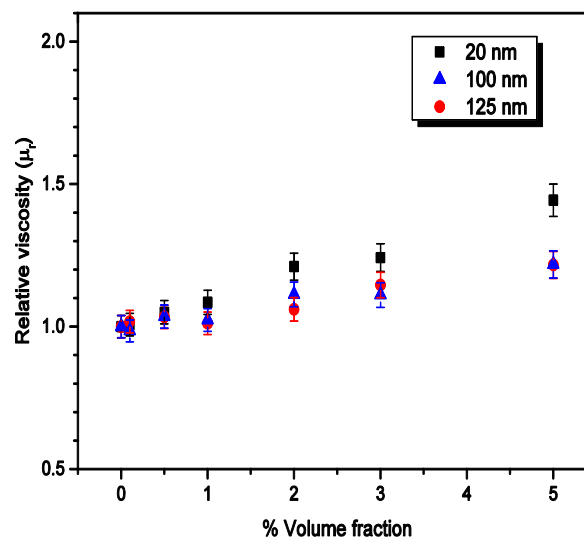
Figure 4.16: The influence of nanoparticle volume fraction on the relative viscosity of MgO-EG nanofluids.

4.4 CHARACTERISATION AND VISCOSITY OF SiO₂-GLYCEROL AND SiO₂-EG NANOFLUIDS

The same procedure applied in sections 4.2 and 4.3 for determining the best homogenised nanofluid was also applied to the SiO₂-glycerol and SiO₂-EG nanofluids. Therefore, the results presented in this section are based on the well-homogenised nanofluids of SiO₂-glycerol and SiO₂-EG.

4.4.1 SiO₂ nanoparticle and nanofluid characterisation

The result of the TEM capture for SiO₂ nanoparticles and the corresponding size analysis based on the TEM is presented in Figure 4.17 (a). The measured APS is ~15 nm as against

the manufacturer's value of 20 nm (Figure 4.17 (b)) and the morphology of the nanoparticles is roughly spherical. Figure 4.18 (a) represents the XRD patterns of the SiO_2 nanoparticles used in this work. The spectra pattern shows that the SiO_2 nanoparticles are in the amorphous phase and correspond to the result of XRD from the manufacturer as shown in Figure 4.18 (b).
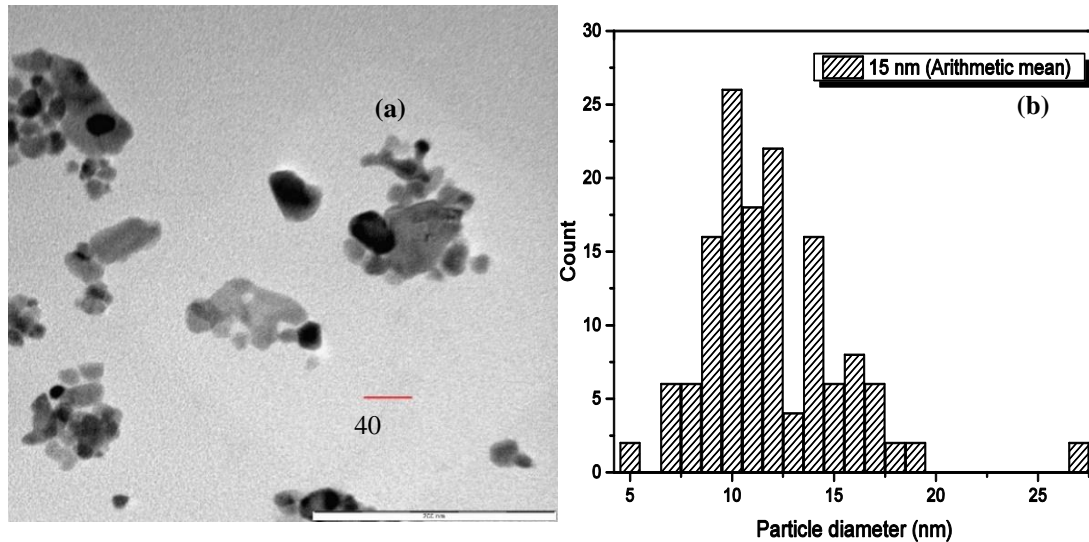
Figure 4.17: TEM and size analyses of SiO$_2$ nanoparticles.
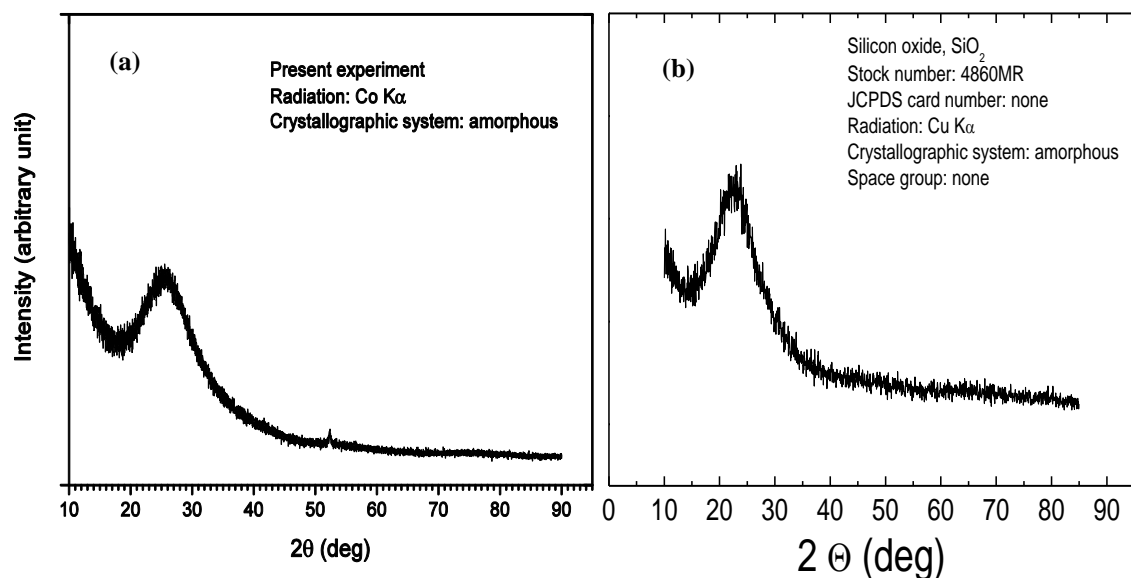
Figure 4.18: XRD pattern for SiO$_2$ nanoparticles: (a) present experiment; (b) manufacturer's result.

96

The result of the UV-visible analyses of both the SiO_2-glycerol and SiO_2-EG nanofluids is presented in Figure 4.19. Figure 4.19 (a and b) shows the UV-visible spectra at different particle concentrations for the SiO_2-glycerol and SiO_2-EG nanofluids respectively. The spectra patterns show maximum absorption at about 266 nm. As seen in Figure 4.19 (a and b), the spectra patterns are similar, but the absorbance value at a given wavelength increases with an increase of SiO_2 nanoparticle concentration.

The spectra structure and absorbance value is also different in the two nanofluids due to the different base fluids. The plots between absorbance and SiO_2 nanoparticle concentration at 266 nm, as presented in Figure 4.19 (c and d), show that the absorbance depends linearly on the SiO_2 nanoparticle concentration, and the data obeyed Beer's Law. The zeta potential characterisation for both SiO_2-glycerol and SiO_2-EG nanofluids gave -315.33 and -21.23 mV respectively. The implication of these results is that the SiO_2-glycerol nanofluid is more stable than the SiO_2-EG nanofluid. It should be noted that the nanofluid samples are stable throughout the course of the experimental investigations.

4.4.2   Influence of temperature

The effective viscosity of both the SiO_2-glycerol and SiO_2-EG nanofluids decrease exponentially as the temperature increases, as presented in Figure 4.20. For all the volume fractions investigated, the temperature dependence of the effective viscosity of the nanofluids is similar to the base fluid's dependence. At higher temperatures, the gaps between the different samples seemed to have reduced due to the influence of the temperature increase breaking down the intermolecular bonding between the fluid molecules. This is also similar to the patterns exhibited by nanofluids of Al_2O_3 and MgO, as explained in sections 4.2.3 and 4.3.3.

4.4.3   Influence of volume fraction

The influence of suspending a SiO_2 nanoparticle and changing its volume fraction on SiO_2-EG and SiO_2-glycerol nanofluids is presented in Figure 4.21. The dispersion of SiO_2 nanoparticles into the base fluids resulted in the nanofluids having a higher viscosity than the ordinary base fluids, as shown in the relative viscosity plot presented in Figure 4.21. The higher the volume fraction of the SiO_2 nanoparticle, the greater the viscosity value.

97

This trend is similar in both nanofluids. Generally, the results are similar to the results of the other nanofluids reported in sections 4.2.4 and 4.3.4.
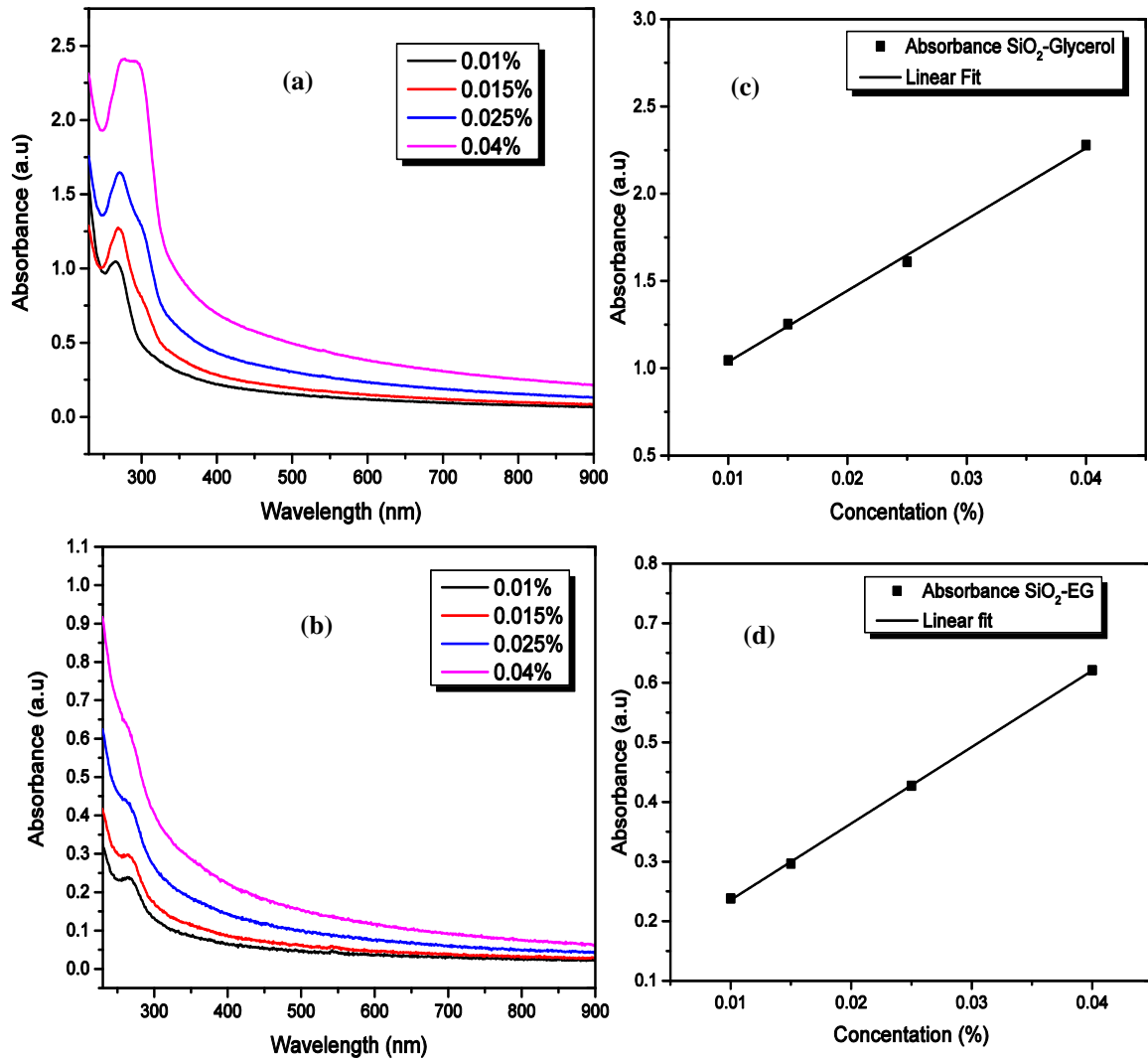
Figure 4.19: UV-visible of SiO$_2$-glycerol and SiO$_2$-EG nanofluids at different concentrations: (a and b) UV-visible spectra between 230 and 900 nm for SiO$_2$-glycerol and SiO$_2$-EG nanofluids respectively; (c and d) relationship between the absorbance and concentration of the nanofluids at 266 nm.
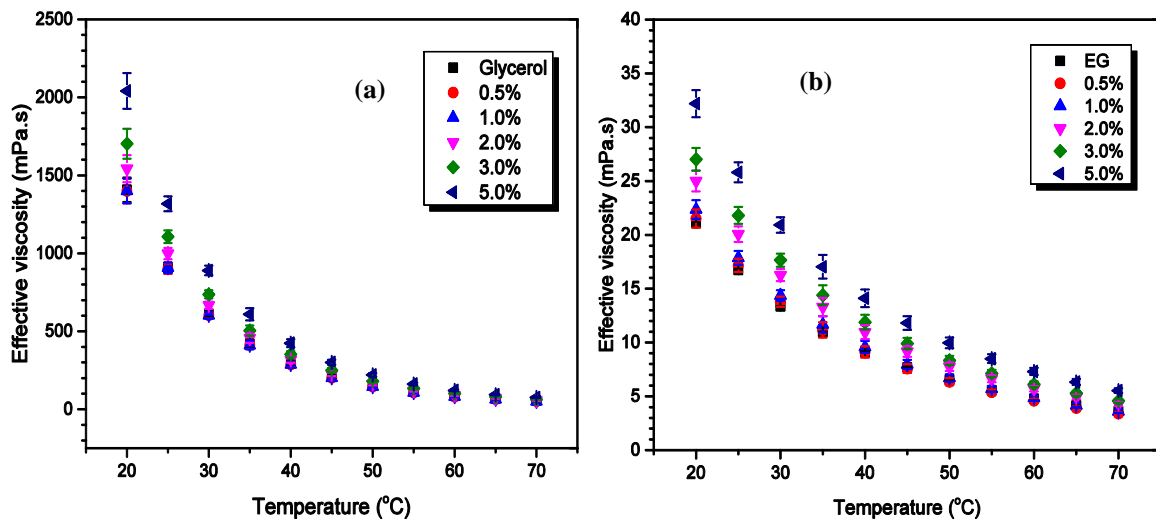
Figure 4.20: The effect of temperature on the effective viscosity at various volume fractions: (a) SiO$_2$-glycerol nanofluid; (b) SiO$_2$-EG nanofluid.
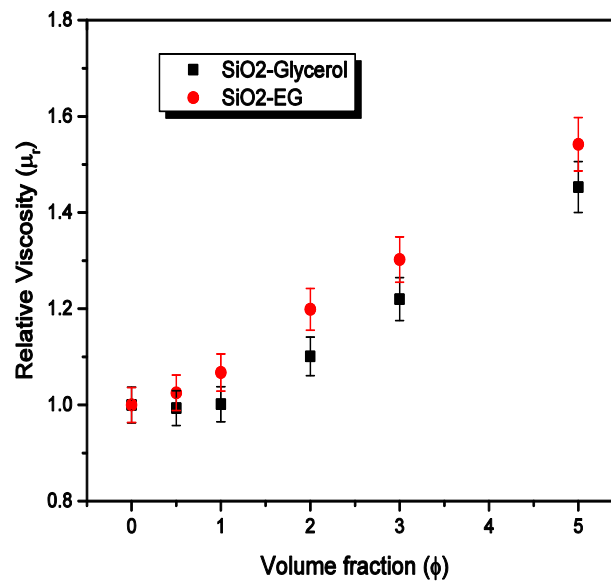
Figure 4.21: The influence of nanoparticle volume fraction on the relative viscosity of SiO$_2$-glycerol and SiO$_2$-EG nanofluids.

4.5 THE EFFECT OF DIFFERENT BASE FLUIDS ON VISCOSITY ENHANCEMENT

Different base fluids possess unique physical and chemical properties, which is why their performance as heat transfer fluids varies. The investigation of the influence of different

99

base fluids on the viscosity of nanofluids was carried out using SiO_2-glycerol and SiO_2-EG nanofluids and the result is presented in Figure 4.21 above. Although, the same trend was observed for the relative viscosity of both nanofluids, the relative viscosity of the SiO_2-EG nanofluid is higher than that of the SiO_2-glycerol nanofluid. Since, the same nanoparticle sample is used in the two base fluids, it is evident that the base fluid characteristics also contribute significantly to the nanofluids' thermophysical properties. A similar result was presented by Syam Sundar et al. [178] on Fe_3O_4 and different EG-water binary mixtures. EG possesses a lower density compared to glycerol. It is believed that the particle-particle interaction and Brownian motion will be more intense in an EG base fluid than glycerol, which explains the higher enhancement observed in the SiO_2-EG nanofluid.

4.6 THE EFFECT OF DIFFERENT NANOPARTICLES ON VISCOSITY ENHANCEMENT

To determine whether the influence of different nanoparticles on the viscosity enhancement of nanofluids is significant, different nanoparticle types of a similar size were dispersed in the same base fluid type. The results of the comparison between the relative viscosity of MgO-EG and SiO_2-EG nanofluids, and the nanofluids of Al_2O_3-glycerol and SiO_2-glycerol are presented in Figure 4.22. The plots showed that the influence of different nanoparticles on the enhancement of nanofluid viscosity is not particularly significant, especially at low-volume fractions up to the Einstein concentration regime ($\phi \leq 2\%$).

However, there was a distinction in the enhancement observed in different nanofluids at a higher volume fraction. Although, different nanoparticles have different physical-chemical properties, including different ionic charge types and ionic concentrations, the implication of the result in Figure 4.22 is that the influence of increased volume fraction, which leads to an increase in particle-particle interactions and higher energy dissipation, is more pronounced than the influence of different nanoparticle types. More studies of this type should be carried out to extract more useful information.

4.7 CONCLUSION AND RECOMMENDATIONS

This chapter presents the experimental results of the influence of temperature, volume fraction, particle size, particle types and base fluid types on the viscosity and viscosity

100

enhancement of nanofluids. The nanofluids of Al_2O_3-glycerol, MgO-EG, SiO_2-glycerol and SiO_2-EG were investigated. Different ultrasonication energy densities were applied for the preparation of the nanofluids. An optimum energy, which gave good dispersion, was obtained to prepare uniformly homogenised nanofluids.
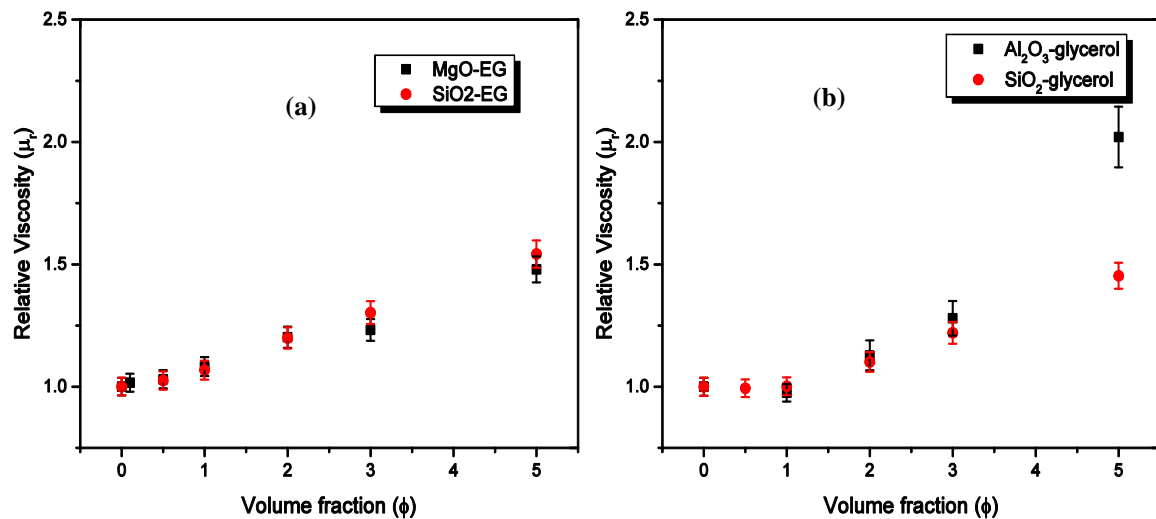
Figure 4.22: The influence of different nanoparticle types on the relative viscosity of nanofluids (a) MgO and SiO2 suspended in EG (b) Al2O3 and SiO2 suspended in glycerol.

The influence of temperature on the viscosity of nanofluids is similar to the trend displayed by the base fluids in all the cases investigated. The viscosity reduced exponentially with an increase in temperature. On the contrary, an increase in the volume fraction of suspended nanoparticles resulted in an increase in the viscosity of the nanofluids. Different nanoparticle sizes displayed different enhancements when dispersed in the base fluid, and the smallest nanoparticle recorded the highest enhancement because of higher particle-particle interactions and increased Brownian motion.

The enhancement recorded for the same nanoparticles in different base fluids showed that base fluid types also have a significant effect on the viscosity of nanofluids. However, the influence of nanoparticle types seemed to be overshadowed by the influence of an increase in nanoparticle volume fractions. Therefore, it is recommended that more investigations should be carried out on the influence of particle types in order to properly understand their level of significance. It is also important to undertake further study to determine which of the base fluid properties is important when it comes to nanofluid viscosity enhancement.

5

CHAPTER 5: THE pH AND ELECTRICAL CONDUCTIVITY OF NANOFLUIDS[1, 2, 3]

5.1 INTRODUCTION

The formation of a stable nanofluid is central to its successful implementation in most engineering systems. For instance, the stability of nanofluids has been shown to affect properties such as viscosity and thermal conductivity. Therefore, to ensure stable nanofluids, a situation where the van der Waals force is lower than the force of repulsion between particles, surface-active agents (surfactants or dispersants) or electrostatic stabilisation have been proposed [271].

In the case of a surface-active agent that is a chemical method, there is no unique formula for adding the chemical surfactant. Consequently, it involves trial and error, which may not be sustainable for the different possible combinations of the available chemical surfactants. Electrostatic stabilisation, on the other hand, is often achieved by modifying the pH of the nanofluids, which affects the ionic state of the nanoparticle surface [224, 225]. Physical preparation methods, such as an ultrasonication assist mechanism, is another factor that has a significant effect in ensuring the stability of nanofluids [272].

In light of the preceding statements, pH modification appears to be the most sustainable stabilisation method, and is a very important parameter that may facilitate investigations of

the fundamental nature of nanofluids [215]. Wong and Kurma [233] also stated that evaluating the electrical conductivity of nanofluids would give a better understanding of the transport properties of the heat transfer fluid. Although some efforts have focused on the study of the effect of the pH value of nanofluids on their heat transfer properties, such as thermal conductivity and viscosity, these studies do not examine the influence of temperature on the pH of nanofluids. Since nanofluids are being proposed for use in heat transfer equipment, such as high-temperature heat exchangers, it is important to understand the influence of temperature on the pH of nanofluids.

As stated in Section 2.5, the electrical conductivity and pH of nanofluids may be related because they are both affected by the ionic configuration within the system [224, 225]. With regard to nanofluids, electrostatic forces become extant and the strength of the electrostatic forces depends on the degree of ionisation of the suspension when nanoparticles are dispersed in the base fluid (e.g. water) [223]. This process alters the electrical properties of the base fluid due to interactions with the particle surface charge. Despite the importance of the electrical conductivity of heat transfer fluids to science and technological advancements, thorough investigations of the electrical conductivity of nanofluids have not been explored. Therefore, there is very limited data available on the electrical conductivity properties of nanofluids.

5.2 THE pH AND ELECTRICAL CONDUCTIVITY OF MgO-EG NANOFLUIDS

5.2.1 The influence of temperature on the pH and electrical conductivity of MgO-EG nanofluids

The pH of a solution can change with temperature due to the effect of temperature on the dissociation of weak acid and base groups and the splitting of the water component into H^+ and OH^-. Figure 5.1 presents the influence of temperature on the pH of MgO-EG nanofluid at various volume fractions alongside the base fluid. The pH of the base fluid measured at 25 ^{o}C was 6.78, which was in agreement with the manufacturer's reference value (i.e. 6 to 7.5) and the value reported by Timofeeva et al. [273] (i.e. 6.8). Table 5.1 shows the measured pH and electrical conductivity of EG and of nanofluid samples at room temperature. The presence of MgO gave approximately 60 and 53% enhancement in the pH value for 20 and 100 nm respectively at 3% volume fraction. However, these

103

values reduced with an increase in temperature. The trends, as presented in Figure 5.1, show a significant reduction in pH values between 20 and 70 ^{o}C. Similar results were published by Konakanchi et al. [223] on PG/water (60:40)-based nanofluids for Al_2O_3, SiO_2 and ZnO. The fact that temperature variation affects the pH value of MgO-EG nanofluid, which is not the case for the base fluid, illustrates the significance of this research on the stability of the nanofluid.
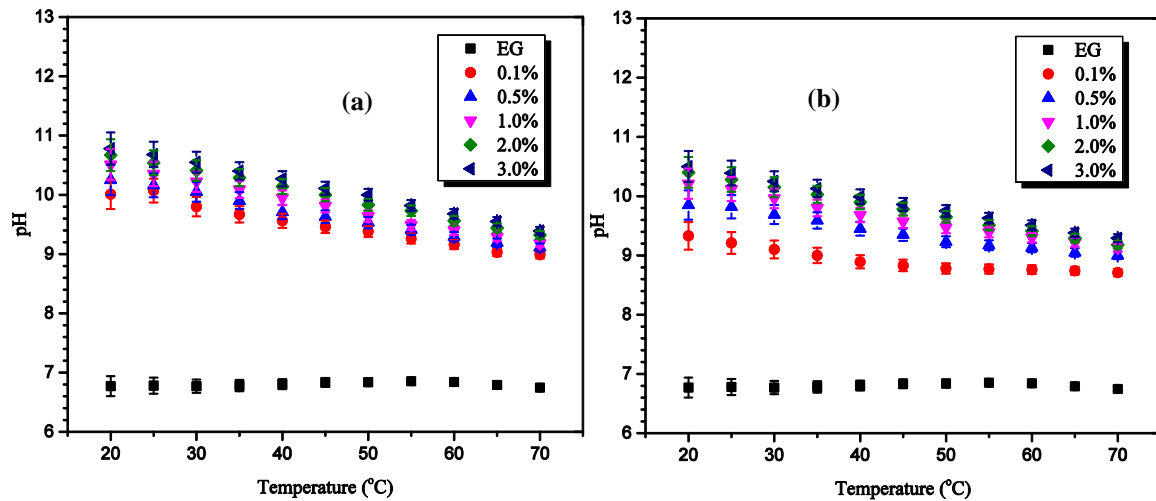
Figure 5.1: The influence of temperature on the pH of MgO-EG nanofluid: (a) 20 nm; (b) 100 nm.

Table 5.1: Experimental values of the pH and electrical conductivity of EG and 20 nm MgO-EG nanofluid at 25 ^{o}C

Volume fraction, ϕ (%)	Electrical conductivity, K (µS/cm)	pH
EG	0.1133	6.78
0.1	3.01	9.66
0.5	6.68	10.14
1.0	8.73	10.33
2.0	11.74	10.3
3.0	14.05	10.84

The behaviour of the electrical conductivity of EG, which is investigated in this study, is somewhat similar to the pH measurement with values changing from 0.11 to 0.35 µS/cm (Figure 5.2). At room temperature, the electrical conductivity value of the EG used in this experiment was 0.11 µS/cm, which totally disagrees with the 1.07 µS/cm reported by

104

Sarojini et al. [33]. However, it is comparable to the value of other glycols [37]. The reason for this disparity could lie in the purity of the EG used in these two experiments. In the present study, the EG had a 99.5% purity, while Sarojini et al. [33] did not provide the detail of the purity of their EG base fluid. Although EG is mildly polar, it is also highly hygroscopic. Therefore, if it is overexposed to the atmosphere, it will absorb moisture, which will alter the purity. Water is a polar liquid [33], which means that moisture will increase its electrical conductivity value.
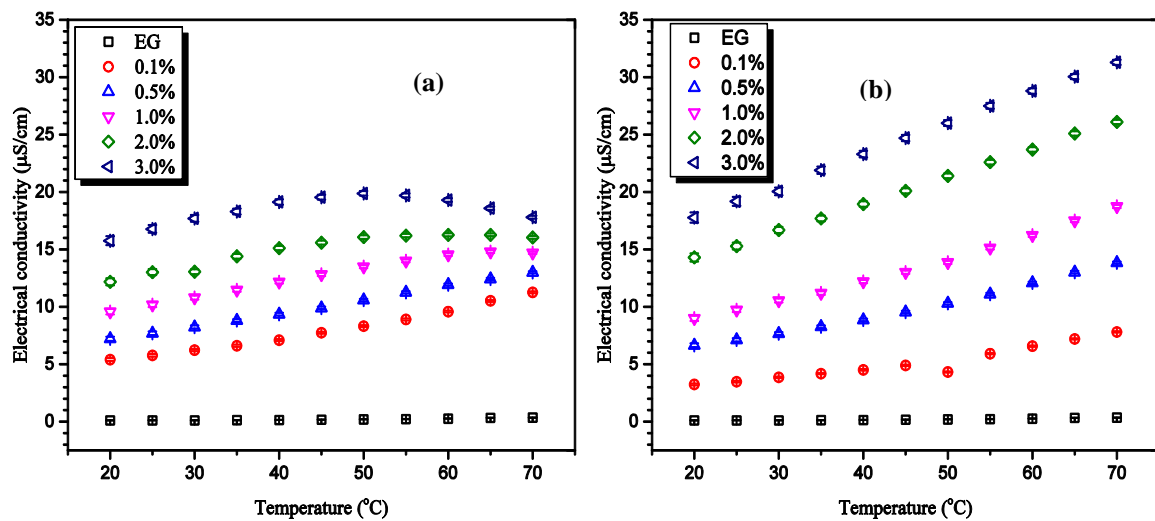
Figure 5.2: The influence of temperature on the electrical conductivity of MgO-EG nanofluid: (a) 20 nm; (b) 100 nm.

The apparently unchanging values of the pH and electrical conductivity of the base fluid with temperature further supports the fact that pH and electrical conductivity are two interrelated processes that are linked with ionic concentration/activity. Figure 5.2 presents the plots of the effective electrical conductivity of MgO-EG nanofluid against temperature at various volume fractions. Adding MgO nanoparticles to EG up to 3% by volume displayed a significant increase in electrical conductivity. The influence of temperature is also significant as the electrical conductivity increased with an increase in sample temperature. Similar behaviour was reported on CuO-EG nanofluids, where electrical conductivity increased with an increase in nanoparticle concentration and temperature [274].

105

The graph of 20 nm MgO in Figure 5.2 (a) shows that there is electrical conductivity saturation at 1% through 3% volume fractions and around 40 to 70 ^{o}C, which is not the case with 100 nm in Figure 5.2 (b). The counterion condensation (i.e. saturation of electrical conductivity-determining ions) was noticed at these volume fractions, and as the temperature increased, the trend remained and became more pronounced.

In 2011, Konakanchi et al. [241] reported similar findings with ZnO-PG/water nanofluids. In Figure 5.3, the electrical conductivity values are normalised in order to study the incremental behaviour of the electrical conductivity of MgO-EG relative to the base fluid within the experimental temperature range. Increasing the temperature up to 30 ^{o}C caused an increase in the relative electrical conductivity to a maximum value, and a further increment in the temperature gave a continual drop in the relative electrical conductivity. This shows that the percentage increment in the electrical conductivity of base fluid as temperature increases is higher than the percentage increment in MgO-EG nanofluids.
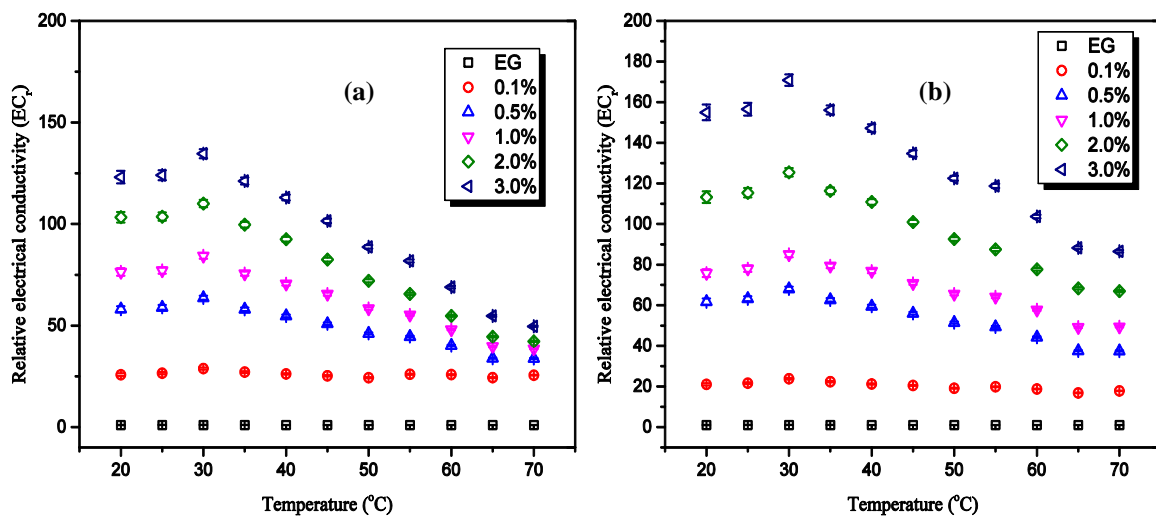
Figure 5.3: Relative electrical conductivity of MgO-EG nanofluid against temperature: (a) 20 nm; (b) 100 nm.

For the base fluid, a 218.2% increment was recorded, while an increment of about 40% was recorded for 20 nm at 3% volume fraction, and between 20 and 70 ^{o}C. Consequently, the normalised electrical conductivity reduced as the temperature increased. MgO is widely used as an electrical insulator in technical devices, such as thermocouples, coaxial heating elements and electrical cables, especially in the temperature region below 1 000 K

[275, 276]. Therefore, the relative electrical conductivity plot in Figure 5.3 depicted electrically insulating nanofluids as the temperature increased. The graphs of the relative pH against temperature, presented in Figure 5.4, show comparable behaviour as noted for electrical conductivity. The values reduced with an increase in nanofluid temperature. Comparable results on the pH for other types of nanofluids were recently reported by Konakanchi et al. [223].

5.2.2 The effect of volume fraction and particle size on the pH and electrical conductivity of MgO-EG nanofluid

As shown in figures 5.5 and 5.6, increasing the volume fraction of MgO nanoparticles significantly increased the electrical conductivity and pH values with regard to the base fluid. In Figure 5.5 (b), the relative electrical conductivity for all the samples of MgO-EG nanofluid with respect to the volume fraction shows that there are significant enhancements in electrical conductivity values, even at a low MgO volume fraction of 0.1%. The enhancement increases with the increase of the volume fraction of MgO. Clearly, in Figure 5.5 (a), the effect of MgO particle size does not have a definitive pattern on the electrical conductivity of the MgO-EG nanofluid. This trend is unlike those reported by Sarojini et al. [33] on Al_2O_3-water nanofluid and White et al. [37] on Al_2O_3-PG nanofluid.
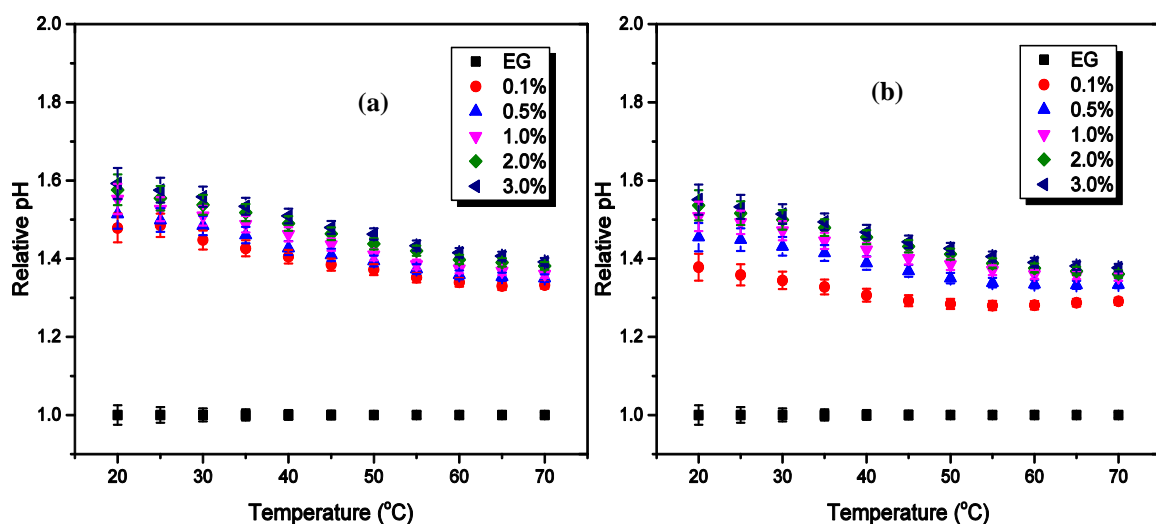
Figure 5.4: Relative pH of MgO-EG nanofluid against temperature: (a) 20 nm; (b) 100 nm.
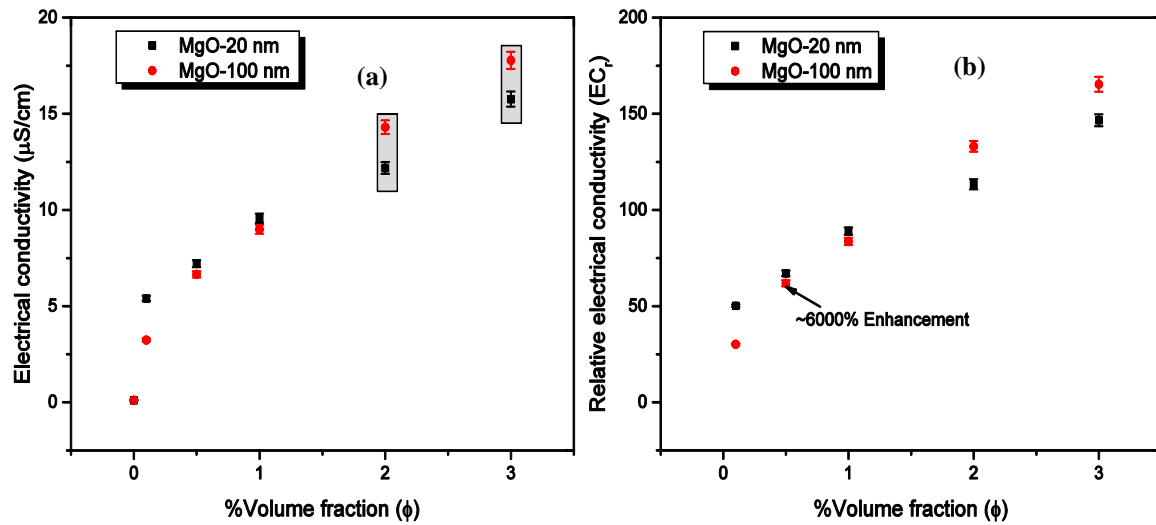
Figure 5.5: The effect of volume fraction on the electrical conductivity of MgO-EG at 20 ^{o}C: (a) effective electrical conductivity; (b) relative electrical conductivity.

The electrical conductivity of the 20 nm MgO was initially slightly higher than that of 100 nm MgO with later trends suggesting the presence of counterion condensation [36, 37]. It is also more pronounced in the 20 nm particles, as highlighted by the shaded bars in Figure 5.5 (a). Usually, there are no ions other than the ones stemming from the suspended particles in a salt-free suspension, such as a MgO-EG nanofluid, which allows for the formation of a thick EDL because of the low ionic strength of the suspension. In this type of system, the ionic conductivity in the EDL is typically greater than the bulk conductivity, so that the surface conductance increases the effective electrical conductivity of the suspension [277].

The surface conductivity has no appreciable influence on the electrical conductivity of the suspension beyond the critical particle surface charge density. Therefore, as the volume fraction increases, it adds to the total charge present, and the electrical conductivity increases until the critical surface charge density is reached. Further increment in volume fraction only increases the amount of counterions that feed the condensation regions (region closest to the particle surface) and leaves the charge and potential in the bulk virtually unchanged. This reduces the electrical conductivity incremental slope and may cause the electrical conductivity to plateau [37, 278].

In terms of the effect of nanoparticle size on the pH of the MgO-EG nanofluid, Figure 5.6 shows that the smaller the particle size, the higher the pH value. The shaded rectangles in Figure 5.6 correspond with those in Figure 5.5 at the point of counterion condensation. Contrary to Minea and Luciu [234] and Ganguly et al. [228], who reported a 379.6 and 833% enhancement in electrical conductivity for alumina nanofluids at 4 and 0.5% volume fractions respectively, the percentage enhancement in the present investigation is as high as ~6000% at a 0.5% volume fraction. This is similar to the value reported by Kole and Dey [279] on functionalised graphene-based-EG nanofluid. The high enhancement value recorded compared to past studies is probably due to the different nanoparticle types, base fluids and nanoparticle size.
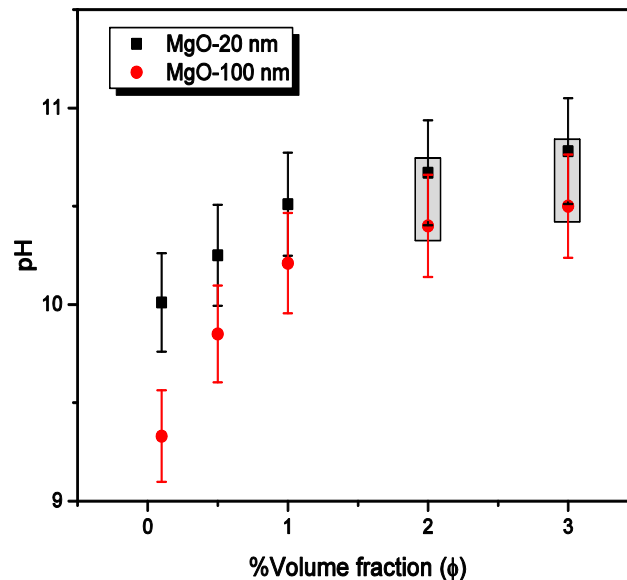
Figure 5.6: The effect of volume fraction on the pH of MgO-EG at 20 $^{\circ}$C.

5.3   THE pH AND ELECTRICAL CONDUCTIVITY OF SiO$_2$-EG AND SiO$_2$-GLYCEROL NANOFLUIDS

The results presented here are based on the nanofluid formulated from the same SiO$_2$ nanoparticle dispersed separately in EG and glycerol base fluids.

5.3.1   The influence of temperature on the pH and electrical conductivity of SiO$_2$-EG and SiO$_2$-glycerol nanofluids

The electrical conductivity value of both glycerol and EC within the experimental temperature range was less than 1.0. As shown in Figure 5.7, the addition of SiO$_2$

109

nanoparticles showed a significant jump, especially in SiO_2-glycerol nanofluid. Furthermore, similar to the behaviour of MgO-EG nanofluids presented in Section 5.2, as the temperature of the nanofluid increased, the electrical conductivity also increased for both the SiO_2-EG and SiO_2-glycerol nanofluids.

Figure 5.8 shows how the pH of the SiO_2-EG and SiO_2-glycerol nanofluids responds to temperature change. The pH of glycerol changed from slightly basic to acidic (7.56 to 5.1) within the investigated temperature regime. The SiO_2-glycerol nanofluid, on the other hand, does not seem to change much with temperature change. The plot, as shown in Figure 5.8 (a), signifies that the nanofluid is in a basic regime and not much has changed as a result of the temperature increment that was observed. The EG base fluid hovers around the neutral pH with values between 6.75 and 6.85. Unlike the SiO_2-glycerol, the pH of a SiO_2-EG nanofluid changed significantly with temperature change, as depicted in Figure 5.8 (b). This trend is similar to the trend displayed by MgO-EG nanofluids that are discussed in Section 5.2.1 and other earlier reported studies [223].
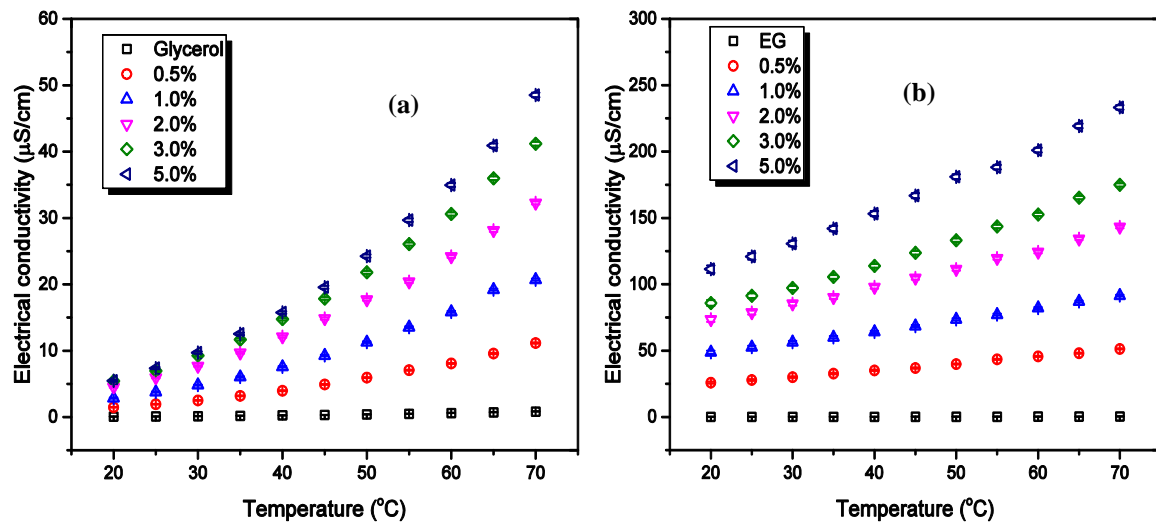
Figure 5.7: The effect of temperature on the electrical conductivity of SiO_2-glycerol and SiO_2-EG nanofluid: (a) SiO_2-glycerol; (b) SiO_2-EG.
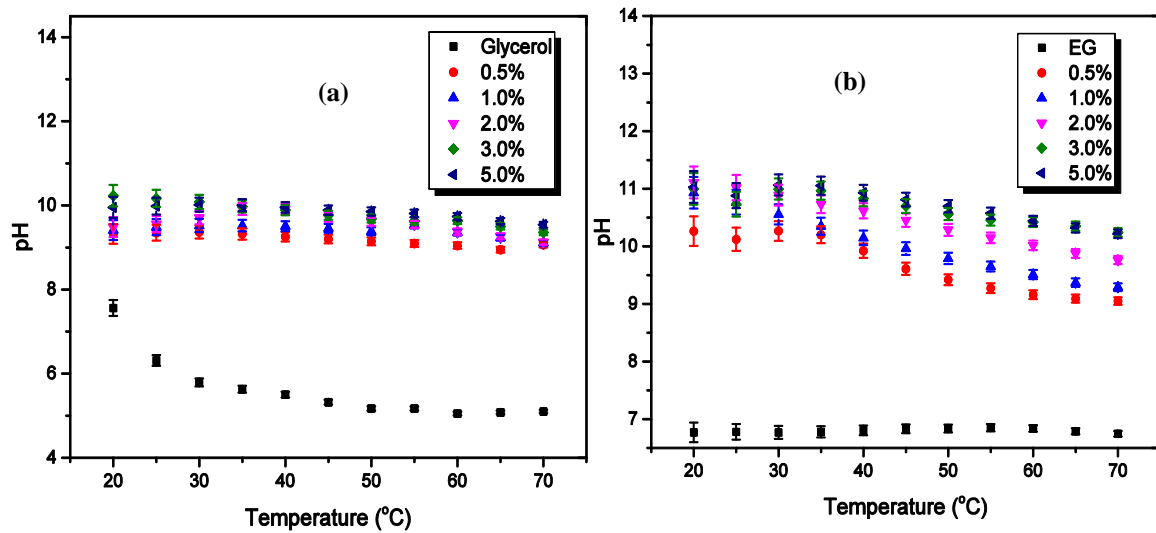
Figure 5.8: The effect of temperature on the pH of SiO₂-glycerol and SiO₂-EG nanofluid: (a) SiO₂-glycerol; (b) SiO₂-EG.

5.3.2 The influence of volume fraction on the pH and electrical conductivity of SiO₂-EG and SiO₂-glycerol nanofluids

Figure 5.9 presents the plots of the electrical conductivity of SiO₂-based nanofluids as a function of volume fraction loading. It is obvious from Figure 5.9 that the electrical conductivity initially increased with an increase in the volume fraction of SiO₂ until it reached around 2.0% volume fraction. Then, the rate of increment reduced until it reached the 5.0% volume fraction investigated. This behaviour is similar to that observed for the MgO-EG nanofluid discussed in Section 5.2 and is as a result of counterion condensation in the EDL that formed around the nanoparticles in the suspension. For suspensions with low surface charge density, an increase in volume fraction gives a fairly linear relationship with the electrical conductivity (i.e. increase in surface potential). However, above a critical value of the surface charge density, the electrical conductivity increases very slowly. This phenomenon is known as counterion condensation [280].

Although, the pH trend for both pure EG and glycerol base fluids are different with respect to temperature change, the dispersion of SiO₂ nanoparticles in both base fluids displayed similar trends as the volume fraction was increased (Figure 5.10). This trend is also similar to the nanofluid of MgO-EG discussed in Section 5.2. From these graphs, it is evident that the suspension of nanoparticles caused an obvious jump in the pH value. The pH increases very slowly with the trends and later flattens out.

111
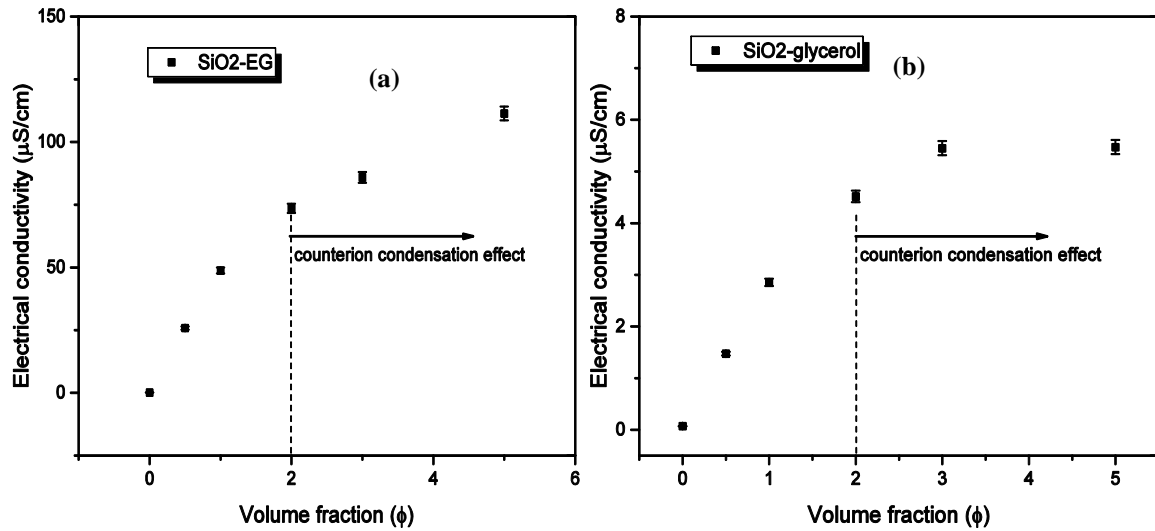
Figure 5.9: The effect of volume fraction on the electrical conductivity of SiO$_2$-based nanofluids: (a) SiO$_2$-EG; (b) SiO$_2$-glycerol nanofluids.
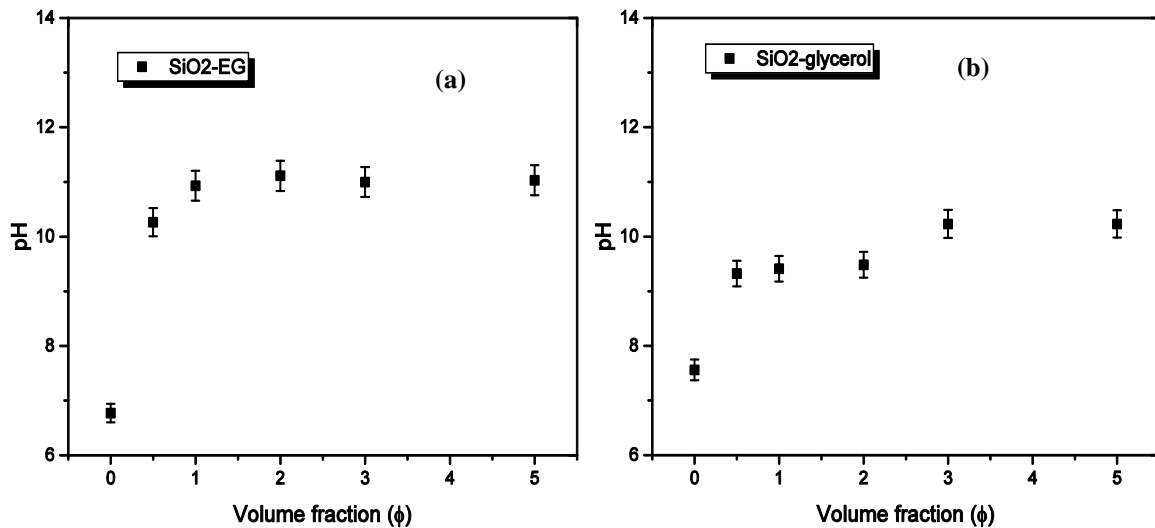
Figure 5.10: The effect of volume fraction on the electrical conductivity of SiO$_2$-based nanofluids: (a) SiO$_2$-EG; (b) SiO$_2$-glycerol nanofluids.

5.4   THE INFLUENCE OF DIFFERENT BASE FLUIDS ON THE PH AND ELECTRICAL CONDUCTIVITY OF NANOFLUIDS

The graph presented in Figure 5.11 represents a comparison of the pH and electrical conductivity of SiO$_2$ dispersed in two different base fluids: EG and glycerol. It is clear from the figure that the type of base fluid dictates the level of enhancement in both the pH and the electrical conductivity. Surprisingly, the enhancement of both the pH and electrical conductivity is higher in SiO$_2$-EG nanofluids. This behaviour may not be

112

unconnected to the ionic activities present in the nanofluid systems, which also affect these two properties significantly.
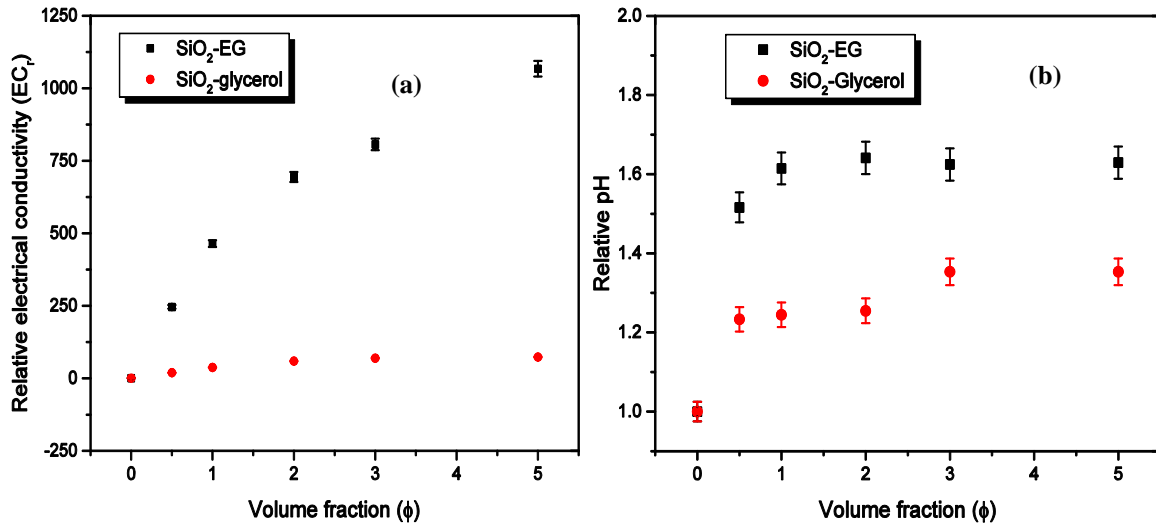
Figure 5.11: The influence of different base fluid on the relative electrical conductivity and relative pH of SiO$_2$-based nanofluids: (a) SiO$_2$-EG nanofluid; (b) SiO$_2$-glycerol nanofluid.

5.5   CONCLUSION AND RECOMMENDATIONS

The influence of temperature, volume fraction, size and different base fluids on the pH and electrical conductivity of nanofluids was investigated and reported in this chapter. The nanofluids selected for the experiment in this category are MgO-EG, SiO$_2$-EG and SiO$_2$-glycerol. All the nanofluids used are uniformly homogenised and there was no sign of sedimentation throughout the course of the experiments. Moreover, samples were continuously stirred during the measurement process.

The values of the electrical conductivity of the base fluids used in this thesis are small and lower than 1.0, even when the temperature changed between 20 and 70 $^{\circ}$C. However, for all the nanofluids investigated, the values of the electrical conductivities are significantly higher than those of the base fluids and there were notable increments in electrical conductivity with an increase in temperature.

Regarding the pH of the nanofluids, the addition of nanoparticles saw a jump in pH compared to the base fluids, and their values generally reduced with temperature increments. This was the case for all the nanofluids investigated in this category. The

113

higher the volume fraction of the nanoparticles in all the cases investigated, the more the pH and electrical conductivity values will increase until a counterion condensation effect sets in. MgO nanoparticles of two different sizes were dispersed in EG in order to investigate the influence of nanoparticle size on pH and electrical conductivity. The smaller MgO nanoparticles showed slightly higher electrical conductivity compared to the larger nanoparticles until the counterion condensation effect set in. At this point, the ionic concentration around the smaller nanoparticles became choked with the increment of volume fraction so that the later trend showed a lower electrical conductivity for the smaller nanoparticles. For the pH, smaller nanoparticles showed higher pH values and larger particles showed lower pH values.

The relative electrical conductivity and relative pH values obtained showed that base fluid types influence the level of enhancement that is obtainable. Therefore, the pH and electrical conductivity increments are functions of temperature, volume fraction, particle size and base fluid types. At 20 ^{o}C, minimum electrical conductivity and pH enhancements of ~6 000% and ~50% respectively were observed in a 0.5% volume fraction of MgO dispersed in EG. The enhancements observed for SiO_2-EG nanofluid are 23 927% and 51.6% for electrical conductivity and pH respectively, while SiO_2-glycerol nanofluid gave 2 004% and 23.3% for electrical conductivity and pH respectively.

Since different base fluids have their unique physical and chemical properties, it is recommended that the influence of these base fluid properties on the pH and electrical conductivity enhancement should be investigated. This will provide information on the properties that are significant determinants for pH and electrical conductivity enhancements.

CHAPTER 6:   MODEL DEVELOPMENT FOR NANOFLUID VISCOSITY[1, 2]

6.1   INTRODUCTION

A good nanofluid should present high thermal conductivity in order to be efficient for thermal management (heat removal). It should also show minimum viscosity in order to minimise pressure drop and pumping costs. Viscosity plays a major role in determining the pumping power requirements of any heat exchanger. Thus, precise knowledge of the nanofluid's viscosity behaviour is important [213]. A key problem with nanofluid research is also the estimation of the effective viscosity of nanofluids. Einstein's model [39] showed that the viscosity of colloidal suspensions of spherical particles increases as the volume fraction of suspended particle increases. Brinkman [43], Krieger and Dougherty [54] and Batchelor [52] all modified Einstein's model to show the effect of particle-particle interactions and concentrated volume fraction on the effective viscosity of the suspension of solid spheres. However, the effects of size and temperature are not included in these models. Therefore, these models have not succeeded in predicting the viscosity of nanofluids.

When experimental data does not indicate the significant influencing factors and how these factors combine to influence the observed results, non-dimensional analysis could be used to obtain a valid relationship between experimental and influential factors. Recently, researchers have paid attention to the application of AI to model engineering

---

115

problems. Many intelligent techniques such as GA, ANN and fuzzy logic have been developed and deployed in various engineering systems using the available empirical data. Since these AI techniques do not consider any assumptions about the characteristics and statistical distribution of data, they are practically more effective in modelling complex engineering systems than most other statistical techniques. An efficient approach for modelling various systems can be created through the combination of fuzzy technique and ANN, GA and GMDH-PNN or GMDH and ANN. The deficiencies in one method can be minimised by another method, which increases the efficiency of a hybrid system.

6.2   MODELLING THE VISCOSITY OF MgO-EG NANOFLUIDS

6.2.1   Modelling the viscosity of MgO-EG nanofluids using non-dimensional analysis

In the present study, essential parameters, including nanoparticle size, volume fraction, temperature, capping layer thickness, the viscosity of the base fluid, the density of the base fluid and the density of the nanofluid are considered as input parameters. These parameters are non-dimensionalised to produce the non-dimensional parameters (π's) presented below:

$$\pi_1 = \frac{\mu_{eff}}{\mu_o} = f\left(\pi_2 = \frac{T}{T_0}, \pi_3 = \phi, \pi_4 = \frac{d_p}{r}, \pi_5 = \frac{\rho_{nf}}{\rho_f}\right). \tag{6.1}$$

In Equation 6.1 above, T is the working temperature, T_0 is the reference temperature taken as 20 $^{\circ}$C, d_p is the particle diameter, r is the thickness of the capping layer taken as 1 nm [25], ρ_f is the density of base fluid and ρ_{nf} is the density of nanofluid. The densities of the nanofluids were calculated based on the mixture model [98] and a correlation matrix was run on 198 data points with each data point containing all four independent non-dimensional parameters. The results of the correlation matrix showed that π_3 and π_5 are highly correlated with a correlation index of over 99%. Consequently, preference is given to π_3 over π_5, since it is part of the input parameters that are considered in the experiment. Therefore, Equation 6.1 is reduced to Equation 6.2:

$$\frac{\mu_{eff}}{\mu_o} = f\left(\frac{T}{T_0}, \phi, \frac{d_p}{r}\right). \tag{6.2}$$

116

Using non-linear regression modelling, the function f in Equation 6.2 is expressed as follows:

$$\frac{\mu_{eff}}{\mu_o} = 1 + a_0(\phi) + a_1\left(\frac{T}{T_0}\right)\phi + a_2\left(\frac{d_p}{h}\right)\phi + a_3\left(\left(\frac{d_p}{h}\right)\phi\right)^2$$
$$+ a_4\left(\left(\frac{T}{T_0}\right)\phi\right)^2 + a_5\phi^2 + a_6\left(\frac{T}{T_0}\right)^2\phi^{\frac{1}{3}}$$

$$(6.3)$$

where a_0 to a_7 are empirical constants presented in Table 6.1. This correlation is valid for a volume fraction of MgO ≤ 5%, temperatures between 20 and 70 ^{o}C and particle sizes between 20 and 125 nm. The coefficient of determination (R^2) of this model is 0.9524. Other statistics on the goodness of the fit, such as the sum of square errors (SSE), means square error (MSE) and RMSE are 0.1543, 0.0008 and 0.0285 respectively.

Table 6.1: Correlation parameters for Equation 6.3

Parameters	Values
a_0	7.0764
a_1	-0.1246
a_2	-0.0346
a_3	-0.0024
a_4	-1.2357
a_5	53.6946
a_6	0.0436

In Figure 6.1, the relative viscosity of the MgO-EG nanofluids is predicted using Equation 6.3 and it is compared with the predictions made by some of the prominent models that are used for nanofluid viscosity. It is obvious that the presented correlation performed better than the other models. The models of Einstein [39], Brinkman [43] and Batchelor [52] all predicted similar results, which fell short of the present results. The deviation from the experimental results becomes more pronounced as the nanoparticle size gets smaller. On the other hand, the empirical models of Kitano et al. [107], who considered particle volume fraction and agglomeration, and Corcione [105], who considered particle size, base fluid properties and volume fraction. These researchers all overpredicted the present experiment.

117
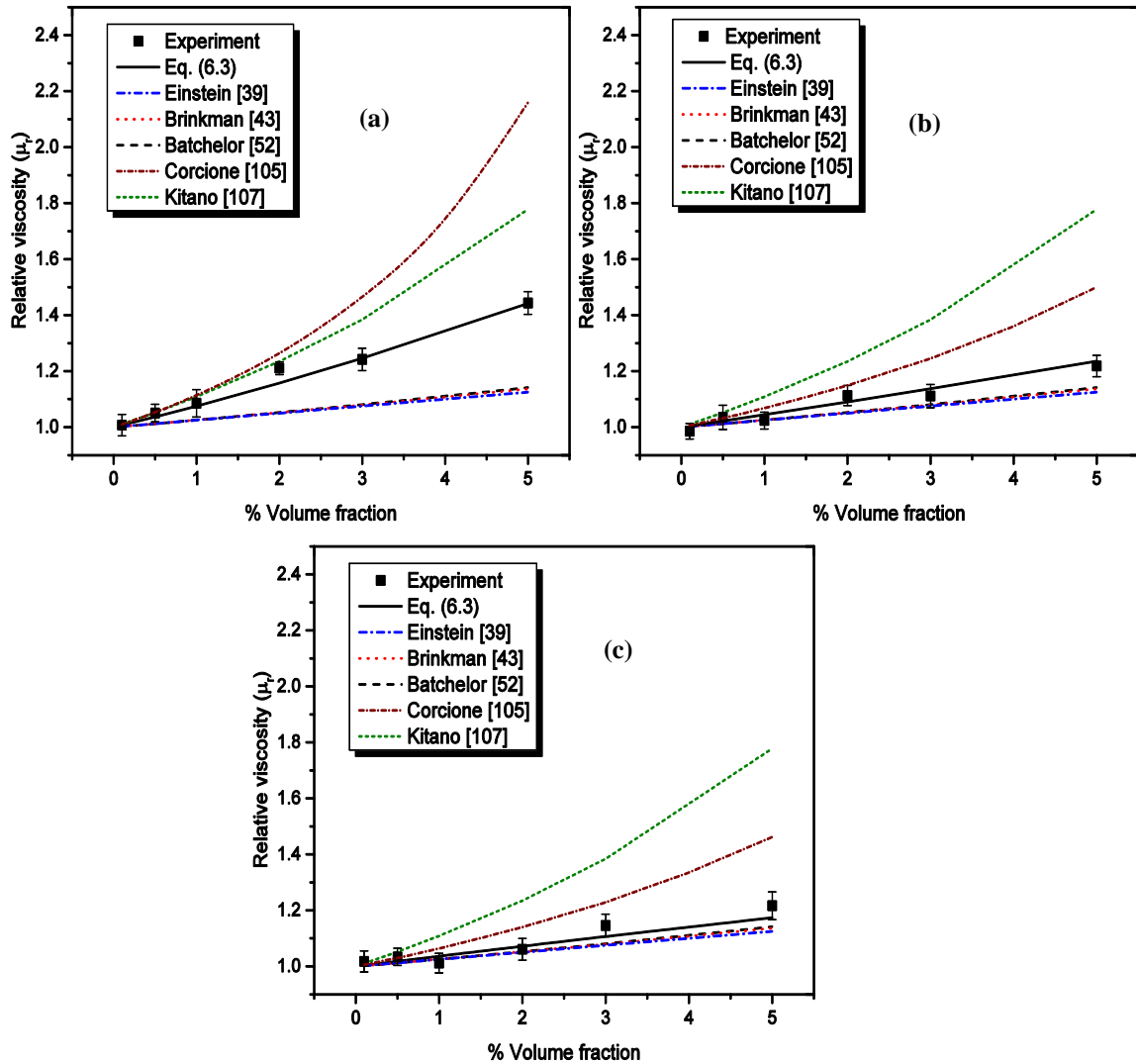
Figure 6.1: Comparison between the present experimental data, proposed correlation and other prominent viscosity models.

In the prediction made by Corcione [105], it can be seen that with smaller nanoparticles, the deviation from experimental data is higher than in samples with bigger nanoparticles. When the correlation in Equation 6.3 was used to estimate the temperature dependence of the effective viscosity of MgO-EG nanofluid containing 20 nm nanoparticles, it resulted in very good agreement, as shown in Figure 6.2. Very similar results were obtained for samples containing nanoparticles of other sizes.

118
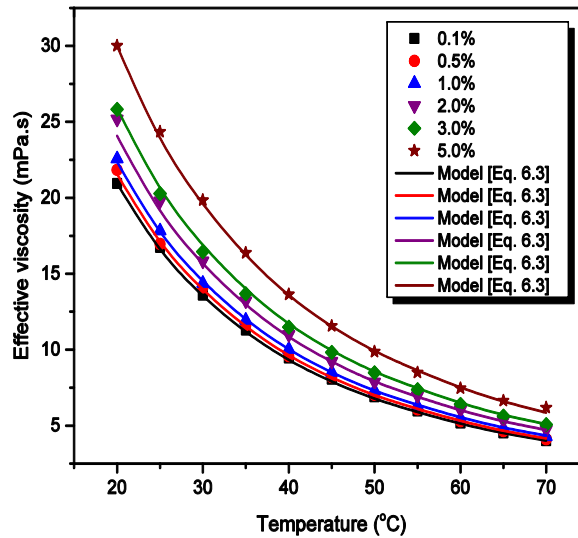
Figure 6.2: Comparison between experimental data (effective viscosity of MgO-EG) and the proposed correlation (Equation 6.3) for different temperatures and various volume fractions, in the case of particles of 20 nm.

6.2.2 Modelling the viscosity of MgO-EG nanofluid using FCM-ANFIS and GA-PNN modelling techniques

As explained under Section 3.7, the structure of ANFIS can be generated using one of the following techniques: fuzzy C-mean clustering, subtractive clustering and grid partitioning. Each of these identification techniques starts with mapping the input variables to the input space partitioning, then choosing the appropriate input membership functions, followed by the creation of the fuzzy rules, selection premise and creation of the concluding part of the fuzzy rules, and selecting the initial parameters for the membership functions. The GA-PNN hybrid system was also applied to modelling the viscosity of MgO-EG nanofluids in the present study. The GA-PNN hybrid system was created by a combination of GA and the GMDH-PNN approaches. Details can be found in Section 3.7.

The present experimental data, comprising 198 input-output data points, is used for the modelling of the viscosity of MgO-EG nanofluids. The experimental data was divided into two, with 154 data points (78%) for training and 44 data points (22%) for testing purposes. The RMSE, mean relative error (MRE) and MAE, as given in Table 6.2, are used as statistical criteria for selecting the optimal model. These criteria show the

119

accuracy of the models used for the prediction of the viscosity of MgO-EG nanofluids for various input variables.

Table 6.2: Statistical criteria used to analyse the results

Statistical criterion	Equation
Mean absolute error	$MAE = \dfrac{1}{n} \sum\limits_{i=1}^{n} \left\| X_{pr} - X_a \right\|$
Mean relative error	$MRE(\%) = \dfrac{100}{n} \sum\limits_{i=1}^{n} \left(\dfrac{\left\| X_{pr} - X_a \right\|}{X_a} \right)$
Root mean square error	$RMSE = \sqrt{\dfrac{1}{n} \sum\limits_{i=1}^{n} \left(X_{pr} - X_a \right)^2}$

The network architecture of the GA-PNN model for predicting the viscosity of MgO-EG nanofluids is shown in Figure 6.3 and corresponds to the genome representation of *3333111222223313,* in which *1, 2* and *3* represent the average particle diameter d_p (nm), volume fraction ϕ (%) and temperature T ($^{\circ}$C) respectively. The equivalent grand polynomial model for the effective viscosity of MgO-EG nanofluids based on the network architecture is presented in Appendix B1.
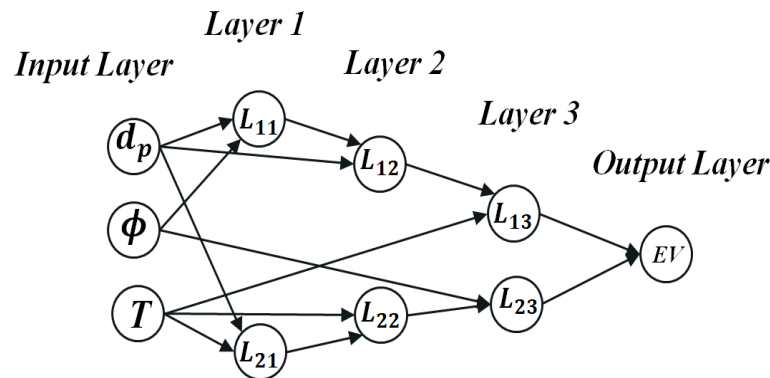
Figure 6.3: Structure of the GA-PNN hybrid system for the effective viscosity of MgO-EG nanofluid modelling.

Figure 6.4 shows the comparison between the present experimental results, the FCM-ANFIS model, the GA-PNN model and the present correlation presented in Equation 6.3

120

for the viscosity of MgO-EG nanofluids with 20 nm MgO at 1% volume fraction and various temperatures. All the models for the effective viscosity of MgO-EG nanofluids agree with the experimental data and present a good degree of accuracy. The following statistics on the goodness of the predictions were obtained: RMSE = 0.095, MRE = 0.87% and MAE = 0.073 for the correlation (Equation 6.3); RMSE = 0.529, MRE = 2.67% and MAE = 0.359 for the GA-PNN model; and RMSE = 0.207, MRE = 1.32% and MAE = 0.148 for FCM-ANFIS model.
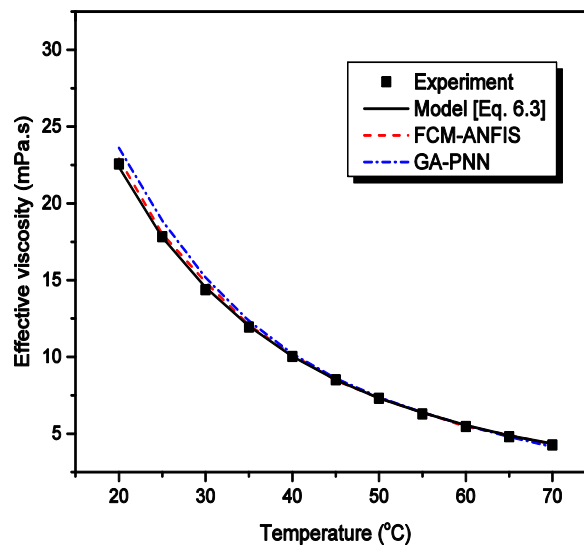
Figure 6.4: Comparison of the experimental data with the GA-PNN model, FCM-ANFIS model and proposed model for the effective viscosity of 20 nm MgO-EG nanofluid at 1% volume fraction.

In figures 6.5 and 6.6, a similar comparison is made between the results of the three modelling techniques presented in this section and the experimental results of MgO-EG nanofluids containing 100 and 125 nm MgO nanofluids, respectively. It can be seen that, for the experimental temperature regime and the different volume fractions, the three models performed very well. Figure 6.5 (a and b) contains experimental data for 100 nm MgO at 0.5 and 2% volume fractions respectively, while Figure 6.6 contains experimental data for 125 nm MgO at 3% volume fraction. The statistics on the goodness of these fits are very similar to those presented for Figure 6.4.
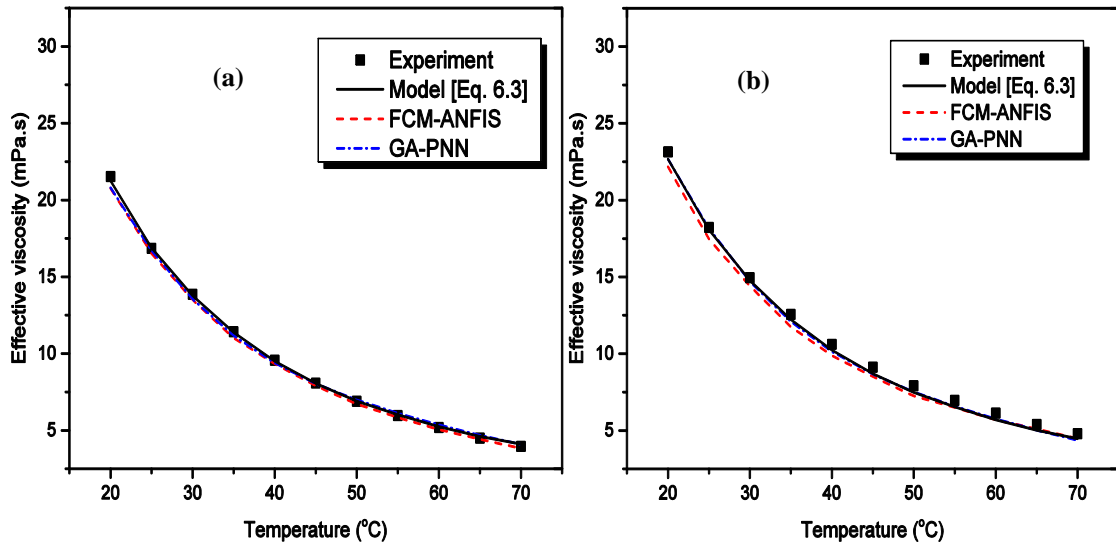
Figure 6.5: Comparison of the experimental data with the GA-PNN model, FCM-ANFIS model and proposed model for the effective viscosity of 100 nm MgO-EG nanofluids: (a) 0.5% volume fraction; (b) 2% volume fraction.
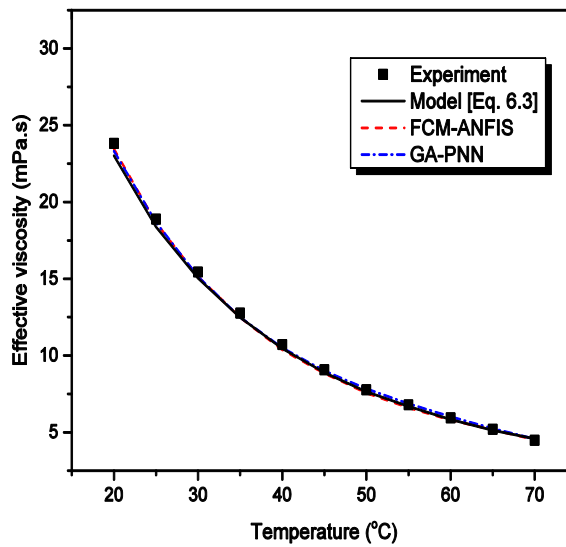
Figure 6.6: Comparison of the experimental data with the GA-PNN model, FCM-ANFIS model and proposed model for the effective viscosity of 125 nm MgO-EG nanofluids at 3% volume fraction.

122

6.3 MODELLING THE VISCOSITY OF Al$_2$O$_3$-GLYCEROL NANOFLUIDS

6.3.1 Modelling the viscosity of Al$_2$O$_3$-glycerol nanofluids using non-dimensional analysis

A method similar to the one used in Section 6.2.1 is employed to model the viscosity of Al$_2$O$_3$-glycerol nanofluids. A total of 132 data points with three independent and one dependent non-dimensional parameters given in Equation 6.2 are used. For the Al$_2$O$_3$-glycerol nanofluids, the function *f* in Equation 6.2 is best expressed as follows:

$$\frac{\mu_{eff}}{\mu_o} = 1 + \Re[\eta] \cdot \left[\left(\frac{T}{T_0} \right)^{\alpha} \cdot \phi^{\sigma} \cdot \left(\frac{d}{r} \right)^{\gamma} \right], \qquad (6.4)$$

where $\Re$ is the system parameter, $[\eta]$ is the intrinsic viscosity, α, ω and γ are correlation coefficients. The $\Re$ and correlation coefficients α, ω and γ for this model are 240.19, 0.807, 2.480 and -0.522, respectively. The parity plot between the predicted results of Equation 6.4 and the experimental data is shown in Figure 6.7. The predicted results using this model show a maximum deviation of about ±15% from the experimental observations. Table 6.3 shows the statistics on the model's accuracy. Although the R^2 of this model is 0.9495, it still outperforms most cited theoretical and empirical models in the prediction of the Al$_2$O$_3$-glycerol viscosity data as explained below.
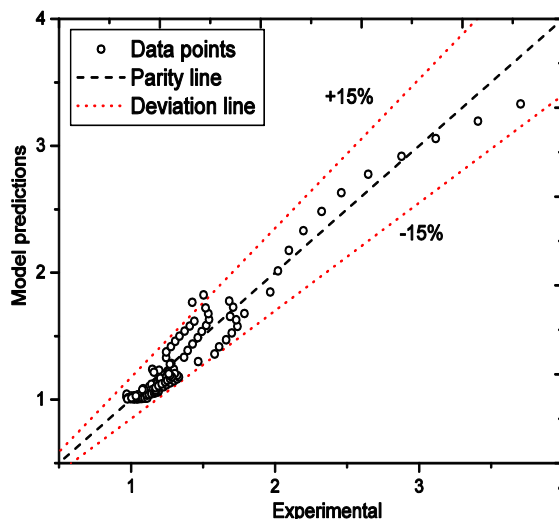
Figure 6.7: Parity plot between the dimensional analysis model (Equation 6.4)'s predictions and experimental data.

123

Table 6.3: Statistics on the accuracy of models

Statistical parameters	Dimensional analysis model	GMDH-NN model
R^2	0.9495	0.9905
RMSE	0.1094	0.0447623
SSE	1.5310	-
MAE	-	0.0346317

Figure 6.8 shows the comparison between the viscosity ratios of Al_2O_3-glycerol nanofluids obtained from the current experiment, the dimensionless empirical correlation based on the current experimental data and some of the several models reported in the literature. These models, which are used for comparison, are selected because of their high level of acceptability and citation in the nanofluid research field.

Most of the developed empirical models were missing some of the input parameters, such as size and temperature, while others did not give the value of the base fluid when there was no nanoparticle addition. For example, the model of Hosseini et al. [25] has all three parameters, as investigated in this work (size, volume fraction and temperature) and it was developed for Al_2O_3-water nanofluids. However, when $\phi = 0$, the model failed to reproduce the base fluid viscosity value. When it is applied to the present data, it does not achieve good correlation results.

As shown in Figure 6.8, the model in Equation 6.4 predicted the experimental data fairly well, unlike the previously published models. The main cause of the difference between the experimental data and the previously published models is that most of the models are based on low concentrations and micron size particles. Moreover, particle size and temperature were never considered in these models, and this may hinder the applicability of the models.

6.3.2 Modelling the viscosity of Al_2O_3-glycerol nanofluids using the GMDH-NN modelling technique

The GMDH algorithm was first introduced by Ivankhnenko [252] as a learning algorithm to perform the generation and selection of model structures based on the neurons that give optimised output. However, numerous researchers have formulated different hybrid

124

network systems based on the GMDH algorithms, such as GA-PNN, GMDH-NN and GMDH-PNN. This is because the initial GMDH algorithm by Ivankhnenko was limited in terms of the number of independent input variables that could be combined at a time during the iterative procedure. This limitation reduced the complexity and accuracy of the algorithm to predict non-linear systems. Since the viscosity data in the present study is non-linear, with particle size, temperature and volume fraction being considered, a hybrid GMDH-NN was achieved by combining GMDH and ANN to model the Al_2O_3-glycerol nanofluid experimental data.
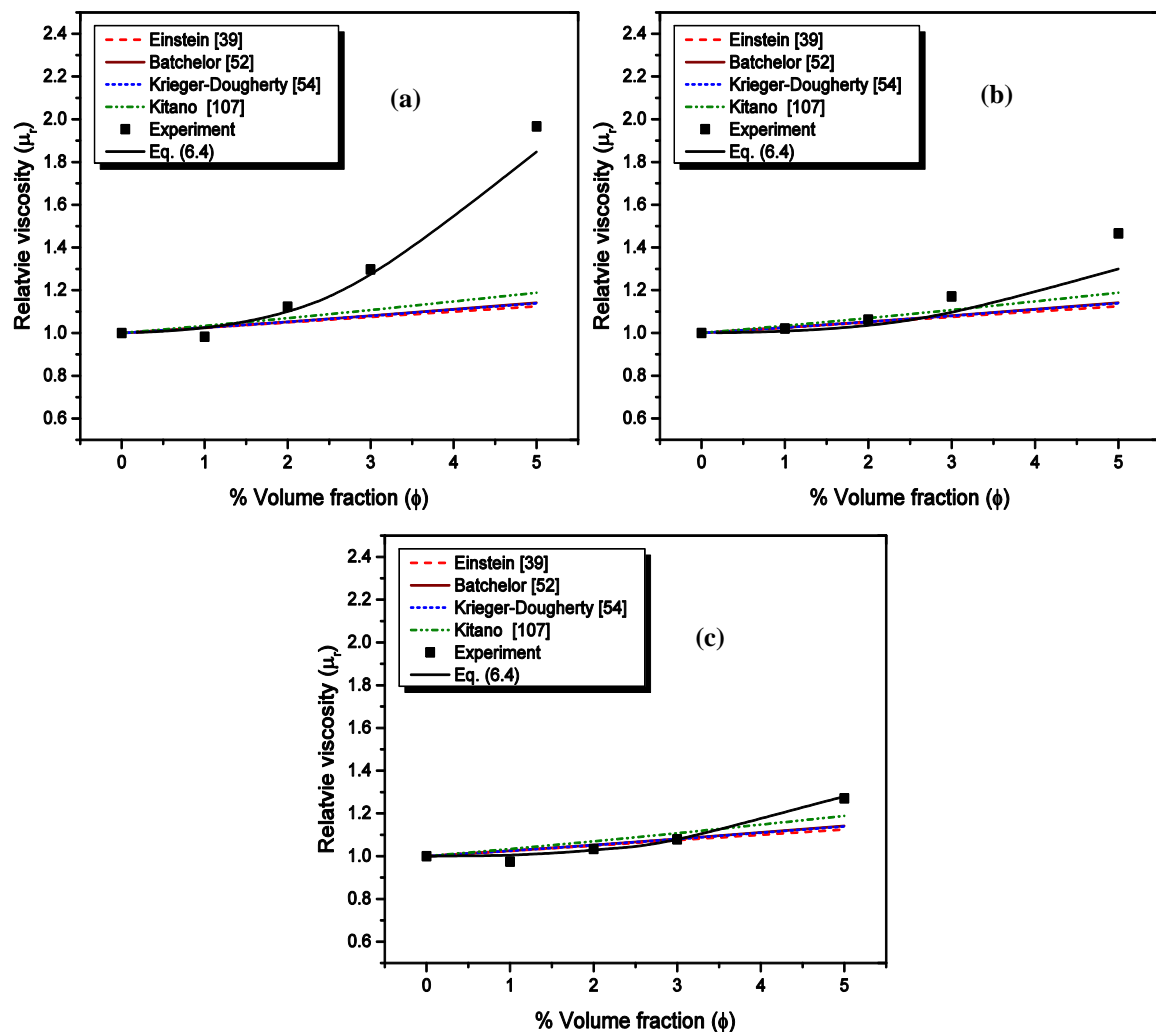
Figure 6.8: Comparison of the experimental relative viscosity of Al_2O_3-glycerol nanofluids with relative viscosity obtained from various model equations as a function of volume fraction: (a) 19 nm; (b) 139 nm; (c) 160 nm.

125

The deviation between the experimental data and the results predicted by the GMDH-NN is monitored using both the MAE and RMSE statistical tools, as in Table 6.3. The experimental data is divided into training and testing sets. The GMDH-NN system provided a polynomial system after it was executed using a random 60% of the 132 data points for training. The remaining 40% was used to validate the system.

The proposed GMDH-NN grand model is presented in Appendix B2. A parity plot between the results predicted by the GMDH-NN and the experimental data is presented in Figure 6.9. It is clear from the figure that the predicted results are on a par with experimentally observed data and the model's R^2 is 0.9905. Other statistics on the accuracy of the model are presented in Table 6.3 above. Figure 6.10 shows the performance of the GMDH-NN in predicting the viscosity of Al_2O_3-glycerol nanofluids with respect to temperature and volume fraction. The GMDH-NN model showed very good agreement with the experimental data for the independent parameters considered.

Considering the statistics provided in Table 6.3, the GMDH-NN model is more accurate than the dimensional analysis model. However, the model in Equation 6.4 is more user-friendly and less complex, especially when it is needed to introduce the formulation in a computational fluid dynamics (CFD) simulation where the nanofluid is employed as a heat transfer fluid.

Figure 6.9: Parity plot between the experimental relative viscosity of Al_2O_3-glycerol nanofluid and the result predicted by the GMDH-NN.

126
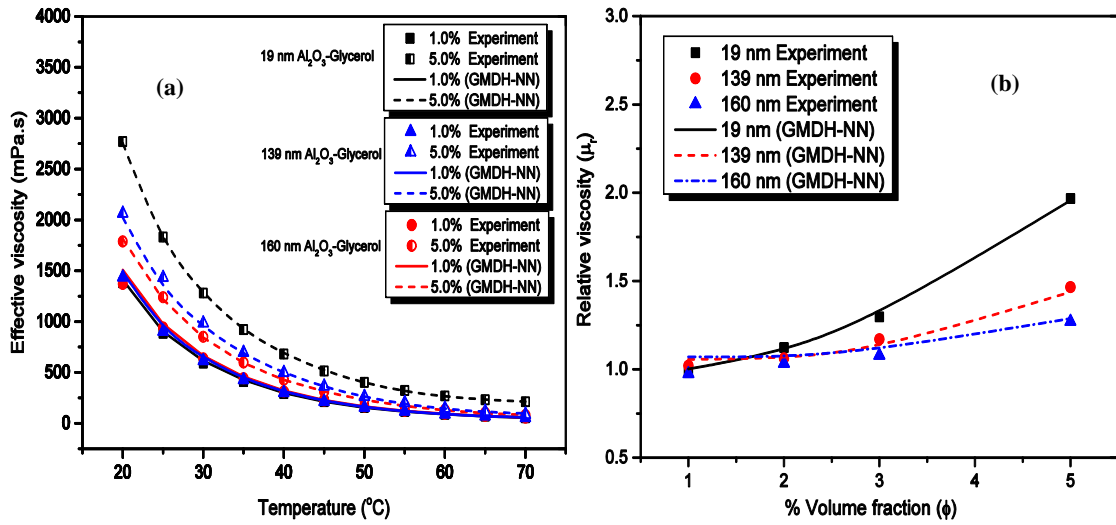
Figure 6.10: GMDH-NN performance in predicting the Al₂O₃-glycerol viscosity data: (a) effective viscosity vs temperature; (b) relative viscosity vs volume fraction.

6.4   MODELLING THE VISCOSITY OF SiO₂-EG AND SiO₂-GLYCEROL NANOFLUIDS

6.4.1   Modelling the viscosity of SiO₂-EG and SiO₂-glycerol nanofluids with non-dimensional analysis

The non-dimensional parameters for the SiO_2-based nanofluids are presented in Equation 6.5. The function *f* in Equation 6.5 is obtained using non-linear regression and presented in equations 6.6 and 6.7 for SiO_2-EG and SiO_2-glycerol respectively:

$$\pi_1 = \frac{\mu_{eff}}{\mu_o} = f\left(\pi_2 = \frac{T}{T_0}, \pi_3 = \phi, \right), \tag{6.5}$$

$$\frac{\mu_{eff}}{\mu_o} = 1 + a_1\phi + a_2\phi^\alpha\left(\frac{T}{T_0}\right) + \left(\phi\frac{T}{T_0}\right)^\sigma, \tag{6.6}$$

$$\frac{\mu_{eff}}{\mu_o} = 1 + a_1\phi + a_2\phi^\alpha\left(\frac{T}{T_0}\right) + a_3\phi\left(\frac{T}{T_0}\right)^\sigma, \tag{6.7}$$

where a_i, α and σ are correlation coefficients presented in Table 6.4. The parity plots between the experimental data and the predicted results of equations 6.6 and 6.7 are shown in Figure 6.11. The parity between the correlations and the experimental data show good agreement. Table 6.5 shows the statistics on the accuracy of the correlations.

127

Table 6.4 Correlation coefficients

Coefficient	Equation 6.6	Equation 6.7
a_1	8.7181	5.3639
a_2	-0.1029	-1.2498
a_3	-	7.8664
α	0.1153	0.5686
σ	0.6055	0.6726
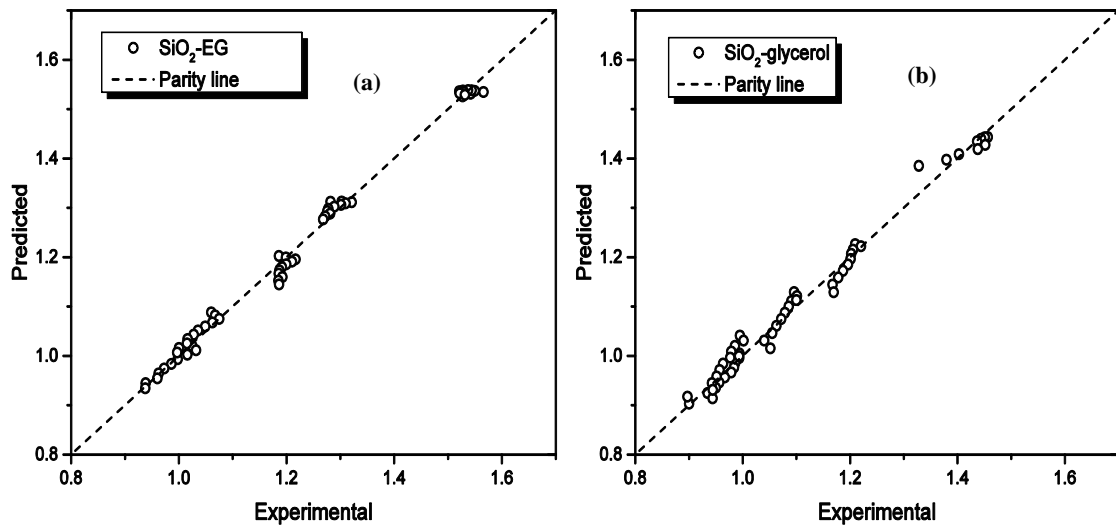
Figure 6.11: Parity plot between the experimental data and the model-predicted relative viscosity of SiO$_2$ based nanofluids: (a) Equation 6.6; (b) Equation 6.7.

Table 6.5: Statistics on the accuracy of models

Statistical parameters	Equation 6.6	Equation 6.7
R^2	0.9939	0.9879
SSE	0.0130	0.0210
MSE	0.0003	0.0004
RMSE	0.0160	0.0205

Presented in Figure 6.12 is the comparison between the correlations in equations 6.6 and 6.7 with some of the prominent viscosity models found in the open literature. It can be seen that the presented correlations performed better than the other models. The

128

behaviour of these prominent models in predicting the viscosity of SiO_2-EG and SiO_2-glycerol is similar to that presented in previous sections on the other nanofluids investigated in this work.
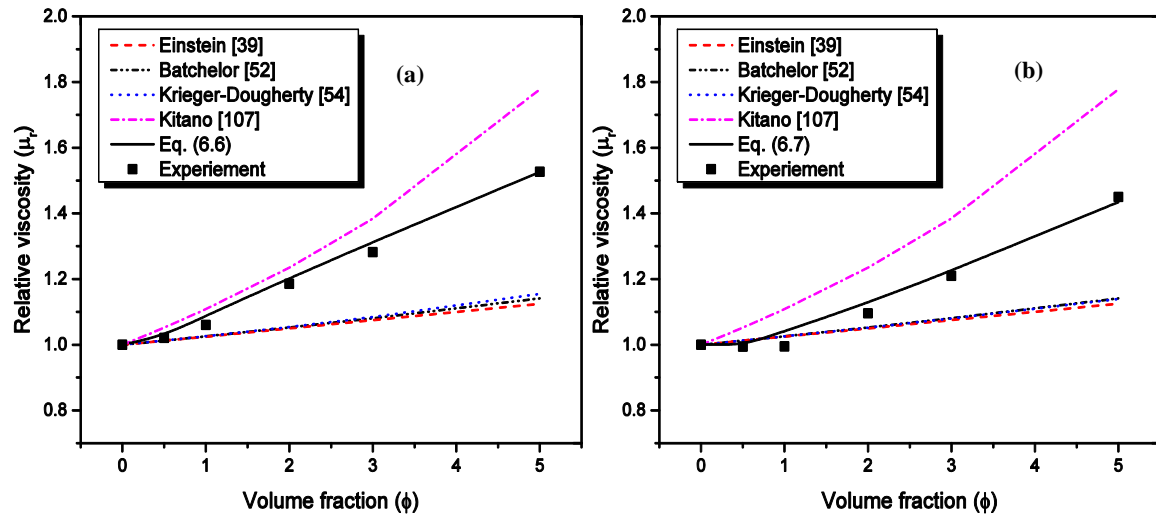
Figure 6.12: Comparison between the models in Equation 6.6 for SiO_2-EG, Equation 6.7 for SiO_2-glycerol and some prominent viscosity models.

6.4.2 Modelling the viscosity of SiO_2-EG and SiO_2-glycerol nanofluids using the GMDH-NN modelling technique

This technique is the same as that applied in Section 6.3.2. However, 55 data points are used to model both the viscosity of SiO_2-EG and the viscosity of SiO_2-glycerol nanofluids. The GMDH-NN modelling technique was executed using a randomised 80% of the data set for training. The remaining 20% was used to test the system's best equation. The proposed GMDH-NN grand model is presented in appendices B3 and B4 for SiO_2-EG and SiO_2-glycerol nanofluids respectively. A parity plot between the results predicted by the GMDH-NN and the experimental data is presented in Figure 6.13 for both SiO_2-EG and SiO_2-glycerol nanofluids. It is clear from Figure 6.13 (a and b) that the predicted results are at parity with experimentally observed data, and the two models have R^2 values of 0.9989 and 0.9985 for SiO_2-EG and SiO_2-glycerol nanofluids respectively. Their respective MAEs are 0.005108 and 0.005254, and their RSMEs are 0.006657 and 0.006715.
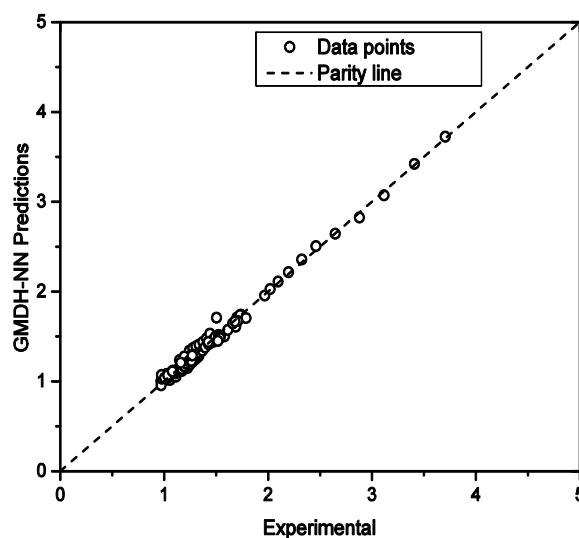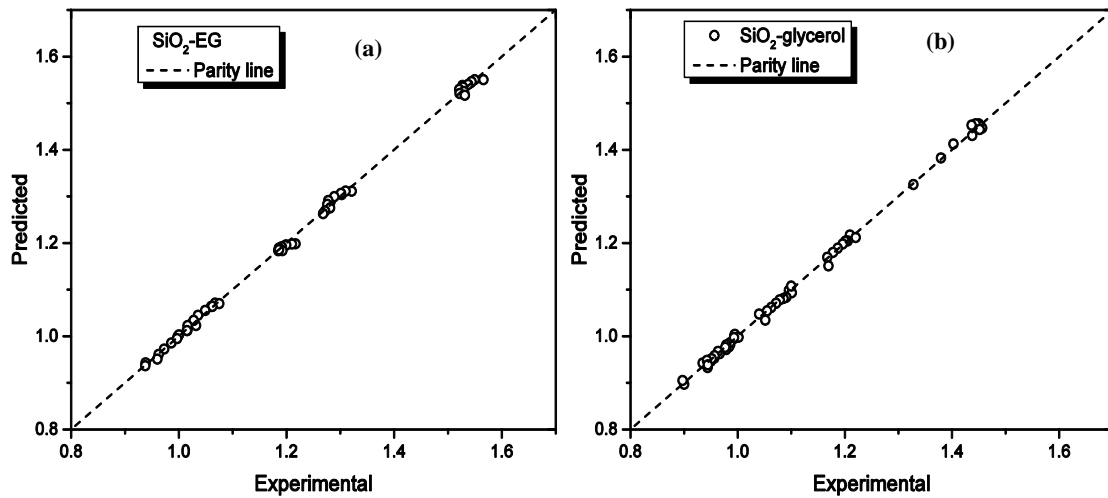
Figure 6.13: Parity plot between the experimental relative viscosity of SiO$_2$-EG and SiO$_2$-glycerol nanofluids and the results predicted by the GMDH-NN.

Figure 6.14 shows the performance of the GMDH-NN in predicting the viscosity of SiO$_2$-EG and SiO$_2$-glycerol nanofluids at various temperature, and Figure 6.15 shows the performance of the models at various volume fractions. The GMDH-NN models showed good agreement with the experiments. Considering the RMSE statistics provided for the two GMDH-NN models and the correlations in equations 6.6 and 6.7, the GMDH-NN models are slightly more accurate than the dimensional analysis models. However, the correlations given in equations 6.6 and 6.7 are simpler and can easily be integrated into numerical models for CFD analysis involving SiO$_2$-EG or SiO$_2$-glycerol nanofluids.
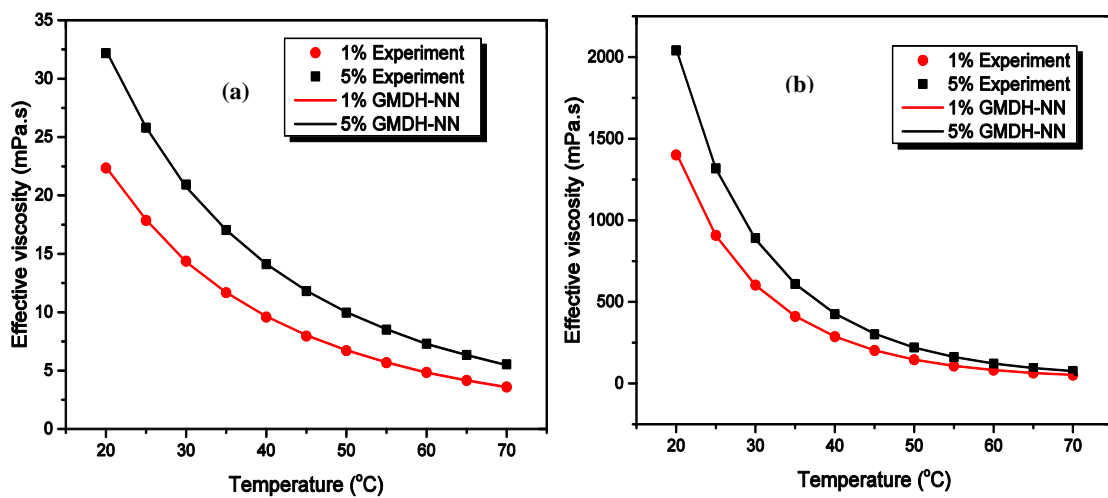
Figure 6.14: GMDH-NN performance in predicting the effective viscosity of the SiO$_2$-based nanofluids: (a) SiO$_2$-EG; (b) SiO$_2$-glycerol.

130
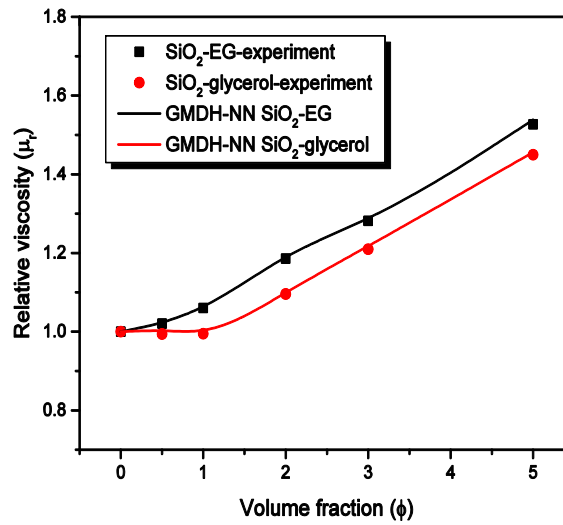
Figure 6.15: GMDH-NN performance in predicting the relative viscosity of the SiO₂-EG and SiO₂-glycerol nanofluids.

6.5   CONCLUSION AND RECOMMENDATION

In this chapter, non-dimensional analysis, regression, GMDH-NN, GA-PNN and FCM-ANFIS modelling techniques have been employed to model the viscosity of different nanofluids considering the following effective parameters: particle size, volume fraction and working temperature. The literature has shown that these parameters are the most influential factors affecting the viscosity of nanofluids.

The results of all the modelling techniques mentioned in the preceding sections were compared with experimental data. In all cases, the predictions matched the experimental data with good degrees of accuracy. The results of the correlations from the dimensional analysis were also compared with several well-cited correlations from literature and, in all the cases, the proposed correlations outperformed the other models. This study further showed the capability of using AI for modelling non-linear engineering problems, such as the viscosity of nanofluids.

In the future, base fluid properties and ultrasonication energy could be introduced as parameters to expand the robustness of the models.

131

CHAPTER 7:   CONCLUSIONS AND RECOMMENDATIONS

7.1   SUMMARY

Nanofluids are modified heat transfer fluids aimed at mitigating the poor heat transfer efficiency of conventional heat transfer fluids such as water, EG, PG, engine oil, glycerol and refrigerants. This new class of heat transfer fluid was first developed nearly two decades ago and much research has been carried out on the fluid since then to either study or improve its properties. Notably, thermophysical properties, such as thermal conductivity and heat transfer performance in different heat exchangers, were the most investigated aspects of the fluid. Rheological properties are next in line, while properties such as electrical conductivity, pH and electrical diffusivity are seldom investigated, despite their scientific and engineering importance.

Surprisingly, most of the experimental investigations on nanofluids were crudely executed because the field is still new and lacking standards in most of the processes involved, especially in the method of preparing nanofluids from the two-step method. Many reported experimental nanofluid investigations in which the two-step method of nanofluid preparation was used only chose an arbitrary time for the preparation process.

In many cases, the power rating of the dispersion-assisting mechanism, setting and/or energy input into the preparation process are left out during the reporting. Arbitrarily choosing the preparation time may not only be inappropriate, as it may be more than what is required or not enough, but it also makes it difficult for the research community to repeat the experimental procedure. Therefore, this research was devoted to creating homogeneous nanofluids, employing a standardised method of preparation and reporting on the energy input into the preparation process. This was achieved by calculating the total energy per unit volume (energy density) from the ultrasonication mechanism into the dispersion process. The dispersion consistency was monitored using the viscosity value at room temperature. The energy density that gave a minimised viscosity value shows a good dispersion of the nanoparticles in the base fluid.

132

The influence of nanoparticle size, volume fraction, temperature, base fluid type and nanoparticle type on the viscosity, electrical conductivity and pH of MgO-EG, Al_2O_3-glycerol, SiO_2-EG and SiO_2-glycerol nanofluids were investigated. The experimental investigation of these thermophysical properties is essential at this stage in nanofluid research, as not much thorough work has been done in this respect. Furthermore, there are still challenges in modelling and predicting the thermophysical properties of nanofluids because it involves too many factors that can affect nanofluid properties. Therefore, research that can find an accurate model for predicting the thermophysical properties of nanofluids, such as viscosity, is vital.

In this dissertation, the methods of dimensional analysis and regression modelling were applied to develop empirical correlations for predicting the viscosity of the different nanofluids considered. The results of the proposed correlations were compared with the experimental data, as well as other prominent correlations in the open literature. The use of AI was also applied by using the GMDH-NN, GA-PNN and FCM-ANFIS modelling techniques, together with the input-output experimental data. All three AI techniques also accurately predicted the experimental data.

7.2 CONCLUSIONS

Chapter 1 of this dissertation provided an overall introduction of the research, and clearly outlined the specific objectives and scope of the work.

Chapter 2 reviewed the theoretical background on the viscosity, electrical conductivity and pH of nanofluids. It included the different classical viscosity models that had been developed for micrometric suspensions, the new theoretical models that considered some of the factors that are pertinent to the viscosity of nanofluids, and models that had been developed based on experimental input-output data. The different factors that affect the viscosity of nanofluids, such as particle size, temperature, volume fraction, base fluid type, shapes and shear stress/shear rate, were all reviewed based on available data in the open literature.

The pH and electrical conductivity of nanofluids are both related to the stability of nanofluids and not much research has been done to systematically investigate the factors

133

that may be responsible for enhancing or changing these two significant properties. Consequently, the influence of some of the aforementioned factors on the pH and electrical conductivity of nanofluids was appraised based on what is available in the literature. Elaborate information and recent improvements on other modelling techniques that border on the use of AI for the prediction of thermophysical properties, such as viscosity and the thermal conductivity of nanofluids, were adequately presented.

Chapter 3 presented the experimental methodology that was adopted in the execution of the experimental investigations of the factors that affect the viscosity, electrical conductivity and pH of nanofluids. It also outlined the modelling techniques used for the development of viscosity models for different nanofluids. The methods used for nanoparticles and nanofluid characterisation based on TEM, XRD, EDS, UV-visible spectrophotometry and zeta potential measurements were detailed.

The results of the characterisations and the experimental investigation on the viscosity of MgO-EG, Al_2O_3-glycerol, SiO_2-EG and SiO_2-glycerol nanofluids were presented in Chapter 4. The nanofluid viscosity reduced as the ultrasonication energy density increased until a minimised viscosity was obtained. The viscosity decreased exponentially as the temperature in the nanofluid increased. The addition of nanoparticles to the base fluids gave higher viscosity values compared to the base fluid, and as the volume fraction of the nanoparticle increased, so the viscosity also increased.

Different particle sizes revealed different viscosity values, even for the same nanoparticle type. Smaller nanoparticles revealed higher viscosity values due to the increased particle number density (more surface contact), Brownian motion and particle-particle interactions. When the same nanoparticle types were dispersed in different base fluids, the relative viscosity showed different enhancements. The implication of this is that base fluid properties are also important factors that should be considered when investigating or designing based on nanofluids. Different nanoparticle types suspended in the same base fluid do not really show much difference in relative viscosity.

In Chapter 5, the results of the experimental investigation of the electrical conductivity and pH of nanofluids were discussed. Present findings showed that, as the temperature of the nanofluid increased, so the electrical conductivity increased, while the pH of the

134

nanofluid decreased. Adding nanoparticles to the base fluid produced an increase in the electrical conductivity and pH values of the nanofluids, and as the volume fraction increased, so the electrical conductivity increased until it reached a critical value of surface charge density at which the counterion condensation effect set in.

Surprisingly, the pH values at the point of counterion condensation also plateau. Different particle types in the same base fluids produce different electrical conductivity and pH values due to different types of ions and valence on the nanoparticles. Different base fluids also produced different electrical conductivity and pH values when the same type of nanoparticle was suspended. Smaller particles showed slightly higher electrical conductivity until counterion condensation effects set in. In terms of pH, the smaller the particle size, the higher the pH enhancement.

Finally, in Chapter 6, the dimensional analysis with a regression technique was used for modelling the viscosity of the nanofluids investigated in Chapter 4. This modelling technique considered the following essential factors: nanoparticle size, volume fraction temperature, capping layer thickness, the viscosity of the base fluid, the density of the base fluid and the density of the nanofluid as input. The factors were reduced to non-dimensional parameters and regression was used to obtain the best combination of non-dimensional parameters based on the experimental input-output data.

The results of the models were compared with the experimental data points and with prominent, well-cited correlations from the literature. The statistics on the goodness of predictions show that the developed models are in good agreement with the experimental data and show improved accuracy with experimental data in comparison with existing models. The results of models that were developed using GMDH-NN, GA-PNN and FCM-ANFIS all showed good agreement with the experimental data. They compared very well in terms of performance with the models generated through dimensional analysis.

7.3   RECOMMENDATIONS

Since ultrasonication energy density influences the level of dispersion of nanoparticles in the base fluids, it is highly recommended that the best ultrasonication energy density

135

should always be sought, especially when nanofluid is prepared using the two-step method. Choosing an arbitrary time for ultrasonication or any other dispersion-assisting mechanism may be counterproductive regarding the time and energy input into the process.

The experimental results showed that the type of base fluid is instrumental in the level of enhancement recorded in the viscosity of the nanofluids. Future research should be directed at understanding which properties of the base fluid may be responsible for viscosity enhancement. More research should also be carried out on the influence of types of nanoparticles on the viscosity of nanofluids. It is important that models like those proposed in this thesis should always be used in CFD simulation if these types of nanofluids are to be implemented rather than the generic theoretical models that underpredicted in every case tested thus far.

Change in temperature significantly affects the pH of nanofluids, while a change in pH affects the stability of nanofluids. Future research should also focus on developing nanofluids that will be stable if kept at a temperature that produces pH that gives good stability. Lastly, the modelling techniques applied in this thesis can be further extended to modelling the evolution of the pH, electrical conductivity, thermal diffusivity, surface tension and other properties of nanofluids.

REFERENCES

[1]   Maxwell, J.C., *Electricity and magnetism*, Oxford, Clarendon, 1873.

[2]   Masoumi, N., Sohrabi, N. and Behzadmehr, A., A new model for calculating the effective viscosity of nanofluids, *Journal of Physics D: Applied Physics*, vol. 42, no. 5, pp. 0555011–0555016, 2009.

[3]   Choi, S.U.S., Enhancing thermal conductivity of fluid with nanoparticles, *Proceeding of the American Society of Mechanical Engineers (ASME)*, pp. 99–109, New York, NY, 1995.

[4]   Lee, S., Choi, U.S. and Li, S., Measuring thermal conductivity of fluids containing oxide nanoparticles, *Journal of Heat Transfer*, vol. 121, pp. 280–289, 1999.

[5]   Murshed, S.M.S., Leong, K.C. and Yang, C., Thermophysical and electrokinetci properties of nanofluids – a critical review, *Applied Thermal Engineering*, vol. 28, pp. 2109–2125, 2008.

[6]   Xiang-Qi, W. and Arun, S.M., A review on nanofluids – Part II: experiments and applications, *Brazilian Journal of Chemical Engineering*, vol. 24, no. 4, pp. 631–648, 2008.

[7]   Vajjha, R.S., Das, D.K. and Namburu, P.K., Numerical study of fluid dynamic and heat transfer performance of Al_2O_3 and CuO nanofluids in the flat tubes of a radiator, *International Journal of Heat and Fluid Flow*, vol. 31, no. 4, pp. 613–621, 2010.

[8]   Peyghambarzadeh, S.M., Hashemabadi, S.H., Jamnani, M.S. and Hoseini, S.M., Improving the cooling performance of automobile radiator with Al_2O_3/water nanofluid, *Applied Thermal Engineering*, vol. 31, no. 10, pp. 1833–1838, 2011.

[9]   Lee, J-H., Hwang, K.S., Jang, S.P., Lee, B.H., Kim, J.H., Choi, S.U.S.S. and Choi, C.J., Effective viscosities and thermal conductivities of aqueous nanofluids containing low volume concentrations of Al_2O_3 nanoparticles, *International Journal of Heat and Mass Transfer*, vol. 51, no. 11–12, pp. 2651–2656, 2008.

[10]   Yu, W., Xie, H., Chen, L. and Li, Y., Investigation of thermal conductivity and viscosity of ethylene glycol based ZnO nanofluid, *Thermochimica Acta*, vol. 491, no. 1–2, pp. 92–96, 2009.

[11]   Eastman, J.A., Phillpot, S.R., Choi, S.U.S. and Keblinski, P., Thermal transport in nanofluids, *Annual Review of Materials Research*, vol. 34, no. 1, pp. 219–246, 2004.

137

[12]   Maïga, S.E., Palm, S.J., Nguyen, C.T., Roy, G. and Galanis, N., Heat transfer enhancement by using nanofluids in forced convection flows, *International Journal for Heat and Fluid Flow*, vol. 26, pp. 530–546, 2005.

[13]   Heyhat, M.M.M., Kowsary, F., Rashidi, A.M.M., Memenpour, M.H., Amrollahi, A. and Momenpour, M.H., Exeprimental investigation of laminar convective heat transfer and pressure drop of water-based Al_2O_3 nanofluids in fuly developed flow regime, *Experimental Thermal and Fluid Science*, vol. 44, pp. 483–489, 2013.

[14]   Quaresma, J.N.N., Macêdo, E.N., Da Fonseca, H.M., Orlande, H.R.B., Cotta, R.M., Macedo, E.N. and Fonseca, H.M.D., An analysis of heat conduction models for nanofluids, *Heat Transfer Engineering*, vol. 31, no. 14, pp. 1125–1136, 2010.

[15]   Wang, J.J., Zheng, R.T., Gao, J.W. and Chen, G., Heat conduction mechanisms in nanofluids and suspensions, *Nano Today*, vol. 7, no. 2, pp. 124–136, 2012.

[16]   Wen, D., Lin, G., Vafaei, S. and Zhang, K., Review of nanofluids for heat transfer applications, *Particuology*, vol. 7, no. 2, pp. 141–150, 2009.

[17]   Philip, J. and Shima, P.D., Thermal properties of nanofluids, *Advances in Colloid and Interface Science*, vol. 183, pp. 30–45, 2012.

[18]   Buschmann, M.H., Thermal conductivity and heat transfer of ceramic nanofluids, *International Journal of Thermal Sciences*, vol. 62, pp. 19–28, 2012.

[19]   Mallick, S.S., Mishra, A. and Kundan, L., An investigation into modelling thermal conductivity for alumina-water nanofluids, *Powder Technology*, vol. 233, pp. 234–244, 2013.

[20]   Fan, J. and Wang, L., Heat conduction in nanofluids: structure-property correlation, *International Journal of Heat and Mass Transfer*, vol. 54, no. 19, pp. 4349–4359, 2011.

[21]   Saleh, R., Putra, N., Prakoso, S.P. and Septiadi, W.N., Experimental investigation of thermal conductivity and heat pipe thermal performance of ZnO nanofluids, *International Journal of Thermal Sciences*, vol. 63, pp. 125–132, 2013.

[22]   Altan, C.L., Elkatmis, A., Yuksel, M., Aslan, N. and Bucak, S., Enhancement of thermal conductivity upon application of magnetic field to Fe_3O_4 nanofluids, *Journal of Applied Physics*, vol. 110, no. 093917, pp. 1–8, 2011.

[23] Gupta, S.S., Siva, M.V, Krishnan, S., Sreeprasad, T.S., Singh, P.K., Pradeep, T. and Das, S.K., Thermal conductivity enhancement of nanofluids containing graphene nanosheets, *Journal of Heat Transfer*, vol. 110, no. 084302, pp. 1–7, 2011.

[24] Chandrasekar, M., Suresh, S. and Bose, A.C., Experimental investigations and theoretical determination of thermal conductivity and viscosity of Al_2O_3/water nanofluid, *Experimental Thermal and Fluid Science*, vol. 34, no. 2, pp. 210–216, 2010.

[25] Hosseini, S., Moghadassi, A. and Henneke, D.E., A new dimensionless group model for determining the viscosity of nanofluids, *Journal of Thermal Analysis and Calorimetry*, vol. 100, pp. 873–877, 2010.

[26] Namburu, P.K., Kulkarni, D.P., Misra, D. and Das, D.K., Viscosity of copper oxide nanoparticles dispersed in ethylene glycol and water mixture, *Experimental Thermal and Fluid Science*, vol. 32, pp. 397–402, 2007.

[27] Rashin, M.N. and Hemalatha, J., Viscosity studies on novel copper oxide − coconut oil nanofluid, *Experimental Thermal and Fluid Science*, vol. 48, pp. 67–72, 2013.

[28] Moosavi, M., Goharshadi, E.K. and Youssefi, A., Fabrication, characterization and measurement of some physicochemical properties of ZnO nanofluids, *International journal of Heat and Fluid Flow*, vol. 31, no. 4, pp. 599–605, 2010.

[29] Abareshi, M., Sajjadi, S.H., Zebarjad, S.M. and Goharshadi, E.K., Fabrication, characterization, and measurement of viscosity of α-Fe_2O_3-glycerol nanofluids, *Journal of Molecular Liquids*, vol. 163, no. 1, pp. 27–32, 2011.

[30] Kole, M. and Dey, T.K., Effect of aggregation on the viscosity of copper oxide-gear oil nanofluids, *International Journal of Thermal Sciences*, vol. 50, no. 9, pp. 1741–1747, 2011.

[31] Avsec, J. and Oblak, M., The calculation of thermal conductivity, viscosity and thermodynamic properties for nanofluids on the basis of statistical nanomechanics, *International Journal of Heat and Mass Transfer*, vol. 50, no. 21–22, pp. 4331–4341, 2007.

[32] Okhio, C., Hodges, D. and Black, J., Review of literature on nanofluid flow and heat transfer properties, *Cyber Journals: Multidisciplinary Journals in Science and Technology, Journal of Selected Areas in Nanotechnology*, pp. 1–8, 2010.

139

[33] Sarojini, K.G.K., Manoj, S.V, Singh, P.K., Pradeep, T. and Das, S.K., Electrical conductivity of ceramic and metallic nanofluids, *Colloids and Surfaces A: Physicochemical and Engineering Aspects*, vol. 417, pp. 39–46, 2013.

[34] Andablo-Reyes, E., Hidalgo-Álvarez, R. and Vicente, J., Controlling friction using magnetic nanofluids, *Soft Matter*, vol. 7, pp. 880–883, 2011.

[35] Yao, G.Z., Yap, F.F., Chen, G., Li, W.H. and Yeo, S.H., MR damper and its application for semi-active control of vehicle suspension system, *Mechatronics*, vol. 12, no. 7, pp. 963–973, 2002.

[36] Modesto-Lopez, L.B. and Biswas, P., Role of the effective electrical conductivity of nanosuspensions in the generation of TiO_2 agglomerates with electrospray, *Journal of Aerosol Science*, vol. 41, no. 8, pp. 790–804, 2010.

[37] White, S.B., Shih, A.J. and Pipe, K.P., Investigation of the electrical conductivity of propylene glycol-based ZnO nanofluids, *Nanoscale Research Letters*, vol. 6, pp. 346–350, 2011.

[38] Meyer, J.P., Nwosu, P., Sharifpur, M. and Ntumba, T., Parametric analysis of effective viscosity models for nanofluids, *Proceedings of the ASME 2012 International Mechanical Engineering Congress and Exposition*, pp. 1–9, Houston, TX, 2012.

[39] Einstein, A., A new determination of molecular dimensions, *Annalen der Physik*, vol. 4, no. 19, pp. 37–62, 1906.

[40] Smoluchowski, M.V, Theoretishche bemerkungen uber die viskositat der kolloide, *Kolloidzschr*, vol. 80, pp. 190–195, 1916.

[41] Jeffery, G.B., The motion of ellipsoidal particles immersed in a viscous fluid, *Proceedings of the Royal Society A: Mathematical, Physical and Engineering Sciences*, vol. 102, no. 715, pp. 161–179, 1922.

[42] Taylor, G.I., The viscosity of a fluid containign small drops of another fluid, *Proceedings of the Royal Society.*, vol. 138, no. 834, pp. 41–48, 1932.

[43] Brinkman, H.C., The viscosity of concentrated suspensions and solutions, *Journal of Chemical Physics*, vol. 20, no. 4, pp. 571, 1952.

[44] Bull, H., The electroviscous effect in egg albumin solutions, *Transactions of the Faraday Society.*, no. 80, pp. 80–84, 1940.

140

[45] Booth, F., The electroviscous effect for suspensions of solid spherical particles, *Proceedings of the Royal Society A: Mathematical, Physical and Engineering Sciences*, vol. 203, no. 1075, pp. 533–551, 1950.

[46] Ward, S. and Whitmore, R., Studies of the viscosity and sedimentation of suspensions Part 1 – the viscosity of suspension of spherical particles, *British Journal of Applied Physics*, vol. 286, pp. 1–6, 1950.

[47] Vand, V., Viscosity of solutions and suspensions. I. Theory, *The Journal of Physical Chemistry*, pp. 277–299, 1948.

[48] Williams, P.S., Flow of concentrated suspensions, *Journal of Applied Chemistry*, vol. 3, no. 3, pp. 120–128, 1953.

[49] Mooney, M., The viscosity of a concentrated suspension of spherical particles, *Journal of Colloid Science*, no. 113, pp. 3–4, 1951.

[50] Roscoe, R., The viscosity of suspensions of rigid spheres, *Journal of Applied Physics*, vol. 267, pp. 3–6, 1952.

[51] Maron, S. and Fok, S., Effect of concentration on flow behavior of glass sphere suspensions, *Journal of Colloid Science*, pp. 540–542, 1953.

[52] Batchelor, G., The effect of Brownian motion on the bulk stress in the suspension of sphrerical particles, *Journal of Fluid Mechanics*, vol. 83, no. 1, pp. 97–117, 1977.

[53] Chen, H., Ding, Y. and Tan, C., Rheological behaviour of nanofluids, *New Journal of Physics*, vol. 9, no. 10, pp. 367–391, 2007.

[54] Krieger, I. and Dougherty, T., A mechanicsm for non-Newtonian flow in suspensions of rigid spheres, *Transactions of the Society. Rheology*, vol. 3, pp. 137–152, 1959.

[55] Kole, M. and Dey, T.K., Thermophysical and pool boiling characteristics of ZnO-ethylene glycol nanofluids, *International Journal of Thermal Sciences*, vol. 62, pp. 61–70, 2012.

[56] Farris, R., Prediction of the viscosity of multimodal suspensions from unimodal viscosity data, *Transactions of the Society of Rheology*, vol. 12, pp. 281–301, 1968.

[57] Chong, J., Christiansen, E. and Baer, A., Rheology of concentrated suspensions, *Journal of Applied Polymer Science*, vol. 15, pp. 2007–2021, 1971.

[58]   Storms, R.F., Ramarao, B.V. and Weiland, R.H., Low shear rate viscosity of bimodally dispersed suspensions, *Powder Technology*, vol. 63, no. 3, pp. 247–259, 1990.

[59]   Dames, B., Morrison, B.R. and Willenbacher, N., An empirical model predicting the viscosity of highly concentrated, bimodal dispersions with colloidal interactions, *Rheologica Acta*, vol. 40, no. 5, pp. 434–440, 2001.

[60]   Muralidharan, G. and Runkana, V., Rheological modeling of spherical polymeric gels and dispersions incorporating the influence of particle size distribution and surface forces, *Industrial and Engineering Chemistry Research*, vol. 48, no. 19, pp. 8805–8811, 2009.

[61]   Servais, C., Jones, R. and Roberts, I., The influence of particle size distribution on the processing of food, *Journal of Food Engineering*, vol. 51, pp. 201–208, 2002.

[62]   Kole, M. and Dey, T.K., Viscosity of alumina nanoparticles dispersed in car engine coolant, *Experimental Thermal and Fluid Science*, vol. 34, no. 6, pp. 677–683, 2010.

[63]   Lundgren, T.S., Slow flow through stationary random beds and suspensions of spheres, *Journal of Fluid Mechanics*, vol. 51, no. 2, pp. 273–299, 1972.

[64]   Graham, A.L., On the viscosity of suspensions of solid spheres, *Applied Scientific Research*, vol. 37, pp. 275–286, 1981.

[65]   Saitô, N., Concentration dependence of the viscosity of high polymer solution, *Journal of the Physical Society of Japan*, vol. 5, pp. 4–8, 1950.

[66]   Hatschek, E., The general theory of viscosity of two phase systems, *Transactions of the Faraday Society*, vol. 9, no. 2, pp. 80–92, 1913.

[67]   Thomas, C.U. and Muthukumar, M., Three-body hydrodynamic effects on viscosity of suspensions of spheres, *The Journal of Chemical Physics*, vol. 94, no. 7, pp. 5180, 1991.

[68]   Frankel, N. and Acrivos, A., On the viscosity of a concentrated suspension of solid spheres, *Chemical Engineering Science*, vol. 22, pp. 847–853, 1967.

[69]   Prasher, R., Bhattacharya, P. and Phelan, P.E., Brownian-motion-based convective-conductive model for the effective thermal conductivity of nanofluids, *Journal of Heat Transfer*, vol. 128, no. 6, pp. 588–595, 2006.

[70]   Graf, W.H., *Hydraulics of Sediment Transport*, New York, NY, McGraw-Hill, 1971.

[71] Batchelor, G.K. and Green, J.T., The hydrodynamic interaction of two small freely-moving spheres in a linear flow field, *Journal of Fluid Mechanics*, vol. 56, no. 3, pp. 401–427, 1972.

[72] Cheng, N. and Law, A., Exponential formula for computing effective viscosity, *Powder Technology*, vol. 129, pp. 156–160, 2003.

[73] Chen, H., Ding, Y., He, Y. and Tan, C., Rheological behaviour of ethylene glycol based titania nanofluids, *Chemical Physics Letters*, vol. 444, pp. 333–337, 2007.

[74] Tseng, W.J. and Chen, C., Effect of polymeric dispersant on rheological behavior of nickel-terpineol suspensions, *Materials Science and Engineering: A*, vol. 347, no. 1, pp. 145–153, 2003.

[75] Tseng, W.J. and Lin, K., Rheology and colloidal structure of aqueous TiO_2 nanoparticle suspensions, *Materials Science and Engineering: A*, vol. 355, pp. 186–192, 2003.

[76] Chen, H., Ding, Y., Lapkin, A. and Fan, X., Rheological behaviour of ethylene glycol-titanate nanotube nanofluids, *Journal of Nanoparticle Research*, vol. 11, pp. 1513–1520, 2009.

[77] Horri, B.A., Ranganathan, P., Selomulya, C. and Wang, H., A new empirical viscosity model for ceramic suspensions, *Chemical Engineering Science*, vol. 66, no. 12, pp. 2798–2806, 2011.

[78] Sahoo, B.C., Vajjha, R.S., Ganguli, R., Chukwu, G.A. and Das, D.K., Determination of rheological behaviour of aluminium oxide nanofluid and development of new viscosity correlations, *Petroleum Science and Technology*, vol. 27, pp. 1757–1770, 2009.

[79] Nguyen, C.T., Desgranges, F., Galanis, N., Roy, G., Maré, T., Boucher, S., Angue Mintsa, H., Maré, T. and Mintsa, H.A., Viscosity data for Al_2O_3-water nanofluid – hysteresis: is heat transfer enhancement using nanofluids reliable?, *International Journal of Thermal Sciences*, vol. 47, no. 2, pp. 103–111, 2008.

[80] Mahbubul, I.M., Saidur, R. and Amalina, M.A., Latest developments on the viscosity of nanofluids, *International Journal of Heat and Mass Transfer*, vol. 55, no. 4, pp. 874–885, 2012.

[81] Hernández Battez, A., Viesca, J.L., González, R., García, A., Reddyhoff, T. and Higuera-Garrido, A., Effect of shear rate, temperature and particle concentration on

143

the rheological properties of ZnO and ZrO$_2$ Nanofluids, *Tribology Transactions*, vol. 57, no. 3, pp. 489–495, 2014.

[82]   Vakili-Nezhaad, G. and Dorany, A., Effect of single-walled carbon nanotube on the viscosity of lubricants, *Energy Procedia*, vol. 14, no. 1998, pp. 512–517, 2012.

[83]   Garg, J., Poudel, B., Chiesa, M., Gordon, J.B., Ma, J.J., Wang, J.B., Ren, Z.F., Kang, Y.T., Ohtani, H., Nanda, J., McKinley, G.H. and Chen, G., Enhanced thermal conductivity and viscosity of copper nanoparticles in ethylene glycol nanofluid, *Journal of Applied Physics*, vol. 103, no. 7, pp. 074301, 2008.

[84]   Godson, L., Raja, B., Lal, D.M. and Wongwises, S., Experimental investigation on the thermal conductivity and viscosity of silver-deionized water nanofluid, *Experimental Heat Transfer*, vol. 23, no. 4, pp. 317–332, 2010.

[85]   Duangthongsuk, W. and Wongwises, S., Measurement of temperature-dependent thermal conductivity and viscosity of TiO$_2$-water nanofluids, *Experimental Thermal and Fluid Science*, vol. 33, no. 4, pp. 706–714, 2009.

[86]   Colla, L., Fedele, L., Scattolini, M. and Bobbo, S., Water-based Fe$_2$O$_3$ nanofluid characterization: thermal conductivity and viscosity measurements and correlation, *Advances in Mechanical Engineering*, vol. 2012, pp. 1–8, 2012.

[87]   Chevalier, J., Tillement, O. and Ayela, F., Rheological properties of nanofluids flowing through microchannels, *Applied Physics Letters*, vol. 91, no. 233103, pp. 1–3, 2007.

[88]   Suganthi, K.S. and Rajan, K.S., Temperature induced changes in ZnO-water nanofluid: zeta potential, size distribution and viscosity profiles, *International Journal of Heat and Mass Transfer*, vol. 55, no. 25–26, pp. 7969–7980, 2012.

[89]   Suganthi, K., Anusha, N. and Rajan, K., Low viscous ZnO-propylene glycol nanofluid: a potential coolant candidate, *Journal of Nanoparticle Research*, vol. 15, no. 1986, pp. 1986–1–6, 2013.

[90]   Singh, D., Timofeeva, E., Yu, W., Routbort, J., France, D., Smith, D. and Lopez-Cepero, J.M., An investigation of silicon carbide-water nanofluid for heat transfer applications, *Journal of Applied Physics*, vol. 105, no. 6, pp. 064306:1–6, 2009.

[91]   Timofeeva, E.V., Routbort, J.L. and Singh, D., Particle shape effects on thermophysical properties of alumina nanofluids, *Journal of Applied Physics*, vol. 106, no. 1, pp. 014304: 1–10, 2009.

144

[92]   Takeuchi, A., Kato, H. and Inoue, A., Vogel-Fulcher-Tammann plot for viscosity scaled with temperature interval between actual and ideal glass transitions for metallic glasses in liquid and supercooled liquid states, *Intermetallics*, vol. 18, pp. 406–411, 2010.

[93]   Żyła, G., Witek, A. and Cholewa, M., Viscosity of diethylene glycol-based Y_2O_3 nanofluids, *Journal of Experimental Nanoscience*, vol. 10, no. 6, pp. 1–8, 2013.

[94]   Kulkarni, D., Das, D. and Chukwu, G.A., Temperature dependent rheological property of copper oxide nanoparticles suspension (nanofluid), *Journal of Nanoscience and Nanotechnology,* vol. 6, no. 4, pp. 679–690, 2009.

[95]   Yiamsawas, T., Dalkilic, A.S., Mahian, O. and Wongwises, S., Measurement and correlation of the viscosity of water-based Al_2O_3 and TiO_2 nanofluids in high temperatures and comparisons with literature reports, *Journal of Dispersion Science and Technology*, vol. 34, no. 12, pp. 1697–1703, 2013.

[96]   Hemmat Esfe, M. and Saedodin, S., An experimental investigation and new correlation of viscosity of ZnO–EG nanofluid at various temperatures and different solid volume fractions, *Experimental Thermal and Fluid Science*, vol. 55, pp. 1–5, 2014.

[97]   Azmi, W.H., Sharma, K.V, Mamat, R., Alias, a B.S. and Misnon, I.I., Correlations for thermal conductivity and viscosity of water based nanofluids, *IOP Conference Series: Materials Science and Engineering*, vol. 36, pp. 012029, 2012.

[98]   Khanafer, K. and Vafai, K., A critical synthesis of thermophysical characteristics of nanofluids, *International Journal of Heat and Mass Transfer*, vol. 54, no. 19–20, pp. 4410–4428, 2011.

[99]   Yu, W., Xie, H., Li, Y. and Chen, L., Experimental investigation on thermal conductivity and viscosity of aluminum nitride nanofluid, *Particuology*, vol. 9, no. 2, pp. 187–191, 2011.

[100]   Halelfadl, S., Estellé, P., Aladag, B., Doner, N. and Maré, T., Viscosity of carbon nanotubes water-based nanofluids: influence of concentration and temperature, *International Journal of Thermal Sciences*, vol. 71, pp. 111–117, 2013.

[101]   Aladag, B., Halelfadl, S., Doner, N., Maré, T., Duret, S., Estellé, P. and Haleifadl, S., Experimental investigations of the viscosity of nanofluids at low temperatures, *Applied Energy*, vol. 97, pp. 876–880, 2012.

145

[102] Syam Sundar, L., Singh, M.K. and Sousa, A.C.M., Investigation of thermal conductivity and viscosity of Fe_3O_4 nanofluid for heat transfer applications, *International Communications in Heat and Mass Transfer*, vol. 44, pp. 7–14, 2013.

[103] Phuoc, T.S.X. and Massoudi, M., Experimental observations of the effects of shear rates and particle concentration on the viscosity of Fe_2O_3-deionized water nanofluids, *Internationl Journal of Thermal Sciences*, vol. 48, no. 7, pp. 1294–1301, 2009.

[104] Prasher, R., Song, D. and Wang, J., Measurements of nanofluid viscosity and its implication for thermal application, *Applied Physics Letters*, vol. 89, pp. 133108:1–3, 2006.

[105] Corcione, M., Empirical correlating equations for predicting the effective thtermal conductivity and dynamic viscosity of nanofluids, *Energy Conversion and Management*, vol. 52, no. 1, pp. 789–793, 2011.

[106] Sekhar, Y.R. and Sharma, K.V., Study of viscosity and specific heat capacity characteristics of water-based Al_2O_3 nanofluids at low particle concentrations, *Journal of Experimental Nanoscience*, vol. 10, no. 2, pp. 86–102, 2013.

[107] Kitano, T., Kataoka, T. and Shirota, T., An empirical equation of the relative viscosity of polymer melts filled with various inorganic fillers, *Rheology Acta*, vol. 20, pp. 207–209, 1981.

[108] Paul, G., Chopkar, M., Manna, I. and Das, P.K., Techniques for measuring the thermal conductivity of nanofluids: a review, *Renewable and Sustainable Energy Reviews*, vol. 14, no. 7, pp. 1913–1924, 2010.

[109] Sundar, L.S., Farooky, M.H., Sarada, S.N. and Singh, M.K., Experimental thermal conductivity of ethylene glycol and water mixture based low volume concentration of Al_2O_3 and CuO nanofluids, *International Communications in Heat and Mass Transfer*, vol. 41, pp. 41–46, 2013.

[110] Vajjha, R.S. and Das, D.K., Experimental determination of thermal conductivity of three nanofluids and development of new correlations, *International Journal of Heat and Mass Transfer*, vol. 52, pp. 4675–4682, 2009.

[111] Mansour, R.B., Galanis, N. and Nguyen, C.T., Experimental study of mixed convection with water-Al_2O_3 nanofluid in inclined tube with uniform wall heat flux, *International Journal of Thermal Sciences*, vol. 50, no. 3, pp. 403–410, 2011.

[112] Fotukian, S.M. and Esfahany, M.N., Experimental study of turbulent convective heat transfer and pressure drop of dilute CuO/water nanofluid inside a circular tube, *International Communications in Heat and Mass Transfer*, vol. 37, no. 2, pp. 214–219, 2010.

[113] Liu, Z-H. and Li, Y-Y., A new frontier of nanofluid research - application of nanofluids in heat pipes, *International Journal of Heat and Mass Transfer*, vol. 55, no. 23–24, pp. 6786–6797, 2012.

[114] Wang, P-Y., Chen, X-J., Liu, Z-H. and Liu, Y-P., Application of nanofluid in an inclined mesh wicked heat pipes, *Thermochimica Acta*, vol. 539, pp. 100–108, 2012.

[115] Hajian, R., Layeghi, M. and Sani, K.A., Experimental study of nanofluid effects on the thermal performance with response time of heat pipe, *Energy Conversion and Management*, vol. 56, pp. 63–68, 2012.

[116] Saidur, R., Meng, T.C., Said, Z., Hasanuzzaman, M. and Kamyar, A., Evaluation of the effect of nanofluid-based absorbers on direct solar collector, *International Journal of Heat and Mass Transfer*, vol. 55, pp. 5899–5907, 2012.

[117] Yousefi, T., Shojaeizadeh, E., Veysi, F. and Zinadini, S., An experimental investigation on the effect of pH variation of MWCNT-H_2O nanofluid on the efficiency of a flat-plate solar collector, *Solar Energy*, vol. 86, no. 2, pp. 771–779, 2012.

[118] Yousefi, T., Veisy, F., Shojaeizadeh, E., Zinadini, S. and Veysi, F., An experimental investigation on the effect of MWCNT-H_2O nanofluid on the efficiency of flat-plate solar collectors, *Experimental Thermal and Fluid Science*, vol. 39, pp. 207–212, 2012.

[119] Yousefi, T., Veysi, F., Shojaeizadeh, E. and Zinadini, S., An experimental investigation on the effect of Al_2O_3-H_2O nanofluid on the efficiency of flat-plate solar collectors, *Renewable Energy*, vol. 39, no. 1, pp. 293–298, 2012.

[120] Nieh, H-M., Teng, T-P. and Yu, C-C., Enhanced heat dissipation of a radiator using oxide nano-coolant, *International Journal of Thermal Sciences*, vol. 77, pp. 252–261, 2014.

[121] Murshed, S.M.S., Leong, K.C. and Yang, C., Determination of the effective thermal diffusivity of nanofluids by the double hot-wire technique, *Journal of Physics D: Applied Physics*, vol. 39, no. 24, pp. 5316–5322, 2006.

[122] Rella, R., Spadavecchia, J., Menera, M.G., Capone, S. and Taurino, A., Acetone and ethanol solid-state gas sensor based on TiO_2 nanoparticles thin film deposited by matrix assisted pulsed laser evaporation, *Sensors and Actuators B*, vol. 127, pp. 426–431, 2007.

[123] Madaria, A.R., Kumar, A., Ishikawa, F.N. and Zhou, C., Uniform, highly conductive, and patterned transparent films of a percolating silver nanowire network on rigid and flexible substrates using a dry transfer technique, *Nano Research*, vol. 3, no. 8, pp. 564–573, 2010.

[124] Anoop, K.B., Kabelac, S., Sundararajan, T. and Das, S.K., Rheological and flow characteristics of nanofluids: influence of electroviscous effects and particle agglomeration, *Journal of Applied Physics*, vol. 106, no. 3, pp. 034909 1–7, 2009.

[125] Janot, R. and Guérard, D., One-step synthesis of maghemite nanometric powers by ball milling, *Journal of Alloys and Compounds*, vol. 333, pp. 302–307, 2002.

[126] Chin, P.P., Ding, J., Yi, J.B. and Liu, B.H., Synthesis of FeS2 and FeS nanoparticles by high-energy mechanical milling and mechanochemical processing, *Journal of Alloys and Compound*, vol. 390, pp. 255–260, 2005.

[127] Lam, C., Zhang, Y.F., Tang, Y.H., Lee, C.S., Bello, I. and Lee, S.T., Large-scale synthesis of ultrafine Si nanoparticles by ball milling, *Journal of Crystal Growth*, vol. 220, pp. 466–470, 2000.

[128] Franzel, L., Bertino, M.F., Huba, Z.J. and Carpenter, E.E., Synthesis of magnetic nanoparticles by paulsed laser ablation, *Applied Surface Science*, vol. 261, pp. 332–336, 2012.

[129] Cristoforetti, G., Pitzalis, E., Spiniello, R., Ishak, R., Giammanco, F., Muniz-Miranda, M. and Caprali, S., Physic-chemical properties of Pd nanoparticles produced by pulsed laser ablation in different organic solvents, *Applied Surface Science*, vol. 258, pp. 3289–3297, 2012.

[130] Mutisya, S., Franzel, L., Barnstein, B.O., Faber, T.W., Ryann, J.J. and Bertino, M.F., Comparison of in situ and ex situ bioconjugate of Au nanoparticles generated by laser ablation, *Applied Surface Science*, vol. 264, pp. 27–30, 2013.

[131] Manera, M.G., Taurino, A., Catalano, M., Rella, R., Caricato, A.P. and Buonsanti, R., Enhancement of the optically activated NO_2 gas sensing response of brookite Ti_2

148

nanorods/nanoparticles thin films deposited by matrix-assisted pulsed-laser evaporation, *Sensors and Actuator B: Chemical*, vol. 161, pp. 869–879, 2012.

[132] Singh, V. and Chauhan, P., Structural and optical characterization of CdS nanoparticles prepared by chemical precipitation, *Journal of Physics and Chemistry of Solids*, vol. 70, pp. 1074–1079, 2009.

[133] Chen, J-F., Wang, Y-H., Guo, F., Wang, X-M. and Zheng, C., Synthesis of nanoparticles with novel technology: high-gravity reactive precipitation, *Industrial and Engineering Chemistry Research*, vol. 39, no. 4, pp. 948–954, 2000.

[134] Hsu, W-C., Chen, S., Kuo, P., Lie, C. and Tsai, W., Preparation of NiCuZn ferrite nanoparticles from chemical co-precipitation method and the magnetic properties after sintering, *Materials Science and Engineering: B*, vol. 111, no. 2–3, pp. 142–149, 2004.

[135] Zhu, J., Liu, S., Palchik, O., Koltypin, Y. and Gedanken, A., Shape-controlled synthesis of silver nanoparticles by pulse sonoelectrochemical methods, *Langmuir*, no. 23, pp. 6396–6399, 2000.

[136] Mastai, Y., Polsky, R., Koltypin, Y., Gedanken, A. and Hodes, G., Pulsed sonoelectrochemical synthesis of cadmium selenide nanoparticles, *Journal of the American Chemical Society*, vol. 121, pp. 10047–10052, 1999.

[137] Zhu, J., Aruna, S.T., Koltypin, Y. and Gedanken, A., A novel method for the preparation of lead selenide: pulse sonoelectrochemical synthesis of lead selenide nanoparticles, *Chemistry Materials*, vol. 12, pp. 143–147, 2000.

[138] Zin, V., Pollet, B.G. and Dabalà, M., Sonoelectrochemical (20kHz) production of platinum nanoparticles from aqueous solutions, *Electrochimica Acta*, vol. 54, no. 28, pp. 7201–7206, 2009.

[139] Lei, H., Tang, Y-J., Wei, J-J., Li, J., Li, X-B. and Shi, H-L., Synthesis of tungsten nanoparticles by sonoelectrochemistry, *Ultrasonics Sonochemistry*, vol. 14, no. 1, pp. 81–3, 2007.

[140] Sáez, V. and Mason, T.J., Sonoelectrochemical synthesis of nanoparticles, *Molecules*, vol. 14, pp. 4284–4299, 2009.

[141] Mueller, R., Mädler, L. and Pratsinis, S.E., Nanoparticle synthesis at high production rates by flame pyrolysis, *Chemical Engineering Science*, vol. 58, pp. 1969–1976, 2003.

[142] Sahm, T., Mädler, L., Gurlo, A., Barsan, N., Pratsinis, S.E. and Weimar, U., Flame spray synthesis of tin dioxide nanoparticles for gas sensing, *Sensors and Actuators B*, vol. 98, pp. 148–153, 2004.

[143] Kong, J., Cassell, A. and Dai, H., Chemical vapor deposition of methane for single-walled carbon nanotubes, *Chemical Physics Letters*, vol. 292, no. 4–6, pp. 567–574, 1998.

[144] Colomer, J-F., Stephan, C., Lefrant, S., Tendeloo, G.V, Willems, I., Kónya, Z., Fonseca, A., Laurent, C. and Nagy, J.B., Large-scale synthesis of single-wall carbon nanotubes by catalytic chemical vapor deposition (CCVD) method, *Chemical Physics Letters*, vol. 317, pp. 83–89, 2000.

[145] Nakaso, K., Han, B., Ahn, K.H., Choi, M. and Okuyama, K., Synthesis of non-agglomerated nanoparticles by an electrospray assisted chemical vapour depostion (ES-CVD) method, *Aerosol Science*, vol. 34, pp. 869–881, 2003.

[146] Sahoo, P.K., Kamal, S.S.K., Premkumar, M., Kumar, T.J., Sreedhar, B., Singh, A.K., Srivastava, S.K. and Sekhar, K.C., Synthesis of tungsten nanoparticles by solvothermal decomposition of tungsten hexacarbonyl, *International Journal of Refractory Metals and Hard Materials,* vol. 27, pp. 567–574, 2009.

[147] Rao, J.P. and Geckeler, K.E., Polymer nanoparticles: preparation techniques and size-control parameters, *Progress in Polymer Science*, vol. 36, pp. 887–913, 2011.

[148] Koch, C.C., The synthesis and structure of nanocrystalline materials produced by mechanical attrition: a review, *Nanostructured Materials*, vol. 2, pp. 109–129, 1993.

[149] Das, S.K., Choi, S.U.S. and Patel, H.E., Heat transfer in nanofluids – a review, *Heat Transfer Engineering*, vol. 27, no. 10, pp. 3–19, 2006.

[150] Fedele, L., Colla, L., Bobbo, S., Barison, S. and Agresti, F., Experimental stability analysis of different water-based nanofluids., *Nanoscale Research Letters*, vol. 6, no. 1, pp. 300–307, 2011.

[151] Zamzamian, A., Oskouie, S.N., Doosthoseini, A., Joneidi, A. and Pazouki, M., Experimental investigation of forced convective heat transfer coefficient in nanofluids of Al_2O_3/EG and CuO/EG in a double pipe and plate heat exchangers under turbulent flow, *Experimental Thermal and Fluid Science*, vol. 35, no. 3, pp. 495–502, 2011.

[152] Singh, A.K. and Raykar, V.S., Microwave synthesis of silver nanofluids with polyvinylpyrrolidone (PVP) and their transport properties, *Colloid and Polymer Science*, vol. 286, no. 14–15, pp. 1667–1673, 2008.

[153] Kim, D., Hwang, Y., Cheong, S.I., Lee, J.K., Hong, D., Moon, S., Lee, J.E. and Kim, S.H., Production and characterization of carbon nano colloid via one-step electrochemical method, *Journal of Nanoparticle Research*, vol. 10, no. 7, pp. 1121–1128, 2008.

[154] Singaravelu, G., Arockiamary, J., Ganesh, K. and Govindaraju, K., A novel extracellular synthesis of monodispersed gold nanoparticles using marine alga, Sargassum wightii grevile, *Colloids and Surface B: Biointerfaces*, vol. 28, pp. 313–318, 2003.

[155] Ahmad, A., Mukherjee, P., Senapati, S., Mandal, D., Khan, M.I., Kumar, R. and Sastry, M., Extracellular biosynthesis of silver nanoparticles using the fungus Fusarium osysporum, *Colloids and Surfaces B: Biointerfaces*, vol. 28, pp. 313–318, 2007.

[156] Bhainsa, K.C. and D'Souza, S.F., Extracellular biosynthesis of silver nanoparticles using the fungus Aspergillus fumigatus, *Colloids Surfaces B: Biointerfaces*, vol. 47, no. 2, pp. 160–164, 2006.

[157] Elumalai, E.K., Prasad, T.N.V.K. V, Hemachandran, J. and Therasa, S.V, Extracellular synthesis of silver nanoparticles using leaves of Euphorbia hirta and their antibacterial activities, *Jorunal of Pharmaceutical Sciences and Research*, vol. 2, no. 9, pp. 549–554, 2010.

[158] Krishnaraj, C., Jagan, E.G., Rajasekar, S., Selvakumar, P., Kalaichelvan, P.T. and Mohan, N., Synthesis of silver nanoparticles using Acalypha indica leaf extracts and its antibacterial activity against water borne pathogens, *Colloids and Surface B: Biointerfaces*, vol. 76, pp. 50–56, 2010.

[159] Huang, J., Li, Q., Sun, D., Lu, Y., Su, Y., Yang, X., Wang, H., Wang, Y., Shao, W., He, N., Hong, J. and Chen, C., Biosynthesis of silver and gold nanoparticles by novel sundried Cinnamomum camphora leaf, *Nanotechnology*, vol. 18, no. 10, pp. 105104, 2007.

[160] Narayanan, K.B. and Sakthivel, N., Coriander leaf mediated biosynthesis of gold nanoparticles, *Materials Letters*, vol. 62, no. 30, pp. 4588–4590, 2008.

[161] Song, J.Y., Jang, H. and Kim, B.S., Biological synthesis of gold nanoparticles using Magnolia kobus and Diopyros kaki leaf extracts, *Process Biochemistry*, vol. 44, pp. 1133–1138, 2009.

[162] Shivaji, S., Madhu, S. and Singh, S., Extracellular synthesis of antibacterial silver nanoparticle using psychrophilic bacteria, *Process Biochemistry*, vol. 46, pp. 1800–1807, 2011.

[163] He, S., Guo, Z., Zhang, Y., Zhang, S., Wang, J. and Gu, N., Biosynthesis of gold nanoparticles using the bacteria Rhodopseudomonas capsulata, *Materials Letters*, vol. 61, pp. 3984–3987, 2007.

[164] Husseiny, M.I., El-Aziz, M.A., Badr, Y. and Mahmoud, M.A., Biosynthesis of gold nanoparticles using Pseudomonas aeruginosa, *Spectrochimica Acta Part A*, vol. 67, pp. 1003–1006, 2007.

[165] Agnihotri, M., Joshi, S., Kumar, A.R., Zinjarde, S. and Kulkarni, S., Biosynthesis of gold nanoparticles by the tropical marine yeast Yarrowia lipolytica NCIM 3589, *Materials Letters*, vol. 63, pp. 1231–1234, 2009.

[166] Apte, M., Girme, G., Nair, R., Bankar, A., Kumar, A.R. and Zinjarde, S., Melanin mediated synthesis of gold nanoparticles by Yarrowia lipolytica, *Materials Letters*, vol. 95, pp. 149–152, 2013.

[167] Krumov, N., Oder, S., Perner-Nochta, I., Angelov, A. and Posten, C., Accumulation of CdS nanoparticles by yeast in a fed-batch bioprocess, *Journal of Biotechnology*, vol. 132, pp. 481–486, 2007.

[168] Jha, A.K. and Prasad, K., A green low-cost biosynthesis of Sb_2O_3 nanoparticles, *Biochemical Engineering Journal*, vol. 43, no. 3, pp. 303–306, 2009.

[169] Inbakandan, D., Sivaleela, G., Magesh Peter, D., Kiurbagaran, R., Venkatesan, R. and Ajmal Khan, S., Marine sponge extract assisted biosynthesis of silver nanoparticles, *Materials Letters*, vol. 87, pp. 66–68, 2012.

[170] Thakkar, K.N., Mhatre, S.S. and Parikh, R.Y., Biological synthesis of metallic nanoparticles, *Nanomedicine: Nanotechnology, Biology, and Medicine*, vol. 6, pp. 257–262, 2010.

[171] Prasher, R., Phelan, P.E. and Bhattacharya, P., Effect of aggregation kinetics on the thermal conductivity of nanoscale colloidal solutions (nanofluid), *Nano Letters*, vol. 6, no. 7, pp. 1529–34, 2006.

152

[172] Samal, S., Satpati, B. and Chaira, D., Production and dispersion stability of ultrafine Al–Cu alloy powder in base fluid, *Journal of Alloys and Compounds*, vol. 504, pp. S389–S394, 2010.

[173] Wang, X., Li, X. and Yang, S., Influence of pH and SDBS on the stability and thermal conductivity of nanofluids, *Energy and Fuels*, vol. 23, no. 16, pp. 2684–2689, 2009.

[174] Shima, P.D., Philip, J. and Raj, B., Magnetically controllable nanofluid with tunable thermal conductivity and viscosity, *Applied Physics Letters*, vol. 95, no. 13, pp. 133112, 2009.

[175] Lee, S.W., Park, S.D., Kang, S., Bang, I.C. and Kim, J.H., Investigation of viscosity and thermal conductivity of SiC nanofluids for heat transfer applications, *International Journal of Heat and Mass Transfer*, vol. 54, no. 1–3, pp. 433–438, 2011.

[176] Phuoc, T.X., Massoudi, M. and Chen, R-H., Viscosity and thermal conductivity of nanofluids containing multi-walled carbon nanotubes stabilized by chitosan, *International Journal of Thermal Sciences*, vol. 50, no. 1, pp. 12–18, 2011.

[177] Kumaresan, V. and Velraj, R., Experimental investigation of the thermo-physical properties of water-ethylene-glycol-mixture-based CNT nanofluids, *Thermochimica Acta*, vol. 545, pp. 180–186, 2012.

[178] Syam Sundar, L., Venkata Ramana, E., Singh, M.K. and De Sousa, A.C.M., Viscosity of low volume concentrations of magnetic Fe_3O_4 nanoparticles dispersed in ethylene glycol and water mixture, *Chemical Physics Letters*, vol. 554, pp. 236–242, 2012.

[179] Das, S.K., Putra, N. and Roetzel, W., Pool boiling characteristics of nano-fluids, *International Journal of Heat and Mass Transfer*, vol. 46, no. 5, pp. 851–862, 2003.

[180] Wang, X., Xu, X. and Choi, S.U., Thermal conductivity of nanoparticle – fluid mixture, *Journal of Thermophysics and Heat Transfer*, vol. 13, no. 4, pp. 474–480, 1999.

[181] Hosseini, M. and Ghader, S., A model for temperature and particle volume fraction effect on nanofluid viscosity, *Journal of Molecular Liquids*, vol. 153, pp. 139–145, 2010.

[182] Suresh, S., Venkitaraj, K.P., Selvakumar, P. and Chandrasekar, M., Synthesis of Al$_2$O$_3$-Cu/water hybrid nanofluids using two step method and its thermo physical properties, *Colloids and Surfaces A: Physicochemical and Engineering Aspects,* vol. 388, pp. 41–48, 2011.

[183] Larson, R.G., *The structure and rheology of complex fluids*, New York, NY, Oxford University Press,1999.

[184] Chen, H., Witharana, S., Jin, Y., Kim, C. and Ding, Y., Predicting thermal conductivity of liquid suspensions of nanoparticles (nanofluids) based on rheology, *Particuology*, vol. 7, no. 2, pp. 151–157, 2009.

[185] Moradpour, H., Chapoy, A. and Tohidi, B., Bimodal model for predicting the emulsion-hydrate mixture viscosity in high water cut systems, *Fuel*, vol. 90, no. 11, pp. 3343–3351, 2011.

[186] Rensing, P.J., Liberatore, M.W., Sum, A.K., Koh, C.A. and Dendy Sloan, E., Viscosity and yield stresses of ice slurries formed in water-in-oil emulsions, *Journal of Non-Newtonian Fluid Mechanics*, vol. 166, no. 14–15, pp. 859–866, 2011.

[187] Singh, N., Chand, G. and Kanagaraj, S., Investigation of thermal conductivity and viscosity of carbon nanotubes-ethylene glycol nanofluids, *Heat Transfer Engineering*, vol. 33, no. 9, pp. 821–827, 2012.

[188] Mahbubul, I.M., Khaleduzzaman, S.S., Saidur, R. and Amalina, M.A., Rheological behavior of Al$_2$O$_3$/R141b nanorefrigerant, *International Journal of Heat and Mass Transfer*, vol. 73, pp. 118–123, 2014.

[189] Yang, Y., Oztekin, A., Neti, S. and Mohapatra, S., Particle agglomeration and properties of nanofluids, *Journal of Nanoparticle Research*, vol. 14, no. 5, pp. 852, 2012.

[190] Keblinski, P., Prasher, R. and Eapen, J., Thermal conductance of nanofluids: is the controversy over?, *Journal of Nanoparticle Research*, vol. 10, pp. 1089–1097, 2008.

[191] Tseng, W.J. and Lin, C.L., Effect of dispersant on rheological behaviour of BaTiO$_3$ poweders in ethano-isopropanol mixtures, *Materials Chemistry and Physics,* vol. 80, pp. 232–238, 2003.

[192] Nguyen, C.T., Desgranges, F., Roy, G., Galanis, N., Maré, T., Boucher, S. and Angue Mintsa, H., Temperature and particle-size dependent viscosity data for water-

154

based nanofluids − hysteresis phenomenon, *International Journal of Heat and Fluid Flow*, vol. 28, no. 6, pp. 1492–1506, 2007.

[193] He, Y., Jin, Y., Chen, H., Ding, Y., Cang, D. and Lu, H., Heat transfer and flow behaviour of aqueous suspensions of TiO$_2$ nanoparticles (nanofluids) flowing upward through a vertical pipe, *International Journal of Heat and Mass Transfer*, vol. 50, no. 11–12, pp. 2272–2281, 2007.

[194] Namburu, P. and Kulkarni, D., Experimental investigation of viscosity and specific heat of silicon dioxide nanofluids, *Micro and Nano Letters*, vol. 2, no. 3, pp. 67–71, 2007.

[195] Pastoriza-Gallego, M.J., Casanova, C., Legido, J.L. and Piñeiro, M.M., CuO in water nanofluid: influence of particle size and polydispersity on volumetric behaviour and viscosity, *Fluid Phase Equilibria*, vol. 300, no. 1–2, pp. 188–196, 2011.

[196] Anoop, K.B., Sundararajan, T. and Das, S.K., Effect of particle size on the convective heat transfer in nanofluid in the developing region, *International Journal of Heat and Mass Transfer*, vol. 52, no. 9–10, pp. 2189–2195, 2009.

[197] Timofeeva, E.V, Smith, D.S., Yu, W., France, D.M., Singh, D. and Routbort, J.L., Particle size and interfacial effects on thermo-physical and heat transfer characteristics of water-based alpha-SiC nanofluids., *Nanotechnology*, vol. 21, no. 215703, pp. 1–10, 2010.

[198] Jia-Fei, Z. and Zhong-Yang, L., Dependence of nanofluid viscosity on particle size and pH value, *Chinese Physics Letters*, vol. 26, no. 6, pp. 10–13, 2009.

[199] Rubio-Hernández, F.J., Ayúcar-Rubio, M.F., Vlaázquez-Navarro, J.F. and Galindo-Rosales, F.J., Intrinsic viscosity of SiO$_2$, Al$_2$O$_3$ and TiO$_2$ aqueous suspensions, *Journal of Colloid and Interface Science*, vol. 298, pp. 967–972, 2006.

[200] Boluk, Y., Lahiji, R., Zhao, L. and McDermott, M.T., Suspension viscosities and shape parameters of cellulose nanocrystals (CNC), *Colloids and Surfaces A:Physicochemical and Engineering Aspects*, vol. 337, pp. 297–303, 2011.

[201] Wierenga, A.M. and Philipse, A.P., Low-shear viscosities of (semi-)dilute, aqueous dispersions of charged boehmite rods: dynamic scaling of double layer effects, *Langmuir*, vol. 13, pp. 4574–4582, 1997.

155

[202] Wierenga, A.M. and Philipse, A.P., Low-shear viscosities of dilute dispersions of colloidal rodlike silica particles in cyclohexane, *Journal of Colloid and Interface Science*, vol. 180, pp. 360–370, 1996.

[203] Rudyak, V.Y. and Krasnolutskii, S.L., Dependence of the viscosity of nanofluids on nanoparticle size and material, *Physics Letters A*, vol. 378, no. 26–27, pp. 1845–1849, 2014.

[204] Huseyin, K. and Muhammet, K., Prediction of thermal conductivity of ethylene glycol – water solutions by using artificial neural networks, *Applied Energy*, vol. 86, pp. 2244–2248, 2009.

[205] Hojjat, M., Etemad, S.G., Bagheri, R. and Thibault, J., Thermal conductivity of non-Newtonian nanofluids: experimental data and modeling using neural network, *International Journal of Heat and Mass Transfer*, vol. 54, pp. 1017–1023, 2011.

[206] Papari, M.M., Yousefi, F., Moghadasi, J., Karimi, J. and Campo, A., Modeling thermal conductivity augmentation of nanofluids using diffusion neural networks, *International Journal of Thermal Sciences*, vol. 50, pp. 44–52, 2011.

[207] Mehrabi, M., Sharifpur, M. and Meyer, J.P., Application of the FCM-based neuro-fuzzy inference system and genetic algorithm-polynomial neural network approaches to modelling the thermal conductivity of alumina-water nanofluids, *International Communications in Heat and Mass Transfer*, vol. 39, pp. 971–997, 2012.

[208] Esfe, M.H., Saedodin, S., Bahiraei, M., Toghraie, D., Mahian, O. and Wongwises, S., Thermal conductivity modeling of MgO/EG nanofluids using experimental data and artificial neural network, *Journal of Thermal Analysis and Calorimetry*, vol. 118, pp. 287–294, 2014.

[209] Esfe, M.H., Saedodin, S., Naderi, A., Alirezaie, A., Karimipour, A. and Wongwises, S., Modeling of thermal conductivity of ZnO-EG using experimental data and ANN methods, *International Communications in Heat and Mass Transfer*, 2015.

[210] Yousefi, F., Karimi, H. and Papari, M.M., Modeling viscosity of nanofluids using diffusional neural networks, *Journal of Molecular Liquids*, vol. 175, pp. 85–90, 2012.

[211] Bahiraei, M., Hosseinalipour, S., Zabihi, K. and Taheran, E., Using neural network for determination of viscosity in water-TiO_2 nanofluids, *Advances in Mechanical Engineering*, vol. 742680, no. 1–10, 2012.

156

[212] Karimi, H. and Yousefi, F., Application of artificial neural network-genetic algorithm (ANN–GA) to correlation of density in nanofluids, *Fluid Phase Equilibria*, vol. 336, pp. 79–83, 2012.

[213] Mehrabi, M., Sharifpur, M. and Meyer, J.P., Viscosity of nanofluids based on an artificial intelligence model, *International Communications in Heat and Mass Transfer*, vol. 43, pp. 6–11, 2013.

[214] Atashrouz, S., Pazuki, G. and Alimoradi, Y., Estimation of the viscosity of nine nanofluids using a hybrid GMDH-type neural network system, *Fluid Phase Equilibria*, vol. 372, pp. 43–48, 2014.

[215] Wamkam, C.T., Opoku, M.K., Hong, H. and Smith, P., Effects of pH on heat transfer nanofluids containing ZrO_2 and TiO_2 nanoparticles, *Journal of Applied Physics*, vol. 109, no. 024305, pp. 1–5, 2011.

[216] Zhao, J., Luo, Z., Ni, M. and Cen, K., Dependence of nanofluid viscosity on particle size and pH value, *Chinese Physics Letters,* vol. 26, no. 066202, pp. 1–3, 2009.

[217] Chandrasekar, M. and Suresh, S., A review on the mechanisms of heat transport in nanofluids, *Heat Transfer Engineering*, vol. 30, no. 14, pp. 1136–1150, 2009.

[218] Xian-Ju, W. and Xin-Fang, L., Influence of pH on nanofluids' viscosity and thermal conductivity, *Chinese Physics Letters*, vol. 26, no. 5, pp. 1–4, 2009.

[219] Li, X.F., Zhu, D.S., Wang, X.J., Wang, N., Gao, J.W. and Li, H., Thermal conductivity enhancement dependent pH and chemical surfactant for Cu-H_2O nanofluids, *Thermochimica Acta*, vol. 469, no. 1–2, pp. 98–103, 2008.

[220] Li, X., Zhu, D. and Wang, X., Evaluation on dispersion behavior of the aqueous copper nano-suspensions, *Journal of Colloid and Interface Science*, vol. 310, no. 2, pp. 456–63, 2007.

[221] Huang, J., Wang, X., Long, Q., Wen, X., Zhou, Y. and Li, L., Influence of pH on the stability characteristics of nanofluids, *Symposium on Photonics and Optoelectronics,* pp. 1–4, Wuhan, IEEE eXpress Conference Publishing, 2009.

[222] Younes, H., Christensen, G., Luan, X., Hong, H. and Smith, P., Effects of alignment, pH, surfactant, and solvent on heat transfer nanofluids containing Fe_2O_3 and CuO nanoparticles, *Journal of Applied Physics*, vol. 111, no. 6, pp. 064308, 2012.

[223] Konakanchi, H., Vajjha, R.S., Chukwu, G. and Das, D.K., Measurements of pH of three nanofluids and development of new correlations, *Heat Transfer Engineering*, vol. 36, no. 1, pp. 81–90, 2014.

[224] Lee, D., Kim, J-W. and Kim, B.G., A new parameter to control heat transport in nanofluids: surface charge state of the particle in suspension., *The Journal of Physical Chemistry. B*, vol. 110, no. 9, pp. 4323–4328, 2006.

[225] Degen, A. and Kosec, M., Effect of pH and impurities on the surface charge of zinc oxide in aqueous solution, *Journal of the European Ceramic Society*, vol. 20, pp. 667–673, 2000.

[226] Delgado, A.V, González-Caballero, F., Hunter, R.J. and Koopal, L.K., Measurement and interpretation of electrokinetic phenomena, *Journal of Colloid and Interface Science*, vol. 309, pp. 194–224, 2007.

[227] Charkraborty, S. and Padhy, S., Anomalous electrical conductivity of nanoscale colloidal suspensions, *ACS Nano*, vol. 2, no. 10, pp. 2029–2036, 2008.

[228] Ganguly, S., Sikdar, S. and Basu, S., Experimental investigation of the effective electrical conductivity of aluminum oxide nanofluids, *Powder Technology*, vol. 196, no. 3, pp. 326–330, 2009.

[229] Baby, T.T. and Ramaprabhu, S., Investigation of thermal and electrical conductivity of graphene based nanofluids, *Journal of Applied Physics*, vol. 108, no. 12, pp. 124308, 2010.

[230] Glory, J., Bonetti, M., Helezen, M., Mayne-L'Hermite, M. and Reynaud, C., Thermal and electrical conductivities of water-based nanofluids prepared with long multiwalled carbon nanotubes, *Journal of Applied Physics*, vol. 103, no. 9, pp. 094309, 2008.

[231] Teng, T-P., Cheng, C-M. and Pai, F-Y., Preparation and characterization of carbon nanofluid by a plasma arc nanoparticles synthesis system., *Nanoscale Research Letters*, vol. 6, no. 1, pp. 293, 2011.

[232] Maddah, H., Rezazadeh, M., Maghsoudi, M. and NasiriKokhdan, S., The effect of silver and aluminum oxide nanoparticles on thermophysical properties of nanofluids, *Journal of Nanostructure in Chemistry*, vol. 3, no. 1, pp. 28, 2013.

[233] Wong, K-F.V. and Kurma, T., Transport properties of alumina nanofluids, *Nanotechnology*, vol. 19, no. 345702, pp. 1–8, 2008.

[234] Minea, A.A. and Luciu, R.S., Investigations on electrical conductivity of stabilized water based Al$_2$O$_3$ nanofluids, *Microfluidand Nanofluid*, vol. 13, no. 6, pp. 977–985, 2012.

[235] Ohshima, H., Dynamic electrophoretic mobility of spherical colloidal particles in concentrated suspensions, *Journal of Colloid and Interface Science*, vol. 148, no. 195, pp. 137–148, 1997.

[236] Ohshima, H., Electrokinetic phenomena in a dilute suspension of spherical colloidal particles in a salt-free medium, *Chinese Physics Letters*, vol. 222, pp. 207–211, 2003.

[237] Ohshima, H., Electrophoretic mobility of soft particles in concentrated suspensions., *Journal of Colloid and Interface Science*, vol. 225, no. 1, pp. 233–242, 2000.

[238] Ohshima, H., Electrical conductivity of a concentrated suspension of spherical colloidal particles., *Journal of Colloid and Interface Science*, vol. 212, no. 2, pp. 443–448, 1999.

[239] Cruz, R.C.D., Reinshagen, J., Oberacker, R., Segadães, A.M. and Hoffmann, M.J., Electrical conductivity and stability of concentrated aqueous alumina suspensions, *Journal of Colloid and Interface Science*, vol. 286, pp. 579–588, 2005.

[240] Turner, J., Two-phase conductivity: the electrical conductance of liquid-fluidized beds of spheres, *Chemical Engineering Science*, vol. 31, no. 6, pp. 487–492, 1976.

[241] Konakanchi, H., Vajjha, R., Misra, D. and Das, D., Electrical conductivity measurements of nanofluids and development of new correlations, *Journal of Nanoscience and Nanotechnology*, vol. 11, no. 8, pp. 6788–6795, 2011.

[242] Gustafsson, J., Mikkola, P., Jokinen, M. and Rosenholm, J.B., The influence of pH and NaCl on the zeta potential and rheology of anatase dispersions, *Colloids and Surfaces A: Physicochemical and Engineering Aspects*, vol. 175, pp. 349–359, 2000.

[243] Li, Y., Zhou, J., Tung, S., Schneider, E. and Xi, S., A review on development of nanofluid preparation and characterization, *Powder Technology*, vol. 196, no. 2, pp. 89–101, 2009.

[244] Mehrali, M., Sadeghinezhad, E., Latibari, S.T., Kazi, S.N., Mehrali, M., Zubir, M.N.B.M. and Metselaar, H.S.C., Investigation of thermal conductivity and rheological properties of nanofluids containing graphene nanoplatelets., *Nanoscale Research Letters*, vol. 9, no. 15, pp. 1–12, 2014.

[245] Miner, C.S. and Dalton, N.N., *Glycerol*, New York, NY, Reinhold Publishing Company, 1953.

[246] Xie, H., Yu, W. and Chen, W., MgO nanofluids: higher thermal conductivity and lower viscosity among ethylene glycol-based nanofluids containing oxide nanoparticles, *Journal of Experimental Nanoscience*, vol. 5, no. 5, pp. 463–472, 2010.

[247] Pastoriza-Gallego, M.J., Lugo, L., Legido, J.L. and Piñeiro, M.M., Thermal conductivity and viscosity measurements of ethylene glycol-based Al_2O_3 nanofluids., *Nanoscale Research Letters*, vol. 6, no. 1, pp. 221–231, 2011.

[248] Figliola, R.S. and Beasley, D.E., *Theory and design for mechanical measurements*, Hoboken, NJ, Wiley, 2011.

[249] Kulkarni, D.P.D., Namburu, P.P.K., Ed Bargar, H. and Das, D.K., Convective heat transfer and fluid dynamic characteristics of sio_2 ethylene glycol/water nanofluid, *Heat Transfer Engineering*, vol. 29, no. 12, pp. 1027–1035, 2008.

[250] Cengel, Y.A. and Cimbala, J.M., *Fluid mechanics – fundamentals and applications*, New York, NY, McGraw-Hill, 2013.

[251] Onwubulu, G.C., *Hybrid self-organizing modeling systems*, Springer, 2009.

[252] Ivakhnenko, A.G., The group method of data handling-a rival of the method of stochastic approximation, *Soviet Automatic Control*, vol. 13, no. 3, pp. 43–55, 1966.

[253] Abdolrahimi, S., Nasernejad, B. and Pazuki, G., Prediction of partition coefficients of alkaloids in ionic liquids based aqueous biphasic systems using hybrid group method of data handling (GMDH) neural network, *Journal of Molecular Liquids*, vol. 191, pp. 79–84, 2014.

[254] Pesteei, S.M. and Mehrabi, M., Modeling of convection heat transfer of supercritical carbon dioxide in a vertical tube at low Reynolds numbers using artificial neural network, *International Communications in Heat and Mass Transfer*, vol. 37, no. 7, pp. 901–906, 2010.

[255] Mehrabi, M., Rezazadeh, S., Sharifpur, M. and Meyer, J.P., Modeling of Proton Exchange Membrane Fuel Cell (PEMFC) performance by using Genetic Algorithm-Polynomial Neural Network (GA-PNN) hybrid system, *ASME 2012 10th International Conference on Fuel Cell Science, Engineering and Technology*, pp. 447–452, San Diego, CA, 2012.

[256] Karimi, H., Yousefi, F. and Rahimi, M.R., Correlation of viscosity in nanofluids using genetic algorithm-neural network (GA-NN), *Heat and Mass Transfer*, vol. 47, no. 11, pp. 1417–1425, 2011.

[257] Jang, J.S.R., ANFIS: adaptive-network-based fuzzy inference system, *IEEE Transactions on Systems, Man and Cybernetics*, vol. 23, no. 3, pp. 665–685, 1993.

[258] Mehrabi, M., Pesteei, S.M. and Pashaee G.T., Modeling of heat transfer and fluid flow characteristics of helicoidal double-pipe heat exchangers using Adaptive Neuro-Fuzzy Inference System (ANFIS), *International Communications in Heat and Mass Transfer*, vol. 38, no. 4, pp. 525–532, 2011.

[259] Mehrabi, M., Sharifpur, M. and Meyer, J.P., Adaptive neuro-fuzzy modeling of the thermal conductivity of alumina-water nanofluids, *ASME 2012 Third International Conference on Micro/Nanoscale Heat and Mass Transfer*, pp. 155–161, Atlanta, GA, 2012.

[260] Choi, S. and Eastman, J., Enhancing thermal conductivity of fluids with nanoparticles, *ASME International Mechanical Engineering Congress and Exposition*, pp. 1–8, San Francisco, CA, 1995.

[261] Peng, H., Ding, G., Jiang, W., Hu, H. and Gao, Y., Measurement and correlation of frictional pressure drop of refrigerant-based nanofluid flow boiling inside a horizontal smooth tube, *International Journal of Refrigeration*, vol. 32, no. 7, pp. 1756–1764, 2009.

[262] Alawi, O.A., Azwadi, N., Sidik, C. and Kherbeet, A.S., Measurements and correlations of frictional pressure drop of TiO_2/R123 flow boiling inside a horizontal smooth tube, *International Communications in Heat and Mass Transfer*, vol. 61, pp. 42–48, 2015.

[263] Mahbubul, I.M., Saidur, R. and Amalina, M.A., Influence of particle concentration and temperature on thermal conductivity and viscosity of Al_2O_3/R141b nanorefrigerant, *International Communications in Heat and Mass Transfer*, vol. 43, pp. 100–104, 2013.

[264] Piriyawong, V., Thongpool, V., Asanithi, P. and Limsuwan, P., Preparation and characterization of alumina nanoparticles in deionized water using laser ablation technique, *Journal of Nanomaterials*, vol. 2012, pp. 1–6, 2012.

[265] Greenwood, R., *Review of the measurement of zeta potentials in concentrated aqueous suspensions using electroacoustics*, vol. 106, pp. 55–81, 2003.

[266] Chung, S.J.J., Leonard, J.P.P., Nettleship, I., Lee, J.K.K., Soong, Y., Martello, D.V.V and Chyu, M.K.K., Characterization of ZnO nanoparticle suspension in water: effectiveness of ultrasonic dispersion, *Powder Technology*, vol. 194, no. 1–2, pp. 75–80, 2009.

[267] Enomoto, N., Maruyama, S. and Nakagawa, Z., Agglomeration of silica spheres under ultrasonication, *Journal of Materials Research*, 1997.

[268] Yiamsawas, T., Mahian, O., Dalkilic, A.S., Kaewnai, S. and Wongwises, S., Experimental studies on the viscosity of TiO_2 and Al_2O_3 nanoparticles suspended in a mixture of ethylene glycol and water for high temperature applications, *Applied Energy*, vol. 111, pp. 40–45, 2013.

[269] Ghazvini, M., Akhavan-Behabadi, M.A., Rasouli, E. and Raisee, M., Heat transfer properties of nanodiamond-engine oil nanofluid in laminar flow, *Heat Transfer Engineering*, vol. 33, no. 6, pp. 525–532, 2012.

[270] Mastuli, M.S., Ansari, N.S., Nawawi, M.A. and Mahat, A.M., Effects of cationic surfactant in sol-gel synthesis of nano sized magnesium oxide, *APCBEE Procedia*, vol. 3, pp. 93–98, 2012.

[271] Yu, W. and Xie, H., A review on nanofluids: preparation, stability mechanisms, and applications, *Journal of Nanomaterials*, vol. 2012, pp. 1–17, 2012.

[272] Ghadimi, A. and Metselaar, I., The influence of surfactant and ultrasonic processing on improvement of stability, thermal conductivity and viscosity of titania nanofluid, *Experimental Thermal and Fluid Science*, vol. 51, pp. 1–9, 2013.

[273] Timofeeva, E.V, Gavrilov, A.N., Mccloskey, J.M., Tolmachev, Y.V, Sprunt, S., Lopatina, L.M. and Selinger, J.V, Thermal conductivity and particle agglomeration in alumina nanofluids: experiment and theory, *Physical Review E*, vol. 76, no. 061203, pp. 1–16, 2007.

[274] Baby, T.T. and Sundara, R., Synthesis and transport properties of metal oxide decorated graphene dispersed nanofluids, *Journal of Physical Chemistry C*, vol. 115, no. 17, pp. 8527–8533, 2011.

162

[275] Kathrein, H. and Freund, F., Electrical conductivity of magnesium oxide single crystal below 1200 K, *Journal of Physics and Chemistry of Solids*, vol. 44, no. 3, pp. 177–186, 1983.

[276] Wilson, I.O., Magnesium oxide as a high-temperature insulant, *IEE Proceedings A Physical Science, Measurement and Instrumentation, Management and Education, Reviews*, vol. 128, no. 3, pp. 159, 1981.

[277] Posner, J.D., Properties and electrokinetic behavior of non-dilute colloidal suspensions, *Mechanics Research Communications*, vol. 36, no. 1, pp. 22–32, 2009.

[278] Carrique, F., Ruiz-reina, E., Arroyo, F.J. and Delgado, V., Cell model of the direct current electrokinetics in salt-free concentrated suspensions : the role of boundary conditions, *Journal of Physical Chemistry B*, vol. 110, pp. 18313–18323, 2006.

[279] Kole, M. and Dey, T.K., Investigation of thermal conductivity, viscosity, and electrical conductivity of graphene based nanofluids, *Journal of Applied Physics*, vol. 113, no. 8, 2013.

[280] Ruiz-Reina, E. and Carrique, F., Electroviscous effect of concentrated colloidal suspensions in salt-free solutions, *Journal of Physical Chemistry C*, vol. 111, no. 1, pp. 141–148, 2007.

A

APPENDIX A: Al_2O_3 NANOPARTICLES EDS ANALYSIS

7.4   APPENDIX A.1 Al_2O_3 EDS RESULTS
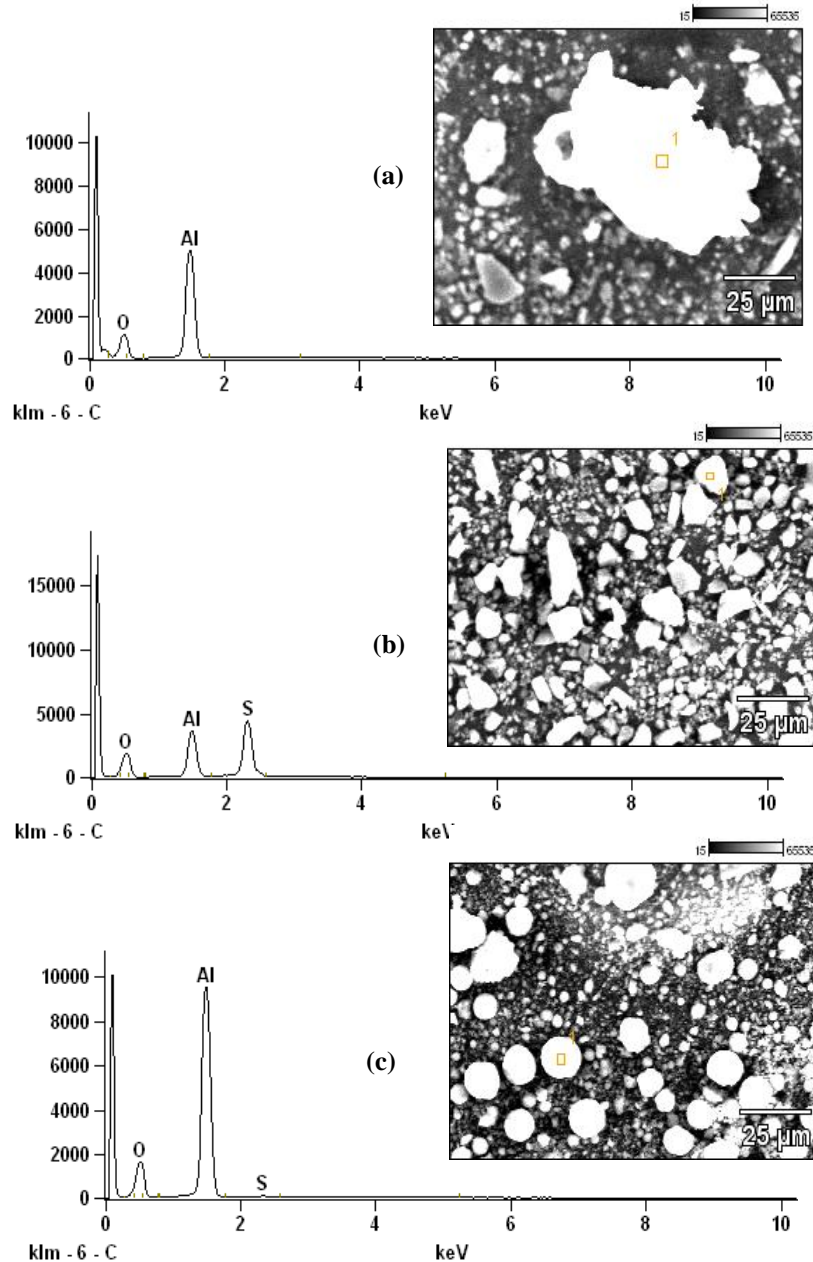
EDS characterisation of Al_2O_3: (a) 19 nm Al_2O_3; (b) 139 nm Al_2O_3; (c) 160 nm Al_2O_3.

164

APPENDIX B: ARTIFICIAL INTELLIGENCE GRAND MODELS

7.5   APPENDIX B.1   HYBRID GA-PNN GRAND MODEL FOR MgO-EG NANOFLUID

Grand GA-PNN model:

$$L_{11} = a_{1,0} + a_{1,1}.d_p + a_{1,2}.\phi + a_{1,3}.d_p.\phi + a_{1,4}.d_p^{\ 2} + a_{1,5}.\phi^2$$

$$L_{21} = a_{2,0} + a_{2,1}.T + a_{2,2}.d_p + a_{2,3}.T.d_p + a_{2,4}.T^2 + a_{2,5}.d_p^{\ 2}$$

$$L_{12} = a_{3,0} + a_{3,1}.d_p + a_{3,2}.L_{11} + a_{3,3}.d_p.L_{11} + a_{3,4}.d_p^{\ 2} + a_{3,5}.L_{11}^{\ 2}$$

$$L_{22} = a_{4,0} + a_{4,1}.\phi + a_{4,2}.L_{21} + a_{4,3}.\phi.L_{21} + a_{4,4}.\phi^2 + a_{4,5}.L_{21}^{\ 2}$$

$$L_{13} = a_{5,0} + a_{5,1}.T + a_{5,2}.L_{12} + a_{5,3}.T.L_{12} + a_{5,4}.T^2 + a_{5,5}.L_{12}^{\ 2}$$

$$L_{23} = a_{6,0} + a_{6,1}.\phi + a_{6,2}.L_{22} + a_{6,3}.\phi.L_{22} + a_{6,4}.\phi^2 + a_{6,5}.L_{22}^{\ 2}$$

$$EV = a_{7,0} + a_{7,1}.L_{13} + a_{7,2}.L_{23} + a_{7,3}.L_{13}.L_{23} + a_{7,4}.L_{13}^{\ 2} + a_{7,5}.L_{23}^{\ 2}$$

Coefficient matrix:

$$
\left[\mathbf{a}_{i,j} \right] =
\begin{bmatrix}
13.04471101 & -0.23643914 & -0.07431895 & 0.00173761 & 0.36614326 & -0.01084868 \\
43.42309576 & -0.02706623 & -1.12543872 & -0.00001994 & 0.00819309 & 0.00044192 \\
14.36973131 & -0.09765461 & -1.28875574 & 0.00050633 & 0.09269148 & 0.00280595 \\
13.73583221 & -0.12049393 & -0.48198892 & -0.00026002 & 0.04173937 & 0.00491979 \\
26.50248649 & -0.77882891 & 1.07065759 & 0.00695986 & 0.00836354 & -0.01844119 \\
-0.14756145 & -0.08250359 & 0.96488446 & 0.00870994 & -0.00369486 & 0.05667468 \\
0.47357046 & -0.07974226 & 0.96704951 & 0.07986601 & 0.05545359 & -0.13097044
\end{bmatrix}
$$

7.6 APPENDIX B2 HYBRID GMDH-NN GRAND MODEL FOR Al$_2$O$_3$-GLYCEROL NANOFLUID

Grand GMDH-NN model:

$$\mu_r = a_{17,0} + a_{11,1} \cdot N_{11} + a_{17,2} \cdot N_{11} \cdot N_{18} + a_{17,3} \cdot N_{11}{}^2 + a_{17,4} \cdot N_{18}{}^2$$

$$N_{11} = a_{1,0} + a_{1,1} \cdot \left(\frac{T}{T_0}\right) + a_{1,2} \cdot N_{25} \cdot \left(\frac{T}{T_0}\right) + a_{1,3} \cdot \left(\frac{T}{T_0}\right)^2 + a_{1,4} \cdot N_{25}$$

$$N_{18} = a_{2,0} + a_{2,1} \cdot N_{35} + a_{2,2} \cdot N_{35} \cdot N_{41} + a_{2,3} \cdot N_{35}{}^2 + a_{2,4} \cdot N_{41}$$

$$N_{25} = a_{3,0} + a_{3,1} \cdot N_{53} + a_{3,2} \cdot N_{53} \cdot N_{63} + a_{3,3} \cdot N_{53}{}^2 + a_{3,4} \cdot N_{63}$$

$$N_{35} = a_{4,0} + a_{4,1} \cdot N_{74} + a_{4,2} \cdot N_{49} \cdot N_{74} + a_{4,3} \cdot N_{74}{}^2 + a_{4,4} \cdot N_{49} + a_{4,5} \cdot N_{49}^2$$

$$N_{41} = a_{5,0} + a_{5,1} \cdot N_{58} + a_{5,2} \cdot N_{58} \cdot N_{68} + a_{5,3} \cdot N_{58}{}^2 + a_{5,4} \cdot N_{68} + a_{5,5} \cdot N_{68}^2$$

$$N_{49} = a_{6,0} + a_{6,1} \cdot N_{74} + a_{6,2} \cdot N_{74} \cdot N_{78} + a_{6,3} \cdot N_{74}{}^2 + a_{6,4} \cdot N_{78}{}^2$$

$$N_{53} = a_{7,0} + a_{7,1} \cdot \left(\frac{d}{h}\right) + a_{7,2} \cdot N_{77} \cdot \left(\frac{d}{h}\right) + a_{7,3} \cdot N_{77} + a_{7,4} \cdot N_{77}{}^2$$

$$N_{58} = a_{8,0} + a_{8,1} \cdot \left(\frac{T}{T_0}\right) + a_{8,2} \cdot N_{74} \cdot \left(\frac{T}{T_0}\right) + a_{8,3} \cdot \left(\frac{T}{T_0}\right)^2 + a_{8,4} \cdot N_{74} + a_{8,5} \cdot N_{74}{}^2$$

$$N_{63} = a_{9,0} + a_{9,1} \cdot \left(\frac{d}{h}\right) + a_{9,2} \cdot N_{79} \cdot \left(\frac{d}{h}\right) + a_{9,3} \cdot N_{79} + a_{9,4} \cdot N_{79}{}^2$$

$$N_{68} = a_{10,0} + a_{10,1} \cdot N_{80} + a_{10,2} \cdot N_{80} \cdot N_{88} + a_{10,3} \cdot N_{80}{}^2 + a_{10,4} \cdot N_{88}$$

$$N_{74} = a_{11,0} + a_{11,1} \cdot \phi + a_{11,2} \cdot \phi \cdot \left(\frac{d}{h}\right)^{\frac{1}{3}} + a_{11,3} \cdot \phi^2 + a_{11,4} \cdot \left(\frac{d}{h}\right)^{\frac{1}{3}}$$

$$N_{77} = a_{12,0} + a_{12,1} \cdot \phi + a_{12,2} \cdot \phi \cdot \left(\frac{T}{T_0}\right)^{\frac{1}{3}} + a_{12,3} \cdot \phi^2 + a_{12,4} \cdot \left(\frac{T}{T_0}\right)^{\frac{2}{3}}$$

$$N_{78} = a_{13,0} + a_{13,1} \cdot \phi + a_{13,2} \cdot \phi \cdot \left(\frac{T}{T_0}\right) + a_{13,3} \cdot \phi^2 + a_{13,4} \cdot \left(\frac{T}{T_0}\right)^2$$

$$N_{79} = a_{14,0} + a_{14,1} \cdot \phi^{\frac{1}{3}} + a_{14,2} \cdot \left(\frac{\phi \cdot T}{T_0}\right)^{\frac{1}{3}} + a_{14,3} \cdot \phi^{\frac{2}{3}} + a_{13,4} \cdot \left(\frac{T}{T_0}\right)^{\frac{2}{3}}$$

$$N_{80} = a_{15,0} + a_{15,1} \cdot \left(\frac{T}{T_0}\right) \cdot \phi^{\frac{1}{3}} + a_{15,2} \cdot \left(\frac{T}{T_0}\right)^2 + a_{15,3} \cdot \phi^{\frac{1}{3}} + a_{15,4} \cdot \phi^{\frac{2}{3}}$$

$$N_{88} = a_{16,0} + a_{16,1} \cdot \left(\frac{d}{h}\right)^{\frac{4}{3}}$$

Coefficients matrix:

$$
\begin{bmatrix} \vec{a}_{i,j} \end{bmatrix} =
\begin{bmatrix}
-0.321517 & 0.25606 & -0.0370338 & -0.048751 & 1.10191 & 0 \\
-0.188348 & 1.23044 & 4.49926 & -2.41921 & -2.13299 & 0 \\
-0.140132 & -2.75747 & -4.79704 & 4.70576 & 3.99177 & 0 \\
-0.0307418 & 0.538185 & -1.53936 & 0.598807 & 0.55801 & 0.880023 \\
0.173143 & -1.92998 & -15.5739 & 8.5577 & 2.74038 & 7.14322 \\
1.49413 & -1.27825 & 2.71316 & -0.68996 & -1.17788 & 0 \\
-0.935389 & 1.15697 & -1.0292 & 1.69105 & 0.127347 & 0 \\
1.43738 & -0.300686 & 0.381542 & -0.0263996 & -0.649262 & 0.228859 \\
-0.482389 & 1.13287 & -1.0101 & 1.0606 & 0.331032 & 0 \\
7.83947 & -6.43514 & 4.69425 & 0.384991 & -5.25237 & 0 \\
0.255487 & 42.7945 & -49.5965 & 423.808 & 0.829561 & 0 \\
1.30942 & -45.7755 & 33.4417 & 399.686 & -0.168446 & 0 \\
1.14943 & -18.5889 & 7.06931 & 400.59 & -0.0217554 & 0 \\
4.53686 & -30.2614 & 8.01848 & 43.5546 & -0.725447 & 0 \\
3.7242 & 1.4423 & -0.0709741 & -23.2172 & 43.6259 & 0 \\
1.53855 & -0.173113 & 0 & 0 & 0 & 0 \\
0.00719965 & 0.968948 & 13.6328 & 6.65067 & 6.99027 & 0
\end{bmatrix}
$$

167

7.7 APPENDIX B3   HYBRID GMDH-NN GRAND MODEL FOR SiO₂-EG NANOFLUID

Grand GMDH-NN model:

$$\mu_r = a_{13,0} + a_{13,1} \cdot N_8 + a_{13,2} \cdot N_9$$

$$N_9 = a_{1,0} + a_{1,1} \cdot N_{56} + a_{1,2} \cdot N_{56} \cdot N_{23} + a_{1,3} \cdot N_{56}^2 + a_{1,4} \cdot N_{23} + a_{1,5} \cdot N_{23}^2$$

$$N_{23} = a_{2,0} + a_{2,1} \cdot N_{36} + a_{2,2} \cdot N_{41}$$

$$N_{41} = a_{3,0} + a_{3,1} \cdot \phi^{\frac{1}{3}} + a_{3,2} \cdot N_{55} \cdot \phi^{\frac{1}{3}} + a_{3,3} \cdot \phi^{\frac{2}{3}} + a_{3,4} \cdot N_{55} + a_{3,4} \cdot N_{55}^2$$

$$N_{36} = a_{4,0} + a_{4,1} \cdot \left(\frac{T}{T_0}\right)^{\frac{1}{3}} + a_{4,2} \cdot N_{60} \cdot \left(\frac{T}{T_0}\right)^{\frac{1}{3}} + a_{4,3} \cdot \left(\frac{T}{T_0}\right)^{\frac{2}{3}} + a_{4,4} \cdot N_{40}$$

$$N_{56} = a_{5,0} + a_{5,1} \cdot N_{58} \cdot N_{62} + a_{5,2} \cdot N_{62}$$

$$N_{62} = a_{6,0} + a_{6,1} \cdot \left(\frac{T}{T_0}\right) + a_{6,2} \cdot \left(\frac{T}{T_0}\right)^{\frac{1}{3}} + a_{6,3} \cdot \left(\frac{T}{T_0}\right)^{\frac{2}{3}}$$

$$N_8 = a_{7,0} + a_{7,1} \cdot N_{58} + a_{7,2} \cdot N_{32}$$

$$N_{32} = a_{8,0} + a_{8,1} \cdot \left(\frac{T}{T_0}\right)^{\frac{1}{3}} + a_{8,2} \cdot N_{42} \cdot \left(\frac{T}{T_0}\right)^{\frac{1}{3}} + a_{8,3} \cdot \left(\frac{T}{T_0}\right)^{\frac{2}{3}} + a_{8,4} \cdot N_{42}$$

$$N_{42} = a_{9,0} + a_{9,1} \cdot N_{55} + a_{9,2} \cdot N_{55} \cdot N_{60} + a_{9,3} \cdot N_{55}^2 + a_{9,4} \cdot N_{60} + a_{9,5} \cdot N_{60}^2$$

$$N_{60} = a_{10,0} + a_{10,1} \cdot \phi + a_{10,2} \cdot (\phi)^{\frac{4}{3}} + a_{10,3} \cdot (\phi)^2 + a_{10,4} \cdot (\phi)^{\frac{1}{3}} + a_{10,5} \cdot (\phi)^{\frac{2}{3}}$$

$$N_{55} = a_{11,0} + a_{11,1} \cdot (\phi)^{\frac{1}{3}} + a_{11,2} \cdot \left(\frac{\phi \cdot T}{T_0}\right)^{\frac{1}{3}} + a_{11,3} \cdot (\phi)^{\frac{2}{3}} + a_{11,4} \cdot \left(\frac{T}{T_0}\right)^{\frac{1}{3}} + a_{11,5} \cdot \left(\frac{T}{T_0}\right)^{\frac{2}{3}}$$

$$N_{58} = a_{12,0} + a_{12,1} \cdot \phi + a_{12,2} \cdot \phi \cdot \left(\frac{T}{T_0}\right) + a_{12,3} \cdot \phi^2 + a_{12,4} \cdot \left(\frac{T}{T_0}\right)^2$$

Coefficient matrix:

$$
\left[\vec{a}_{i,j} \right] =
\begin{bmatrix}
-0.000627144 & 0.487834 & 0.512688 & 0 & 0 & 0 \\
0.0439827 & -2.47133 & -94.0591 & 48.0503 & 3.39193 & 46.0402 \\
-0.00111379 & 0.5878 & 0.413127 & 0 & 0 & 0 \\
1.23612 & 15.3554 & -30.3722 & 39.601 & -4.46816 & 5.64538 \\
0.0220551 & 0.368961 & 0.234737 & -0.295086 & 0.697561 & 0 \\
1.03135 & 0.826603 & -0.852156 & 0 & 0 & 0 \\
-7.6187 & 3.60075 & 19.971 & -14.8094 & 0 & 0 \\
0.00327297 & -1.01163 & 2.00891 & 0 & 0 & 0 \\
-0.376273 & 0.522309 & -0.0867539 & -0.174847 & 1.11026 & 0 \\
-0.0701683 & 2.96384 & -17.2466 & 7.6602 & -1.86796 & 9.55329 \\
3.99572 & 212.213 & -1108.44 & 2430.24 & -37.6939 & 111.698 \\
0.962521 & -2.96796 & 0.733451 & 8.90803 & 0.484774 & -0.306703 \\
0.957334 & 12.3012 & 0.501123 & -21.3242 & -0.00712839 & 0
\end{bmatrix}
$$

7.8   APPENDIX B4   HYBRID GMDH-NN GRAND MODEL FOR SiO$_2$-GLYCEROL NANOFLUID

Grand GMDH-NN model:

$$\mu_r = a_{6,0} + a_{6,1} \cdot (\phi)^{\frac{1}{3}} \cdot N_{15} + a_{6,2} \cdot N_{15} \cdot (\phi)^{\frac{2}{3}} + a_{6,3} \cdot N_{15} + a_{6,4} \cdot N_{15}^2$$

$$N_{15} = a_{1,0} + a_{1,1} \cdot N_{52} + a_{1,2} \cdot N_{52} \cdot N_{29} + a_{1,3} \cdot N_{52}^2 + a_{1,4} \cdot N_{29}^2$$

$$N_{29} = a_{2,0} + a_{2,1} \cdot N_{38} + a_{2,2} \cdot N_{38} \cdot N_{40} + a_{2,3} \cdot N_{38}^2 + a_{2,4} \cdot N_{40} + a_{2,5} \cdot N_{40}^2$$

$$N_{40} = a_{3,0} + a_{3,1} \cdot (\phi)^{\frac{1}{3}} + a_{3,2} \cdot (\phi)^{\frac{2}{3}} + a_{3,3} \cdot \left(\frac{T}{T_0}\right)^{\frac{1}{3}} + a_{3,4} \cdot \left(\frac{T}{T_0}\right)^{\frac{2}{3}}$$

$$N_{38} = a_{4,0} + a_{4,1} \cdot \left(\frac{T}{T_0}\right) + a_{4,2} \cdot \left(\frac{T}{T_0}\right)^2 + a_{4,3} \cdot (\phi)^{\frac{1}{3}} + a_{4,4} \cdot (\phi)^{\frac{2}{3}}$$

$$N_{41} = a_{5,0} + a_{5,1} \cdot \left(\frac{T}{T_0}\right)^{\frac{1}{3}} + a_{5,2} \cdot \left(\frac{T}{T_0}\right)^{\frac{2}{3}}$$

Coefficient matrix:

$$\left[\vec{a}_{i,j}\right] = \begin{bmatrix} -0.0127672 & -1.66122 & 3.65348 & 1.01789 & 0.179252 & 0 \\ -3.76918 & 7.88574 & 1.04186 & -4.11105 & -0.0696878 & 0 \\ -0.0072149 & -11.7977 & 2178 & -1082.93 & 12.8227 & -1095.08 \\ 0914388 & -5.12665 & 13.9785 & 0.992816 & -0.455421 & 0 \\ 1.43103 & 0.0368856 & -0.0157883 & -5.1183 & 13.9623 & 0 \\ -0.868837 & 3.30514 & -1.34924 & 0 & 0 & 0 \end{bmatrix}$$